uOttawa

L'Université canadienne
Canada's university

FACULTÉ DES ÉTUDES SUPÉRIEURES ET POSTOCTORALES

uOttawa

L'Université canadienne
Canada's university

FACULTY OF GRADUATE AND POSDOCTORAL STUDIES

Recep Emre Erkmen
AUTEUR DE LA THÈSE / AUTHOR OF THESIS

Ph.D. (Civil Engineering)
GRADE / DEGREE

Department of Civil Engineering
FACULTÉ, ÉCOLE, DÉPARTEMENT / FACULTY, SCHOOL, DEPARTMENT

Finite Element Formulations for Thin-walled Members

TITRE DE LA THÈSE / TITLE OF THESIS

Magdi Mohareb
DIRECTEUR (DIRECTRICE) DE LA THÈSE / THESIS SUPERVISOR

CO-DIRECTEUR (CO-DIRECTRICE) DE LA THÈSE / THESIS CO-SUPERVISOR

EXAMINATEURS (EXAMINATRICES) DE LA THÈSE / THESIS EXAMINERS

Heng Khoo

Kenneth Will (teleconference)

Beatriz Martin-Perez

Dan Palerdmo

Gary W. Slater
Le Doyen de la Faculté des études supérieures et postdoctorales / Dean of the Faculty of Graduate and Postdoctoral Studies

Finite Element Formulations for Thin-walled Members

By

R. Emre Erkmen

A Thesis submitted to
the Faculty of Graduate Studies and Research
in partial fulfillment of
the requirement for the degree of

DOCTOR OF PHILOSOPHY
In Civil Engineering

Department of Civil Engineering
University of Ottawa
Ottawa, Ontario, Canada

December 2006

The Ph.D in Civil Engineering is a joint program with the
Carleton University, administrated by the Ottawa-Carleton Institute for Civil Engineering

Your file Votre référence
ISBN: 978-0-494-25867-5
Our file Notre référence
ISBN: 978-0-494-25867-5

To Serra

Acknowledgements

The author would like to express his gratitude to his supervisor, Dr. Magdi Mohareb for his guidance, valuable suggestions and advice throughout the course of this research.

The author also would like to thank to the members of his thesis proposal committee; Dr. Khoo, Dr. Redekop and Dr. Martin-Perez for their valuable suggestions and encouragement.

Special thanks to Dr. Murat Saatcioglu, Metin Bayulken, Ismail Ozerdinc, Aysun Ozerdinc and Rengin Mahruki for their encouragement and moral support.

Deepest thanks go to author's parents Tulin Erkmen and A. Cahit Erkmen for their immense support and guidance, and to his brother Atilla Erkmen for all the joy and happiness.

The author wishes to express his highest appreciations to his wife Serra Cimilli-Erkmen for her love and support.

Abstract

Conventional solutions for the equations of equilibrium based on the well known Vlasov thin-walled beam theory uncouple the equations by adopting orthogonal coordinate systems. This technique introduces several modeling complications and limitations where eccentric supports or abrupt cross-sectional changes exist (in elements with rectangular holes, coped flanges, or longitudinal stiffened members, etc.).

In this study, a general solution of the Vlasov thin-walled beam theory based on a non-orthogonal coordinate system is developed. A finite element formulation, which yields nodal values in exact agreement with those based on the closed form solution of the Vlasov field equations and boundary conditions, is derived. The advantages and modeling capabilities of the formulation are discussed in detail. General expressions for normal and shearing stresses under non-orthogonal coordinate systems are developed. For design purposes, an elastic interaction equation for general open thin-walled section is derived.

The shear deformation effect due to warping torsion is included in the torsional analysis of open thin-walled beams of general cross-section. The principle of stationary complementary energy is adopted to formulate the governing field compatibility condition. The variational principle is then extended to formulate a finite element, which captures shear deformation effects and allows the use of a minimal number of elements. For squat beams, shear deformation effects are shown to gain significance.

Field equations and boundary conditions are obtained for the buckling analysis of thin-walled members by using the principle of stationary complementary energy. Subsequently a finite element is derived which incorporates shear deformation effects, a feature that is neglected in most available buckling solutions. It is shown that conventional solutions which neglect shear deformation effects can overestimate the predicted buckling load in some cases. The proposed finite element formulation can be used for the problems of column flexural buckling and torsional buckling, as well as beam lateral torsional buckling under linear moment gradients for doubly symmetric, mono-symmetric and channel sections. By adopting a non-orthogonal coordinate system, the solution is able to successfully capture load position effects relative to the shear centre. The efficiency and availability of the formulation is shown through comparisons to results based on shell finite element analysis solutions and other closed form or numerical solutions in the literature.

Table of Contents

CHAPTER I

INTRODUCTION AND SUMMARY

General

Open section thin-walled members are commonly used in steel structures. A member can be characterized as thin-walled when the characteristic thickness t is in the order of $1/10^{th}$ of the characteristic depth of the cross-section i.e., $t \approx d/10$ (Fig.I.1). A number of theories were developed in the literature in order to analyze thin-walled members. In this thesis, the Vlasov theory is adopted and modified to analyze the behavior under static loading and buckling behavior of thin-walled beams. Several finite elements are formulated as numerical tools to systematically solve the governing equations subject to boundary conditions.

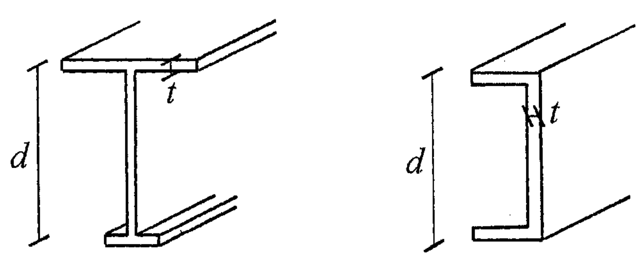

Fig.I.1 Open Thin-walled cross-sections

Contents of the Thesis

The thesis is organized in a paper format. In Chapter II (paper [I.1]), three finite element families are developed for the analysis of thin-walled members based on the well-known Vlasov theory. The equilibrium equations and the boundary conditions are derived in terms of the displacement fields by using the principle of virtual work. Unlike the conventional approach in which the orthogonal system of coordinates is selected to uncouple the differential equations, the differential equilibrium equations are solved in the general coupled form. The homogenous solution of the differential equations is used to interpolate the displacement field in deriving the first finite element. This approach yields to exact nodal values under general loading conditions. Two additional elements are subsequently derived for the special cases of long elements in which the warping stiffness is negligible and, short element in which the warping stiffness is dominant.

In Chapter III (paper [I.2]), the advantages of the elements formulated in Chapter II in modeling practical problems are illustrated through examples. It is shown that the formulation seamlessly handles members with abrupt cross-sectional changes (e.g., rectangular holes Fig.I.2a or coped beams Fig. I.2b), and eccentric boundary conditions (e.g., Fig.I.2c).

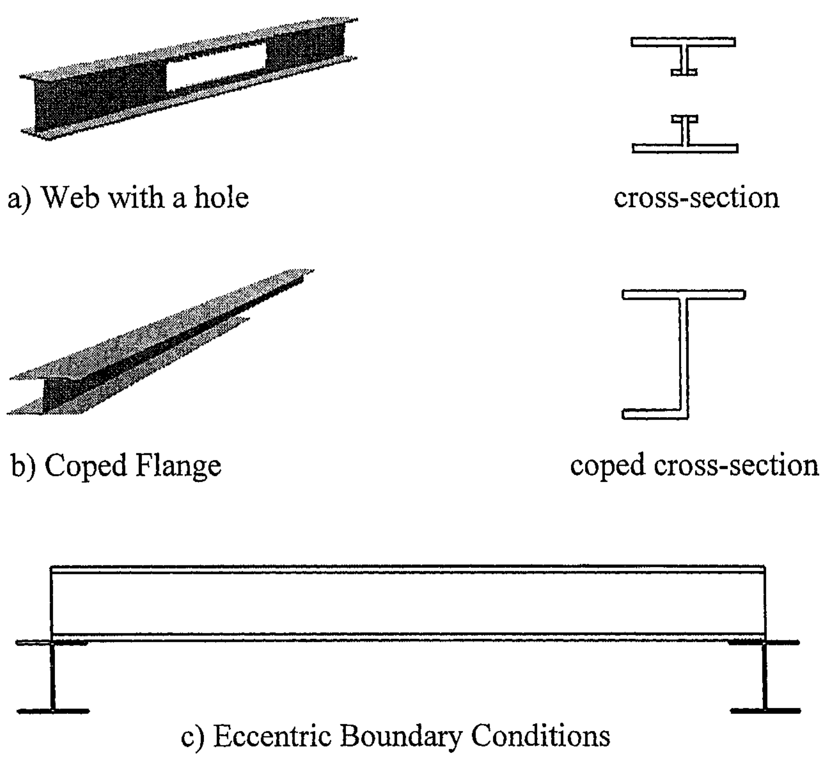

Figure I.2 Cross-section discontinuities and Eccentric Boundary Conditions

In Chapter IV (paper [I.3]) generalized expressions of normal and shear stresses in terms internal forces are derived for the proposed finite element solution scheme based on non-orthogonal coordinates. It is shown that for the special case of an orthogonal system of coordinates, the expressions coincide with the conventional ones.

A restriction of Vlasov's theory is the fact that it does not incorporate transverse shear deformation effects. For squat thin-walled members (Fig.I.3), neglecting shear effect may cause significant errors. In Chapter V (paper [I.4]), the effect of shear deformation is included in torsional analysis of thin-walled prismatic beams through a modified version of the Vlasov theory. The field equations and boundary conditions are derived by using the principle of stationary complementary energy. A new cross-sectional property associated with the distribution of shear stresses over the cross-section arises in the formulation. The solution scheme for hand calculations is illustrated through a practical example. Two finite elements based on the new theory are formulated. The first element provides a solution suitable for short elements in which the warping stiffness is dominant. The second element is derived based on the interpolation functions which satisfy the homogenous solution of the field equations, which is proved to provide exact nodal values within the limitations of the theory. An example is given to illustrate the effectiveness of the finite element solution scheme. Solutions based on the new theory are compared with those based on the theories of Vlasov and Benscoter.

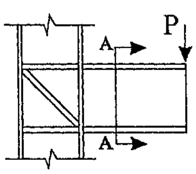

a) Elevations

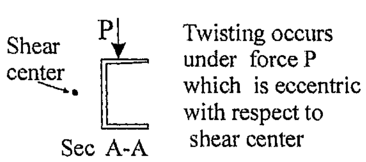

b) cross-section

Figure I.3- Squat thin-walled beam subject to a loading condition that causes twisting

In Chapter VI (paper [I.5]), a formulation for the buckling analysis of thin-walled members is developed based on the principle of stationary complementary energy. Material, stress and strain measures of finite elasticity are adopted. The deformation gradient tensor is decomposed into a finite rotation tensor and a right extensional stretch tensor according to Polar decomposition theory. The Euler-Rodrigues expressions are adopted to express the rotation tensor in terms of the three mutually independent rotation vectors. The Jaumann stress tensor is used to refer to the stress configuration. Some aspects of the Vlasov theory is adopted to describe the behavior of members under buckling deformation. Thus, the cross-section is assumed to remain rigid under deformation in agreement with the first Vlasov assumption. The stress-stress resultant relations are postulated to be in agreement with the Vlasov theory as obtained in Paper [I.3]. Pre-buckling deformations are neglected. The equilibrium equations are satisfied at the stress level. Equilibrium and compatibility equations are derived in terms of the stress resultants and displacement fields. It is shown that the formulation based on the complementary energy functional may provide lower bound buckling load predictions in torsional buckling modes (Fig, I.4), a characteristic which is unattainable under displacement based formulations and preferable from the designer point of view.

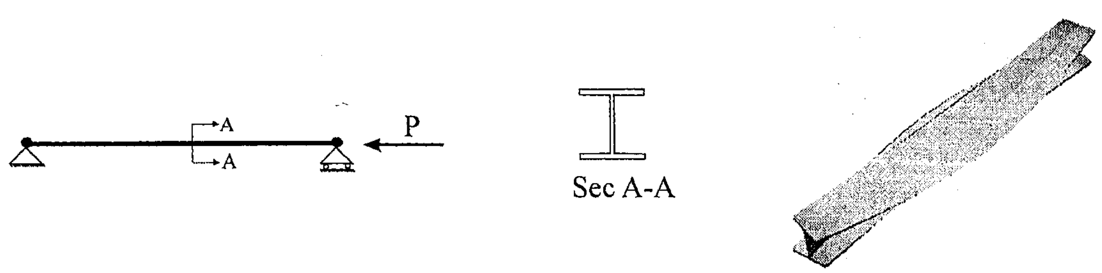

(a) Boundary conditions and loading (b) Cross-section (c) Buckled shape

Figure I.4- Torsional buckling mode of a simply supported beam under axial load

Finite element formulation is derived based on a general non-orthogonal system of coordinates. Thus, the load position effects in the plane of the cross-section are captured (e.g., Fig. I.5). Mono-symmetric properties are generalized to non-orthogonal coordinates. New cross-sectional properties associated with the distribution of shear stresses over the cross-section arise within the new formulation. Unlike other theories in the literature, the effect of shear deformation on buckling load predictions of open section thin-walled beams and columns is successfully captured. Several examples illustrate the validity and versatility of the proposed solution. It is shown that in some cases of short span members (Fig. I.5) in which global buckling occurs prior to yielding of the material or local buckling, shear deformation can have significant effect in predicting buckling loads.

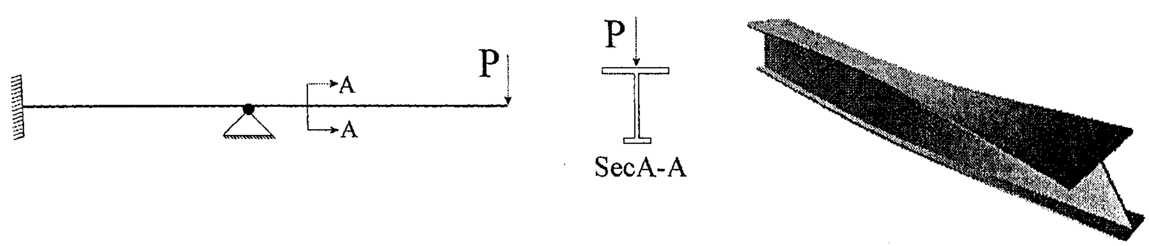

(a) Boundary conditions and loading (b) Cross-section (c) Buckled shape

Figure I.5- Lateral torsional buckling of a mono-symmetric beam under top flange load

In Chapter VII, the main contributions of the thesis are summarized and proposed extensions of the research are recommended.

References

[I.1] Erkmen, R. E. and Mohareb, M. (2006). "Non-orthogonal solution for thin-walled members I. Finite Element Formulation", Canadian Journal of Civil Engineering 2006; Vol. 33(4): 421-439

[I.2] Erkmen, R. E. and Mohareb, M. (2006). "Non-orthogonal solution for thin-walled members II. Applications and Modelling Considerations", Canadian Journal of Civil Engineering 2006; Vol. 33(4): 440-450

[I.3] Erkmen, R. E. and Mohareb, M. "Non-orthogonal solution for thin-walled members-Generalized Expression for Stresses", accepted for presentation in The Eighth International Conference on Computational Structures Technology September 2006

[I.4] Erkmen, R. E. and Mohareb, M. (2006). "Torsion Analysis of Thin-Walled Beams Including Shear Deformation Effects", accepted for publication in Thin-Walled Structures

[I.5] Erkmen, R. E. and Mohareb, M. (2006). "Buckling Analysis of Thin-walled open members based on Complementary Energy functional", to be sent to an International Journal

Chapter II

Non-orthogonal solution for thin-walled members - Finite Element Formulation

Abstract

Conventional solutions for the equations of equilibrium based on the well known Vlasov thin-walled beam theory uncouple the equations by adopting orthogonal coordinate systems. Although this technique considerably simplifies the resulting field equations, it introduces several modeling complications and limitations. As a result, when analyzing problems where eccentric supports or abrupt cross-sectional changes exist (in elements with rectangular holes, coped flanges, or longitudinal stiffened members, etc..), the Vlasov theory has been avoided in favour of shell finite element which offer modeling flexibility at higher computational cost. In this chapter, a general solution of the Vlasov thin-walled beam theory based on a non-orthogonal coordinate system is developed. The field equations are then exactly solved and the obtained displacement field expressions are used to formulate a finite element. Two additional finite elements are subsequently derived to cover the special cases where: a) the St. Venant torsional stiffness is negligible, and b) the warping torsional stiffness is negligible. The advantages and modeling functionality of the new formulation scheme are illustrated through examples in the next chapter.

Keywords

Open sections, warping effect, finite element, thin-walled beams, asymmetric sections.

Introduction and Scope

The well known thin-walled beam theory (Vlasov 1961) results into four coupled differential equations of equilibrium. The equilibrium equations are formulated in terms of the three translational rigid body displacements of the cross-section and the in-plane angle of rotation. Conventional solution techniques for the Vlasov equilibrium equations attempt to eliminate the coupling between the four field equations (Murray 1984). This is realized by adopting an orthogonal system of coordinates (adopting the centroidal principal axes, and selecting the line joining the section shear center and principal sectorial origin as a fixed radius-Appendix II.A). While this approach successfully uncouples the equations of equilibrium, it generally suffers from a number of drawbacks including: (a) the necessity to perform coordinate transformations; (b) the difficulties in handling cross-section discontinuities where members undergo abrupt sectional changes (e.g., members with holes, flange copes, presence of longitudinal stiffening plates, etc.); (c) the boundary conditions may remain or become uncoupled after transformation; (d) the adoption of an orthogonal system of coordinates may necessitate resolving the internal and external forces along the orthogonal coordinate systems. As a result, the use of conventional solution techniques has been limited to very simple applications. The idea of this paper is to avoid the modeling complications arising from the conventional technique by developing a direct and exact solution of the coupled system of equilibrium equations.

Literature review

Several finite element solutions for the torsion of thin-walled sections are reported in the literature. Krajcinovic (1969) formulated a displacement based finite element for the analysis of thin-walled sections under non-uniform torsion by adopting shape functions based on the homogenous solutions of the uncoupled differential equations of Vlasov. Another solution (Krajcinovic 1970) using a force based approach was presented. Finite element formulations by Barsoum (1970) and Barsoum and Gallagher (1970) were based on cubic and fifth order Hermitian polynomial interpolations of the rotation field. Tso and Ghobarah (1971) developed an elastic geometrically nonlinear solution for the torsion of thin-walled sections. Using the principle of virtual work, Murray and Rajasekaran (1975) formulated the governing equations and associated boundary conditions for thin-walled beam under general loading. Gunnlaugson and Pedersen (1981) formulated a finite element for arbitrary thin-walled sections. In their derivation, they included the contributions of bending and warping shear deformations. An attempt to formulate the stiffness matrix of a thin-walled beam-column including second order effects due to axial forces was presented by Chaudhary (1982). The derived stiffness matrix has several limitations (Hancock 1984; Aly and Sato 1984) including: (a) the applied bending moments are assumed constant throughout the length of the thin-walled element; (b) the formulation is limited to mono-symmetric sections; and (c) warping is assumed to be restrained at both ends. An elasto-plastic finite element for wide flange sections was developed by Gellin et al. (1983). Friberg (1985) developed a finite element formulation for the vibration of thin-walled beams. A hybrid finite element formulation for thin-walled beams based on the Hellinger-Reissner variational principle was presented by Tralli (1986). Later on, an element similar to the one developed in Krajcinovic (1969) was presented in Dvorkin et al. (1989) and applied to the analysis of curved beams as an approximate solution. Chen and Blandford (1989) developed a finite element formulation, which included the effects of shear deformations using a hybrid Vlasov-Timoshenko beam formulation. A comprehensive comparative study of finite elements for thin-walled elements was presented by de Ville de Goyet (1989). Batoz and Dhatt (1990) presented a 14 degree of freedom (DOF) thin-wall beam element based an exact orthogonal solution of the differential equations of equilibrium. A modified Hellinger-Reissner functional was employed by Gendy et al. (1992) to derive a thin-walled beam finite element free of shear-locking. Shakourzadeh et al. (1995) derived an exact finite element based on Benscoter thin walled beam theory (Benscoter 1954). Eisenberger and Cohen (1995) developed exact series solutions for non-prismatic torsional flexural buckling of thin-walled members under variable axial loads. Prokic (1996) developed an advanced thin-walled beam theory and a finite element formulation based on an advanced warping function. A generalized warping torsion formulation was developed by Schultz and Filippou (1998) by relaxing the transversely rigid assumption for the cross-section commonly adopted in other formulations. Back and Will (1999) adopted a modified Vlasov theory in formulating a shear-flexible thin-walled finite element. Mohareb and Nowzartash (2003) mathematically demonstrated that torsion finite elements based on hyperbolic shape functions (Krajcinovic 1969; Batoz and Dhatt 1990) yield nodal displacements in exact agreement with the Vlasov thin-walled theory, irrespective of twisting moment distributions. A common feature among the previous formulations is the adoption of orthogonal coordinate systems. In contrast, the current paper presents a finite element for members subjected to general loading conditions based on the Vlasov thin-walled beam theory using a general non-orthogonal coordinate system.

Assumptions

The formulation is restricted to prismatic thin-walled members of arbitrary cross-sections. Material is assumed to behave elastically. For general loading inducing twisting moments, the elastic assumption is justified by the fact that, given the weak torsional stiffness of open sections, they typically undergo significant angles of twists (a serviceability limit state) prior exhibiting plastic deformations (Driver and Kennedy 1989). Small displacements and rotations are assumed. Thus, geometric non-linear effects are considered negligible. The formulation is based on the two classical kinematic assumptions of the thin-walled beam theory (Vlasov 1961). These are: (a) no distortion of cross-section during deformation; (b) shearing strains acting on the middle surface are negligible.

Review of Vlasov thin-walled beam theory

According to the first Vlasov assumption, cross-sectional distortions throughout deformation are assumed negligible. As a result, the horizontal and vertical components of the displacement $u_s(s,z)$ and $v_s(s,z)$ of an arbitrary point B_p located on the section mid-surface can be expressed in terms of the horizontal and vertical displacement components $u(z)$ and $v(z)$ of an arbitrarily located pole $A_p(a_x,a_y)$ and the angle of twist $\phi(z)$ of the cross-section (Fig. II.1a). Coordinate s, measured from an arbitrary sectorial origin S_0 located on the section profile, identifies coordinates $[x(s),y(s)]$ of point B_p. Thus,

$$u_s(s,z) = u(z) - \left[y(s) - a_y\right]\phi(z) \tag{II.1}$$

$$v_s(s,z) = v(z) + \left[x(s) - a_x\right]\phi(z) \tag{II.2}$$

The component of the displacement $\eta_s(s,z)$ along the tangent to the profile (Fig. II.1a) at point $B_p[x(s),y(s)]$ is related to the displacement components $u_s(s,z)$ and $v_s(s,z)$ by projecting displacement vector $[u_s(s,z),v_s(s,z)]$ on to the unit tangent vector $\vec{t}[\cos\alpha(s),\sin\alpha(s)]$ at point B_p i.e.,

$$\eta_s(s,z)=u_s(s)\cos\alpha(s)+v_s(s)\sin\alpha(s) \tag{II.3}$$

in which $\alpha(s)$ is the angle between the tangent to the profile and the x axis. According to the second Vlasov assumption, the shear strain $\gamma_{z\eta}$ at the middle surface is negligible, i.e., $\gamma_{z\eta}=\partial w_s/\partial s+\partial\eta_s/\partial z\approx 0$. The expression for the shear strain $\gamma_{z\eta}$ is integrated with respect to coordinates and the identities in Eqs. (II.1), (II.2) and (II.3) are used to obtain an expression for the longitudinal displacement $w_s(s,z)$ of point $B_p(s,z)$ on the section profile. One obtains

$$w_s(s,z)=\int\left\{\left[u'(z)-(y-a_y)\phi'(z)\right]\cos\alpha(s)+\left[v'(z)+(x-a_x)\phi'(z)\right]\sin\alpha(s)\right\}ds \tag{II.4}$$

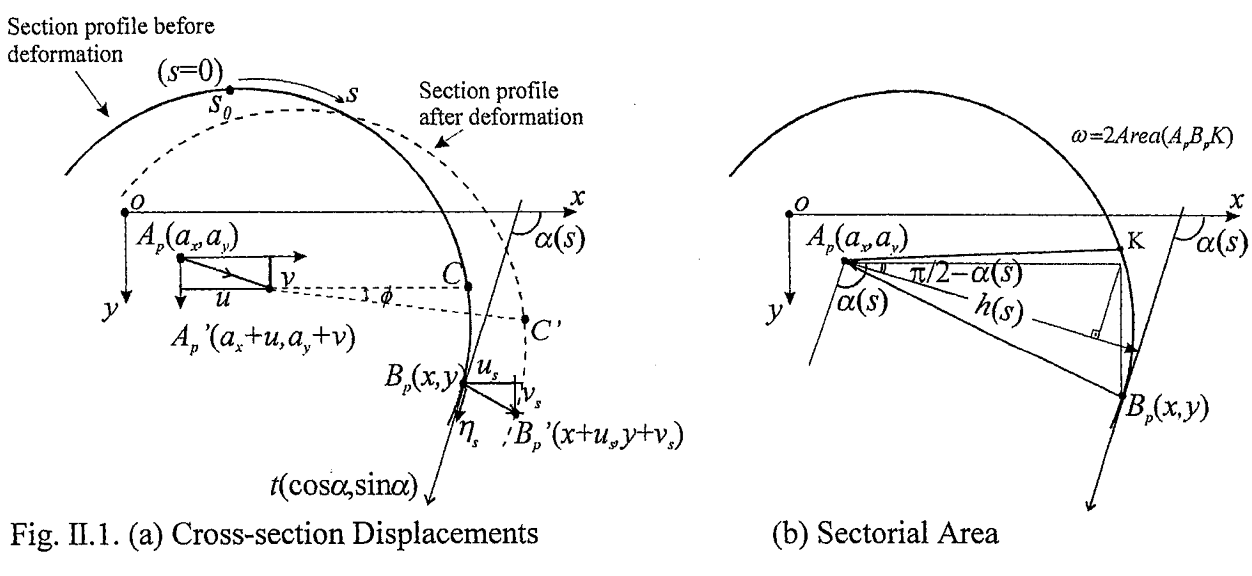

Fig. II.1. (a) Cross-section Displacements (b) Sectorial Area

All primes denote differentiation with respect to longitudinal coordinate z. By denoting the normal distance from the pole $A_p(a_x, a_y)$ to the tangent at point $B_p(x, y)$ as $h(s) = (x - a_x)\sin\alpha(s) - (y - a_y)\cos\alpha(s)$ (Fig. II.1b), defining the change in the sectorial coordinate as $d\omega(s) = h(s)ds$, and noting that $dx = ds\cos\alpha(s)$ and $dy = ds\sin\alpha(s)$, Eq. (II.4) is expressed as

$$w_s(s,z) = w(z) - x(s)u'(z) - y(s)v'(z) - \omega(s)\phi'(z) \tag{II.5}$$

in which $w(z)$ is an arbitrary function which arises when integrating Eq. (II.4) with respect to coordinate s. The longitudinal strain $\varepsilon_{zz}(s,z)$ is obtained by differentiating Eq. (II.5) with respect to coordinate z yielding

$$\varepsilon_{zz}(s,z) = \mathbf{x}_{1\times4}^{\mathrm{T}}\mathbf{u}(z)_{4\times1} \tag{II.6}$$

in which the vector of coordinates $\mathbf{x}_{1\times4}^{\mathrm{T}} = \langle 1 \quad -x(s) \quad -y(s) \quad -\omega(s)\rangle$ and the vector of displacement derivatives $\mathbf{u(z)}_{1\times4}^{\mathrm{T}} = \langle w'(z) \quad u''(z) \quad v''(z) \quad \phi''(z)\rangle$ have been defined. In thin-walled beam analysis, it is common to neglect the normal stresses σ_{ss} acting along the s coordinate (Vlasov 1961). Thus, the approximate constitutive relation $\varepsilon_{zz} = (\sigma_{zz} - \mu\sigma_{ss})/E \approx \sigma_{zz}/E$ is used to relate the longitudinal stress $\sigma_{zz}(s,z)$ to the longitudinal strain $\varepsilon_{zz}(s,z)$. In line with the Vlasov theory (Vlasov 1961), the normal stresses are assumed constant across the section thickness while the shear stresses are assumed to have a linear distribution.

Variational formulation under a non-orthogonal coordinate system

General

A prismatic thin-walled beam element of arbitrary cross-section is considered. The element (Fig. II.2) is subject to externally applied tractions $\bar{\sigma}_0 = \bar{\sigma}_{zz}(s,0,r)$ and $\bar{\tau}_0 = \bar{\tau}_{zs}(s,0,r)$ acting at end $z=0$, and $\bar{\sigma}_l = \bar{\sigma}_{zz}(s,l,r)$ and $\bar{\tau}_l = \bar{\tau}_{zs}(s,l,r)$ acting at end $z=l$, in addition to general member tractions $\mathbf{p}(s,z)^{\mathrm{T}}_{1\times 3} = \langle p_x \quad p_y \quad p_z \rangle_{1\times 3}$. Coordinate r is the normal distance from the mid-surface (Fig. II.2). According to the principle of stationary potential energy, the equilibrium conditions are given by

$$\delta\pi = (\delta U_n + \delta U_s) - (\delta V_1 + \delta V_2) = 0 \tag{II.7}$$

In Eq. (II.7), $\delta\pi$ is the first variation of the total potential energy, δU_n is the internal virtual work induced by normal stresses, δU_s is the internal virtual work induced by the St. Venant shear stresses, δV_1 is the external virtual work induced by the end tractions, and δV_2 is the external virtual work induced by the tractions acting along the member.

Internal Virtual Work

In Eq. (II.7), the internal virtual work terms are given by

$$\delta U_n = \int_V \sigma_{zz}\delta\varepsilon_{zz} dV = E\int_0^l \int_A \delta\mathbf{u}(z)^{\mathrm{T}}_{1\times 4}\mathbf{x}_{4\times 1}\mathbf{x}^{\mathrm{T}}_{1\times 4}\mathbf{u}(z)_{4\times 1} dA dz \tag{II.8}$$

$$\delta U_s = GJ_d \int_0^l \delta\phi'\phi' dz \tag{II.9}$$

in which l is the length of the member, $dA = t(s)ds$, where $t(s)$ is the thickness, the operator δ denotes the variation of the argument displacement functions, and V denotes the volume of the element.

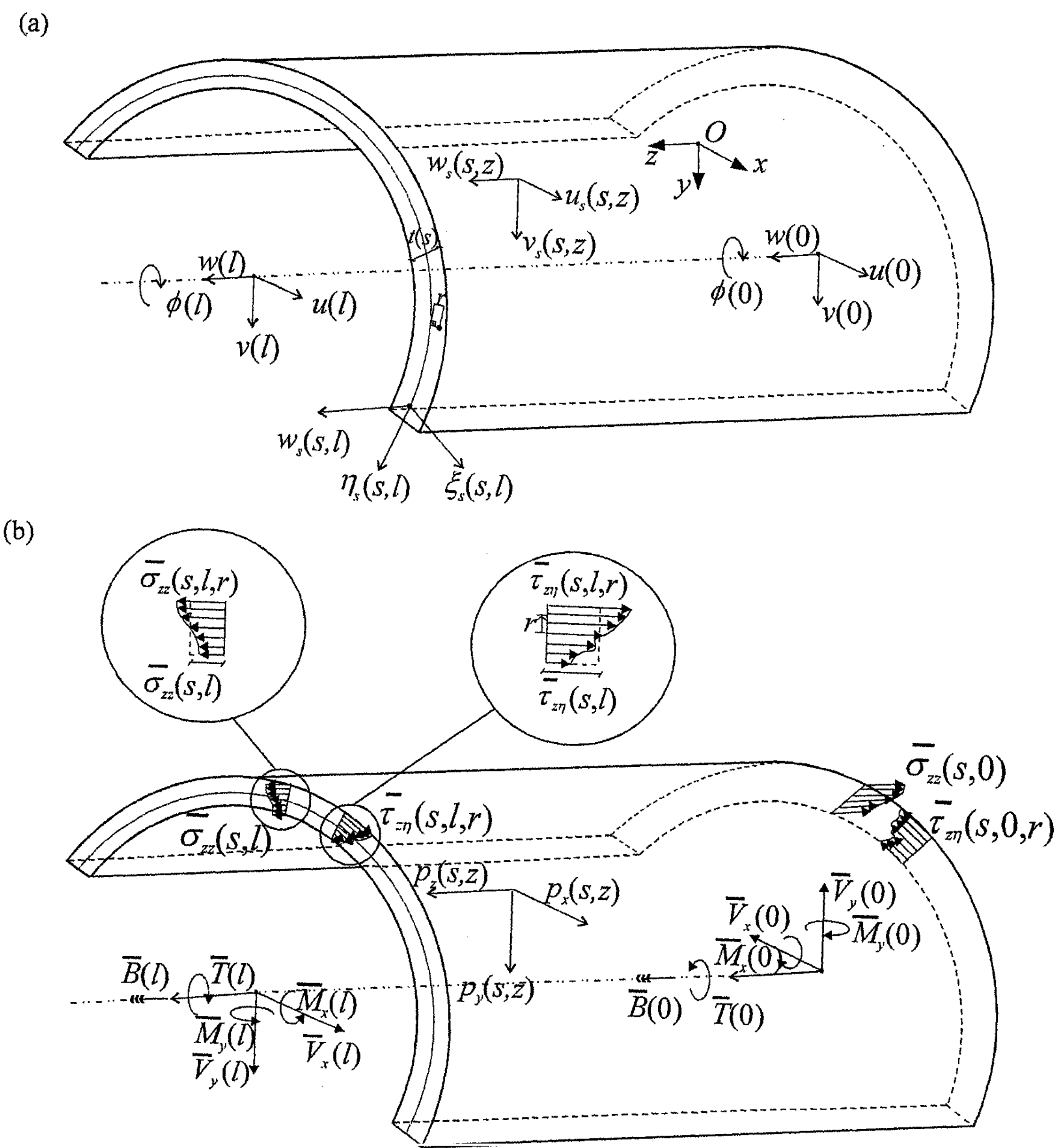

Fig. II.2 Thin wall beam geometry (a) generalized displacements, (b) generalized forces and stresses

For a thin-walled section consisting of n thin-walled rectangular pieces of constant thickness t_k and width b_k, $k = (1...n)$, the St. Venant torsional rigidity constant, is $J_d \approx \sum_{c=1}^{n} b_c t_c^{\,3}/3$ (Boresi and Sidebottom 1985). By defining the matrix of section properties $\mathbf{D}_{4\times4}$ as

$$\mathbf{D}_{4\times4} = \int_A \mathbf{x}_{4\times1}\mathbf{x}_{1\times4}^{\mathrm{T}} dA = \begin{bmatrix} A & -S_y & -S_x & -S_\omega \\ -S_y & J_{yy} & J_{xy} & J_{\omega x} \\ -S_x & J_{xy} & J_{xx} & J_{\omega y} \\ -S_\omega & J_{\omega x} & J_{\omega y} & J_{\omega\omega} \end{bmatrix} \tag{II.10}$$

in which section constants $A = \int_A dA$, $S_y = \int_A x dA$, $S_x = \int_A y dA$, $S_\omega = \int_A \omega dA$, $J_{xx} = \int_A y^2 dA$, $J_{xy} = \int_A xy dA$, $J_{yy} = \int_A x^2 dA$, $J_{\omega x} = \int_A \omega x dA$, $J_{\omega y} = \int_A \omega y dA$, $J_{\omega\omega} = \int_A \omega^2 dA$ are defined, the internal virtual work due to normal strains is expressed as

$$\delta U_n = E\int_0^l \delta\mathbf{u}(z)_{1\times4}^{\mathrm{T}} \mathbf{D}_{4\times4}\mathbf{u}(z)_{4\times1} dz \tag{II.11}$$

In conventional solutions (Vlasov 1961; Murray 1984), it is customary to select an orthogonal system of coordinates x, y, ω, which vanishes the off diagonal terms of matrix $\mathbf{D}_{4\times4}$, i.e. enforcing the conditions $S_x = S_y = S_\omega = J_{xy} = J_{\omega x} = J_{\omega y} = 0$. When matrix $\mathbf{D}_{4\times4}$ is diagonal, the subsequent formulations become simple and the energy conjugate boundary terms were well established in the literature. In contrast, this study considers the general case where matrix $\mathbf{D}_{4\times4}$ is a full matrix (arising when a non-orthogonal coordinate system is adopted). In this case, the energy conjugate stress resultants are not known. The objective of the following section is to formulate the energy conjugate stress resultants for a non-orthogonal system of coordinates.

External virtual work due to end tractions

Given the general specified tractions $\bar{\sigma}_0 = \bar{\sigma}(s,0,r)$, $\bar{\tau}_0 = \bar{\tau}(s,0,r)$ acting at the end $z = 0$ and $\bar{\sigma}_l = \bar{\sigma}(s,l,r)$, $\bar{\tau}_l = \bar{\tau}(s,l,r)$ acting at the end $z = l$ of the member and noting that both ends undergo virtual displacements $\delta u(0)$, $\delta v(0)$, $\delta w(0)$, $\delta\phi(0)$, $\delta u'(0)$, $\delta v'(0)$, $\delta\phi'(0)$, $\delta u(l)$, $\delta v(l)$, $\delta w(l)$, $\delta\phi(l)$, $\delta u'(l)$, $\delta v'(l)$, and, $\delta\phi'(l)$, the corresponding virtual work done by the externally applied tractions is

$$\begin{aligned}\delta V_1 = &-\int_A \bar{\sigma}_0 \delta\left[w(0) - x(s)u'(0) - y(s)v'(0) - \omega(s)\phi'(0)\right] dA \\ &-\int_A \bar{\tau}_0 \cos\alpha(s) \delta\left[u(0) - \left(y(s) - a_y\right)\phi(0)\right] dA \\ &-\int_A \bar{\tau}_0 \sin\alpha(s) \delta\left[v(0) + \left(x(s) - a_x\right)\phi(0)\right] dA \\ &+\int_A \bar{\sigma}_l \delta\left[w(l) - x(s)u'(l) - y(s)v'(l) - \omega(s)\phi'(l)\right] dA \\ &+\int_A \bar{\tau}_l \cos\alpha(s) \delta\left[u(l) - \left(y(s) - a_y\right)\phi(l)\right] dA \\ &+\int_A \bar{\tau}_l \sin\alpha(s) \delta\left[v(l) + \left(x(s) - a_x\right)\phi(l)\right] dA\end{aligned} \tag{II.12}$$

By regrouping terms, Eq. (II.12) can be expressed as

$$\begin{aligned}\delta V_1 = &-\bar{N}(0)\delta w(0) - \bar{V}_x(0)\delta u(0) - \bar{V}_y(0)\delta v(0) \\ &-\bar{M}_y(0)\delta u'(0) - \bar{M}_x(0)\delta v'(0) - \bar{T}(0)\delta\phi(0) - \bar{B}(0)\delta\phi'(0) \\ &+\bar{N}(l)\delta w(l) + \bar{V}_x(l)\delta u(l) + \bar{V}_y(l)\delta v(l) \\ &+\bar{M}_y(l)\delta u'(l) + \bar{M}_x(l)\delta v'(l) + \bar{T}(l)\delta\phi(l) + \bar{B}(l)\delta\phi'(l)\end{aligned} \tag{II.13}$$

in which the following energy conjugate stress resultants arise naturally.

$$\bar{N}(0) = \int_A \bar{\sigma}_0 dA, \quad \bar{M}_y(0) = -\int_A \bar{\sigma}_0 x(s) dA, \quad \bar{M}_x(0) = -\int_A \bar{\sigma}_0 y(s) dA, \quad \bar{B}(0) = -\int_A \bar{\sigma}_0 \omega(s) dA,$$

$$\bar{V}_x(0) = \int_A \bar{\tau}_0 \cos\alpha(s) dA, \ \bar{V}_y(0) = \int_A \bar{\tau}_0 \sin\alpha(s) dA,$$

$$\bar{T}(0) = \int_A \left\{ -\bar{\tau}_0(s,z)\cos\alpha(s)\left[y(s)-a_y\right] + \bar{\tau}_0(s,z,r)\sin\alpha(s)\left[x(s)-a_x\right] \right\} dA$$

$$\bar{N}(l) = \int_A \bar{\sigma}_l dA, \quad \bar{M}_y(l) = -\int_A \bar{\sigma}_l x(s) dA, \quad \bar{M}_x(l) = -\int_A \bar{\sigma}_l y(s) dA, \quad \bar{B}(l) = -\int_A \bar{\sigma}_l \omega(s) dA,$$

$\bar{V}_x(l) = \int_A \bar{\tau}_l \cos\alpha(s)\, dA$, $\bar{V}_y(l) = \int_A \bar{\tau}_l \sin\alpha(s)\, dA$, and

$$\bar{T}(l) = \int_A \left\{ -\bar{\tau}_l(s,z)\cos\alpha(s)\left[y(s)-a_y\right] + \bar{\tau}_l(s,z,r)\sin\alpha(s)\left[x(s)-a_x\right] \right\} dA \tag{II.14}$$

The conjugate stress resultants defined in Eqs. (II.14) have a general significance in the sense that they are applicable to any non-orthogonal coordinate system. Specifically, the moments $\bar{M}_y(0) = -\int_A \bar{\sigma}_0 x(s) dA$, $\bar{M}_x(0) = -\int_A \bar{\sigma}_0 y(s) dA$, $\bar{M}_y(l) = -\int_A \bar{\sigma}_l x(s) dA$, and $\bar{M}_x(l) = -\int_A \bar{\sigma}_l y(s) dA$ are those about an origin which does not necessarily coincide with the centroidal axis of the longitudinal tractions acting at the cross-sections $z = 0$ and $z = l$. In the special case where an orthogonal system of coordinates is adopted, the above terms revert to the conventional moment definitions about the centroidal axis. Also, the bimoment terms $\bar{B}(0) = -\int_A \bar{\sigma}_0 \omega(s) dA$ and $\bar{B}(l) = -\int_A \bar{\sigma}_l \omega(s) dA$ are related to a sectorial origin which does not necessarily coincide with the principal sectorial origin as defined by the orthogonality condition $S_\omega = 0$. Finally, the twisting moments $\bar{T}(0)$ and $\bar{T}(l)$ are the moments of the tractions tangent to the end cross-sections $z = 0$ and $z = l$ about a pole (a_x, a_y) which does not necessarily coincide with the section shear centre. Again, in conventional solutions based on orthogonal coordinates, the pole $\left(a_x, a_y\right)$ is selected to coincide with the shear centre defined by the orthogonality conditions

$J_{\omega x} = J_{\omega y} = 0$, and the twisting moment definition in Eq. (II.14) becomes that about the shear centre.

External virtual work due to member tractions

The effect of member tractions $\mathbf{p}(s,z)$ is obtained by pre-multiplying the traction vector by the corresponding virtual displacements $\delta\mathbf{u}_s(s,z)^{\mathrm{T}}$ and integrating over the member middle surface, i.e,

$$\delta V_2 = \int_0^l \int_s \delta\mathbf{u}_s(s,z)_{1\times3}^T \mathbf{p}(s,z)_{3\times1} ds dz \tag{II.15}$$

In Eq. (II.15), the virtual displacements at any point on the midsurface $\delta\mathbf{u}_s(s,z)_{1\times3}^{\mathrm{T}} = \langle \delta u_s(s,z) \quad \delta v_s(s,z) \quad \delta w_s(s,z)\rangle$ can be related to those at the pole displacements through Eqs. (II.1), (II.2) and (II.5). By defining the resultant forces per unit length as $q_x(z) = \int_s p_x(s,z) ds$, $q_y(z) = \int_s p_y(s,z) ds$, $q_z(z) = \int_s p_z(s,z) ds$ and resultant twisting moments per unit length $m(z)$ induced by the action of traction components p_x, p_y acting in the plane of the cross-section about pole $A_p(a_x, a_y)$ as $m(z) = \int_s -p_x(s,z)(y(s)-a_y) + p_y(s,z)(x(s)-a_x) ds$, Eq. (II.15) is rewritten as

$$\begin{aligned} \delta V_2 = & \int_0^l \delta w(z) q_z(z) dz + \int_0^l \delta u(z) q_x(z) dz + \int_0^l \delta v(z) q_y(z) dz + \int_0^l \delta\phi(z) m(z) dz \\ & - \int_0^l \int_s \delta u'(z) x(s) p_z(s,z) ds dz - \int_0^l \int_s \delta v'(z) y(s) p_z(s,z) ds dz - \int_0^l \int_s \delta\phi'(z) \omega(s) p_z(s,z) ds dz \end{aligned} \tag{II.16}$$

Field Equations

Equations (II.9), (II.11), (II.13) and (II.16) are substituted into Eq. (II.7) and all terms including $\delta w'$ and $\delta\phi'$ are integrated once by parts, and all those including the terms $\delta u''$, $\delta v''$ and $\delta\phi''$ are integrated twice by parts. Noting that the virtual displacement fields $\delta\mathbf{d}(z)^{\mathrm{T}}_{1\times 4} = \langle \delta w(z) \quad \delta u(z) \quad \delta v(z) \quad \delta\phi(z) \rangle$ are arbitrary, the well known Vlasov field equations are recovered

$$E\left[\begin{array}{ccc|c} -AD^2 & S_yD^3 & S_xD^3 & S_\omega D^3 \\ -S_yD^3 & J_{yy}D^4 & J_{xy}D^4 & J_{\omega x}D^4 \\ -S_xD^3 & J_{xy}D^4 & J_{xx}D^4 & J_{\omega y}D^4 \\ \hline -S_\omega D^3 & J_{\omega x}D^4 & J_{\omega y}D^4 & J_{\omega\omega}D^4 - E^{-1}GJ_dD^2 \end{array}\right]\left\{\begin{array}{c} w \\ u \\ v \\ \hline \phi \end{array}\right\} = \left\{\begin{array}{c} q_z \\ q_x + \int_s x\,\partial p_z/\partial z\,ds \\ q_y + \int_s y\,\partial p_z/\partial z\,ds \\ \hline m + \int_s \omega\,\partial p_z/\partial z\,ds \end{array}\right\} \qquad \text{(II.17)}$$

in which the differentiation operators, $D^2 = d^2/dz^2$, $D^3 = d^3/dz^3$, and $D^4 = d^4/dz^4$ have been defined.

Boundary conditions in non-orthogonal coordinate system

The boundary terms arising from the integration by parts performed in the previous section provide the 14 boundary conditions associated with the above field equations. These are found to coincide with those reported in Gjelsvik (1981).

$$\left\{E(Aw'-S_y u''-S_x v''-S_\omega \phi'')-\bar{N}\right\}\delta w\Big|_0^l=0$$

$$\left\{E(S_y w''-J_{yy}u'''-J_{xy}v'''-J_{\omega x}\phi''')-\bar{V}_x+\int_s p_z(s,z)x(s)ds\right\}\delta u\Bigg|_0^l=0$$

$$\left\{E(S_x w''-J_{xy}u'''-J_{xx}v'''-J_{\omega y}\phi''')-\bar{V}_y+\int_s p_z(s,z)y(s)ds\right\}\delta v\Bigg|_0^l=0$$

$$\left\{E(S_\omega w''-J_{\omega x}u'''-J_{\omega y}v'''-J_{\omega\omega}\phi'''+GJ_d E^{-1}\phi')-\bar{T}+\int_s p_z(s,z)\omega(s)ds\right\}\delta\phi\Bigg|_0^l=0 \qquad \text{(II.18)}$$

$$\left\{E(-S_y w'+J_{yy}u''+J_{xy}v''+J_{\omega x}\phi'')-\bar{M}_y\right\}\delta u'\Big|_0^l=0$$

$$\left\{E(-S_x w'+J_{xy}u''+J_{xx}v''+J_{\omega y}\phi'')-\bar{M}_x\right\}\delta v'\Big|_0^l=0$$

$$\left\{E(-S_\omega w'+J_{\omega x}u''+J_{\omega y}v''+J_{\omega\omega}\phi'')-\bar{B}\right\}\delta\phi'\Big|_0^l=0$$

In applications where an abrupt cross-sectional change occurs (e.g., Example III.1 in Chapter III), Equations (II.18) provide clear and systematic means of expressing the continuity conditions at the location of the cross-sectional change.

It can be verified that for an orthogonal coordinate system, the above boundary terms coincide with the well known boundary terms in orthogonal solutions. For instance, under an orthogonal coordinate system, the conditions $S_y = J_{xy} = J_{\omega x} = 0$ are met. Also, the origin coincides with the section centroid. Thus $\bar{M}_y(0)$ becomes the integral of the moments of the longitudinal tractions acting at the end $z=0$ about the section *centroid.* Also the boundary term $\left[E(-S_y w'(0)+J_{yy}u''(0)+J_{xy}v''(0)+J_{\omega x}\phi''(0)-\bar{M}_y(0)\right]\delta u'(0)=0$ simplifies to the well known boundary condition $\left[EJ_{yy}u''(0)-\bar{M}_y(0)\right]\delta u'(0)=0$, i.e., either the displacement boundary condition $u'(0)$ has to be specified or the natural boundary condition $\left[EJ_{yy}u''(0)=\bar{M}_y(0)\right]$ has to be met.

Homogeneous displacement field expressions

The homogeneous solution is obtained by setting the right hand side terms of Eq. (II.17) to zero. The resulting coupled system of differential equations is then solved and the resulting integration constants are related to the the nodal displacements $\mathbf{U}^{\mathbf{T}}_{\mathrm{N}14\times1} = \langle \mathbf{w}_{\mathrm{N}2\times1} \mid \mathbf{u}_{\mathrm{N}4\times1} \mid \mathbf{v}_{\mathrm{N}4\times1} \mid \boldsymbol{\varphi}_{\mathrm{N}4\times1} \rangle$, in which the sub-vectors $\mathbf{w}^{\mathbf{T}}_{\mathrm{N}4\times1} = \langle w(0) \quad w(l) \rangle$, $\mathbf{u}^{\mathbf{T}}_{\mathrm{N}4\times1} = \langle u(0) \quad u'(0) \quad u(l) \quad u'(l) \rangle$, $\mathbf{v}^{\mathbf{T}}_{\mathrm{N}4\times1} = \langle v(0) \quad v'(0) \quad v(l) \quad v'(l) \rangle$, and $\boldsymbol{\varphi}^{\mathbf{T}}_{\mathrm{N}4\times1} = \langle \phi(0) \quad \phi'(0) \quad \phi(l) \quad \phi'(l) \rangle$ are defined.

The main idea of the solution is to differentiate the first row of Eq. (II.17) with respect to z, expand the top partition of Eq. (II.17) to express the $D^4\phi$ in terms of the displacement derivatives D^3w, D^4u, D^4v through a 3x3 sub-matrix of coefficients, performing a symbolic inversion of the resulting matrix to express the displacement fields in terms of the rotation field, and substituting the result into the bottom partition, yielding an uncoupled differential equation in the rotation field vector. The obtained differential equation is then exactly integrated, and the integration constants are related to the rotational and warping nodal displacements and the result is back-substituted into the remaining field equations which are then integrated to yield exact expressions for the displacement fields. The new integration constants are then expressed in terms of the displacement and slope nodal displacements. The reader is referred Appendix II.B for the mathematical details of the formulation. The final solution is

$$\phi(z) = \mathbf{L}(z)^{\mathbf{T}}_{1\times4}\, \boldsymbol{\varphi}_{\mathrm{N}4\times1} \tag{II.19}$$

$$u(z) = \mathbf{N}(z)^{\mathbf{T}}_{1\times4}\, \mathbf{u}_{\mathrm{N}4\times1} + C_2\left(\mathbf{L}(z)^{\mathbf{T}}_{1\times4} - \mathbf{N}(z)^{\mathbf{T}}_{1\times4}\right) \boldsymbol{\varphi}_{\mathrm{N}4\times1} \tag{II.20}$$

$$v(z) = \mathbf{N}(z)^{\mathbf{T}}_{1\times4}\mathbf{v}_{\mathrm{N4\times1}} + C_3\left(\mathbf{L}(z)^{\mathbf{T}}_{1\times4} - \mathbf{N}(z)^{\mathbf{T}}_{1\times4}\right)\boldsymbol{\varphi}_{\mathrm{N4\times1}} \tag{II.21}$$

$$\begin{aligned} w(z) = {} & \mathbf{M}(z)^{\mathbf{T}}_{1\times2}\mathbf{w}_{\mathrm{N2\times1}} + \frac{S_y}{A}\left[\mathbf{N}'(\mathbf{z})^{\mathbf{T}}_{1\times4} - \mathbf{M}^*(z)^{\mathbf{T}}_{1\times4}\right]\mathbf{u}_{\mathrm{N4\times1}} + \frac{S_x}{A}\left[\mathbf{N}'(z)^{\mathbf{T}}_{1\times4} - \mathbf{M}^*(z)^{\mathbf{T}}_{1\times4}\right]\mathbf{v}_{\mathrm{N4\times1}} \\ & + \frac{S_y C_2}{A}\left[\mathbf{L}'(z)^{\mathbf{T}}_{1\times4} - \mathbf{N}'(z)^{\mathbf{T}}_{1\times4}\right]\boldsymbol{\varphi}_{\mathrm{N4\times1}} + \frac{S_x C_3}{A}\left[\mathbf{L}'(z)^{\mathbf{T}}_{1\times4} - \mathbf{N}'(z)^{\mathbf{T}}_{1\times4}\right]\boldsymbol{\varphi}_{\mathrm{N4\times1}} \\ & + \frac{S_\omega}{A}\left[\mathbf{L}'(z)^{\mathbf{T}}_{1\times4} - \mathbf{M}^*(z)^{\mathbf{T}}_{1\times4}\right]\boldsymbol{\varphi}_{\mathrm{N4\times1}} \end{aligned} \tag{II.22}$$

In Eqs.(II.19) through (II.22), the following hyperbolic shape function vectors were defined as

$$\mathbf{L}(z)_{4\times1} = \frac{1}{2-2C+klS}\left\{\begin{array}{c} (1-C)\cosh kz + S\sinh kz - Skz + (1-C+klS) \\ \frac{1}{k}\left[(S-klC)\cosh kz + (1-C+klS)\sinh kz + (1-C)kz - (S-klC)\right] \\ -(1-C)\cosh kz - S\sinh kz + Skz + (1-C) \\ \frac{1}{k}\left[(kl-S)\cosh kz - (1-C)\sinh kz + (1-C)kz + (S-kl)\right] \end{array}\right\} \tag{II.23}$$

where constants $C = \cosh kl$, $S = \sinh kl$, and $k = \sqrt{GJ_d/EC_w}$ have been defined. In Eqs. (II.19) through (II.22) the Hermitian and linear interpolation function vectors have been used

$$\mathbf{N}(z)^{\mathbf{T}}_{1\times4} = \left\langle \left(1 - \frac{3z^2}{l^2} + \frac{2z^3}{l^3}\right) \;\; \left(z - \frac{2z^2}{l} + \frac{z^3}{l^2}\right) \;\; \left(\frac{3z^2}{l^2} - \frac{2z^3}{l^3}\right) \;\; \left(-\frac{z^2}{l} + \frac{z^3}{l^2}\right) \right\rangle \tag{II.24}$$

$$\mathbf{M}(z)^{\mathbf{T}}_{1\times2} = \left\langle (1-z/l) \;\; z/l \right\rangle,\; \mathbf{M}^*(z)^{\mathbf{T}}_{1\times4} = \left\langle 0 \;\; (1-z/l) \;\; 0 \;\; z/l \right\rangle \tag{II.25}$$

Also, the following constants have been defined

$$C_2 = \frac{\left\langle \left(S_y J_{xx} - S_x J_{xy}\right) \;\; \left(AJ_{xx} - S_x^{\,2}\right) \;\; \left(S_y S_x - AJ_{xy}\right) \right\rangle}{-AJ_{xx}J_{yy} + AJ_{xy}^{\,2} + S_x^{\,2}J_{yy} - 2S_xS_yJ_{xy} + S_y^{\,2}J_{xx}} \left\{\begin{array}{c} -S_\omega \\ J_{\omega x} \\ J_{\omega y} \end{array}\right\} \tag{II.26}$$

$$C_3 = \frac{\left\langle \left(S_x J_{yy} - S_y J_{xy}\right) \quad \left(S_y S_x - A J_{xy}\right) \quad \left(A J_{yy} - S_y^{\,2}\right) \right\rangle}{-A J_{xx} J_{yy} + A J_{xy}^{\,2} + S_x^{\,2} J_{yy} - 2 S_x S_y J_{xy} + S_y^{\,2} J_{xx}} \begin{Bmatrix} -S_\omega \\ J_{\omega x} \\ J_{\omega y} \end{Bmatrix} \tag{II.27}$$

$$C_w = J_{\omega\omega} - \left\langle -S_\omega \quad J_{\omega x} \quad J_{\omega y} \right\rangle \begin{bmatrix} A & -S_y & -S_x \\ -S_y & J_{yy} & J_{xy} \\ -S_x & J_{xy} & J_{xx} \end{bmatrix}^{-1} \begin{Bmatrix} -S_\omega \\ J_{\omega x} \\ J_{\omega y} \end{Bmatrix} \tag{II.28}$$

Equation (II.28) is a new expression for the warping constant C_w in terms of other sectional properties based on a non-orthogonal coordinate system. The expression naturally arises when comparing the torsion differential equation based on the current non-orthogonal solution scheme to the torsion differential equation resulting from the conventional solution based on an orthogonal coordinate system (Appendix II.B). It is observed that the hyperbolic shape functions in Eq. (II.23) coincide with those presented in Krajcinovic (1969) derived for members under torsion.

Finite element formulation in a non-orthogonal coordinate system

From Eqs. (II.19) through (II.22), the vector of displacement derivatives can be related to the nodal displacement vector $\mathbf{U}^{\mathbf{T}}_{\mathrm{N}14\times1}$ through

$$\mathbf{u}(z)_{14\times1} = \begin{Bmatrix} w'(z) \\ u''(z) \\ v''(z) \\ \phi''(z) \end{Bmatrix} = \mathbf{B}(z)_{4\times14}\, \mathbf{U}_{\mathrm{N}14\times1} \tag{II.29}$$

in which the strain-nodal displacement matrix $\mathbf{B}(z)_{4\times14}$ is given by

$$\mathbf{B}(z)_{4\times 14}=\left[\begin{array}{c|c|c|c}\mathbf{M}'(z)^{\mathrm{T}}_{1\times 2} & \mathbf{C}_4{}'(z)^{\mathrm{T}}_{1\times 4} & \mathbf{C}_5{}'(z)^{\mathrm{T}}_{1\times 4} & \mathbf{C}_6{}'(z)^{\mathrm{T}}_{1\times 4}-\mathbf{C}_7{}'(z)^{\mathrm{T}}_{1\times 4}\\ \hline \mathbf{0}_{1\times 2} & \mathbf{N}''(z)^{\mathrm{T}}_{1\times 4} & \mathbf{0}_{1\times 4} & \mathbf{C}_8{}''(z)^{\mathrm{T}}_{1\times 4}\\ \hline \mathbf{0}_{1\times 2} & \mathbf{0}_{1\times 4} & \mathbf{N}''(z)^{\mathrm{T}}_{1\times 4} & \mathbf{C}_9{}''(z)^{\mathrm{T}}_{1\times 4}\\ \hline \mathbf{0}_{1\times 2} & \mathbf{0}_{1\times 4} & \mathbf{0}_{1\times 4} & \mathbf{L}''(z)^{\mathrm{T}}_{1\times 4}\end{array}\right] \tag{II.30}$$

In Eq. (II.30), the following vectors are defined

$$\mathbf{C}_4(z)^{\mathrm{T}}_{1\times 4}=\frac{S_y}{A}\left[\mathbf{N}'(z)^{\mathrm{T}}_{1\times 4}-\mathbf{M}^*(z)^{\mathrm{T}}_{1\times 4}\right] \tag{II.31}$$

$$\mathbf{C}_5(z)^{\mathrm{T}}_{1\times 4}=\frac{S_x}{A}\left[\mathbf{N}'(z)^{\mathrm{T}}_{1\times 4}-\mathbf{M}^*(z)^{\mathrm{T}}_{1\times 4}\right] \tag{II.32}$$

$$\mathbf{C}_6(z)^{\mathrm{T}}_{1\times 4}=\frac{1}{A}(S_yC_2+S_xC_3+S_\omega)\left[\mathbf{L}'(z)^{\mathrm{T}}_{1\times 4}-\mathbf{M}^*(z)^{\mathrm{T}}_{1\times 4}\right] \tag{II.33}$$

$$\mathbf{C}_7(z)^{\mathrm{T}}_{1\times 4}=\frac{1}{A}(S_yC_2+S_xC_3)\left[\mathbf{N}'(z)^{\mathrm{T}}_{1\times 4}-\mathbf{M}^*(z)^{\mathrm{T}}_{1\times 4}\right] \tag{II.34}$$

$$\mathbf{C}_8(z)^{\mathrm{T}}_{1\times 4}=C_2\left[\mathbf{L}(z)^{\mathrm{T}}_{1\times 4}-\mathbf{N}(z)^{\mathrm{T}}_{1\times 4}\right] \tag{II.35}$$

$$\mathbf{C}_9(z)^{\mathrm{T}}_{1\times 4}=C_3\left[\mathbf{L}(z)^{\mathrm{T}}_{1\times 4}-\mathbf{N}(z)^{\mathrm{T}}_{1\times 4}\right] \tag{II.36}$$

From Eqs. (II.9) , (II.11), (II.13), (II.16), (II.29) and (II.30) by substituting into Eq. (II.7), one obtains

$$\delta\pi=\delta\mathbf{U}^{\mathrm{T}}_{1\times 14}\left(\mathbf{K}_{14\times 14}\mathbf{U}_{\mathrm{N}14\times 1}-\mathbf{P}_{14\times 1}-\mathbf{R}_{14\times 1}\right)=\mathbf{0}_{14\times 1} \tag{II.37}$$

in which the nodal force vector due to end tractions $\mathbf{P}_{14\times 1}$

$$\mathbf{P}^{\mathrm{T}}_{1\times 14}=\left\langle \bar{N}(0)\;\; \bar{N}(l)\;\vdots\; \bar{V}_x(0)\;\; \bar{M}_y(0)\;\; \bar{V}_x(l)\;\; \bar{M}_y(l)\;\vdots\; \bar{V}_y(0)\;\; \bar{M}_x(0)\;\; \bar{V}_y(l)\;\; \bar{M}_x(l)\;\vdots\; \bar{T}(0)\;\; \bar{B}(0)\;\; \bar{T}(l)\;\; \bar{B}(l)\right\rangle \tag{II.38}$$

and energy equivalent nodal force vector due to member loads $\mathbf{R}_{14\times 1}$ is given by

$$\mathbf{R}_{14\times 1}=\int_0^l \mathbf{H}(z)^{\mathrm{T}}_{14\times 7}\int_s \mathbf{A}(s)^{\mathrm{T}}_{7\times 3}\mathbf{p}_{3\times 1}\,ds\;dz \tag{II.39}$$

in which the following matrices are defined

$$\mathbf{A}(s)_{3\times 7} = \begin{bmatrix} 1 & 0 & 0 & 0 & -x(s) & -y(s) & -\omega(s) \\ 0 & 1 & 0 & -(y(s)-a_y) & 0 & 0 & 0 \\ 0 & 0 & 1 & (x(s)-a_x) & 0 & 0 & 0 \end{bmatrix} \tag{II.40}$$

and

$$\mathbf{H}(z)_{7\times 14} = \left[\begin{array}{c:c:c:c} \mathbf{M}(z)^{\mathbf{T}}_{1\times 2} & \mathbf{C}_4(z)_{1\times 4} & \mathbf{C}_5(z)_{1\times 4} & \mathbf{C}_6(z)_{1\times 4} - \mathbf{C}_7(z)_{1\times 4} \\ \hdashline \mathbf{0}_{1\times 2} & \mathbf{N}(z)^{\mathbf{T}}_{1\times 4} & \mathbf{0}_{1\times 4} & \mathbf{C}_8(z)_{1\times 4} \\ \hdashline \mathbf{0}_{1\times 2} & \mathbf{0}_{1\times 4} & \mathbf{N}(z)^{\mathbf{T}}_{1\times 4} & \mathbf{C}_9(z)_{1\times 4} \\ \hdashline \mathbf{0}_{1\times 2} & \mathbf{0}_{1\times 4} & \mathbf{0}_{1\times 4} & \mathbf{L}(z)^{\mathbf{T}}_{1\times 4} \\ \hdashline \mathbf{0}_{1\times 2} & \mathbf{N}'(z)^{\mathbf{T}}_{1\times 4} & \mathbf{0}_{1\times 4} & \mathbf{C}_8{}'(z)_{1\times 4} \\ \hdashline \mathbf{0}_{1\times 2} & \mathbf{0}_{1\times 4} & \mathbf{N}'(z)^{\mathbf{T}}_{1\times 4} & \mathbf{C}_9{}'(z)_{1\times 4} \\ \hdashline \mathbf{0}_{1\times 2} & \mathbf{0}_{1\times 4} & \mathbf{0}_{1\times 4} & \mathbf{L}'(z)^{\mathbf{T}}_{1\times 4} \end{array}\right] \tag{II.41}$$

The application of Eq. (II.39) is illustrated in Appendix II.C, in which the expression is used to formulate the energy equivalent nodal force vector for the case of a line load per unit length $\langle P_x, P_y, P_z \rangle$ for which the line of action is defined by the coordinates $\left(x\left(s_p\right) \quad y\left(s_p\right) \quad \omega\left(s_p\right)\right)$ relative to section origin.

The stiffness matrix $\mathbf{K}$ in Eq. (II.37) is expressed by

$$\mathbf{K}_{14\times 14} = E\int_0^l \mathbf{B}(z)^{\mathbf{T}}_{14\times 4}\,\mathbf{D}_{4\times 4}\mathbf{B}(z)_{4\times 14}\,dz + GJ_d\int_0^l \left[\begin{array}{c:c} \mathbf{0}_{10\times 10} & \mathbf{0}_{10\times 4} \\ \hdashline \mathbf{0}_{4\times 10} & \mathbf{L}'(z)^{\mathbf{T}}_{4\times 1}\,\mathbf{L}'(z)_{1\times 4} \end{array}\right] dz \tag{II.42}$$

The first integral in Eq. (II.42) represents the normal stress contribution to the stiffness of the element while the second integral represents the St. Venant contribution. The finite element formulated in this section will subsequently be referred to as the NOVEE14 (Non-Orthogonal Vlasov Element based on Exact shape functions with 14 degrees of freedom). The entries of the stiffness matrix for NOVEE14 as defined by Eq. (II.42) are presented in Appendix II.D.

Exactness of the solution based on NOVEE14

The NOVEE14 formulation is based on shape functions which exactly meet the *homogeneous* form of the Vlasov equilibrium equations. Therefore, the formulation is expected to yield nodal displacement values in exact agreement with a closed form solution of the Vlasov equations for the case of *zero member loads*. A question arises regarding the ability of the stiffness formulation to exactly predict nodal generalized displacements for members subject to *non-zero* member loads. It can be mathematically proved (Appendix II.E) that indeed this will be the case regardless of the member load distributions. This is also numerically illustrated in Example III.4 in Chapter III, in which a member under non-zero member loads is solved using (a) a single NOVEE14 element, and (b) 16 NOVEE14 elements. The results obtained in both solutions exactly matched.

Special case 1: members with negligible St. Venant stiffness

For elements with relatively short spans, the condition $kl \to 0$ is approached. This signifies that the warping stiffness becomes predominant relative to the St. Venant stiffness. As $kl \to 0$, the hyperbolic shape function vector $\mathbf{L(z)}_{1\times4}^{\mathbf{T}}$ can be demonstrated to approach the Hermitian shape function vector $\mathbf{N(z)}_{1\times4}^{\mathbf{T}}$ (e.g., Batoz and Dhatt, 1990). By substituting into Eqs. (II.19) through (II.22), simplified displacement field expressions are obtained for the limiting case $kl \to 0$ (In the following, all "0" subscripts denote variables under the limiting condition $kl \to 0$)

$$\phi_0(z) = \mathbf{L}(z)_{1\times4}^{\mathbf{T}}\boldsymbol{\varphi}_{\mathrm{N}4\times1} \tag{II.43}$$

$$u_0(z) = \mathbf{N}(z)_{1\times4}^{\mathbf{T}}\mathbf{u}_{\mathrm{N}4\times1} \tag{II.44}$$

$$v_0(z) = \mathbf{N}(z)_{1\times4}^{\mathbf{T}}\mathbf{v}_{\mathrm{N}4\times1} \tag{II.45}$$

$$w_0(z) = \mathbf{M}(z)_{1\times2}^{\mathrm{T}}\mathbf{w}_{\mathrm{N}2\times1} + \frac{S_y}{A}\left[\mathbf{N}'(z)_{1\times4}^{\mathrm{T}} - \mathbf{M}*(z)_{1\times4}^{\mathrm{T}}\right]\mathbf{u}_{\mathrm{N}4\times1} + \frac{S_x}{A}\left[\mathbf{N}'(z)_{1\times4}^{\mathrm{T}} - \mathbf{M}*(z)_{1\times4}^{\mathrm{T}}\right]\mathbf{v}_{\mathrm{N}4\times1}$$
$$+\frac{S_\omega}{A}\left[\mathbf{L}'(z)_{1\times4}^{\mathrm{T}} - \mathbf{M}*(z)_{1\times4}^{\mathrm{T}}\right]\boldsymbol{\varphi}_{\mathrm{N}4\times1} \tag{II.46}$$

It is of interest to note that, in contrast to the formulation of NOVEE14, the transverse displacements u_0, v_0 in elements with short spans become independent from the rotation field, while the longitudinal displacement w_0 remains dependent on the nodal rotations and transverse displacements. By substitution into the virtual work expression, a different stiffness matrix $\mathbf{K}_0$ for the limiting case $kl \to 0$ is obtained. The resulting finite element will subsequently be referred to as the NOVEC14 (Non-Orthogonal Vlasov Element based on Cubic shape functions with 14 degrees of freedom). The entries of the stiffness matrix for NOVEC14 are given in Appendix II.F. The modifications necessary to formulate the energy equivalent nodal force vector for a uniformly distributed line load were presented in Appendix II.C.

Special Case 2: members with negligible warping stiffness

Elements with negligible warping stiffness include tee-shaped and angle sections. Also, for relatively long members, the condition $kl \to \infty$ can be approached for other thin-walled sections. Under the condition $kl \to \infty$, it can be demonstrated (Appendix II.G) that the rotation field $\phi_\infty(z)$ approaches a linear distribution, i.e.,

$$\phi_\infty(z) = \mathbf{M}(z)_{1\times2}^{\mathrm{T}}\boldsymbol{\varphi}_{\infty\mathrm{N}2\times1} \tag{II.47}$$

It is noted here, that unlike elements NOVEE14 and NOVEC14, the nodal rotation vector $\boldsymbol{\varphi}_{\infty\mathrm{N}1\times2}^{\mathrm{T}} = \langle \phi(0) \quad \phi(l) \rangle$ is independent of the nodal warping deformations. By substituting Eq. (II.47) into Eq. (II.17), the following displacement field expressions are obtained

$$u_\infty(z) = \mathbf{N}(z)^{\mathrm{T}}_{1\times4}\mathbf{u}_{\mathrm{N}4\times1} \tag{II.48}$$

$$v_\infty(z) = \mathbf{N}(z)^{\mathrm{T}}_{1\times4}\mathbf{v}_{\mathrm{N}4\times1} \tag{II.49}$$

$$w_\infty(z) = \mathbf{M}(z)^{\mathrm{T}}_{1\times2}\mathbf{w}_{\mathrm{N}2\times1} + \frac{S_y}{A}\left[\mathbf{N}'(z)^{\mathrm{T}}_{1\times4} - \mathbf{M}^*(z)^{\mathrm{T}}_{1\times4}\right]\mathbf{u}_{\mathrm{N}4\times1} + \frac{S_x}{A}\left[\mathbf{N}'(z)^{\mathrm{T}}_{1\times4} - \mathbf{M}^*(z)^{\mathrm{T}}_{1\times4}\right]\mathbf{v}_{\mathrm{N}4\times1} \tag{II.50}$$

In contrast to the displacement fields developed for elements NOVEE14 and NOVEC14, the longitudinal displacement field $w_\infty(z)$ is independent from the rotation field $\phi_\infty(z)$. By substitution into the virtual work expression, another stiffness matrix expression is obtained

$$\mathbf{K}_{\infty12\times12} = E\int_0^l \mathbf{B}_\infty(z)^{\mathrm{T}}_{12\times4}\mathbf{D}_{4\times4}\mathbf{B}_\infty(z)_{4\times12}\,dz + GJ_d\int_0^l \left[\begin{array}{c|c} \mathbf{0}_{10\times10} & \mathbf{0}_{10\times2} \\ \hline \mathbf{0}_{2\times10} & \mathbf{M}'(z)^{\mathrm{T}}_{2\times1}\mathbf{M}'(z)_{1\times2} \end{array}\right]dz \tag{II.51}$$

in which, the following matrix has been defined

$$\mathbf{B}_\infty(z)_{4\times12} = \left[\begin{array}{c|c|c|c} \mathbf{M}'(z)^{\mathrm{T}}_{1\times2} & \frac{S_y}{A}\left[\mathbf{N}'(z)^{\mathrm{T}}_{1\times4} - \mathbf{M}^{*}{}'(z)^{\mathrm{T}}_{1\times4}\right] & \frac{S_x}{A}\left[\mathbf{N}'(z)^{\mathrm{T}}_{1\times4} - \mathbf{M}^{*}{}'(z)^{\mathrm{T}}_{1\times4}\right] & \mathbf{0}_{1\times2} \\ \hline \mathbf{0}_{1\times2} & \mathbf{N}''(z)^{\mathrm{T}}_{1\times4} & \mathbf{0}_{1\times4} & \mathbf{0}_{1\times2} \\ \hline \mathbf{0}_{1\times2} & \mathbf{0}_{1\times4} & \mathbf{N}''(z)^{\mathrm{T}}_{1\times4} & \mathbf{0}_{1\times2} \\ \hline \mathbf{0}_{1\times2} & \mathbf{0}_{1\times4} & \mathbf{0}_{1\times4} & \mathbf{0}_{1\times2} \end{array}\right] \tag{II.52}$$

The element formulated in this section will subsequently be referred to as NOVEL12 (Non-Orthogonal Vlasov Element based on Linear shape functions with 12 degrees of freedom). The entries of the stiffness matrix for NOVEL12 as defined in Eq. (II.51) are presented in Appendix II.G. It is noted that as element NOVEL12 is based on zero warping torsion, it is equally applicable to other thick beam elements, in which the warping stiffness is negligible.

Summary and Conclusions

A general non-orthogonal solution for the Vlasov thin-walled beam theory has been developed. The associated energy conjugate stress resultants were derived from energy principles. Subsequently, three finite elements were derived. Element NOVEE14 yields nodal values in exact agreement with those based on a closed form solution of the Vlasov field equations and boundary conditions. Element NOVEC14 is suitable for modeling short elements while element NOVEL12 is suitable for modeling elements where the torsional stiffness is approached. The finite elements developed provide a powerful analysis tool capable of capturing the behavior of thin-walled elements. The advantages and modeling capabilities of the formulation are discussed in details in the next Chapter.

Appendix II.A-Procedure to Identify an Orthogonal System of Coordinates

The equilibrium equations based on the Vlasov thin-walled beam theory (Eqs. II.17) are coupled. While the formulation presented in Chapter II, III and IV are based on the general solution of the coupled system of equations, the conventional solution scheme uncouples the field equations by adopting an orthogonalization process.

The first step of the orthogonalization process is to obtain the coordinates of centroid of the section. Based on an arbitrary chosen coordinate system (x_1, y_1) (Fig. II.A.1), the static moment of areas defined as $S_{x_1} = \int_A x_1 dA$ and $S_{y_1} = \int_A y_1 dA$.

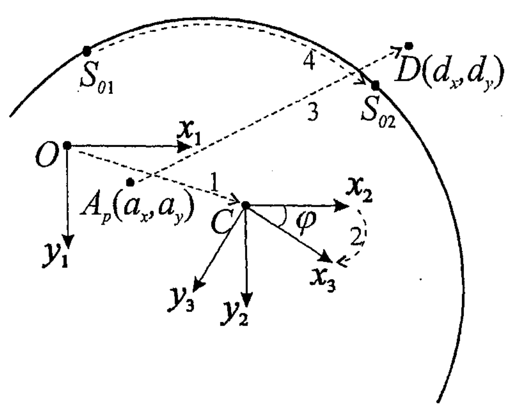

Fig. II.A.1- Orthogonalization process

The coordinates of the section centroid are calculated as $\overline{x}_1 = S_{x_1}/A$ and $\overline{y}_1 = S_{y_1}/A$. The origin is shifted to the location of centroid $x_2 = x_1 - \overline{x}_1$ and $y_2 = y_1 - \overline{y}_1$. The moments of inertias J_{xx}, J_{yy} and J_{xy} are calculated based on coordinate system x_2 and y_2 in Fig. II.A.1, or directly obtained from the parallel axis theorem i.e., $J_{x_2x_2} = J_{xx} - A\overline{y}_1^2$, $J_{y_2y_2} = J_{yy} - A\overline{x}_1^2$ and $J_{x_2y_2} = J_{xy} - A\overline{x}_1\overline{y}_1$. Given the moments of inertia $J_{x_2x_2}$, $J_{y_2y_2}$ and

$J_{x_2y_2}$ based on the coordinate system (x_2, y_2), a new coordinate system having the same origin with different orientation is obtained for which the product of inertia $J_{x_3y_3}$ vanishes. The angle between the new coordinate system (x_3, y_3) and the coordinate system (x_2, y_2) is obtained by the formula (Fig. II.A.1)

$$\varphi = \frac{1}{2}\arctan\left[-\frac{2J_{x_2y_2}}{\left(J_{x_2x_2} - J_{y_2y_2}\right)}\right] \qquad \text{II.A(1)}$$

By using the angle in Eq. (1), the new moments of inertia in terms of the coordinate system (x_2, y_2) can be calculated as

$$J_{x_3x_3} = J_{y_2y_2}\sin^2\varphi + J_{x_2x_2}\cos^2\varphi - 2J_{x_2y_2}\sin\varphi\cos\varphi \qquad \text{II.A(2)}$$

$$J_{y_3y_3} = J_{y_2y_2}\cos^2\varphi + J_{x_2x_2}\sin^2\varphi + 2J_{x_2y_2}\cos\varphi\sin\varphi \qquad \text{II.A(3)}$$

So far, the orthogonalization process is identical to that of the Euler-Bernoulli beam. In the following steps, the pole A_p will be located such that the sectorial products of inertia $J_{\omega x} = \int_A \omega x dA$, $J_{\omega y} = \int_A \omega y dA$ vanish. The sectorial coordinate $\omega\left(S_{01}, A_p, s(x_3, y_3)\right)$ based on an arbitrary pole A_p and arbitrary sectorial origin S_{01} in the coordinate system (x_3, y_3) can be written in terms of a sectorial coordinate $\omega\left(S_{01,}D, s(x_3, y_3)\right)$ based on the shear center D and sectorial origin S_{01}

$$\omega\left(S_{01}, A_p, s(x_3, y_3)\right) = \omega\left(S_{01}, D, s(x_3, y_3)\right) + \left(a_y - d_y\right)\left(x_3 - x_{3S01}\right) - \left(a_x - d_x\right)\left(y_3 - y_{3S01}\right) \text{II.A(4)}$$

In which $a_x, a_y, d_x, d_y, x_{3S01}$ and y_{3S01} are the coordinates of the arbitrary pole A_p, shear center D and a sectorial origin S_{01} in the coordinate system (x_3, y_3) respectively. By multiplying Eq. II.A(4) by x_3 and integrating over the cross-sectional area A, one obtains the sectorial product of inertia based on an arbitrary pole A_p $J_{\omega x_3}\left(S_{01}, A_p\right) = \int\limits_A \omega\left(S_{01}, A_p, s(x_3, y_3)\right) x_3 dA$ in terms the sectorial product of inertia based on the shear center D as

$$J_{\omega x_3}\left(S_{01}, A_p\right) = J_{\omega x_3}\left(S_{01}, D\right) + (a_y - d_y) J_{y_3 y_3} \qquad \text{II.A(5)}$$

In a similar fashion by multiplying Eq. II.A(4) by y_3 and integrating over the cross-sectional area A one obtains

$$J_{\omega y_3}\left(S_{01}, A_p\right) = J_{\omega y_3}\left(S_{01}, D\right) - (a_x - d_x) J_{x_3 x_3} \qquad \text{II.A(6)}$$

Since the products of inertia $J_{\omega x_3}\left(S_{01}, D\right)$ and $J_{\omega y_3}\left(S_{01}, D\right)$ vanish for an orthogonal system, from Eqs. II.A(5) and II.A(6), the location of the shear center is determined as (Fig. II.A.1)

$$d_y = a_y - J_{\omega x_3}\left(S_{01}, A_p\right) / J_{y_3 y_3} \qquad \text{II.A(7)}$$

and

$$d_x = a_x + J_{\omega y_3}\left(S_{01}, A_p\right) / J_{x_3 x_3} \qquad \text{II.A(8)}$$

The remaining orthogonality condition is the vanishing of the first moment of sectorial coordinate i.e., $S_\omega = \int\limits_A \omega dA = 0$. Sectorial area coordinate based a sectorial origin S_{01} $\omega\left(S_{01}, D, s(x_3, y_3)\right)$ can be decomposed as

$$\omega\left(S_{01}, D, s(x_3, y_3)\right) = \omega\left(S_{01}, D, S_{02}\right) + \omega\left(S_{02}, D, s(x_3, y_3)\right) \qquad \text{II.A(9)}$$

In which $\omega(S_{01}, D, S_{02})$ is the sectorial area traced between S_{01} and S_{02} based on the shear center D and $\omega(S_{02}, D, s(x_3, y_3))$ is the sectorial coordinate based on a sectorial origin S_{02} and the shear center D. By integrating Eq. II.A(9) over the cross-sectional area A, the transformation rule which relates a moment of sectorial area based on a sectorial origin S_{01} and the shear center D to a moment of sectorial area based on a another sectorial origin S_{02} and the shear center D can be obtained as

$$S_\omega(S_{01}, D) = S_\omega(S_{02}, D) + A\omega(S_{01}, D, S_{02}) \qquad \text{II.A(10)}$$

In Eq. II.A(10), $S_\omega(S_{01}, D)$ is the first moment of sectorial coordinate based on sectorial origin S_{01} and pole D, and $S_\omega(S_{02}, D)$ is the first moment of sectorial coordinate based on a sectorial origin S_{02} and pole D. Since the moment of sectorial area $S_\omega(S_{02}, D)$ vanishes at the new sectorial origin S_{02} the sectorial coordinate of the required sectorial origin is determined as (Fig. II.A.1)

$$\omega(S_{01}, D, S_{02}) = \frac{S_\omega(S_{01}, D)}{A} \qquad \text{II.A(11)}$$

The new sectorial coordinate diagram based on the sectorial origin S_{02} and the shear center D is reconstructed. And the warping constant $J_{\omega\omega} = \int_A \omega^2 dA$ is calculated. Based on the orthogonal coordinate system, the differential equations of equilibrium (Eq. (II.17)) become uncoupled. In contrast to the above procedure, Chapter II directly solves the coupled differential equations in Eq. (II.17) and the natural boundary conditions are obtained based on the non-orthogonal coordinate system. This eliminates the need to pursue the orthogonalization process described in this appendix.

Appendix II.B Exact solution of Equilibrium Equations for the homogenous case

This appendix presents the details of the solutions of the equilibrium equations (Eq. II.17) for the case of zero member tractions, i.e., $\mathbf{p}(s,z)=\mathbf{0}$ and $\delta V_2=0$. Under this condition, the equilibrium equations take the form

$$\left[\begin{array}{ccc:c} AD^2 & -S_yD^3 & -S_xD^3 & -S_\omega D^3 \\ -S_yD^3 & J_{yy}D^4 & J_{xy}D^4 & J_{\omega x}D^4 \\ -S_xD^3 & J_{xy}D^4 & J_{xx}D^4 & J_{\omega y}D^4 \\ \hdashline -S_\omega D^3 & J_{\omega x}D^4 & J_{\omega y}D^4 & J_{\omega\omega}D^4 - GJ_dE^{-1}D^2 \end{array}\right]\begin{Bmatrix} w \\ u \\ v \\ \phi \end{Bmatrix} = \begin{Bmatrix} 0 \\ 0 \\ 0 \\ 0 \end{Bmatrix} \qquad \text{II.B(1)}$$

By differentiating the first row of Eq. II.B(1) once with respect to coordinate z and expanding the upper portion of the partitioned system in Eq. II.B(1), the displacements w, u and v are expressed in terms of the angle of twist ϕ as

$$\begin{Bmatrix} D^3w \\ D^4u \\ D^4v \end{Bmatrix} = -\begin{bmatrix} A & -S_y & -S_x \\ -S_y & J_{yy} & J_{xy} \\ -S_x & J_{xy} & J_{xx} \end{bmatrix}^{-1} \begin{Bmatrix} -S_\omega \\ J_{\omega x} \\ J_{\omega y} \end{Bmatrix} D^4\phi = \begin{Bmatrix} C_1 \\ C_2 \\ C_3 \end{Bmatrix} D^4\phi \qquad \text{II.B(2)}$$

in which

$$C_1 = \frac{\left\langle \left(J_{yy}J_{xx} - J_{xy}^{\ 2}\right) \;\; \left(S_yJ_{xx} - S_xJ_{xy}\right) \;\; \left(S_xJ_{yy} - S_yJ_{xy}\right) \right\rangle}{-AJ_{xx}J_{yy} + AJ_{xy}^{\ 2} + S_x^{\ 2}J_{yy} - 2S_xS_yJ_{xy} + S_y^{\ 2}J_{xx}} \begin{Bmatrix} -S_\omega \\ J_{\omega x} \\ J_{\omega y} \end{Bmatrix} \qquad \text{II.B(3)}$$

$$C_2 = \frac{\left\langle \left(S_yJ_{xx} - S_xJ_{xy}\right) \;\; \left(AJ_{xx} - S_x^{\ 2}\right) \;\; \left(S_yS_x - AJ_{xy}\right) \right\rangle}{-AJ_{xx}J_{yy} + AJ_{xy}^{\ 2} + S_x^{\ 2}J_{yy} - 2S_xS_yJ_{xy} + S_y^{\ 2}J_{xx}} \begin{Bmatrix} -S_\omega \\ J_{\omega x} \\ J_{\omega y} \end{Bmatrix} \qquad \text{II.B(4)}$$

$$C_3 = \frac{\left\langle \left(S_xJ_{yy} - S_yJ_{xy}\right) \;\; \left(S_yS_x - AJ_{xy}\right) \;\; \left(AJ_{yy} - S_y^{\ 2}\right) \right\rangle}{-AJ_{xx}J_{yy} + AJ_{xy}^{\ 2} + S_x^{\ 2}J_{yy} - 2S_xS_yJ_{xy} + S_y^{\ 2}J_{xx}} \begin{Bmatrix} -S_\omega \\ J_{\omega x} \\ J_{\omega y} \end{Bmatrix} \qquad \text{II.B(5)}$$

From Eq. II.B(2), by substituting into the last row of Eq. II.B(1), one obtains

$$E\left(J_{\omega\omega}-\langle -S_{\omega}\quad J_{\omega x}\quad J_{\omega y}\rangle\begin{bmatrix} A & -S_y & -S_x \\ -S_y & J_{yy} & J_{xy} \\ -S_x & J_{xy} & J_{xx}\end{bmatrix}^{-1}\begin{Bmatrix} -S_{\omega} \\ J_{\omega x} \\ J_{\omega y}\end{Bmatrix}\right)D^4\phi - GJ_d D^2\phi = 0 \qquad \text{II.B(6)}$$

By comparing Eq. II.B(6) to the well known torsional equilibrium equation in an orthogonal system $EC_w D^4\phi - GJ_d D^2\phi = 0$, in which constant C_w denotes the warping constant, a new expression of the warping constant C_w in terms of other section properties in a general non-orthogonal coordinate system is obtained as

$$C_w = J_{\omega\omega}-\langle -S_{\omega}\quad J_{\omega x}\quad J_{\omega y}\rangle\begin{bmatrix} A & -S_y & -S_x \\ -S_y & J_{yy} & J_{xy} \\ -S_x & J_{xy} & J_{xx}\end{bmatrix}^{-1}\begin{Bmatrix} -S_{\omega} \\ J_{\omega x} \\ J_{\omega y}\end{Bmatrix} \qquad \text{II.B(7)}$$

It is noted that Eq. II.B(7) is the same as Eq. (II.28). From the solution of $EC_w D^4\phi - GJ_d D^2\phi = 0$ one obtains

$$\phi(z) = a_1\cosh kz + a_2\sinh kz + a_3 z + a_4 \qquad \text{II.B(8)}$$

in which $k = \sqrt{GJ_d / EC_w}$. By referring to Mohareb and Nowzartash (2003) the above integration constants are related to the nodal angle of twists and their derivative. Thus, the relation $\phi(z) = \mathbf{L}(z)^{\mathrm{T}}_{1\times 4}\boldsymbol{\varphi}_{\mathrm{N}4\times 1}$ (Eq. II.19) is obtained, in which the nodal rotation vector is $\boldsymbol{\varphi}^{\mathrm{T}}_{\mathrm{N}4\times 1} = \langle \phi(0)\quad \phi'(0)\quad \phi(l)\quad \phi'(l)\rangle$ and the shape function vector $\mathbf{L}(z)_{4\times 1}$ (e.g., Krajcinovic, 1969) is given in Eq. (II.23). From Eq. II.B(8) by substituting into Eq. II.B(2) and integrating the second and third rows four times with respect to z one obtains

$$u(z) = C_2\mathbf{L}(z)^{\mathrm{T}}_{1\times 4}\boldsymbol{\varphi}_{\mathrm{N}4\times 1} + b_3 z^3 + b_2 z^2 + b_1 z + b_0 \qquad \text{II.B(9)}$$

$$v(z) = C_3\mathbf{L}(z)^{\mathrm{T}}_{1\times 4}\boldsymbol{\varphi}_{\mathrm{N}4\times 1} + c_3 z^3 + c_2 z^2 + c_1 z + c_0 \qquad \text{II.B(10)}$$

By applying the displacement boundary conditions, integration constants b_0 through b_3 and c_0 through c_3 are related to the nodal displacement vectors $\mathbf{u}_{N4\times1}^{T} = \langle u(0) \quad u'(0) \quad u(l) \quad u'(l)\rangle$ and $\mathbf{v}_{N4\times1}^{T} = \langle v(0) \quad v'(0) \quad v(l) \quad v'(l)\rangle$ through

$$u(z) = \mathbf{N}(z)_{1\times4}^{T}\mathbf{u}_{N4\times1} + C_2\left(\mathbf{L}(z)_{1\times4}^{T} - \mathbf{N}(z)_{1\times4}^{T}\right)\boldsymbol{\varphi}_{N4\times1} \qquad \text{II.B(11)}$$

$$v(z) = \mathbf{N}(z)_{1\times4}^{T}\mathbf{v}_{N4\times1} + C_3\left(\mathbf{L}(z)_{1\times4}^{T} - \mathbf{N}(z)_{1\times4}^{T}\right)\boldsymbol{\varphi}_{N4\times1} \qquad \text{II.B(12)}$$

in which the shape function vector $\mathbf{N}(z)_{4\times1}$ is given in Eq. (II.24). Note that Eqs. II.B(11) and II.B(12) coincide with Eqs. (II.20) and (II.21) respectively. From Eqs. II.B(8), II.B(11) and II.B(12), by substituting into the first row of Eq. II.B(1) and integrating twice, the longitudinal displacement $w(z)$ is obtained as

$$\begin{aligned} w(z) = {} & \frac{S_y}{A}\left[\mathbf{N}'(z)_{1\times4}^{T}\mathbf{u}_{N4\times1} + C_2\left(\mathbf{L}'(z)_{1\times4}^{T} - \mathbf{N}'(z)_{1\times4}^{T}\right)\boldsymbol{\varphi}_{N4\times1}\right] \\ & + \frac{S_x}{A}\left[\mathbf{N}'(z)_{1\times4}^{T}\mathbf{v}_{N4\times1} + C_3\left(\mathbf{L}(z)_{1\times4}^{T} - \mathbf{N}(z)_{1\times4}^{T}\right)\boldsymbol{\varphi}_{N4\times1}\right] + \frac{S_\omega}{A}\mathbf{L}'(z)_{1\times4}^{T}\boldsymbol{\varphi}_{N4\times1} + d_1 z + d_0 \end{aligned} \qquad \text{II.B(13)}$$

By enforcing the displacement boundary conditions, constants d_0 and d_1 are related to the longitudinal nodal displacement vector $\mathbf{w}_{N2\times1}$, i.e.,

$$\begin{aligned} w(z) = {} & \mathbf{M}(z)_{1\times2}^{T}\mathbf{w}_{N2\times1} + \frac{S_y}{A}\left[\mathbf{N}'(\mathbf{z})_{1\times4}^{T} - \mathbf{M}^*(z)_{1\times4}^{T}\right]\mathbf{u}_{N4\times1} + \frac{S_x}{A}\left[\mathbf{N}'(z)_{1\times4}^{T} - \mathbf{M}^*(z)_{1\times4}^{T}\right]\mathbf{v}_{N4\times1} \\ & + \frac{S_y C_2}{A}\left[\mathbf{L}'(z)_{1\times4}^{T} - \mathbf{N}'(z)_{1\times4}^{T}\right]\boldsymbol{\varphi}_{N4\times1} + \frac{S_x C_3}{A}\left[\mathbf{L}'(z)_{1\times4}^{T} - \mathbf{N}'(z)_{1\times4}^{T}\right]\boldsymbol{\varphi}_{N4\times1} + \frac{S_\omega}{A}\left[\mathbf{L}'(z)_{1\times4}^{T} - \mathbf{M}^*(z)_{1\times4}^{T}\right]\boldsymbol{\varphi}_{N4\times1} \end{aligned}$$

II.B(14)

In which the shape function matrices $\mathbf{M}^*(z)_{4\times1} = \langle 0 \quad (1 - z/l) \quad 0 \quad z/l\rangle$ and $\mathbf{M}(z)_{2\times1}$ are given in Eq. (II.25 a and b). Note that Eqs. II.B(13) coincides with Eq. (II.22).

From Eq. II.B(7) by post-multiplying both sides by $\mathbf{J}^{\mathrm{T}}$ where $\mathbf{J}^{\mathrm{T}} = \langle -S_{\omega} \quad J_{\omega x} \quad J_{\omega y} \rangle$, and pre-multiplying both sides by vector $\mathbf{J}$, one obtains the matrix identity $\mathbf{J}\mathbf{J}^{\mathrm{T}}\left\{\mathbf{A}^{-1}\mathbf{J}\mathbf{J}^{\mathrm{T}} - (J_{\omega\omega} - C_w)\mathbf{I}_{3\times 3}\right\} = \mathbf{0}_{3\times 3}$ in which

$$\mathbf{A} = \begin{bmatrix} A & -S_y & -S_x \\ -S_y & J_{yy} & J_{xy} \\ -S_x & J_{xy} & J_{xx} \end{bmatrix} \qquad \text{II.B(15)}$$

The above equation is satisfied under two possible scenarios, either when $\mathbf{J}^{\mathrm{T}} = \mathbf{0}$, i.e., when the pole is located at the shear centre $J_{\omega x} = J_{\omega y} = 0$ and the principal sectorial origin is adopted ($S_{\omega} = 0$), or $\mathbf{J}\mathbf{J}^{\mathrm{T}} = (J_{\omega\omega} - C_w)\mathbf{A}$ (assuming $\left[\mathbf{J}\mathbf{J}^{\mathrm{T}}\right]^{-1}$ exists) is satisfied. Since matrices $\mathbf{J}\mathbf{J}^{\mathrm{T}}$ and $\mathbf{A}$ are symmetric, this relation leads to the following six alternative expressions for the warping constant.

$$\begin{aligned} C_w &= \left(J_{\omega\omega} - \frac{S_{\omega}^{2}}{A}\right) = \left(J_{\omega\omega} - \frac{S_{\omega}J_{\omega x}}{S_y}\right) = \left(J_{\omega\omega} - \frac{S_{\omega}J_{\omega y}}{S_x}\right) \\ &= \left(J_{\omega\omega} - \frac{J_{\omega x}^{2}}{J_{yy}}\right) = \left(J_{\omega\omega} - \frac{J_{\omega y}^{2}}{J_{xx}}\right) = \left(J_{\omega\omega} - \frac{J_{\omega x}J_{\omega y}}{J_{xy}}\right) \end{aligned} \qquad \text{II.B(16)}$$

The author was unable to find similar expressions in the literature, and thus Eq. II.B(16) are, to the best of his knowledge, original.

Appendix II.C - Energy Equivalent Nodal Forces Due to uniformly distributed line load

Given a thin-walled prismatic element subjected to an externally uniformly distributed line load per unit length (P_x, P_y, P_z) acting at an axis located on the element cross-section defined by the coordinates $(x(s_p), y(s_p), \omega(s_p)) = (x_p, y_p, \omega_p)$, the required energy equivalent force vector $\mathbf{R}_{14\times1}$ consistent with element NOVEE14 formulation is given by mathematically expressing the traction function vector in terms of the Dirac delta function as $\mathbf{p}_{3\times1}^{\mathrm{T}} = \delta(s - s_p)(P_x, P_y, P_z)$, substituting into Eq. (II.42), and performing the necessary integrals. One obtains

$$
\mathbf{R}_{14\times 1} = \left\{ \begin{array}{c}
\dfrac{p_z l}{2} \\
\dfrac{p_z l}{2} \\
\hdashline
\dfrac{1}{2} p_x l \\
-\dfrac{p_z l}{2}\dfrac{S_y}{A} + \dfrac{p_x l^2}{12} \\
\dfrac{1}{2} p_x l \\
-\dfrac{p_z l}{2}\dfrac{S_y}{A} - \dfrac{p_x l^2}{12} \\
\hdashline
\dfrac{1}{2} p_y l \\
-\dfrac{p_z l}{2}\dfrac{S_x}{A} + \dfrac{p_y l^2}{12} \\
\dfrac{1}{2} p_y l \\
-\dfrac{p_z l}{2}\dfrac{S_x}{A} - \dfrac{p_y l^2}{12} \\
\hdashline
\left[\left(a_y - y_p\right) p_x - \left(a_x - x_p\right) p_y\right]\dfrac{l}{2} \\
-\dfrac{S_\omega}{A}\dfrac{p_z l}{2} - \left(p_x C_2 + p_y C_3\right)\Psi_1 + \dfrac{1}{2}\left[\left(a_y - y_p\right) p_x - \left(a_x - x_p\right) p_y\right]\Psi_2 \\
\left[\left(a_y - y_p\right) p_x - \left(a_x - x_p\right) p_y\right]\dfrac{l}{2} \\
-\dfrac{S_\omega}{A}\dfrac{p_z l}{2} + \left(p_x C_2 + p_y C_3\right)\Psi_1 - \dfrac{1}{2}\left[\left(a_y - y_p\right) p_x - \left(a_x - x_p\right) p_y\right]\Psi_2
\end{array} \right\} \qquad \text{II.C(1)}
$$

in which

$$
\Psi_1 = \frac{k^2 l^2 \cosh kl + 12\cosh kl - k^2 l^2 - 6kl \sinh kl - 12}{12k^2\left(-1 + \cosh kl\right)} \qquad \text{II.C(2)}
$$

and

$$
\Psi_2 = \frac{kl \sinh kl - 2\cosh kl + 2}{k^2\left(-1 + \cosh kl\right)} \qquad \text{II.C(3)}
$$

For Element NOVEC14, a similar formulation yields the required equivalent nodal forces. Alternatively, the result can be obtained by taking the limits of $\mathbf{R}_{14\times 1}$ as $kl \rightarrow 0$.

The equivalent nodal forces are found identical to those based on the NOVEE14 except for the bimoment terms which are:

$$R_{12}=\frac{l}{12A}\left\{-6S_{\omega}p_z+Al\left[\left(a_y-y_p\right)p_x-\left(a_x-x_p\right)p_y\right]\right\} \tag{II.C(4)}$$

and

$$R_{14}=-\frac{l}{12A}\left\{6S_{\omega}p_z+Al\left[\left(a_y-y_p\right)p_x-\left(a_x-x_p\right)p_y\right]\right\} \tag{II.C(5)}$$

Appendix II.D Stiffness Matrix for NOVEE14

Matrix $\mathbf{K}$ for element NOVEE14 is expressed in a partitioned format as

$$\mathbf{K}_{14\times14}=E\left[\begin{array}{c|c|c|c} \mathbf{K}_{11} & \mathbf{K}_{12} & \mathbf{K}_{13} & \mathbf{K}_{14} \\ \hline \mathbf{K}_{12}{}^{\mathrm{T}} & \mathbf{K}_{22} & \mathbf{K}_{23} & \mathbf{K}_{24} \\ \hline \mathbf{K}_{13}{}^{\mathrm{T}} & \mathbf{K}_{23}{}^{\mathrm{T}} & \mathbf{K}_{33} & \mathbf{K}_{34} \\ \hline \mathbf{K}_{14}{}^{\mathrm{T}} & \mathbf{K}_{24}{}^{\mathrm{T}} & \mathbf{K}_{34}{}^{\mathrm{T}} & \mathbf{K}_{44} \end{array}\right] \qquad \text{II.D(1)}$$

in which the following sub-matrices are defined

$$\mathbf{K}_{11}=\frac{A}{l}\begin{bmatrix} 1 & -1 \\ -1 & 1 \end{bmatrix} \qquad \text{II.D(2)}$$

$$\mathbf{K}_{12}=\frac{S_y}{l}\begin{bmatrix} 0 & -1 & 0 & 1 \\ 0 & 1 & 0 & -1 \end{bmatrix} \qquad \text{II.D(3)}$$

$$\mathbf{K}_{13}=\frac{S_x}{l}\begin{bmatrix} 0 & -1 & 0 & 1 \\ 0 & 1 & 0 & -1 \end{bmatrix} \qquad \text{II.D(4)}$$

$$\mathbf{K}_{14}=\frac{S_\omega}{l}\begin{bmatrix} 0 & -1 & 0 & 1 \\ 0 & 1 & 0 & -1 \end{bmatrix} \qquad \text{II.D(5)}$$

$$\mathbf{K}_{22}=\frac{1}{l^3}\begin{bmatrix} 12\left(J_{yy}-\dfrac{S_y{}^2}{A}\right) & 6\left(J_{yy}-\dfrac{S_y{}^2}{A}\right)l & -12\left(J_{yy}-\dfrac{S_y{}^2}{A}\right) & 6\left(J_{yy}-\dfrac{S_y{}^2}{A}\right)l \\ & \left(4J_{yy}-3\dfrac{S_y{}^2}{A}\right)l^2 & -6\left(J_{yy}-\dfrac{S_y{}^2}{A}\right)l & \left(2J_{yy}-3\dfrac{S_y{}^2}{A}\right)l^2 \\ \mathit{Sym.} & & 12\left(J_{yy}-\dfrac{S_y{}^2}{A}\right) & -6\left(J_{yy}-\dfrac{S_y{}^2}{A}\right)l \\ & & & \left(4J_{yy}-3\dfrac{S_y{}^2}{A}\right)l^2 \end{bmatrix} \qquad \text{II.D(6)}$$

$$
\mathbf{K}_{23}=\frac{1}{l^3}\begin{bmatrix}
12\left(J_{xy}-\frac{S_yS_x}{A}\right) & 6\left(J_{xy}-\frac{S_yS_x}{A}\right)l & -12\left(J_{xy}-\frac{S_yS_x}{A}\right) & 6\left(J_{xy}-\frac{S_yS_x}{A}\right)l \\
 & \left(4J_{xy}-3\frac{S_yS_x}{A}\right)l^2 & -6\left(J_{xy}-\frac{S_yS_x}{A}\right)l & \left(2J_{xy}-3\frac{S_yS_x}{A}\right)l^2 \\
 & Sym. & 12\left(J_{xy}-\frac{S_yS_x}{A}\right) & -6\left(J_{xy}-\frac{S_yS_x}{A}\right)l \\
 & & & \left(4J_{xy}-3\frac{S_yS_x}{A}\right)l^2
\end{bmatrix} \quad \text{II.D(7)}
$$

$$
\mathbf{K}_{24}=\frac{1}{l^3}\begin{bmatrix}
12\left(J_{x\omega}-\frac{S_yS_\omega}{A}\right) & 6\left(J_{x\omega}-\frac{S_yS_\omega}{A}\right)l & -12\left(J_{x\omega}-\frac{S_yS_\omega}{A}\right) & 6\left(J_{x\omega}-\frac{S_yS_\omega}{A}\right)l \\
 & \left(4J_{x\omega}-3\frac{S_yS_\omega}{A}\right)l^2 & -6\left(J_{x\omega}-\frac{S_yS_\omega}{A}\right)l & \left(2J_{x\omega}-3\frac{S_yS_\omega}{A}\right)l^2 \\
 & Sym. & 12\left(J_{x\omega}-\frac{S_yS_\omega}{A}\right) & -6\left(J_{x\omega}-\frac{S_yS_\omega}{A}\right)l \\
 & & & \left(4J_{x\omega}-3\frac{S_yS_\omega}{A}\right)l^2
\end{bmatrix} \quad \text{II.D(8)}
$$

$$
\mathbf{K}_{33}=\frac{1}{l^3}\begin{bmatrix}
12\left(J_{xx}-\frac{S_x^{\,2}}{A}\right) & 6\left(J_{xx}-\frac{S_x^{\,2}}{A}\right)l & -12\left(J_{xx}-\frac{S_x^{\,2}}{A}\right) & 6\left(J_{xx}-\frac{S_x^{\,2}}{A}\right)l \\
 & \left(4J_{xx}-3\frac{S_x^{\,2}}{A}\right)l^2 & -6\left(J_{xx}-\frac{S_x^{\,2}}{A}\right)l & \left(2J_{xx}-3\frac{S_x^{\,2}}{A}\right)l^2 \\
 & Sym. & 12\left(J_{xx}-\frac{S_x^{\,2}}{A}\right) & -6\left(J_{xx}-\frac{S_x^{\,2}}{A}\right)l \\
 & & & \left(4J_{xx}-3\frac{S_x^{\,2}}{A}\right)l^2
\end{bmatrix} \quad \text{II.D(9)}
$$

$$
\mathbf{K}_{34}=\frac{1}{l^3}\begin{bmatrix}
12\left(J_{y\omega}-\frac{S_xS_\omega}{A}\right) & 6\left(J_{y\omega}-\frac{S_xS_\omega}{A}\right)l & -12\left(J_{y\omega}-\frac{S_xS_\omega}{A}\right) & 6\left(J_{y\omega}-\frac{S_xS_\omega}{A}\right)l \\
 & \left(4J_{y\omega}-3\frac{S_xS_\omega}{A}\right)l^2 & -6\left(J_{y\omega}-\frac{S_xS_\omega}{A}\right)l & \left(2J_{y\omega}-3\frac{S_xS_\omega}{A}\right)l^2 \\
 & Sym. & 12\left(J_{y\omega}-\frac{S_xS_\omega}{A}\right) & -6\left(J_{y\omega}-\frac{S_xS_\omega}{A}\right)l \\
 & & & \left(4J_{y\omega}-3\frac{S_xS_\omega}{A}\right)l^2
\end{bmatrix} \quad \text{II.D(10)}
$$

and,

$$\mathbf{K}_{44}=\delta\begin{bmatrix} \frac{\sinh kl}{k}+\frac{12\beta}{\delta l^3} & \frac{(\cosh kl-1)}{k^2}+\frac{6\beta}{\delta l^2} & -\frac{\sinh kl}{k}-\frac{12\beta}{\delta l^3} & \frac{(\cosh kl-1)}{k^2}+\frac{6\beta}{\delta l^2} \\ & \alpha+\frac{4\beta}{\delta l}+\frac{S_\omega^{\ 2}}{\delta Al} & \frac{(1-\cosh kl)}{k^2}-\frac{6\beta}{\delta l^2} & \frac{(\sinh kl-kl)}{k^3}+\frac{2\beta}{\delta l}-\frac{S_\omega^{\ 2}}{\delta Al} \\ Sym. & & \frac{\sinh kl}{k}+\frac{12\beta}{\delta l^3} & \frac{(\cosh kl-1)}{k^2}-\frac{6\beta}{\delta l^2} \\ & & & \alpha+\frac{4\beta}{\delta l}+\frac{S_\omega^{\ 2}}{\delta Al} \end{bmatrix}$$

II.D(11)

in which $\alpha=\dfrac{(kl\cosh kl-\sinh kl)}{k^3}$, $\beta=J_{\omega\omega}-S_\omega^{\ 2}/A-C_\omega$ and $\delta=\dfrac{k^4C_\omega}{(2-2\cosh kl+kl\sinh kl)}$. Remaining terms of matrix $\mathbf{K}_{14\times14}$ are obtained from symmetry.

Appendix II.E Exactness of the solution based on NOVEE14 for the non-homogeneous case

The NOVEE14 formulation is based on the exact solution of the *homogeneous* equilibrium equations. This appendix demonstrates that, in the *non-homogeneous* case, the stiffness matrix for the *homogeneous* case still yields nodal variables in *exact* agreement with those based on the exact solution of the *non-homogeneous* differential equations of equilibrium, as long as the proper modifications are made to the member load vector. The implications are that a prismatic member under *non-zero member loads* can always be modeled using a *single* finite element while yielding the *exact* nodal values. The proof of exactness presented in this appendix is the generalization of the proof provided for the special case of torsional analysis in Mohareb and Nowzartash (2003) to the analysis under coupled axial, bi-flexural and torsional deformation in non-orthogonal coordinate system.

The exact displacement field $\mathbf{d}(z)_{1\times4}^{\mathrm{T}}=\langle w(z) \quad u(z) \quad v(z) \quad \phi(z)\rangle$ for a member subject to end displacements and member loads can be considered to consist of two components $\mathbf{d}(z)_{4\times1}=\mathbf{d}_{\mathrm{h}}(z)_{4\times1}+\mathbf{d}_{\mathrm{p}}(z)_{4\times1}$ corresponding to the homogenous solution $\mathbf{d}_{\mathrm{h}}(z)_{1\times4}^{\mathrm{T}}$ and the particular solution $\mathbf{d}_{\mathrm{p}}(z)_{1\times4}^{\mathrm{T}}$ respectively, where $\mathbf{d}_{\mathrm{h}}(z)_{1\times4}^{\mathrm{T}}=\langle w_h(z) \quad u_h(z) \quad v_h(z) \quad \phi_h(z)\rangle$ and $\mathbf{d}_{\mathrm{p}}(z)_{1\times4}^{\mathrm{T}}=\langle w_p(z) \quad u_p(z) \quad v_p(z) \quad \phi_p(z)\rangle$. By expressing the homogeneous displacement vector $\mathbf{d}_{\mathrm{h}}(z)_{4\times1}$ in terms of nodal displacements one obtains

$$\mathbf{d}_{\mathrm{h}}(z)_{4\times1}=\begin{Bmatrix} w_h(z) \\ u_h(z) \\ v_h(z) \\ \phi_h(z) \end{Bmatrix}=\begin{bmatrix} \mathbf{Z}(z)^{\mathrm{T}}_{1\times14} \\ \mathbf{X}(z)^{\mathrm{T}}_{1\times14} \\ \mathbf{Y}(z)^{\mathrm{T}}_{1\times14} \\ \mathbf{W}(z)^{\mathrm{T}}_{1\times14} \end{bmatrix}\mathbf{U}_{\mathrm{NH}\ 14\times1} \qquad \text{II.E(1)}$$

in which $\mathbf{U}_{\mathrm{NH}\ 14\times1}$ is the vector of nodal displacements, $\mathbf{Z}(z)^{\mathrm{T}}_{1\times14}$, $\mathbf{X}(z)^{\mathrm{T}}_{1\times14}$, $\mathbf{Y}(z)^{\mathrm{T}}_{1\times14}$ and $\mathbf{W}(z)^{\mathrm{T}}_{1\times14}$ represent the interpolation functions satisfying the homogenous form of equation in Eq. (II.17). From Eqs. (II.19), through (II.22), these are expressed as

$$\begin{bmatrix} \mathbf{Z}(z)^{\mathrm{T}}_{1\times14} \\ \mathbf{X}(z)^{\mathrm{T}}_{1\times14} \\ \mathbf{Y}(z)^{\mathrm{T}}_{1\times14} \\ \mathbf{W}(z)^{\mathrm{T}}_{1\times14} \end{bmatrix}=\left[\begin{array}{c:c:c:c} \mathbf{M}(z)^{\mathrm{T}}_{1\times2} & \dfrac{S_y}{A}\times\left[\mathbf{N}'(z)^{\mathrm{T}}_{1\times4}-\mathbf{M}*(z)^{\mathrm{T}}_{1\times4}\right] & \dfrac{S_x}{A}\times\left[\mathbf{N}'(z)^{\mathrm{T}}_{1\times4}-\mathbf{M}*(z)^{\mathrm{T}}_{1\times4}\right] & \begin{array}{c}\left(\dfrac{S_yC_2}{A}+\dfrac{S_xC_3}{A}\right)\\ \times\left[\mathbf{L}'(z)^{\mathrm{T}}_{1\times4}-\mathbf{N}'(z)^{\mathrm{T}}_{1\times4}\right]\\ +\dfrac{S_\omega}{A}\left[\mathbf{L}'(z)^{\mathrm{T}}_{1\times4}-\mathbf{M}*(z)^{\mathrm{T}}_{1\times4}\right]\end{array} \\ \hdashline \mathbf{0} & \mathbf{N}(z)^{\mathrm{T}}_{1\times4} & \mathbf{0} & C_2\left[\mathbf{L}(z)^{\mathrm{T}}_{1\times4}-\mathbf{N}(z)^{\mathrm{T}}_{1\times4}\right] \\ \hdashline \mathbf{0} & \mathbf{0} & \mathbf{N}(z)^{\mathrm{T}}_{1\times4} & C_3\left[\mathbf{L}(z)^{\mathrm{T}}_{1\times4}-\mathbf{N}(z)^{\mathrm{T}}_{1\times4}\right] \\ \hdashline \mathbf{0} & \mathbf{0} & \mathbf{0} & \mathbf{L}(z)^{\mathrm{T}}_{1\times4} \end{array}\right]$$

II.E(2)

The particular solution vector $\mathbf{d}_{\mathrm{p}}(\mathbf{z})_{4\times1}$ can be expressed as the sum of two components

$$\mathbf{d}_{\mathrm{p}}(z)_{4\times1}=\begin{Bmatrix} w_p(z) \\ u_p(z) \\ v_p(z) \\ \phi_p(z) \end{Bmatrix}=\boldsymbol{\mu}(\mathbf{z})_{4\times1}+\begin{bmatrix} \mathbf{Z}(z)^{\mathrm{T}}_{1\times14} \\ \mathbf{X}(z)^{\mathrm{T}}_{1\times14} \\ \mathbf{Y}(z)^{\mathrm{T}}_{1\times14} \\ \mathbf{W}(z)^{\mathrm{T}}_{1\times14} \end{bmatrix}\mathbf{U}_{\mathrm{NP}\ 14\times1} \qquad \text{II.E(3)}$$

In Eq. II.E(3), the first displacement component $\boldsymbol{\mu}^{\mathrm{T}}(z)_{4\times1}=\langle \mu_w(z) \quad \mu_u(z) \quad \mu_v(z) \quad \mu_\phi(z)\rangle$ consists of any displacement functions satisfying the equilibrium equations *in the presence of load terms.* The second displacement field vector consists of any linear combination of the *homogeneous* solution. These are the displacement functions defined in Eq. II.E(2) multiplied by a set of 14 arbitrary constants $\mathbf{U}_{\mathrm{NP}\ 14\times1}$. Thus, if vector $\boldsymbol{\mu}^{\mathrm{T}}(z)_{4\times1}$ is a particular solution for the differential equations of equilibrium, vector $\mathbf{d}_{\mathrm{p}}(z)$ must also be a particular solution irrespective of the magnitude of the arbitrary constants in vector $\mathbf{U}_{\mathrm{NP}\ 14\times1}$. Conventionally, once a particular solution is determined, the entries vector $\mathbf{U}_{\mathrm{NP}\ 14\times1}$ are selected to vanish for simplicity. In contrast, we deviate from this convention in this proof by selecting the entries $\mathbf{U}_{\mathrm{NP}\ 14\times1}$ to satisfy the conditions

$$\begin{aligned} &u_p(0)=v_p(0)=w_p(0)=\phi_p(0)=u'_p(0)=v'_p(0)=\phi'_p(0)=0 \\ &u_p(l)=v_p(l)=w_p(l)=\phi_p(l)=u'_p(l)=v'_p(l)=\phi'_p(l)=0 \end{aligned} \qquad \text{II.E(4)}$$

The vector of displacement derivatives $\mathbf{u}(z)_{4\times1}$ which appears in Eq. (II.6) can be written in terms of the homogeneous and particular parts as

$$\mathbf{u}(z)_{4\times1}=\mathbf{u}_{\mathrm{h}}(z)_{4\times1}+\mathbf{u}_{\mathrm{p}}(z)_{4\times1}=\begin{Bmatrix} w'_h(z) \\ u''_h(z) \\ v''_h(z) \\ \phi''_h(z) \end{Bmatrix}+\begin{Bmatrix} w'_p(z) \\ u''_p(z) \\ v''_p(z) \\ \phi''_p(z) \end{Bmatrix} \qquad \text{II.E(5)}$$

By expressing $\mathbf{u}_{\mathrm{h}}(\mathbf{z})_{4\times1}$ in terms of nodal displacements one obtains,

$$\mathbf{u}(z)_{4\times1}=\boldsymbol{\beta}(z)_{4\times1}+\mathbf{B}(z)_{4\times14}\left(\mathbf{U}_{\mathrm{NH}\ 14\times1}+\mathbf{U}_{\mathrm{NP}14\times1}\right) \qquad \text{II.E(6)}$$

in which.

$$\boldsymbol{\beta}^{\mathrm{T}}(\mathbf{z})_{1\times4}=\langle \mu_w' \quad \mu_u'' \quad \mu_v'' \quad \mu_\phi'' \rangle \qquad \text{II.E(7)}$$

Noting that the variation of the prescribed components of the displacement vector in Eq. II.E(6) vanishes, one obtains $\boldsymbol{\delta}\mathbf{u}(z)_{4\times1}=\mathbf{B}(z)_{4\times14}\boldsymbol{\delta}\mathbf{U}_{\mathrm{NH}\ 14\times1}$

For the non-homogeneous case, the exact virtual work expression must be based on the assumed displacement fields defined in Eq. II.E(6) as opposed to the displacement fields of the homogeneous case (from Eqs. (II.19), through (II.22)). By substituting the displacement fields defined in Eq. II.E(6) into Eq. (II.7), one obtains the virtual work expression $\delta\pi_{NH}$ for the non-homogeneous case

$$\delta\pi_{NH} = \delta\mathbf{U}_{\mathbf{NH}1\times14}^{\mathbf{T}} \int_0^l E\left[\mathbf{B}(z)_{14\times4}^{\mathbf{T}}\mathbf{D}_{4\times4}\mathbf{B}(z)_{4\times14}\right]dz\mathbf{U}_{\mathbf{NH}14\times1} + \delta\mathbf{U}_{\mathbf{NH}1\times14}^{\mathbf{T}} \int_0^l GJ_d\left[\mathbf{W}'(z)_{14\times1}^{\mathbf{T}}\mathbf{W}'(z)_{1\times14}\right]dz\mathbf{U}_{\mathbf{NH}14\times1}$$
$$-\delta\mathbf{U}_{\mathbf{NH}1\times14}^{\mathbf{T}}\mathbf{P}_{14\times1} - \delta\mathbf{U}_{\mathbf{NH}\ 1\times14}^{\mathbf{T}}\mathbf{R}_{14\times1} + \delta\pi_e \tag{II.E(8)}$$

in which

$$\delta\pi_e = \delta\mathbf{U}_{\mathbf{NH}\ 1\times14}^{\mathbf{T}}\left(E\int_0^l \mathbf{B}(z)_{14\times4}^{\mathbf{T}}\mathbf{D}_{4\times4}\mathbf{u}_{\mathbf{p}4\times1}(z)\,dz + GJ_d\int_0^l \mathbf{W}'(z)_{14\times1}^{\mathbf{T}}\phi'_p(z)\,dz\right) \tag{II.E(9)}$$

Apart from the contribution $\delta\pi_e$, the virtual work expression as given by Eq. II.E(8) is found to exactly match the one given in Eq. (II.37). In the following it will be shown that the extra term in virtual work expression $\delta\pi_e$ vanishes. This signifies that the *stiffness matrix and the energy equivalent nodal force vector for the non-homogenous case is identical to that of the homogenous case*. The extra term $\delta\pi_e$ can be rewritten as

$$\delta\pi_e = E\int_0^l \left\langle \delta w'_h(z) \quad \delta u''_h(z) \quad \delta v''_h(z) \quad \delta\phi''_h(z)\right\rangle \begin{bmatrix} A & -S_y & -S_x & -S_\omega \\ -S_y & J_{yy} & J_{xy} & J_{\omega x} \\ -S_x & J_{xy} & J_{xx} & J_{\omega y} \\ -S_\omega & J_{\omega x} & J_{\omega y} & J_{\omega\omega} \end{bmatrix} \begin{Bmatrix} w'_p(z) \\ u''_p(z) \\ v''_p(z) \\ \phi''_p(z) \end{Bmatrix} dz$$
$$+GJ_d\int_0^l \phi'_h(z)\phi'_p(z)\,dz \tag{II.E (10)}$$

By integrating the terms including w_p' and ϕ_p' once by parts, and those including the terms u_p'', v_p'' and ϕ_p'' twice by parts, $\delta\pi_e$ is expressed as

$$\delta\pi_e = E\int_0^l \langle \Lambda_1 \quad \Lambda_2 \quad \Lambda_3 \quad \Lambda_4 \rangle \begin{Bmatrix} w_p \\ u_p \\ v_p \\ \phi_p \end{Bmatrix} dz - E \left. \begin{Bmatrix} \delta w''_h A - \delta u'''_h S_y - \delta v'''_h S_x - \delta\phi'''_h S_\omega \\ -\delta w''_h S_y + \delta u'''_h J_{yy} + \delta v'''_h J_{xy} + \delta\phi'''_h J_{\omega x} \\ -\delta w''_h S_x + \delta u'''_h J_{xy} + \delta v'''_h J_{xx} + \delta\phi'''_h J_{\omega y} \\ -\delta w''_h S_\omega + \delta u'''_h J_{\omega x} + \delta v'''_h J_{\omega y} + \delta\phi'''_h J_{\omega\omega} \end{Bmatrix}^{\mathrm{T}} \begin{Bmatrix} 0 \\ u_p \\ v_p \\ \phi_p \end{Bmatrix} \right|_0^l$$

$$+ E \left. \begin{Bmatrix} \delta w'_h A - \delta u''_h S_y - \delta v''_h S_x - \delta\phi''_h S_\omega \\ -\delta w'_h S_y + \delta u''_h J_{yy} + \delta v''_h J_{xy} + \delta\phi''_h J_{\omega x} \\ -\delta w'_h S_x + \delta u''_h J_{xy} + \delta v''_h J_{xx} + \delta\phi''_h J_{\omega y} \\ -\delta w'_h S_\omega + \delta u''_h J_{\omega x} + \delta v''_h J_{\omega y} + \delta\phi''_h J_{\omega\omega} \end{Bmatrix}^{\mathrm{T}} \begin{Bmatrix} w_p \\ u'_p \\ v'_p \\ \phi'_p \end{Bmatrix} \right|_0^l + GJ_d\phi'_h(z)\phi_p(z)\Big|_0^l$$

II.E(11)

In which

$$\Lambda_1 = -\delta w''_h A + \delta u'''_h S_y + \delta v'''_h S_x + \delta\phi'''_h S_\omega \qquad \text{II.E(12)}$$

$$\Lambda_2 = -\delta w'''_h S_y + \delta u''''_h J_{yy} + \delta v''''_h J_{xy} + \delta\phi''''_h J_{\omega x} \qquad \text{II.E(13)}$$

$$\Lambda_3 = -\delta w'''_h S_x + \delta u''''_h J_{xy} + \delta v''''_h J_{xx} + \delta\phi''''_h J_{\omega y} \qquad \text{II.E(14)}$$

$$\Lambda_4 = -\delta w'''_h S_\omega + \delta u''''_h J_{\omega x} + \delta v''''_h J_{\omega y} + \delta\phi''''_h J_{\omega\omega} \qquad \text{II.E(15)}$$

By using the relations $\delta w_h(z) = \mathbf{Z}(z)^{\mathrm{T}}_{1\times14}\delta\mathbf{U}_{\mathrm{NH}\ 14\times1}$, $\delta u_h(z) = \mathbf{X}(z)^{\mathrm{T}}_{1\times14}\delta\mathbf{U}_{\mathrm{NH}\ 14\times1}$, $\delta v_h(z) = \mathbf{Y}(z)^{\mathrm{T}}_{1\times14}\delta\mathbf{U}_{\mathrm{NH}\ 14\times1}$ and $\delta\phi_h(z) = \mathbf{W}(z)^{\mathrm{T}}_{1\times14}\delta\mathbf{U}_{\mathrm{NH}\ 14\times1}$ in Eqs. II.E(12) through II.E(15)one obtains

$$\Lambda_1 = \left\langle -A\mathbf{Z}''(z)^{\mathrm{T}}_{1\times14} + S_y\mathbf{X}'''(z)^{\mathrm{T}}_{1\times14} + S_x\mathbf{Y}'''(z)^{\mathrm{T}}_{1\times14} + S_\omega\mathbf{W}'''(z)^{\mathrm{T}}_{1\times14} \right\rangle \delta\mathbf{U}_{\mathrm{NH}\ 14\times1} \qquad \text{II.E(16)}$$

$$\Lambda_2 = \left\langle -S_y\mathbf{Z}'''(z)^{\mathrm{T}}_{1\times14} + J_{yy}\mathbf{X}''''(z)^{\mathrm{T}}_{1\times14} + J_{xy}\mathbf{Y}''''(z)^{\mathrm{T}}_{1\times14} + J_{\omega x}\mathbf{W}''''(z)^{\mathrm{T}}_{1\times14} \right\rangle \delta\mathbf{U}_{\mathrm{NH}\ 14\times1} \qquad \text{II.E(17)}$$

$$\Lambda_3 = \left\langle -S_x\mathbf{Z}'''(z)^{\mathrm{T}}_{1\times14} + J_{xy}\mathbf{X}''''(z)^{\mathrm{T}}_{1\times14} + J_{xx}\mathbf{Y}''''(z)^{\mathrm{T}}_{1\times14} + J_{\omega y}\mathbf{W}''''(z)^{\mathrm{T}}_{1\times14} \right\rangle \delta\mathbf{U}_{\mathrm{NH}\ 14\times1} \qquad \text{II.E(18)}$$

$$\Lambda_4 = \left\langle -S_\omega\mathbf{Z}'''(z)^{\mathrm{T}}_{1\times14} + J_{\omega x}\mathbf{X}''''(z)^{\mathrm{T}}_{1\times14} + J_{\omega y}\mathbf{Y}''''(z)^{\mathrm{T}}_{1\times14} + J_{\omega\omega}\mathbf{W}''''(z)^{\mathrm{T}}_{1\times14} - \frac{G}{E}J_d\mathbf{W}'' \right\rangle \delta\mathbf{U}_{\mathrm{NH}\ 14\times1}$$

II.E(19)

Since the homogenous form of Eq. (II.17) is satisfied by the interpolation field given in (II.19) through (II.22) from Eq. II.E(2), by substituting into Eqs. II.E(16) through II.E(19) one obtains, $\Lambda_1 = \Lambda_2 = \Lambda_3 = \Lambda_4 = 0$

By substituting Eq. II.E(4) into Eq. II.E (11), it can be also shown that the boundary terms in $\delta\pi_e$ vanish. This signifies that, by using the solution of the homogenous equation as the interpolation functions, the obtained stiffness matrix gives the exact nodal values, and for a member subject to a general load distribution, the product of the exact *homogenous* stiffness matrix by the exact nodal displacement vector is equal to the sum of the generalized force vector due to externally applied generalized nodal forces and the energy equivalent member load vector based on an exact *homogenous* displacement field.

Appendix II.F Stiffness Matrix for NOVEC14

Matrix $\mathbf{K}_0$ for element NOVEC14 can be expressed in a partitioned format as

$$\mathbf{K}_{0\,14\times14}=E\left[\begin{array}{c:c:c:c}\mathbf{K}_{011} & \mathbf{K}_{012} & \mathbf{K}_{013} & \mathbf{K}_{014}\\ \hdashline \mathbf{K}_{012}^{\mathrm{T}} & \mathbf{K}_{022} & \mathbf{K}_{023} & \mathbf{K}_{024}\\ \hdashline \mathbf{K}_{013}^{\mathrm{T}} & \mathbf{K}_{023}^{\mathrm{T}} & \mathbf{K}_{033} & \mathbf{K}_{034}\\ \hdashline \mathbf{K}_{014}^{\mathrm{T}} & \mathbf{K}_{024}^{\mathrm{T}} & \mathbf{K}_{034}^{\mathrm{T}} & \mathbf{K}_{044}\end{array}\right] \qquad \text{II.F(1)}$$

It can be mathematically demonstrated that all sub-matrices $\mathbf{K}_{0\mathrm{ij}}$ (except for sub-matrix $\mathbf{K}_{044}$), are identical to the corresponding sub-matrices $\mathbf{K}$, given in Appendix II.D i.e., $\mathbf{K}_{0\mathrm{ij}}=\mathbf{K}_{\mathrm{ij}}$. The entries of sub-matrix $\mathbf{K}_{044}$ are

$$\mathbf{K}_{044}=\frac{1}{l^3}\begin{bmatrix} 12\left(J_{\omega\omega}-\dfrac{S_\omega^{\ 2}}{A}\right) & 6\left(J_{\omega\omega}-\dfrac{S_\omega^{\ 2}}{A}\right)l & -12\left(J_{\omega\omega}-\dfrac{S_\omega^{\ 2}}{A}\right) & 6\left(J_{\omega\omega}-\dfrac{S_\omega^{\ 2}}{A}\right)l\\ & \left(4J_{\omega\omega}-3\dfrac{S_\omega^{\ 2}}{A}\right)l^2 & -6\left(J_{\omega\omega}-\dfrac{S_\omega^{\ 2}}{A}\right)l & \left(2J_{\omega\omega}-3\dfrac{S_\omega^{\ 2}}{A}\right)l^2\\ \mathit{Sym.} & & 12\left(J_{\omega\omega}-\dfrac{S_\omega^{\ 2}}{A}\right) & -6\left(J_{\omega\omega}-\dfrac{S_\omega^{\ 2}}{A}\right)l\\ & & & \left(4J_{\omega\omega}-3\dfrac{S_\omega^{\ 2}}{A}\right)l^2\end{bmatrix}$$

$$+\frac{GJ_d}{E}\begin{bmatrix}\dfrac{6}{5l} & \dfrac{1}{10} & -\dfrac{6}{5l} & \dfrac{1}{10}\\ & \dfrac{2l}{15} & -\dfrac{1}{10} & -\dfrac{l}{30}\\ & & \dfrac{6}{5l} & -\dfrac{1}{10}\\ \mathit{sym.} & & & \dfrac{2l}{15}\end{bmatrix} \qquad \text{II.F(2)}$$

In the following, the identity equation $\mathbf{K}_{34}=\mathbf{K}_{034}$ is demonstrated as an example. By substituting Eq. (II.10) and Eqs. (II.30) through (II.36) into Eq. (II.42), sub-matrices $\mathbf{K}_{34}$ and $\mathbf{K}_{034}$ appearing in Eqs. II.D(1) and II.F(1) are obtained as

$$\mathbf{K}_{43} = \left[I_{y\omega} - \frac{S_x S_\omega}{A} \right] \int_0^l \mathbf{N''(z)}_{4\times1} \mathbf{L''(z)}_{1\times4}^{\mathbf{T}} dz + \left[\frac{1}{A}(S_y S_x C_2 + S_x{}^2 C_3) \right] \int_0^l [\mathbf{N''(z)}_{4\times1} - \mathbf{L''(z)}_{4\times1}] \mathbf{M*'(z)}_{1\times4}^{\mathbf{T}} dz$$
$$+ \int_0^l \left[S_x S_\omega A^{-1} \right] \mathbf{M*'(z)}_{4\times1} \mathbf{M*'(z)}_{1\times4}^{\mathbf{T}} dz$$

II.F(3)

$$\mathbf{K}_{043} = \left[I_{y\omega} - \frac{S_x S_\omega}{A} \right] \int_0^l \mathbf{N''(z)}_{4\times1} \mathbf{N''(z)}_{1\times4}^{\mathbf{T}} dz + \int_0^l \left[S_x S_\omega A^{-1} \right] \mathbf{M*'(z)}_{4\times1} \mathbf{M*'(z)}_{1\times4}^{\mathbf{T}} dz \qquad \text{II.F(4)}$$

By integrating the first two terms in Eqs. II.F(3) and II.F(4) twice by parts, one obtains

$$\int_0^L \mathbf{N''(z)}_{4\times1} \mathbf{N''(z)}_{1\times4}^{\mathbf{T}} dz = \mathbf{N''(z)}_{4\times1} \mathbf{N'(z)}_{1\times4}^{\mathbf{T}} \Big|_0^L - \mathbf{N'''(z)}_{4\times1} \mathbf{N(z)}_{1\times4}^{\mathbf{T}} \Big|_0^L + \int_0^L \mathbf{N}^{\mathbf{IV}}\mathbf{(z)}_{4\times1} \mathbf{N(z)}_{1\times4}^{\mathbf{T}} dz \qquad \text{II.F(5)}$$

$$\int_0^L \mathbf{N''(z)}_{4\times1} \mathbf{L''(z)}_{1\times4}^{\mathbf{T}} dz = \mathbf{N''(z)}_{4\times1} \mathbf{L'(z)}_{1\times4}^{\mathbf{T}} \Big|_0^L - \mathbf{N'''(z)}_{4\times1} \mathbf{L(z)}_{1\times4}^{\mathbf{T}} \Big|_0^L + \int_0^L \mathbf{N}^{\mathbf{IV}}\mathbf{(z)}_{4\times1} \mathbf{L(z)}_{1\times4}^{\mathbf{T}} dz \qquad \text{II.F(6)}$$

Noting that $\mathbf{N}^{\mathbf{IV}}\mathbf{(z)}_{4\times1} = 0$, $\mathbf{N'(z)}_{1\times4}^{\mathbf{T}} \Big|_0^L = \mathbf{L'(z)}_{1\times4}^{\mathbf{T}} \Big|_0^L$ and $\mathbf{N(z)}_{1\times4}^{\mathbf{T}} \Big|_0^L = \mathbf{L(z)}_{1\times4}^{\mathbf{T}} \Big|_0^L$ one can prove the identity $\int_0^l \mathbf{N''(z)}_{4\times1} \mathbf{L''(z)}_{1\times4}^{\mathbf{T}} dz = \int_0^l \mathbf{N''(z)}_{4\times1} \mathbf{N''(z)}_{1\times4}^{\mathbf{T}} dz$ which makes the first term in Eqs. II.F(3) identical to the first term in Eq. II.F(4).

Also, by applying a similar technique, it can be demonstrated that $\int_0^l \mathbf{N''(z)}_{4\times1} \mathbf{M*'(z)}_{1\times2}^{\mathbf{T}} dz = \int_0^l \mathbf{L''(z)}_{4\times1} \mathbf{M*'(z)}_{1\times2}^{\mathbf{T}} dz$. Thus, the second term in Eq. II.F(3) must vanish. The relation $\mathbf{K}_{34} = \mathbf{K}_{034}$ is proved. Similar proofs can be formulated for the remaining sub-matrices $\mathbf{K}_{\mathbf{0ij}} = \mathbf{K}_{\mathbf{ij}}, i \neq 4, j \neq 4$.

Appendix II.G Finite element approximation for members with negligible warping stiffness

For long elements or for elements with negligible warping constants (e.g., tee and angle sections), the condition $kl \to \infty$ is approached and the torsional differential equation approaches $d^2\phi/d\varsigma^2 = 0$, in which $\varsigma = z/L$. The corresponding solution takes the linear solution form $\phi_\infty(z) = a_1 z + a_2$. The rotation field $\phi_\infty(z)$ is expressed in terms of nodal displacements $\boldsymbol{\varphi}_{\infty N2\times1}$ as

$$\phi_\infty(z) = \mathbf{M}(z)_{1\times2}^{\mathbf{T}} \boldsymbol{\varphi}_{\infty N2\times1} \tag{II.G(1)}$$

in which the nodal rotation vector $\boldsymbol{\varphi}_{\infty N}{}^{\mathrm{T}}{}_{2\times1} = \langle \phi_1 \quad \phi_2 \rangle$ does not include the nodal warping deformation. Eq. II.G(1) is substituted into Eq. II.B(2). The second and third rows of the resulting matrix are integrated four times with respect to z and the displacement boundary conditions are evoked leading to

$$u_\infty(z) = \mathbf{N}(z)_{1\times4}^{\mathbf{T}} \mathbf{u}_{N4\times1} \tag{II.G(2)}$$

$$v_\infty(z) = \mathbf{N}(z)_{1\times4}^{\mathbf{T}} \mathbf{v}_{N4\times1} \tag{II.G(3)}$$

Equations II.G(1) through II.G(3) are substituted into the first row of Eq. II.B(1) and the resulting equation is integrated twice. The longitudinal displacement boundary conditions are then enforced. The following expression for the longitudinal displacement $w(z)$ is obtained

$$w_\infty(z) = \mathbf{M}(z)_{1\times2}^{\mathbf{T}} \mathbf{w}_{N2\times1} + \frac{S_y}{A}\left[\mathbf{N'(z)}_{1\times4}^{\mathbf{T}} - \mathbf{M}*(z)_{1\times4}^{\mathbf{T}}\right]\mathbf{u}_{N4\times1} + \frac{S_x}{A}\left[\mathbf{N'(z)}_{1\times4}^{\mathbf{T}} - \mathbf{M}*(z)_{1\times4}^{\mathbf{T}}\right]\mathbf{v}_{N4\times1} \tag{II.G(4)}$$

From Eq. II.G(1) through II.G(4), the vector of displacement derivatives $\mathbf{u}_\infty(z)^{\mathrm{T}}_{1\times4} = \langle w_\infty{}'(z) \quad u_\infty{}''(z) \quad v_\infty{}''(z) \quad \phi_\infty{}''(z)\rangle$ can be related to the nodal displacement vector $\mathbf{U}^{\mathrm{T}}_{\infty\mathrm{N}12\times1} = \langle \mathbf{w}_{\mathrm{N}2\times1} \mid \mathbf{u}_{\mathrm{N}4\times1} \mid \mathbf{v}_{\mathrm{N}4\times1} \mid \boldsymbol{\varphi}_{\infty\mathrm{N}2\times1}\rangle$ through

$$\mathbf{u}_\infty(z)_{4\times1} = \begin{Bmatrix} w_\infty{}'(z) \\ u_\infty{}''(z) \\ v_\infty{}''(z) \\ \phi_\infty{}''(z) \end{Bmatrix} = \mathbf{B}_\infty(z)_{4\times12}\,\mathbf{U}_{\infty\mathrm{N}\,12\times1} \qquad \text{II.G(5)}$$

in which matrix $\mathbf{B}_\infty(z)_{4\times12}$ is given by

$$\mathbf{B}_\infty(z)_{4\times12} = \left[\begin{array}{c|c|c|c} \mathbf{M}'(z)^{\mathrm{T}}_{1\times2} & \dfrac{S_y}{A}\left[\mathbf{N}'(z)^{\mathrm{T}}_{1\times4} - \mathbf{M}^{*\prime}(z)^{\mathrm{T}}_{1\times4}\right] & \dfrac{S_x}{A}\left[\mathbf{N}'(z)^{\mathrm{T}}_{1\times4} - \mathbf{M}^{*\prime}(z)^{\mathrm{T}}_{1\times4}\right] & \mathbf{0}_{1\times2} \\ \hline \mathbf{0}_{1\times2} & \mathbf{N}''(z)^{\mathrm{T}}_{1\times4} & \mathbf{0}_{1\times4} & \mathbf{0}_{1\times2} \\ \hline \mathbf{0}_{1\times2} & \mathbf{0}_{1\times4} & \mathbf{N}''(z)^{\mathrm{T}}_{1\times4} & \mathbf{0}_{1\times2} \\ \hline \mathbf{0}_{1\times2} & \mathbf{0}_{1\times4} & \mathbf{0}_{1\times4} & \mathbf{0}_{1\times2} \end{array}\right] \qquad \text{II.G(6)}$$

By adopting a procedure as in Eq. (II.51), the stiffness matrix can be expressed as

$$\mathbf{K}_{\infty12\times12} = E\int_0^l \mathbf{B}_\infty(\mathbf{z})^{\mathrm{T}}_{12\times4}\,\mathbf{D}_{4\times4}\mathbf{B}_\infty(\mathbf{z})_{4\times12}\,dz + GJ_d\int_0^l \left[\begin{array}{c|c} \mathbf{0}_{10\times10} & \mathbf{0}_{10\times2} \\ \hline \mathbf{0}_{2\times10} & \mathbf{M}'(\mathbf{z})^{\mathrm{T}}_{2\times1}\mathbf{M}'(\mathbf{z})_{1\times2} \end{array}\right] dz \qquad \text{II.G(7)}$$

The element formulated in this section will subsequently be referred to as the NOVEL12 (Non-Orthogonal Vlasov Element based on Linear shape functions with 12 degrees of freedom). The entries of the stiffness matrix $\mathbf{K}_\infty$ for NOVEL12 are expressed in a partitioned form as

$$\mathbf{K}_{\infty} = E\left[\begin{array}{c|c|c|c} \mathbf{K}_{\infty 11} & \mathbf{K}_{\infty 12} & \mathbf{K}_{\infty 13} & \mathbf{K}_{\infty 14} \\ \hline \mathbf{K}_{\infty 12}{}^{\mathrm{T}} & \mathbf{K}_{\infty 22} & \mathbf{K}_{\infty 23} & \mathbf{K}_{\infty 24} \\ \hline \mathbf{K}_{\infty 13}{}^{\mathrm{T}} & \mathbf{K}_{\infty 23}{}^{\mathrm{T}} & \mathbf{K}_{\infty 33} & \mathbf{K}_{\infty 34} \\ \hline \mathbf{K}_{\infty 14}{}^{\mathrm{T}} & \mathbf{K}_{\infty 24}{}^{\mathrm{T}} & \mathbf{K}_{\infty 34}{}^{\mathrm{T}} & \mathbf{K}_{\infty 44} \end{array}\right] \qquad \text{II.G(8)}$$

in which the following sub-matrices are defined as

$$\mathbf{K}_{\infty 11\ \ 2\times 2} = A\int_0^l \mathbf{M}'(z)_{2\times 1}\mathbf{M}'(z)^{\mathrm{T}}_{1\times 2}dz = \frac{A}{l}\begin{bmatrix} 1 & -1 \\ -1 & 1 \end{bmatrix} \qquad \text{II.G(9)}$$

$$\mathbf{K}_{\infty 21\ \ 4\times 2} = \int_0^l S_y\mathbf{M}^{*}{}'(z)_{4\times 1}\mathbf{M}'(z)^{\mathrm{T}}_{1\times 2}dz = \frac{S_y}{l}\begin{bmatrix} 0 & 0 \\ 1 & -1 \\ 0 & 0 \\ -1 & 1 \end{bmatrix} \qquad \text{II.G(10)}$$

$$\mathbf{K}_{\infty 31\ \ 4\times 2} = \int_0^l S_x\mathbf{M}^{*}{}'(z)_{4\times 1}\mathbf{M}'(z)^{\mathrm{T}}_{1\times 2}dz = \frac{S_x}{l}\begin{bmatrix} 0 & 0 \\ 1 & -1 \\ 0 & 0 \\ -1 & 1 \end{bmatrix} \qquad \text{II.G(11)}$$

$$\mathbf{K}_{\infty 41\ \ 4\times 2} = \mathbf{0}_{2\times 2} \qquad \text{II.G(12)}$$

$$\mathbf{K}_{\infty 22\ \ 4\times 4} = \int_0^l \left[J_{yy} - \frac{S_y{}^2}{A}\right]\mathbf{N}''(z)_{4\times 1}\mathbf{N}''(z)^{\mathrm{T}}_{1\times 4} + \frac{S_y{}^2}{A}\mathbf{M}^{*}{}'(z)_{4\times 1}\mathbf{M}^{*}{}'(z)^{\mathrm{T}}_{4\times 1}dz$$

$$= \left[J_{yy} - \frac{S_y{}^2}{A}\right]\begin{bmatrix} \frac{12}{l^3} & \frac{6}{l^2} & -\frac{12}{l^3} & \frac{6}{l^2} \\ \frac{6}{l^2} & \frac{4}{l} & -\frac{6}{l^2} & \frac{2}{l} \\ -\frac{12}{l^3} & -\frac{6}{l^2} & \frac{12}{l^3} & \frac{-6}{l^2} \\ \frac{6}{l^2} & \frac{2}{l} & \frac{-6}{l^2} & \frac{4}{l} \end{bmatrix} + \frac{S_y{}^2}{Al}\begin{bmatrix} 0 & 0 & 0 & 0 \\ 0 & 1 & 0 & -1 \\ 0 & 0 & 0 & 0 \\ 0 & -1 & 0 & 1 \end{bmatrix} \qquad \text{II.G(13)}$$

$$\mathbf{K}_{\infty 23\quad 4\times 4} = \int_0^l \left[J_{xy} - \frac{S_x S_y}{A} \right] \mathbf{N}''(z)_{4\times 1} \mathbf{N}''(z)_{1\times 4}^{\mathrm{T}} + \frac{S_x S_y}{A} \mathbf{M}^{*\prime}(z)_{4\times 1} \mathbf{M}^{*\prime}(z)_{4\times 1}^{\mathrm{T}} dz$$

$$= \left[J_{yy} - \frac{S_x S_y}{A} \right] \begin{bmatrix} \frac{12}{l^3} & \frac{6}{l^2} & -\frac{12}{l^3} & \frac{6}{l^2} \\ \frac{6}{l^2} & \frac{4}{l} & -\frac{6}{l^2} & \frac{2}{l} \\ -\frac{12}{l^3} & -\frac{6}{l^2} & \frac{12}{l^3} & \frac{-6}{l^2} \\ \frac{6}{l^2} & \frac{2}{l} & \frac{-6}{l^2} & \frac{4}{l} \end{bmatrix} + \frac{S_x S_y}{Al} \begin{bmatrix} 0 & 0 & 0 & 0 \\ 0 & 1 & 0 & -1 \\ 0 & 0 & 0 & 0 \\ 0 & -1 & 0 & 1 \end{bmatrix} \qquad \text{II.G(14)}$$

$$\mathbf{K}_{\infty 42\quad 2\times 2} = \mathbf{0}_{2\times 2} \qquad \text{II.G(15)}$$

$$\mathbf{K}_{\infty 33\quad 4\times 4} = \int_0^l \left[J_{xx} - \frac{S_x^{\ 2}}{A} \right] \mathbf{N}''(z)_{4\times 1} \mathbf{N}''(z)_{1\times 4}^{\mathrm{T}} + \frac{S_x^{\ 2}}{A} \mathbf{M}^{*\prime}(z)_{4\times 1} \mathbf{M}^{*\prime}(z)_{4\times 1}^{\mathrm{T}} dz$$

$$= \left[J_{xx} - \frac{S_y^{\ 2}}{A} \right] \begin{bmatrix} \frac{12}{l^3} & \frac{6}{l^2} & -\frac{12}{l^3} & \frac{6}{l^2} \\ \frac{6}{l^2} & \frac{4}{l} & -\frac{6}{l^2} & \frac{2}{l} \\ -\frac{12}{l^3} & -\frac{6}{l^2} & \frac{12}{l^3} & \frac{-6}{l^2} \\ \frac{6}{l^2} & \frac{2}{l} & \frac{-6}{l^2} & \frac{4}{l} \end{bmatrix} + \frac{S_x^{\ 2}}{Al} \begin{bmatrix} 0 & 0 & 0 & 0 \\ 0 & 1 & 0 & -1 \\ 0 & 0 & 0 & 0 \\ 0 & -1 & 0 & 1 \end{bmatrix} \qquad \text{II.G(16)}$$

$$\mathbf{K}_{\infty 43\quad 2\times 2} = \mathbf{0}_{2\times 2} \qquad \text{II.G(17)}$$

$$\mathbf{K}_{\infty 44\quad 2\times 2} = \frac{GJ_d}{E} \int_0^l \mathbf{M}'(z)_{2\times 1}^{\mathrm{T}} \mathbf{M}'(z)_{1\times 2} dz = \frac{GJ_d}{El} \begin{bmatrix} 1 & -1 \\ -1 & 1 \end{bmatrix} \qquad \text{II.G(18)}$$

Chapter II References

[II.1] Aly, A.G., and Sato, N. 1984. Generalized stiffness matrix for thin walled beams-Discussion. Journal of Structural Engineering, ASCE, 110 (2): 421-422.

[II.2] Back, S.Y., and Will, K.M. 1998. A shear-flexible element with warping for thin-walled open beams. International Journal for Numerical Methods in Engineering, 43 (7): 1173-1191.

[II.3] Barsoum, R.S., 1970. A finite element formulation for the general stability analysis of thin walled members. Ph. D. thesis, Cornell University, Ithaca, New York, USA

[II.4] Barsoum, R.J., and Gallagher, R.H. 1970. Finite element analysis of torsional and torsional-flexural stability problems. International Journal for Numerical Methods in Engineering, 2: 335-352.

[II.5] Batoz, J.L., and Dhatt, G., 1990. Modélisation des structures par éléments finis. Vol. 2, poutres et plaques. (Modeling of structures with finite elements, Vol. 2, Beams and plates). Hermes edition, Paris. (in French).

[II.6] Benscoter, S.U. 1954. A theory of torsion bending for multicell beams. Journal of Applied Mechanics, 53: 25-34.

[II.7] Boresi, A.P., Sidebottom, O.M., 1985. Advanced Mechanics of Materials. Fourth Edition, John Wiley & Sons, New York, USA.

[II.8] Chaudhary, A.B., 1982. Generalized stiffness matrix for thin walled beams. Journal of Structural Engineering, ASCE, 108(2): 559-577.

[II.9] Chen, H., Blandford, G.E., 1989. A C^0 finite element formulation for thin-walled beams. International Journal for Numerical Methods in Engineering, 20(10): 2239-2255.

[II.10] de Ville de Goyet, V. 1989. L'analyse statique non linéaire par la méthode des éléments finis des poutres a section non symétrique (Nonlinear static analysis of beams with unsymmetrical cross sections by the finite element method), Ph. D. thesis, Université de Liége, Belgium (in French).

[II.11] Driver, R.G., Kennedy, D.J.L., 1989. Combined flexural torsion of I-shape steel beams. Canadian Journal for Civil Engineering, 16(2): 124-139.

[II.12] Dvorkin, E.N., Celentano, D., Cuitino, A., and Gioia, G., 1989. A Vlassov beam element. Computers and Structures, 33(1): 187-196.

[II.13] Eisenberger, M., and Cohen, R., 1995. Flexural-Torsional Buckling of Variable and Open Cross-Section Members, Journal of Engineering Mechanics, ASCE, 121(2): 244-254.

[II.14] Erkmen, R.E. and Mohareb, M. 2006. Non-orthogonal solution for thin-walled beams – A Finite Element Formulation, Canadian Journal of Civil Engineering, Vol.33, No.4, 421-439.

[II.15] Erkmen, R.E. and Mohareb, M. 2006. Non-orthogonal solution for thin-walled beams – Applications and Modelling considerations, Canadian Journal of Civil Engineering, Vol.33, No.4, 440-450.

[II.16] Friberg, P.O., 1985. Beam element matrices derived from Vlasov's theory of open thin-walled elastic beams. International Journal for Numerical Methods in Engineering, 21(7): 1205-1228.

[II.17] Gellin, S., Lee, G.C., and Chern, J.H., 1983. A finite element model for thin-walled members. International Journal for Numerical Methods in Engineering. 19 (1): 59-71.

[II.18] Gendy, A.S., Saleeb, A.F., and Chang, T.Y.P., 1992. Generalized thin-walled beam models for flexural-torsional analysis. Computers and Structures, 42(4): 531-550.

[II.19] Gjlesvik, A. 1981. The theory of thin walled bars, John Wiley and Sons, New York, U.S.A.

[II.20] Gunnlaugsson, G.A., and Pedersen, P.T., 1982. A finite element formulation for beams with thin walled cross-sections. Computers and Structures, 15(6): 691-699.

[II.21] Hancock, G.J., 1984. Generalized stiffness matrix for thin walled beams-Discussion. Journal of Structural Engineering, ASCE, 110(2): 422-424.

[II.22] Krajcinovic, D., 1969. A consistent discrete elements technique for thin wall assemblages. International Journal for Solids and Structures, 5: 639-662.

[II.23] Krajcinovic, D., 1970. Matrix force analysis of thin-walled structures. Journal of Structural Engineering, ASCE, 96(1): 107-120.

[II.24] Mohareb, M., and Nowzartash, F., 2003. Exact finite element for warping torsion of open sections. Journal of Structural Engineering, ASCE. 129(2): 215-223.

[II.25] Murray, D.W., Rajasekaran, S. 1975. Technique for formulating beam equations. Journal of the Engineering Mechanics Division, ASCE. 101(5): 561-573.

[II.26] Murray, N.W., 1984. Introduction to the theory of thin-walled structures. Claredon Press, Oxford, United Kingdom.

[II.27] Prokic, A., 1996. New Warping Function for Thin-Walled Beams. I: Theory. Journal of Structural Engineering, ASCE, 122(12): 1437-1442.

[II.28] Schulz, M., Filippou, F.C. 1998. Generalized Warping Torsion Formulation. Journal of Engineering Mechanics, ASCE, 124(3): 339-347.

[II.29] Shakourzadeh, H., Guo, Y.Ch., and Batoz, J.L., 1995. A torsional bending element for thin-walled beams with open and closed cross sections. Computers and Structures, 55(6): 1045-1054.

[II.30] Tso, W.K., and Ghobarah, A.A., 1971. Nonlinear Nonuniform Torsion of Thin-Walled beams. International Journal of Mechanical Sciences, 13(12): 1039-1047.

[II.31] Tralli, A., 1986. A Simple Hybrid Model for Torsion and Flexure of Thin-Walled Beams. Computers and Structures, 22(4): 649-658.

[II.32] Vlasov, V.Z., 1961. Thin Walled Elastic Beams. Second Edition, Israel Program for Scientific Translations, Jerusalem, Israel.

Chapter II List of symbols

The following symbols were used in this paper

A	=	cross-sectional area (Fig. II.1);
A_p	=	arbitrary pole (Fig. II.1);
$\mathbf{A}(s)_{7\times 3}^{\mathbf{T}}$	=	displacement transformation matrix;
a_x, a_y	=	coordinates of arbitrary pole A_p (Figs. II.1, II.2);
b_c	=	width of the of c^{th} thin-wall segment;
B	=	bimoments;
$\overline{B}$	=	end bimoments (Fig. II.2);
B_p	=	arbitrary point on mid-surface (Fig. II.1);
$\mathbf{B}(z)_{4\times 14}$	=	matrix relating the displacement derivative vector $\{\mathbf{u}\}_{4\times 1}$ to the nodal displacements;
C_w	=	warping constant;
$\mathbf{d}$	=	exact displacement field vector;
$\mathbf{D}_{4\times 4}$	=	matrix containing cross-sectional properties;
D	=	shear center (Fig. II.A.1);
d_x, d_y	=	coordinates of the shear center (Fig. II.A.1);
E	=	modulus of elasticity;
$\mathbf{F}_{14\times 1}$	=	load vector due to end tractions;
G	=	shear modulus;

$h(s)$	=	normal distance between pole and the tangent to mid-surface;
$\mathbf{H}(z)^{\mathrm{T}}_{14\times 7}$	=	matrix containing shape functions to calculate energy equivalent nodal forces for member loads;
$J_{xx}, J_{yy}, J_{xy}, J_{\omega x}, J_{\omega y}$	=	section moments of inertia and products of inertia;
$J_{x2x2}, J_{y2y2}, J_{x2y2}$	=	moments of inertias based on the shifted axes x_2, y_2 (Fig. II.A.1);
$J_{x3x3}, J_{y3y3}, J_{\omega x3}, J_{\omega y3}$	=	moments of inertias based on the principal axes x_3, y_3 (Fig. II.A.1);
J_d	=	St. Venant's torsional constant;
$J_{\omega\omega}$	=	second moment of the sectorial coordinate;
k	=	constant $\sqrt{GJ/EC_w}$
$\mathbf{K}_{14\times 14}$	=	stiffness matrix of NOVEE14 element;
$\mathbf{K}_{0\,14\times 14}$	=	stiffness matrix of NOVEC14 element;
$\mathbf{K}_{\infty\,12\times 12}$	=	stiffness matrix of NOVEL12 element;
l	=	length of finite element;
$\mathbf{L}(z)^{\mathrm{T}}_{1\times 4}$	=	vector of hyperbolic shape functions;
$m(z)$	=	twisting moments per unit length about polar axis;
$\mathbf{M}(z)^{\mathrm{T}}_{1\times 2}, \mathbf{M}^*(z)^{\mathrm{T}}_{1\times 4}$	=	linear shape function vectors;
M_x, M_y	=	bending moments;

$\overline{M}_x, \overline{M}_y$	=	end bending moments induced by tractions about the polar axis (Fig. II.2);
n	=	number of segments defining a cross-section;
$\overline{N}$	=	axial force at the end of the beam;
$\mathbf{N}(z)^{\mathrm{T}}_{1\times4}$	=	cubic shape function vector;
NOVEE14	=	Non-Orthogonal Vlasov Element based on Exact shape functions with 14 degrees of freedom
NOVEC14	=	Non-Orthogonal Vlasov Element based on Cubic shape functions with 14 degrees of freedom
NOVEL12	=	Non-Orthogonal Vlasov Element based on Linear shape functions with 12 degrees of freedom
$\mathbf{p}(s,z)_{3\times1}$	=	member traction vector acting on member mid-surface (Fig. II.2) in force per unit area;
$\mathbf{P}_{14\times1}$	=	nodal force vector due to externally applied tractions at member ends;
q_x, q_y, q_z	=	resultant of traction vector (force per unit length);
$\mathbf{R}_{14\times1}$	=	energy equivalent nodal force vector due to member loads;
r	=	coordinate normal to the section mid surface (Fig. II.2);
S_0	=	sectorial origin (Figs. II.1, II.2);
S_{01}	=	arbitrary sectorial origin (Figs. II.A.1);
S_{02}	=	principal sectorial origin (Figs. II.A.1);
S_x, S_y, S_ω	=	first moments of area of coordinates x, y, and ω;

S_{x1}, S_{y1} = first moments of area of coordinates in coordinates; x_1, y_1 (Fig. II.A.1);

s = curvilinear coordinate along mid surface (Fig. II.1,Fig.II.2);

$\vec{t}$ = tangent vector to the cross-section (Fig. II.1, Fig. II.2);

t_c = thickness of c^{th} thin-wall segment;

T_{sv} = St.Venant torsion (Fig. II.2);

T_w = warping torsion (Fig. II.2);

T = total twisting moment;

$\overline{T}$ = end twisting moments about the polar axis (Fig. II.2);

$\mathbf{U_N}$ = nodal displacement vector for the homogeneous case;

$u(z), v(z)$ = displacements along x, y directions of arbitrary pole (Fig. II.1);

$u_s(s,z), v_s(s,z)$ = horizontal and vertical displacements of arbitrary point B_p located on section mid-surface (Fig. II.1);

V = volume of element;

$\overline{V}_x, \overline{V}_y$ = shear stress resultants at the end of the beam (Fig. II.2);

$w(z)$ = function related to the longitudinal displacement of the section

$w_s(s,z)$ = longitudinal displacement of arbitrary point B_p on the mid-surface (Fig. II.1);

x, y, z = coordinates of arbitrary point B_p (Figs. II.1, II.2);

x_1, y_1 = arbitrary chosen system of coordinates for cross-section (Figs. II.A.1);

x_2, y_2 = shifted coordinate system (Figs. II.A.1);

x_3, y_3 = principal coordinate system (Figs. II.A);

$\mathbf{x}_{1\times4}^{\mathrm{T}}$ = displacement vector;

$\delta\pi$ = total virtual work;

$\boldsymbol{\delta}\mathbf{u}_{\mathrm{s}}(s,z)_{1\times3}^{\mathrm{T}}$ = virtual displacement vector of point (s,z) on mid-surface;

δU_n = internal virtual work induced by normal stresses;

δU_s = internal virtual work induced by the St. Venant shear stresses;

ε_{zz} = longitudinal strain;

$\phi(z)$ = angle of twist about the longitudinal axis;

$\boldsymbol{\varphi}_{\mathrm{N}4\times1}, \mathbf{u}_{\mathrm{N}4\times1}, \mathbf{v}_{\mathrm{N}4\times1}, \mathbf{w}_{\mathrm{N}2\times1}$ = nodal displacement vectors;

$\gamma_{z\eta}$ = shear strain at mid-surface;

$\eta_s(s,z)$ = displacements along the tangential direction to the section profile at point B_p (Fig. II.2);

σ_{ss} = normal stress along the tangential coordinate;

σ_{zz} = longitudinal stress;

$\bar{\sigma}, \bar{\tau}$ = externally applied tractions at the ends of the element;

ω = sectorial area;

Chapter II List of Figures

Chapter III

Non-orthogonal solution for thin-walled members - Applications and Modelling Considerations

Abstract

In the previous chapter, three finite elements based on the Vlasov thin-walled beam theory were formulated under a non-orthogonal coordinate system. Although the associated derivations are more elaborate than in more conventional solutions based on orthogonal coordinates, the new elements offer more modelling capabilities and flexibility in modelling structural steel members, a feature that is illustrated in this chapter. In this context, the current chapter presents four details in steel construction which were conveniently modeled within the new solution scheme. The applications involve thin-walled members with coped flanges, rectangular holes reinforced with longitudinal stiffeners, and eccentric supports. Comparisons with established shell finite element models under ABAQUS, suggest the validity of the new solution.

Keywords: Open sections, finite element analysis, thin-walled members, coped flanges, rectangular holes, eccentric supports

Overview of Chapter II

In the previous chapter, three finite elements were developed based on the Vlasov thin-walled beam theory (Vlasov 1961). The solutions developed adopt non-conventional coordinate systems in contrast to conventional formulations in which orthogonal coordinate systems are used ($S_x = \int_A x dA = 0$, $S_y = \int_A y dA = 0$, $S_\omega = \int_A \omega dA = 0$, $J_{xy} = \int_A xy dA = 0$, $J_{\omega x} = \int_A \omega x dA = 0$, $J_{\omega y} = \int_A \omega y dA = 0$). Coordinates $x = x(s), y = y(s)$ are those of a point located on the section mid surface denoted by a curvilinear coördinate s measured from an arbitrary sectorial origin s_0 on the mid surface. The sectorial coordinate $\omega = \omega(s_0, s)$ is twice the area enclosed by the fixed radius Os_0 (where O is an arbitrarily selected origin point in the plane of the cross-section), the mobile radius Os, and the curved sector $s_0 s$ (Fig. II.1 in chapter II). All integrals are performed over the cross-sectional area A.

The first element, NOVEE14 (Non-Orthogonal Vlasov Element based on Exact shape functions, with 14 degrees of freedom), is based on shape functions which exactly satisfy the coupled form of the Vlasov homogeneous form of the differential equations of equilibrium. As a result, it is expected to yield nodal displacements in exact agreement with those based on an exact solution of the Vlasov equations. The second element, NOVEC14 (Non-Orthogonal Vlasov Element based on Cubic shape functions, with 14 degree of freedom), is based on simplified Hermitian shape functions for the angle of twist. Unlike element NOVEE14, element NOVEC14 involves a discetization error which is expected to decrease as the element size is decreased. Element NOVEC14 should be ideal for simulating the cases where the warping torsional stiffness is predominant in comparison to the St. Venant torsional stiffness. The third element NOVEL12 (Non-Orthogonal Vlasov Element based on Linear shape functions with 12 degrees of freedom) is based on a linear shape function for the angle of twist and is ideal for simulated cases where the warping torsional stiffness is negligible in relation to the St. Venant torsional stiffness. This is the case for members made of angles and T sections, and possibly for long members made of other sections.

Limitations

The formulations are based on assumed elastic material behaviour, and do not account for the presence of residual stresses which exist in structural steel members. As a result, they provide accurate deformation response predictions only in cases where the effective stresses due to the combined effect of external loading and residual stresses are less than the material yield point.

Geometric non-linear effects are not modelled and thus the formulation is expected to yield accurate results only in cases where the loads applied are significantly less than elastic buckling loads. Since the formulation is based on the Vlasov thin-walled beam theory, stability effects related to plate buckling and distortional buckling are not captured in the solution.

Objectives and Scope of Current Chapter

In the above context, the primary objective of the current Chapter is to illustrate the applicability of the finite element solutions developed in Chapter II to a variety of problems within the steel construction industry for which the application of the more conventional solutions under the Vlasov thin-walled beam theory is particularly difficult.

The examples were selected with the primary objective of illustrating the modelling capabilities of the new formulation.

The four applications selected involve: a) a member subjected to a concentrated twisting moment with half of its span having a coped flange resulting in an asymmetric cross-section, b) a concentrically loaded eccentrically braced vertical member, c) a transversely loaded beam with a rectangular hole in the web; and d) an eccentrically supported beam under uniformly distributed lateral load. The quality of the predictions based on the approximate element NOVEC14 is assessed and the validity of the more exact solution under element NOVEE14 is examined through a comparative study with established shell finite element models under ABAQUS.

Selected Cross-Section

The same wide flange cross-section is adopted in all four examples (flange width $b = 400mm$, total section depth $d = 420mm$, flange thickness $t = 20mm$ and web thickness $w = 12mm$). In examples III.1 and III.3, modifications are introduced to the section to incorporate the flange copes (in Example III.1), and web holes and longitudinal stiffeners (in Example III.3). For a yielding strength of 350 MPa, the section meets Class 3 requirements as defined in the Canadian Standards (CAN/CSA S16 -2001) and thus is expected to develop its fully elastic resistance prior undergoing local buckling (under any combination of axial force and bending moments). Common structural steel material properties are adopted in all solutions (modulus of elasticity $E = 2\times10^5 MPa$ and Poisson's Ratio $\mu = 0.3$, and a corresponding shear modulus $G = 77\times10^3 MPa$).

Details of Shell Finite Element Models

The results based on the new formulation are compared with finite element shell models developed under ABAQUS, a general purpose finite element program. The objective of this section is to describe the ABAQUS finite element model features common to all four problems considered. Additional details specific to each problem are also provided separately for each example.

The ABAQUS four nodded shell element (S4R) with reduced integration is adopted in all models. The S4R element is efficient and reliable for large displacements, large rotations and finite membrane strains extensively used by many researchers to model steel structure behaviour (Mohareb and Dabbas 2003, Zinoviev and Mohareb 2004). The main advantages of reduced integration are; i) it avoids shear locking that occurs in fully integrated elements and ii) it reduces the CPU time necessary for the analysis of the model and gives more accurate results for thin shells. The multiple point constraints MPC type SLIDER (Hibbit et al. 2001a,b) are adopted in order to approximately impose the first Vlasov assumption. This type of MPC keeps the specified node(s) on a straight line defined by two other nodes but allows the possibility of the node of moving along that line and allows the line to change in length. For all cross-sections along the beam, MPCs type SLIDER were adopted to constrain all nodes of the web to remain collinear throughout deformation. Also, similar constrains were enforced for the nodes of the top and bottom flanges. These artificial constraints were added in order to approximately simulate the Vlasov first assumption which does not capture possible distortional effects in the web and flanges. Previous studies (Mohareb and Dabbas 2003) have shown that the relaxation of the first Vlasov assumption (by removing the MPC -Slider constraints) for sections similar to the one investigated in this study caused a difference in results in the order of only a few percents. In all ABAQUS models developed in this study, the web is subdivided into ten elements and each half flange is subdivided into five elements. The number of the elements used in the longitudinal direction was selected in each application so that the aspect ratio of the S4R element used was close to unity. According to numerous studies (Mohareb and Dabbas 2003; Zinoviev and Mohareb 2004), the S4R element yields most accurate results when the aspect ratio tends to unity.

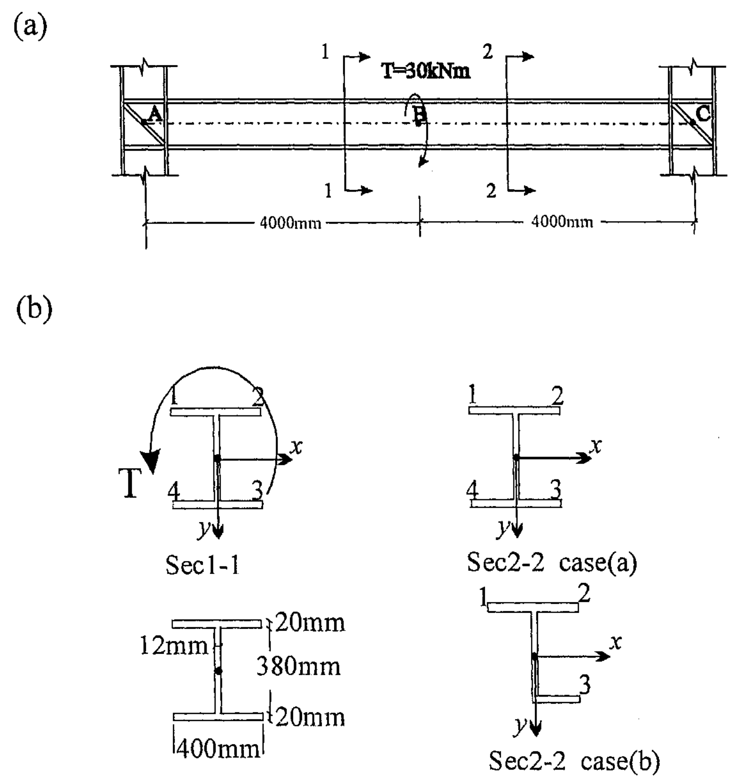

Fig.III.1 Example III.1:beam with coped flange. (a) Geometry, (b) cross-sectional dimensions

Example III.1: Beam with coped flange under Concentrated Twist

Statement of the problem

An eight meter span beam fully fixed at both ends is made of the wide flange section and subject to a 30 kNm twisting moment acting at mid span (Fig. III.1a). The cross-sectional geometries were previously given and are illustrated in Fig. III. 1b. Two cases are considered: Case a) the beam cross section is prismatic throughout the whole span AC, and Case b) Span AB remains identical to Case A while span BC has half of the bottom flange coped (Fig. III. 1b) possibly because of a spatial conflict with existing mechanical equipment. It is required to plot the displacement and the stress resultant diagrams.

This example illustrates the ability and efficiency of Element NOVEE14 to model members with stepwise cross-sectional changes, either due to coped flanges (as is the case in this example) or due to the addition of longitudinal stiffeners, or flange stiffening plates. It is recognized that, conventionally, the detail in Case b would in general be avoided by most engineers due to the associated complexities arising in the analysis. Nevertheless, the example remains a particularly suitable medium to convey key modeling ideas and concepts and provides insight on interpretation of results when applying the new solution scheme to other details.

Finite Element Mesh

In the ABAQUS model the beam is sub-divided into 200 elements in the longitudinal direction, consequently for case (a) 6,000 S4R elements were used whereas in case (b) 5,500 S4R elements were used. In contrast, only two NOVEE14 elements were adopted in each case.

Modeling complications under orthogonal coordinates

Under the conventional orthogonal solution scheme, the centroid of the section is a logical selection for the origin for Case a. Because the section is doubly symmetric, the centroid coincides with a) the shear centre, and b) the principal sectorial origin. The resulting system of equilibrium equations and the boundary conditions are uncoupled, a feature that considerably simplifies the solution of the equilibrium differential equations.

If the conventional technique based on orthogonal coordinates is to be adopted for case b, the centroid of the section along span AB remains the logical choice for the origin for the reasons outlined under Case a. For Span BC, an orthogonal system of coordinates necessitates to select an origin which coincides with the centroid of the *coped* section, (i.e. enforcing the conditions, $S_x = S_y = 0$). As a result, the polar axes for segments AB and BC become offset. Also, the orientation of the principal axes would have to be determined for segment BC (by enforcing the condition $J_{xy} = 0$), the shear centre would have to be located (by enforcing the conditions $J_{\omega x} = J_{\omega y} = 0$), and a principal sectorial coordinate would have to be determined (by enforcing the condition $S_\omega = 0$). Only then, would the equilibrium equations become uncoupled. The solution of the resulting uncoupled system of differential equations is relatively simple. However, the imposition of the compatibility relations at section B becomes quite cumbersome. For example, when expressing the continuity condition of the lateral displacement at point B, it is noted that the in-plane displacements at the pole $u(z), v(z)$ are no longer oriented in the horizontal and vertical directions, respectively. Also, they are no longer defined along the centerline of segment AB. More complications arise when expressing the remaining 13 compatibility relations at point B. (Also, if end C were simply supported, additional difficulties arise when attempting to express the seven boundary conditions at C. Such difficulties do not appear for a fully fixed support as all degrees of freedom at point C vanish). The above difficulties make the conventional solution difficult to implement for problems where a member experiences stepwise cross-sectional changes.

Modeling considerations under non-orthogonal coordinates

A non-orthogonal formulation provides more convenient means of avoiding these complications. For Spans AB and BC, the *pole* is selected to coincide with the *centroid of the un-coped section.* Thus displacements $u(z)$ and $v(z)$ will coincide with those of the centroid of the un-coped section. This selection also facilitates the imposition of boundary conditions at point C and the compatibility relations at point B. Secondly, in order to assign a physical significance to function $w(z)$ arising in the longitudinal displacement expression $w_s(s,z) = w(z) - x(s)u'(z) - y(s)v'(z) - \omega(s)\phi'(z)$ in which $\phi(z)$ is the angle of twist of the section about the longitudinal axis and all primes denote differentiation with respect to coordinate *z*, the *sectorial origin* is selected to coincide with the axes *origin*, i. e., $s = 0$ at $x(s) = y(s) = 0$. Also, the sectorial coordinate $\omega(s)$ will vanish at the origin, i.e., $\omega(s) = \omega(0) = 0$. By referring to the longitudinal displacement expression $w_s(s,z) = w(z) - x(s)u'(z) - y(s)v'(z) - \omega(s)\phi'(z)$, and noting that $x(0) = y(0) = \omega(0) = 0$, function $w(z) = w_s(0,z)$ becomes the longitudinal displacement at the *origin*. In contrast, in an orthogonal system, function $w(z)$, apart from being the average longitudinal displacement of the section, would not necessarily correspond to the displacement of any physical point on the cross-section. Thirdly, as the longitudinal displacement $w(z)$ function is now defined at the *origin* while the transverse displacements $u(z)$ and $v(z)$ are defined at the *pole*, it is desirable to make the *pole* and *origin* coincide, so that all three displacement components become defined at a single point. In most applications, the selection of an origin coinciding with the sectorial origin and pole will lead to simplifications in modeling and data interpretation. The selected point has to lie on the cross-section and should be located so as to simplify the application of the boundary conditions. The above scheme considerably facilitates the expression of the boundary conditions at point C and the continuity conditions at point B. In contrast, the equilibrium equations for span BC become uncoupled. This apparent complication has already been remedied as the general solution for the coupled field equations was provided in the previous chapter. Also, the corresponding NOVEE14 element is capable of numerically solving the coupled equilibrium equations without introducing any dicretization errors.

Results and Discussions

The close agreement between the new solution and ABAQUS-S4R results is observed for the longitudinal displacements (Fig. III.2a), the horizontal and vertical displacements (Fig. III.2b) and the angle of twist (Fig. III.2c). It is noted that all results displayed (displacements and forces) are related to the polar axis ABC (Fig. III.1) located at the centroid of the uncoped section, which also coincides with the origin and the sectorial origin axes. The longitudinal displacement for Case (b) is illustrated in Figure III.2a. Along segment AB, the longitudinal displacement assumes a linear distribution since the adopted coordinate system is orthogonal, thus eliminating the coupling between the longitudinal displacement and other flexural degrees of freedom. The first equilibrium equation for span AB reduces to the simple form $EA\, dw^2/dz^2 = 0$ which corresponds to a linear distribution for the longitudinal displacement $w(z)$. For segment BC, as the chosen coordinate system is non-orthogonal, the coupling between the longitudinal displacements and the flexural and torsional degrees of freedom is responsible for the observed non-linear distribution of the longitudinal displacement.

Unlike Case a, transverse displacements $u(z)$ and $v(z)$ for Case b do not vanish (Fig. III. 2b). For span BC, the presence of a twisting angle $\phi(z)$ introduces transverse displacements at any point not coinciding with the shear centre such as point B. This tendency is somewhat reduced (but not eliminated) due to the restraining action of span AB. The transverse displacements at end B are thus associated with biaxial bending moments and shears at node B. As a result, member AB can be regarded as subject to end bending moments and shears. This explains the linear bending moment distributions (Fig. III. 2d) and constant shear distributions along Span AB (not shown). Figure III.2d depicts the conjugate moment resultants $M_x = E(-S_x w' + J_{xy} u'' + J_{xx} v'' + J_{\omega y} \phi'')$ and $M_y = E(-S_y w' + J_{yy} u'' + J_{xy} v'' + J_{\omega x} \phi'')$ in which M_x and M_y are the moments of the stresses about the axis of reference ABC, and $J_{xx} = \int_A y^2 dA, J_{yy} = \int_A x^2 dA$ are the moments of inertia of the section about axis ABC. For segment AB, J_{xx}, J_{yy} are the principal centroidal moments of inertia, while for segment BC, they are non-centroidal and non-principal. The expressions for M_x and M_y naturally arose as boundary terms in Eq. (II.18) in Chapter II. Similar terms are also found in Gjelsvik (1981). For span AB, as the coordinates are orthogonal, the expressions simplify to the well-known moment curvature relationships $M_x = EJ_{xx}v''$ and $M_y = EJ_{yy}u''$. For span BC, such a simplification does not exist, and the conjugate expressions can be interpreted as the bending moment terms associated with *the selected origin.* It is of interest to note that the moment distribution along span BC remains linear. Figure III.2c provides a comparison of the angle of twist for Case a and Case b of NOVEE14 and ABAQUS S4R solutions. As expected, the peak value for the angle of twist is larger for the coped beam and the ABAQUS analysis gives slightly higher magnitudes for the transverse displacements and angle of twist relative to NOVEE14 analysis.

Figure III.2e depicts the twisting moment distributions along the coped and un-coped beams respectively. The St. Venant twisting moments exhibit a slight discontinuity at point B. At this location, although the derivative of the angle of twist is continuous, there is an abrupt change in the magnitude of St. Venant torsional constant due to the stepwise cross-sectional change. The conjugate warping twisting moments $E(S_\omega w'' - J_{\omega x}u''' - J_{\omega y}v''' - J_{\omega\omega}\phi''')$ naturally arising as boundary terms in Eq. (II.18) of Chapter II is also presented ($J_{\omega\omega} = \int_A \omega^2 dA$ is the second moment of the sectorial coordinate which coincides with the warping constant C_w only for orthogonal coordinates). The expression can be interpreted as the twisting moments associated with *the selected pole.* The warping twisting moment $-EC_w\phi'''$ is plotted for comparison. It is of interest to note that both expressions coincide only when a) the pole coincides with the shear center i.e., $J_{\omega x} = J_{\omega y} = 0$, and b) when the principal sectorial origin is adopted, i.e., $S_\omega = 0$. This is the case for span AB and is not for span BC.

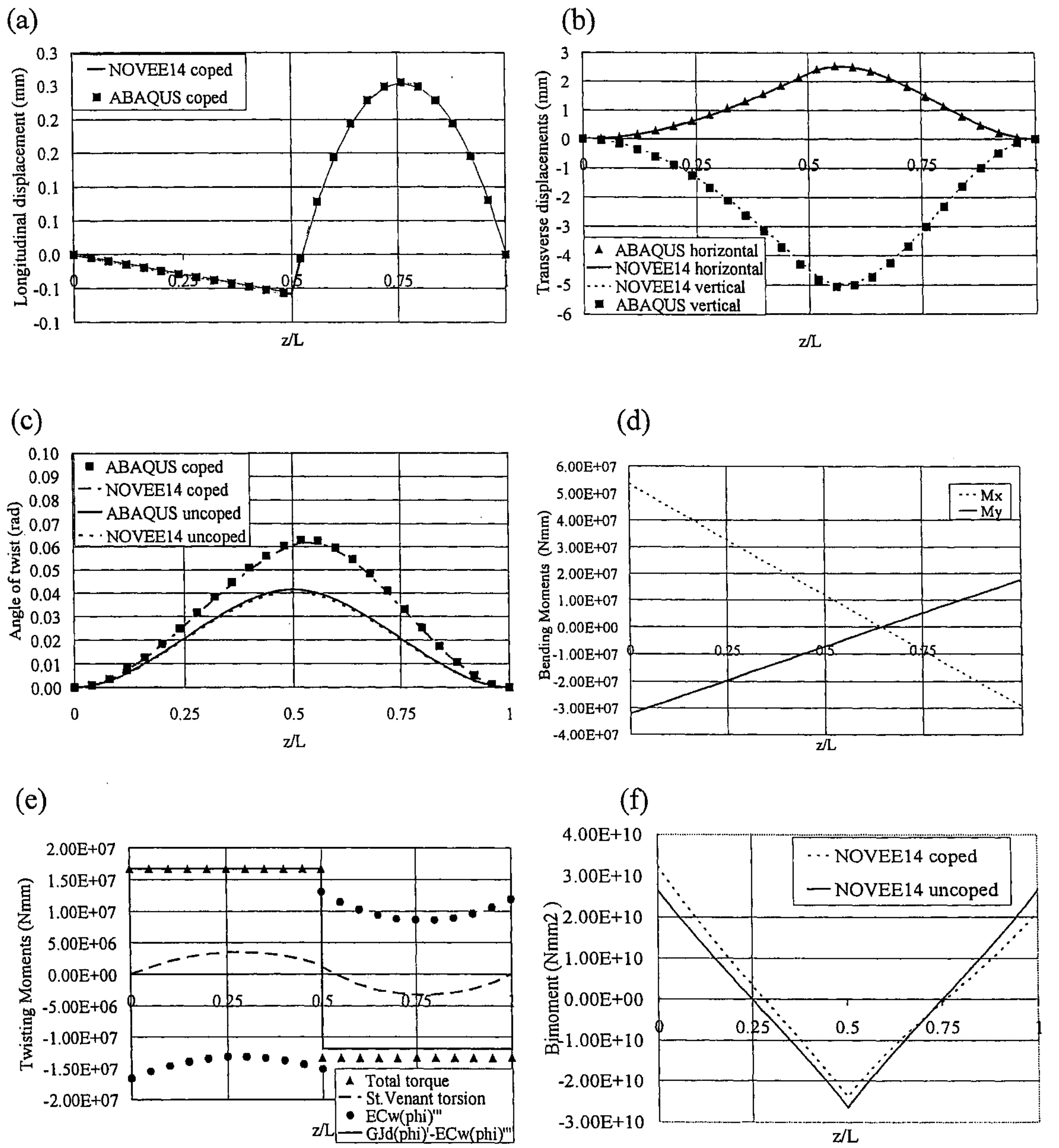

Fig. III.2 Displacements and internal forces for example III.1: (a) longitudinal displacements case B, (b) transversal displacements case B, (c) angle of twist, (d) bending moments for case B, and (f) bimoments

Figure III.2f depicts the energy conjugate bimoment expressions $E\left(-S_\omega w'+J_{\omega x}u''+J_{\omega y}v''+J_{\omega\omega}\phi''\right)$ for the coped and un-coped sections. At point A, the bimoments are larger for the coped beam (Case a) than for the un-coped beam (Case b). At point C, a reverse observation can be made. As expected, the stronger span AB in

Case b attracts more bimoments than the weaker span BC. It is of interest to note that the bimoments to the left of point B for the coped beam are slightly less than those for the un-coped beam.

Figures III.3a through III.3c depict the normal and shear stress distributions immediately to the left and to right of section B for case (a) (Fig. III. 3a), and Figs. III.3b,c for case (b) where the nodal internal force vector was obtained by pre-multiplying the nodal displacement vector by the element stiffness matrix. The nodal stress resultants are then substituted into stress-stress resultant relations. It is important to note that the stress – stress resultant relations provided in many texts (Vlasov 1961, Seaburg and Carter 1997) are applicable only to orthogonal coordinate systems. Under non-orthogonal coordinates, a complete formulation for stress-stress resultant relations is provided in the next chapter. Some of the ingredients of the solution are also found in Gjlesvik (1981). It is noted that by adopting a solution based on a conventional orthogonal coordinate system, the stress distributions obtained are expected to exactly match the ones reported in this study.

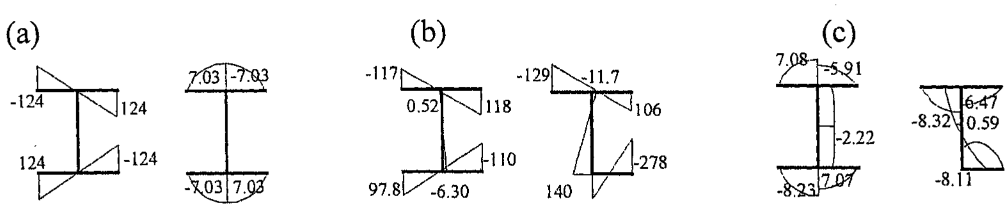

Fig. III.3 Stress diagrams for example III.1. (a) Normal and shear stress (MPa) at section B for case A. (b) Normal stress (MPa) at section B for case C. (c) Shear stress (MPa) at section B for case B.

Example III.2: Eccentrically Braced Member Subject to Concentric Force

Eccentrically Braced Members

In steel construction, a concentrically loaded vertical member such as the vertical member C_TC_B in Figures III.4a would normally be detailed such that the centroidal axis of the inclined brace would pass through point C_T located on the centreline of the vertical member.

Due to an obstacle along the desired line of action of the brace, the orientation of the brace is shifted to pass through point O_T located on the centroid of the left flange of the column instead. As a result, the vertical member becomes eccentrically braced.

Statement of the Problem

Member C_TC_B in Fig. III. 4a-d has the same cross-section as that of Example III.1 with a member height of $10{,}000mm$. The member is subjected to a concentrated load $P = 200kN$ applied at end $z = 0$ acting at the section centroid. The member is assumed completely fixed at the bottom end $z = 10{,}000mm$ and partially restrained at the top end $z = 0$ by the action of a) a brace with an angle of inclination of 2: 1; and b) a horizontal beam. The effect of the braces is incorporated in the analysis by modelling them as linearly elastic springs. The horizontal spring constant k_1=160 *kN/mm* incorporates the effects of a) the flexibility of the beam in the axial direction; and b) the flexibility of the supporting frame. The inclined spring constant k_2=120 *kN/mm* is obtained from the axial stiffness of the brace. It is required to determine the bending moment diagram and deflected shape of the vertical member under the given load and support conditions.

Shell finite element mesh

The general aspects of the shell FEA model were provided in the section titled "Details of the Shell Finite Element Models". The specifics of the model related to this example are: the member is subdivided into 250 elements along the longitudinal direction. The model thus consists of 7,500 S4R elements. The fixed end is modeled by restraining all six degree of freedom at all nodes at the bottom end, whereas the eccentric support is modelled by two linear springs acting along the directions of the eccentric braces.

Numerical solution based on NOVEE14

The load applied represents about 20% of the flexural buckling load of a column fixed at the bottom and completely free at the top. Thus, the geometric non-linear effects are assumed negligible in the analysis. The partial restraint provided by the beam and brace are modelled as two elastic springs acting at point O_T.

Member C_TC_B is modelled using a single NOVEE14 element. By selecting a conventional orthogonal coordinate system (the pole, origin, and sectorial origin to coincide on axis C_TC_B), the boundary conditions at the top of the column become complex and the resulting system becomes somewhat tedious to resolve by hand. This difficulty is remedied by selecting the origin, pole and the sectorial origin to coincide at the point of action of the eccentric braces (along axis O_TO_B) instead. This unconventional selection simplifies the expressions for the boundary conditions at the top of the member but leads to coupled equations of equilibrium. Since element NOVEE14 seamlessly resolves such a coupled system, this difficulty is not transparent to the analyst and the later solution is associated with a smaller modeling effort than the former one.

Results and Discussions

Figure III.4f shows excellent agreement between the displacements predicted by the NOVEE14 model (using a single element) and the ABAQUS S4R model (using 7500 elements), in which the ABAQUS model exhibits a slightly more flexible behaviour. This is attributed to the fact that the ABAQUS shell solution incorporates shear deformation effects while the Vlasov formulation on which element NOVEE14 is based neglects this effect. It is noted that by using multiple NOVEE14 elements, the results obtained are in exact agreement with those based on a single element. This is a natural outcome of the fact that NOVEE14 is based on shape functions which exactly satisfy the Vlasov equilibrium equations and thus involves no discretization errors.

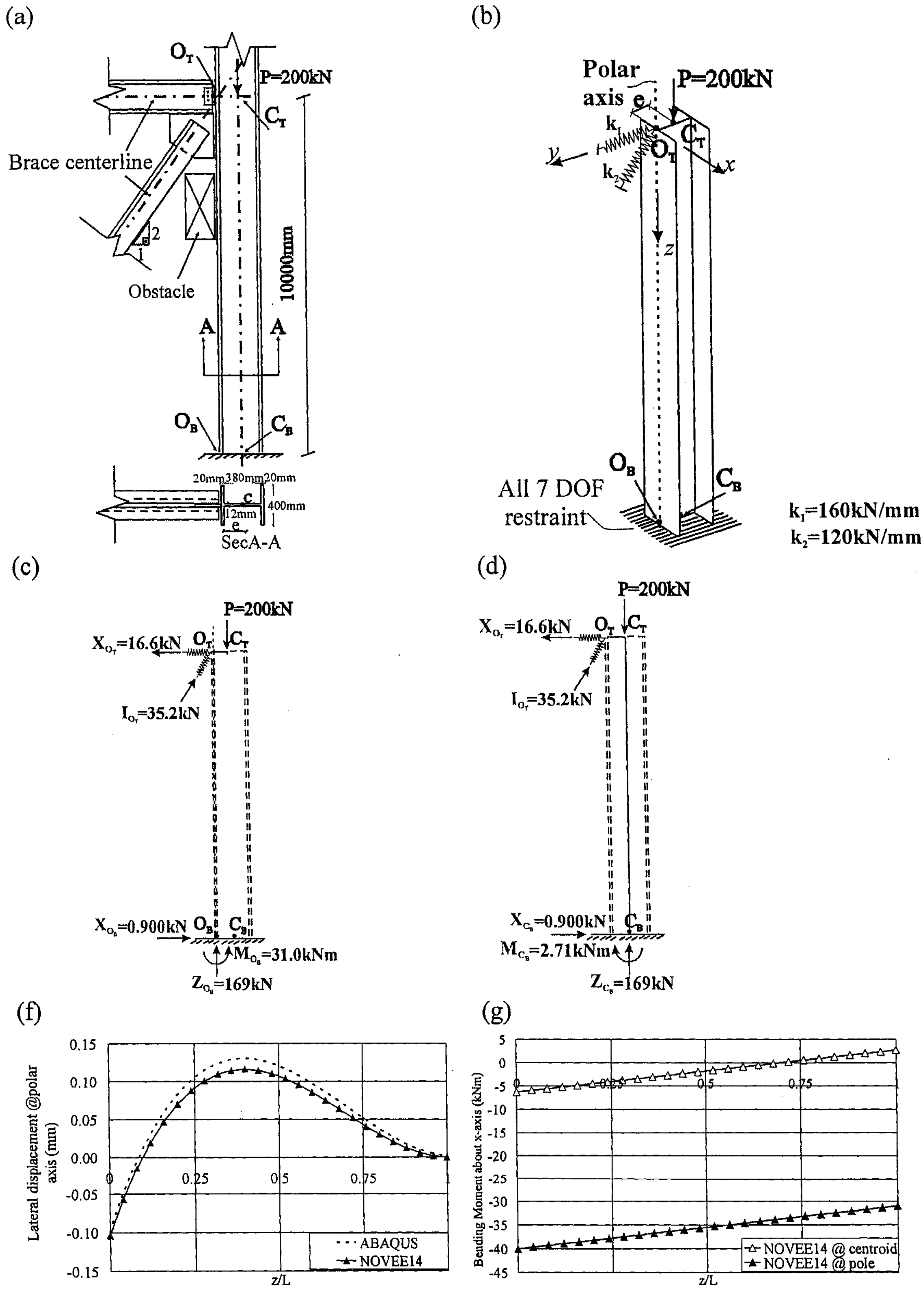

Figure III.4 Example III.2-Eccentrically braced member (a) Vertical member braced by eccentric diagonal and horizontal members (b) Column with eccentric support (c) Idealization based on a polar axis O_TO_B (d) Conventional model for Example III.2 based on centroidal axis C_TC_B (e) Transverse displacement (f) Bending moments

Figure III.4g provides a comparison between the bending moment diagrams based on the NOVEE14 model defined with respect to the eccentric origin (Axis O_TO_B), as obtained from the energy expression (Eq. (II.18) in chapter II) and the conventional bending moments defined with respect to the centroidal axis (Axis C_TC_B) by taking the free body diagram for the member after the forces in the braces have been determined. It can be verified that difference between the two bending moments as given in Figs. III.4c,d $M_{O_b} - M_{C_b} = 31.0 - (-2.71) = 33.7\,kNm$ is equal to the product of eccentricity e=200 *mm* by the vertical support reaction $R \times e = 168.5kN \times 0.20 = 33.7kNm$

Example III.3: Beam with rectangular hole

Rectangular holes in steel members are frequently needed to accommodate heating ducts, ventilation and air conditioning (HVAC) and other utility pipes. Longitudinal stiffeners are conventionally welded around the holes, in order to reinforce the weakened hole zone (Fig. III. 5a, b).

Statement of the problem

A 6,000 *mm* span simply supported beam has a rectangular hole spanning 2,000 *mm* located in the middle of the beam span. The beam is subject to a vertical load of 50 *kN* applied to the top flange of the beam at mid-span (Fig. III. 5a). The cross-section dimensions are presented in Fig. III. 5b. It is required to obtain the vertical displacements of the beam based on NOVEE14 model and to compare the results with those based on ABAQUS shell formulation

Modelling Considerations

The ABAQUS finite element shell mesh is illustrated in Fig. III. 5c. At the supports, the cross-section centroid is restrained against the three translational degrees of freedom. The NOVEE14 model consists of four elements (Fig. III. 5d). Elements 2 and 3 spanning between nodes 2 and 3 represent the members above and below the rectangular hole, respectively. The origin, pole and sectorial origins of all four elements coincide with the beam centroidal axis in order to directly impose the boundary conditions $u = v = w = 0$ at both ends of the beam. Consequently, the sectorial origins for elements 2 and 3 do not lie within the cross-section, resulting in an apparent conceptual contradiction with the Vlasov formulation, in which the sectorial origin has to lie within the cross-section. This contradiction can be resolved by conceiving the sections of elements 2 and 3 as having fictitious arms of zero thickness, joining the cross section of the element to the centroidal axis of the beam (Fig. III. 5d).

Results and Discussion

Figure III.5e provides a comparison of the vertical displacements based on NOVEE14 and ABAQUS S4R models. The displacements of the top and bottom flanges based on ABAQUS S4R model are depicted. The NOVEE14 model produces the displacement curves at the poles of the elements. For the current example, the angle of twist vanishes. Thus, as a result of the first Vlasov assumption, the vertical displacements for all points of a cross-section are equal. The NOVEE14 solution provides distinct deflection curves for elements 2 and 3 (Fig. III. 5e). As expected, under the load locally applied to element 2, the member exhibits more deflection than element 3. In contrast to conventional beam analysis in which members 2 and 3 would be considered as a single element, the shrinking of the hole under load P is successfully captured. The results are found to be in very close agreement with the ABAQUS S4R model.

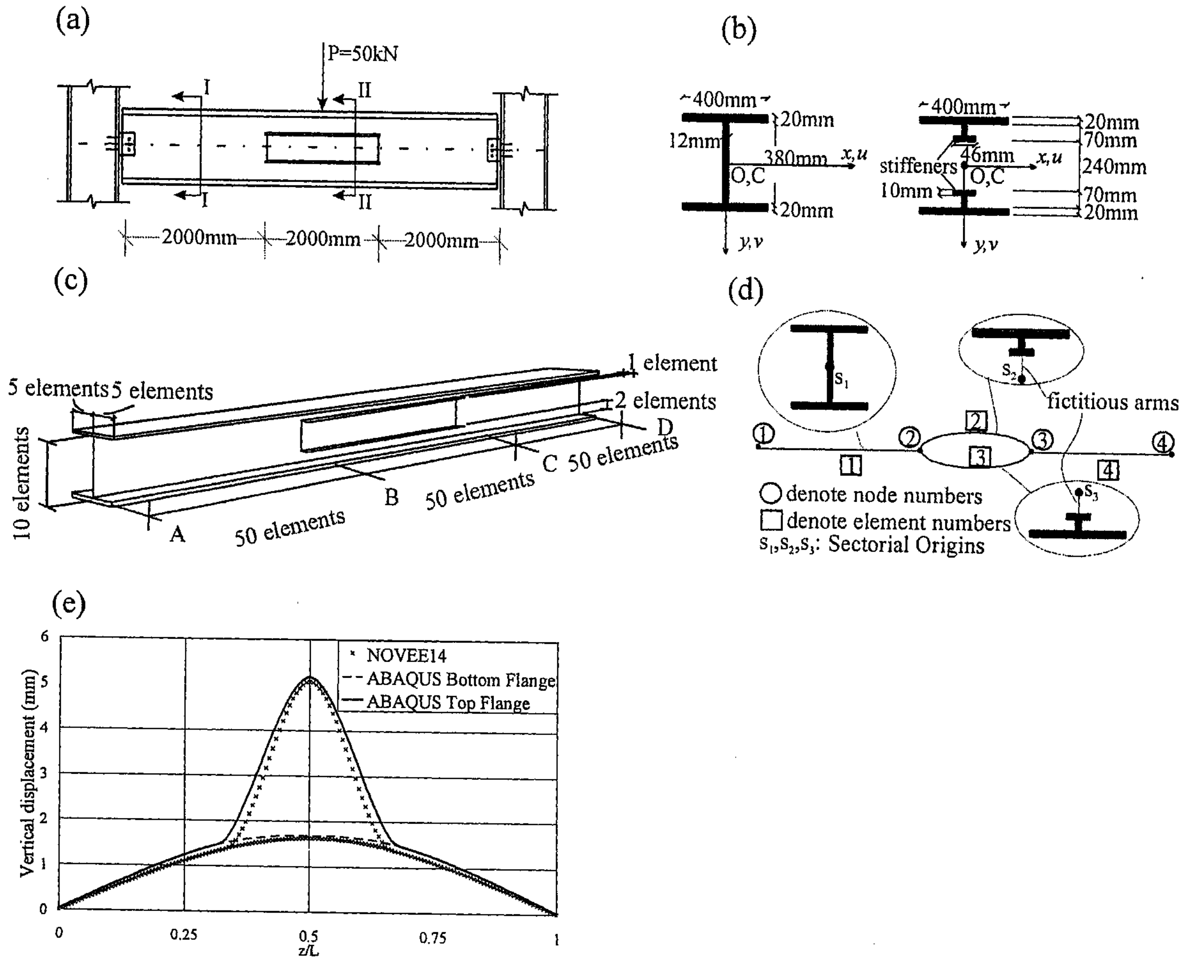

Figure III.5 Example III.3-Beam with rectangular hole (a) Geometry (b) Cross-section dimensions (c) Mesh for shell Finite element (d) Mesh of NOVEE14 model (e) vertical displacements

Modelling considerations for un-reinforced holes

It is of interest to note that, had the hole been un-reinforced, the middle section of the beams would have resulted into two tee sections, each having zero warping stiffness (under the Vlasov theory). If the loading applied involves lateral and/or torsional forces, Element NOVEL12 based on zero warping stiffness should be used for the modeling of elements 2, and 3 while Element NOVEE14 should be used for elements 1 and 4. That is because for sections with zero warping stiffness, $k = \sqrt{GJ_d / EC_w} \rightarrow \infty$ can not be used in calculating stiffness coefficients of the sub-matrix $\mathbf{K}_{44}$ (Appendix II.D). One can pursue the analysis with element NOVEC14 (Appendix II.F). However, for a zero warping constant, the torsional behaviour of element NOVEC14 is overly stiff and the results based on this element converge to those based on element NOVEL12 only when the number of NOVEC14 elements is increased. This is illustrated in Appendix III.A.

Example III.4: Eccentrically supported beam under uniform lateral load

Statement of the problem

Occasionally, beams in industrial plants as well as purlins and girts in steel buildings, are welded on top of other structural steel components. Conceptually, the behaviour of such members, which are eccentrically supported relative to the line of action of lateral loads, tend to twist, a feature that is successfully captured by the current formulation. Figures III.6a, b illustrate such a beam with a span of 16,000 *mm* (maximum slenderness ratio $L/r_y \cong 160$, in which the minimum radius of gyration $r_y = \sqrt{J_{yy}/A}$). For the shown beam, while the bottom flange is fully restrained against displacements and rotations, the top flange is free to rotate. The boundary conditions are such that the degrees of freedom u, v, w, ϕ, u', v' are restrained at the centerline of the *bottom* flange (as opposed to the centroid of the section in the case of a conventional concentric support). A laterally distributed load $q = 1.0 kN/m$ is applied through the centroidal axis of the member (Figs.

III.6a, b). It is required to analyze the problem using ABAQUS-S4R, NOVEE14 and NOVEC14 models.

Shell finite element model

The ABAQUS model is subdivided into 400 elements in the longitudinal direction. Thus, a total of 12,000 shell elements are used. The boundary conditions are applied at both ends by restraining all six degrees of freedom of point O (Fig. III. 6a) located at the centre of the bottom flange.

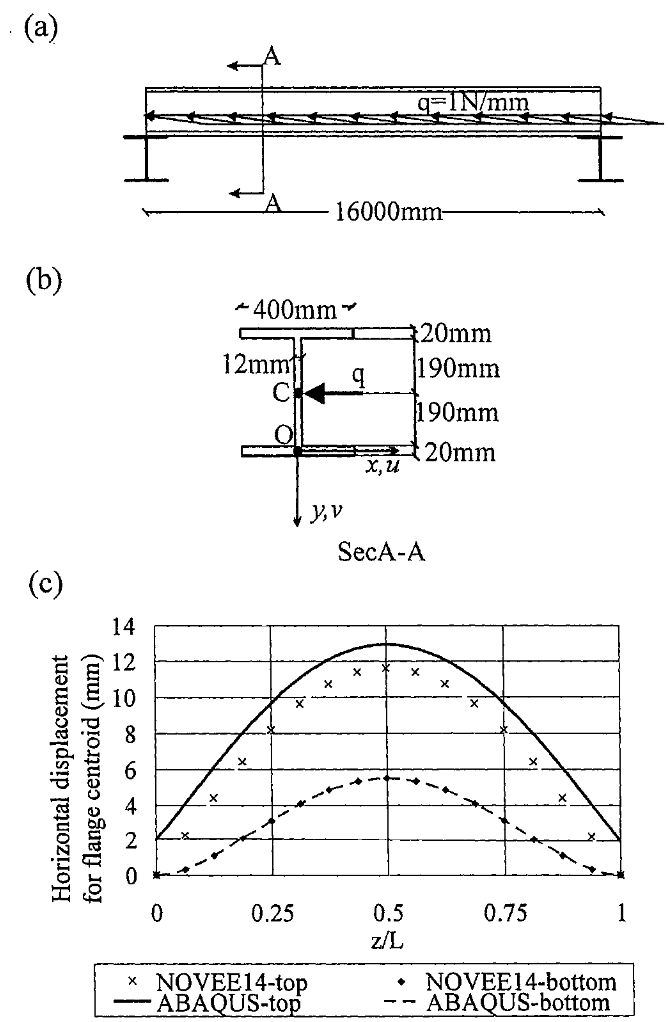

Figure III.6 Example III.4-Eccentrically supported beam (a) Geometry (b) Cross-section dimensions (c) Horizontal displacements

Finite element details for NOVEE14 and NOVEC14

In the NOVEE14 and NOVEC14 models, the origin, pole and sectorial origin are selected to coincide at the center of the bottom flange (Fig. III. 6b). This selection is particularly convenient to impose the boundary conditions $w = u = v = \phi = u' = v' = 0$ at the centroid of the bottom flange at the supports (the bottom flange thickness is considered negligible in this example). As the distributed load $q = 1.0kN/m$ is offset from the selected pole, the line of action of the load is represented by the axis defined by the coordinates $x = 0$, $y = -200mm$ and $\omega = 0$. Two NOVEE14 solutions are conducted using a single element and 16 elements, respectively. For the NOVEC14 element five analyses were conducted using a single, two, four, eight and 16 elements of equal length. Expressions for the energy equivalent nodal forces based on an applied line load under both NOVEE14 and NOVEC14 were developed in chapter II and are used in the solution of this problem.

Results

Table III.1 provides a comparison of the derivative of the angle of twist at the end nodes, which is the only active degree freedom at the supports. It is of interest to note that, although the FEA formulation is based on the exact solution of the homogeneous case, and that in the given example, the differential equations of equilibrium are non-homogeneous due to the presence of the member line load, the solution based on a single NOVEE14 element exactly matches that based on 16 NOVEE14 elements. As a general comment, this will always be the case irrespective of the loading function applied. A formal proof of this statement is presented in Appendix II.E in Chapter II, which extends the exactness of the FEA nodal values for the general non-homogeneous in the case of Element NOVEE14.

In contrast, as the displacement fields in NOVEC14 formulation do not satisfy the exact equilibrium conditions, the solution involves a discretization error. For a single NOVEC14 element, the dimensionless parameter $kl = \sqrt{GJ/EC_w} l = 5.067$ is quite large, and the approximate solution based on the limiting value $kl = 0$ causes a relatively large error of 13.85 %. For 16 elements, $kl = 0.317$ for each element and the error significantly reduces to 0.0005 %. In this case, the solution approaches the one provided by the NOVEE14 model.

Figure III.6c provides a comparison between the horizontal displacements of the top and bottom flanges based on the ABAQUS-S4R and NOVEE14 solutions. Sixteen NOVEE14 elements were used in order to directly obtain the displacements at intermediate nodes shown. The displacements of top flange based on the NOVEE14 model were calculated simply by adding the effect of the cross-section rotation to the horizontal displacement at the bottom flange based on the first Vlasov assumption. Excellent agreement between the two solutions is obtained for the bottom flange. For the top flange, reasonable agreement is obtained between the two solutions. It is noted that under the NOVEE14 solution, the top flange out of plane displacement vanishes. This is a direct result of the fact that the element enforces the first Vlasov kinematic assumption $u_s(s,z) = u(z) - \left[y(s) - a_y \right] \phi(z)$ which relates the displacement $u_s(s,z)$ to the shear centre displacement $u(z)$ (a_y is the y coordinate of the shear centre and vanishes in this example). For instance, the left support $z = 0$, is such that the lateral displacement at the pole displacement $u(0)$ and the angle of twist $\phi(0)$ are zeros. As a result, the transverse displacement for any point $u(s,0)$ at the section $z = 0$ vanishes as well. In contrast, in the ABAQUS S4R model, relative lateral movement between the two flanges is allowed. As a result, the top flange undergoes a small displacement relative to the bottom flange as depicted in Figure III.6c.

If the beam is considered as simply supported, the lateral displacement δ predicted by the closed form solution available in many texts $\delta = 5ql^4/384EJ_{yy}$ is 20.0 *mm*. On the other extreme, if the beam is considered as fixed at both ends, the lateral displacement predicted by the closed form solution $\delta = ql^4/384EJ_{yy}$ reduces to 4.0 *mm*. These values exactly coincide with those obtained based on two NOVEE14 solutions. The corresponding ABAQUS S4R predictions are 20.2 *mm* and 4.05 *mm* respectively.

Table III.1 Comparison of results based on elements NOVEE14 and NOVEC14 for Example III.4

Element Type	Number of Elements	Corresponding *kl*	warping at supports (rad/mm)	Percentage Difference
NOVEE14	1	5.067	5.665E-06	0.0000%
NOVEE14	16	0.317	5.665E-06	0.0000%
NOVEC14	1	5.067	4.880E-06	13.8500%
NOVEC14	2	2.533	5.585E-06	1.4100%
NOVEC14	4	1.267	5.659E-06	0.1100%
NOVEC14	8	0.633	5.664E-06	0.0083%
NOVEC14	16	0.317	5.665E-06	0.0005%

Under the Vlasov assumptions, the bottom flange can be considered as fixed ($u(0)=0, u'(0)=0$ at the flange centroid) while the top flange is considered as simply supported (the centroid of top flange is laterally restrained under Vlasov's kinematic assumption as explained previously) while it remains free to warp since $\phi'(z=0) \neq 0$. Thus, the support condition depicted lies somewhere between the fully fixed condition and the simply supported condition. As a result, it is expected that the lateral displacements would lie between these two bounds. Indeed, this is found to be the case since the lateral displacement based on the NOVEE14 model is found to be 5.8 *mm* for the bottom flange and 11.8 *mm* for the top flange with an average value of 8.8 *mm*, which lies in between the expected bounds 4 *mm* and 20 *mm*.

Conclusions

The finite element solution presented in Chapter II is shown capable of extending the applicability of the Vlasov theory to a wide range of applications involving steel members made of open sections. This includes members with stepwise cross-sectional changes, rectangular holes and longitudinal stiffeners, and eccentric supports in an efficient and seamless way. Irrespective of member load distributions, the NOVEE14 formulation yields nodal displacements and internal forces in exact agreement with the Vlasov thin-walled beam theory, while using a remarkably small number of degrees of freedom.

It is important to stress that, although the solutions based on finite element NOVEE14 exactly match those based on the Vlasov thin-walled beam theory, its applicability to practical situations is limited by the assumptions/simplifications made within the theory. Specifically, the Vlasov theory neglects material nonlinear behaviour, residual stress effects, local, distortional, and member buckling effects. The agreement of results based on the new solution with those based on elastic ABAQUS-S4R shell finite element models in which the above effects were deliberately suppressed, provides an indication of the correctness of the formulations presented in Chapter II. However, this agreement should not be misconstrued to suggest that the assumptions of the Vlasov theory nor the FEA formulations developed based upon these assumptions will invariably represent real response of structural steel members as observed in the field nor in experiments. For example, members of very thin webs may undergo web distortion, which is neither captured by the present formulation, nor the ABAQUS FEA model both based on Vlasov assumptions.

Appendix III.A-Torsional analysis of a member with zero warping stiffness

The objective of this appendix is to illustrate the convergence characteristics of the elements NOVEE14, NOVEC14 and NOVEL12 when modeling a beam with zero warping stiffness. Elements NOVEL12 and NOVEC14 are used to model a 2,000 mm span cantilever beam of tee cross-sections. An external torsional moment of 50Nm is applied at the tip of the cantilever as shown in Fig. III.A.1a. The cross-section dimensions are presented in Fig. III.A.1b. The origin, pole and sectorial origin are chosen to coincide at the point of connection of the flange and the web of the cross-section.

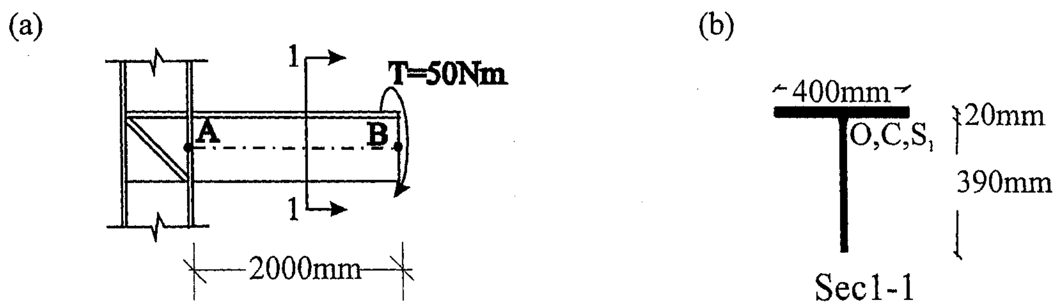

Figure III.A.1 Cantilever beam with tee section (a) Geometry (b) Cross-section dimensions

Table III.A.1 provides a comparison of the angle of twist at the tip of the cantilever (point B in Fig. III.6a) calculated by using elements NOVEL12 and NOVEC14. The results show that element NOVEL12 provides exact nodal values where element NOVEC14 underestimates the angle of twist and the discretization errors in the analysis based on NOVEC14 reduces to 0.71% for 16 elements.

Table III.A.1 Comparison of results based on elements NOVEL12 and NOVEC14 for a cantilever subject to torsion

Element Type	Number of Elements	Angle of twist at the tip (rad)	Percentage Difference
NOVEL12	1	1.002E-03	0.00%
NOVEL12	16	1.002E-03	0.00%
NOVEC14	1	8.909E-04	11.09%
NOVEC14	2	9.433E-04	5.86%
NOVEC14	4	9.727E-04	2.92%
NOVEC14	8	9.875E-04	1.45%
NOVEC14	16	9.949E-04	0.71%

It is of interest to note that when attempting the solve the problem using element NOVEE14, an overflow error was found to occur as the hyperbolic functions $\sinh kl$ and $\cosh kl$ in stiffness terms of this element (Appendix II.D) are infinite for $k \to \infty$.

Chapter III References

[III.1] CAN/CSA-S16-2001 Limit states design of steel structures. Canadian Standard Association, Rexdale, Ontario.

[III.2] Erkmen, R.E. 2006. Finite element formulations for the analysis of thin-walled members. Ph. D. Thesis, Department of Civil Engineering, University of Ottawa, Ottawa, ON, Canada.

[III.3] Erkmen, R.E. and Mohareb, M., 2006. Non-orthogonal solution for thin-walled members - A Finite Element Formulation, Canadian Journal for Civil Engineering, this issue.

[III.4] Hibbit, H.D., Karlsson, B.I., and Sorensen, E.P. 2001. ABAQUS User's manual. Version 6.5, Pawtucket, U.S.A.

[III.5] Hibbit, H.D., Karlsson, B.I., and Sorensen, E.P. 2001. ABAQUS Theory manual. Version 6.5, Pawtucket, U.S.A.

[III.6] Gjlesvik, A. 1981. The theory of thin walled bars, John Wiley and Sons, New York, U.S.A.

[III.7] Mohareb, M., and Dabbas, A. 2003. Lateral stability of partially restrained cantilever supports. Annual Stability Conference Baltimore. Maryland, April 2003.

[III.8] Seaburg, P.A., and Carter, C.J., 1997. Torsional Analysis of Structural Steel Members. American Institute of Steel Construction, Chicago, IL, USA.

[III.9] Vlasov, V.Z., 1961. Thin Walled Elastic Beams. Second Edition, Israel Program for Scientific Translations, Jerusalem, Israel.

[III.10] Zbirohowski-Koscia, K. Thin Walled Beams, From theory to practice, Crosby Lockwood & Sons, London.

[III.11] Zinoviev, I., and Mohareb, M. 2004. Analysis and design of laterally unsupported portal frames for out-of-plane stability". Canadian Journal of Civil Engineering, 31(3), 440-452.

Chapter III List of symbols

The following symbols were used in this paper

A	=	cross-sectional area;
b	=	flange width;
C_w	=	warping constant;
d	=	section depth;
E	=	modulus of elasticity;
G	=	shear modulus;
$J_{xx}, J_{yy}, J_{xy}, J_{\omega x}, J_{\omega y}$	=	section moments of inertia and products of inertia;
$J_{\omega\omega}$	=	second moment of the sectorial coordinate;
$M_x(z), M_y(z)$	=	bending moments in a non-orthogonal coordinate system;
NOVEE14	=	Non-Orthogonal Vlasov Element based on Exact shape functions with 14 degrees of freedom
NOVEC14	=	Non-Orthogonal Vlasov Element based on Cubic shape functions with 14 degrees of freedom
NOVEL12	=	Non-Orthogonal Vlasov Element based on Linear shape functions with 12 degrees of freedom
S_x, S_y, S_ω	=	first moments of area of coordinates *x, y,* and ω;
s	=	curvilinear coordinate along mid surface (Fig. III.1, Fig. III.2);
t	=	flange thickness;
$u(z), v(z)$	=	displacements along x, y directions of arbitrary pole

$w(z)$	=	displacement function appearing when expressing the longitudinal displacement function $w_s(s,z)$ of any point s located on the section contour;
w	=	web thickness;
z	=	longitudinal coordinate;
$\phi(z)$	=	angle of twist about the longitudinal axis;
μ	=	Poisson's ratio; and
$\omega(s_0,s)$	=	sectorial area based on sectorial origin s_0;

Chapter III List of Tables

Chapter III List of Figures

Chapter IV

Non-orthogonal solution for thin-walled members – Generalized Expressions for Stresses

Abstract

The Vlasov thin-walled beam theory (Vlasov 1961) leads to four differential equations of equilibrium. In general, these equations are coupled. Conventional solution techniques attempt to eliminate the coupling between the equations by adopting an orthogonal system of coordinates. (i. e., adopting the centroidal principal axes, and adopting the line joining the section shear centre and principal sectorial origin as a fixed radius). This approach generally suffers from a number of drawbacks including: a) the necessity to perform coordinate transformations, b) the difficulties in handling cross-section discontinuities where members undergo stepwise sectional changes (e.g., members with holes, flange copes, presence of longitudinal stiffening plates, etc.), c) the boundary conditions may remain or become uncoupled after transformation, and; d) the adoption of an orthogonal system of coordinates may necessitate resolving the internal and external forces along the orthogonal coordinate systems. As a result, the use of the conventional solution technique has been limited to very simple applications. In Chapter II a general solution of the Vlasov thin-walled beam theory under non-orthogonal coordinate system was developed in a finite element context, which offers a number of modelling advantages when compared to conventional solutions based on orthogonal coordinates. The objective of the current chapter is to complement the study in Chapters II and III by developing general expressions for normal and shearing stresses under non-orthogonal coordinate systems.

Keywords: Finite Element, thin-walled beams, non-orthogonal coordinate systems, stress expressions.

Introduction and Scope

The thin-walled beam theory developed by Vlasov (1961) leads to four coupled differential equations of equilibrium. The equilibrium equations are formulated in terms of the cross-section rigid body displacements and in-plane rotation. Conventional solution techniques for the equilibrium equations attempt to eliminate the coupling between the differential equations of equilibrium (e.g., Murray 1984). This is realized by adopting an orthogonal system of coordinates. (i. e., adopting the centroidal principal axes, and adopting the line joining the section shear center and principal sectorial origin as a fixed radius). While this approach successfully uncouples the equations of equilibrium, it generally suffers from a number of drawbacks including: a) the necessity to perform coordinate transformations, b) the difficulties in handling cross-section discontinuities where members undergo abrupt section changes (e.g., members with holes, flange copes, presence of longitudinal stiffening plates, etc.), c) the boundary conditions may remain or become uncoupled after transformation, and; d) the adoption of an orthogonal system of coordinates may necessitate resolving the internal and external forces along the orthogonal coordinate systems. As a result, the conventional solution technique has been used for very simple applications.

Assumptions

The formulation is restricted to prismatic thin-walled elements of arbitrary cross-sections. Material is assumed to behave elastically. Small displacements and rotations are assumed. Thus, geometric non-linear effects are assumed negligible. The formulation is based on the two classical assumptions of the thin-walled beam theory (Vlasov 1961). These are: a) no distortion of cross-section during deformation, and; b) shearing strains acting on the middle surface are negligible.

Description of the Problem

A prismatic thin walled beam element of arbitrary cross-section is considered. The element (Fig. IV.1) is subject to externally applied tractions $\bar{\sigma}_0 = \bar{\sigma}_{zz}(s,0,r)$ and $\bar{\tau}_0 = \bar{\tau}_{zs}(s,0,r)$ acting at end $z=0$, and $\bar{\sigma}_l = \bar{\sigma}_{zz}(s,l,r)$ and $\bar{\tau}_l = \bar{\tau}_{zs}(s,l,r)$ acting at end $z=l$, in addition to general member tractions $\mathbf{p}(\mathbf{s},\mathbf{z})^{\mathrm{T}}_{1\times3} = \langle p_x \quad p_y \quad p_z \rangle_{1\times3}$. Coordinate r is the normal distance from the mid-surface. The displacement fields, governing equilibrium equations, and boundary conditions for such a beam are provided in the following sections.

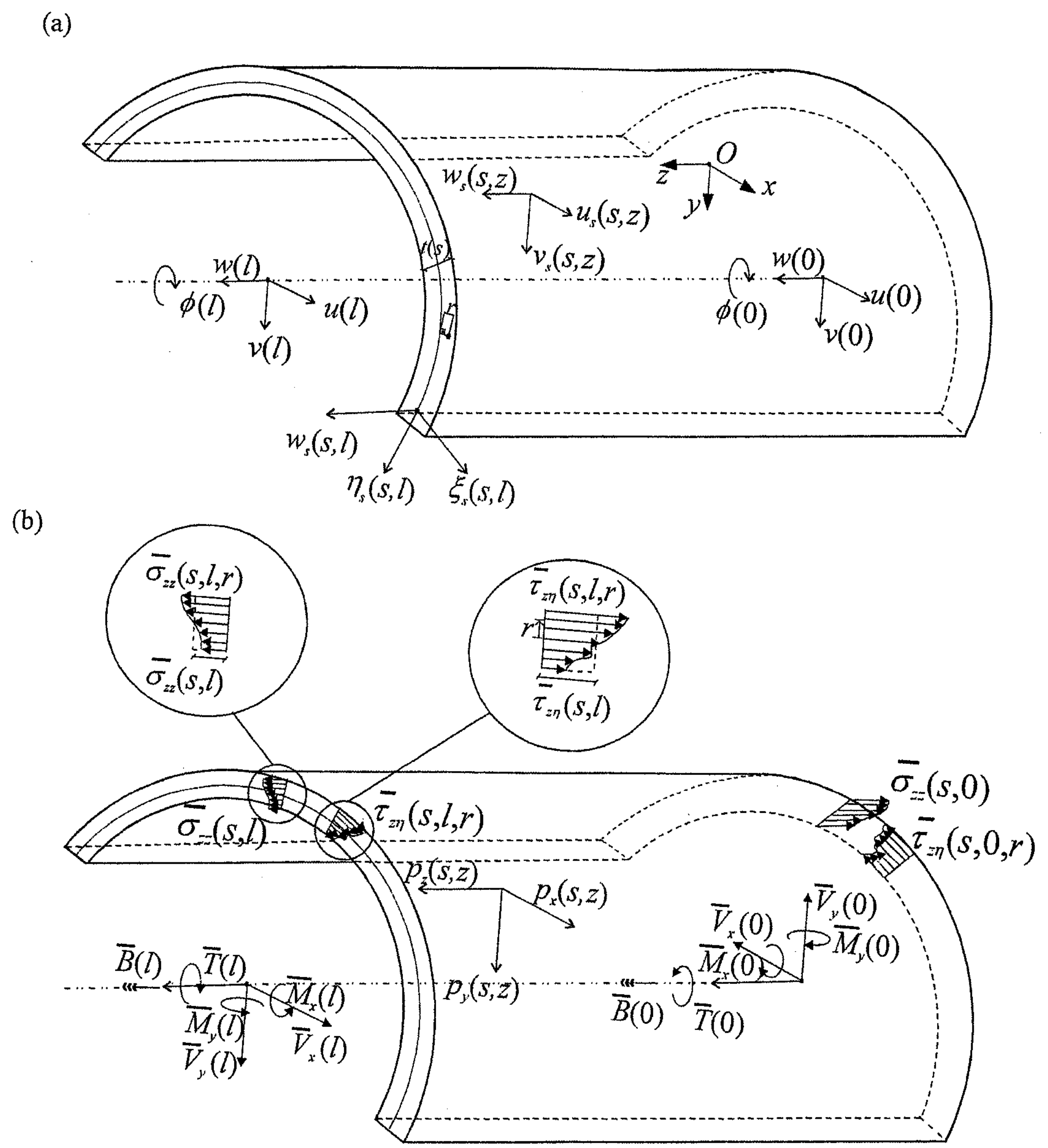

Fig. IV.1- Thin wall beam geometry (a) generalized displacements, (b) generalized forces and stresses

Displacement Fields

Under the Vlasov theory, the in-plane components of the displacement $u_s(s,z)$ and $v_s(s,z)$ of an arbitrary point B_p located on the section mid-surface is expressed in terms of a) the angle of twist $\phi(z)$ of the cross-section and; b) the in-plane displacement components $u(z)$ and $v(z)$ of a pole $A_p(a_x, a_y)$ arbitrarily located in the plane of the cross-section (Fig. IV.2.a). Coordinate s, measured from an arbitrary sectorial origin S_0 located on the section profile, identifies coordinates $[x(s), y(s)]$ of point B_p. Thus,

$$u_s(s,z) = u(z) - \left[y(s) - a_y\right]\phi(z) \tag{IV.1}$$

$$v_s(s,z) = v(z) + \left[x(s) - a_x\right]\phi(z) \tag{IV.2}$$

Also, the longitudinal displacement is expressed as

$$w_s(s,z) = w(z) - x(s)u'(z) - y(s)v'(z) - \omega(s)\phi'(z) \tag{IV.3}$$

in which $d\omega(s) = h(s)ds$, $h(s) = (x - a_x)\sin\alpha(s) - (y - a_y)\cos\alpha(s)$ (Fig. IV.2.b) and $w(z)$ is a longitudinal displacement function representing the average longitudinal displacement of the section when an orthogonal coordinate system is employed.

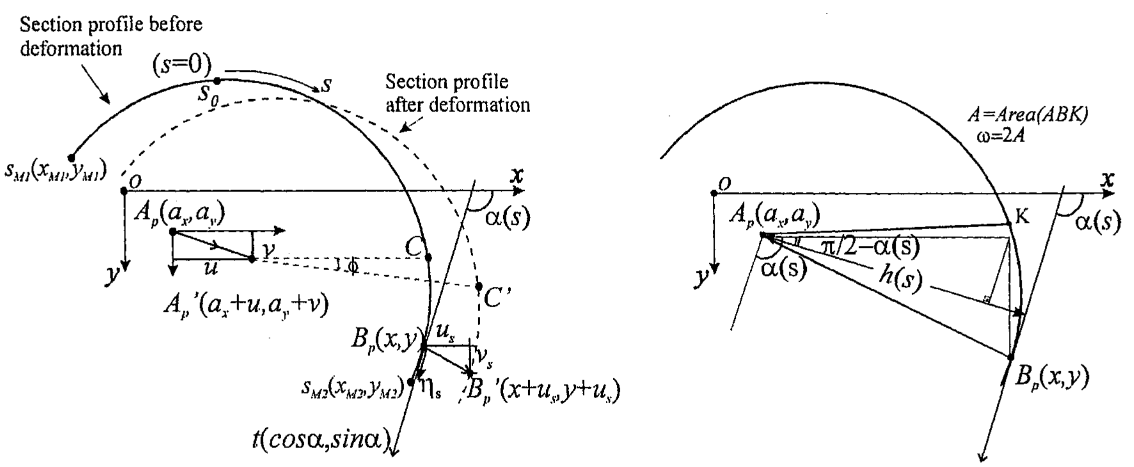

Fig. IV. 2. Cross-section (a) Displacements, (b) Sectorial Area

Equilibrium Equations and Boundary Conditions

By using Eqs. (IV.1), (IV.2) and (IV.3) in conjunction with the principle of virtual work (Chapter II), one recovers the well known Vlasov equilibrium equations (Vlasov 1961)

$$E\begin{bmatrix} -AD^2 & S_yD^3 & S_xD^3 & S_\omega D^3 \\ -S_yD^3 & J_{yy}D^4 & J_{xy}D^4 & J_{\omega x}D^4 \\ -S_xD^3 & J_{xy}D^4 & J_{xx}D^4 & J_{\omega y}D^4 \\ -S_\omega D^3 & J_{\omega x}D^4 & J_{\omega y}D^4 & J_{\omega\omega}D^4 - E^{-1}GJ_dD^2 \end{bmatrix}\begin{Bmatrix} w \\ u \\ v \\ \phi \end{Bmatrix} = \begin{Bmatrix} q_z \\ q_x + \int_s x\,\partial p_z/\partial z\,ds \\ q_y + \int_s y\,\partial p_z/\partial z\,ds \\ m + \int_s \omega\,\partial p_z/\partial z\,ds \end{Bmatrix} \tag{IV.4}$$

in which the operators $D^2 = d^2/dz^2$, $D^3 = d^3/dz^3$, and $D^4 = d^4/dz^4$ and the section

section constants $A = \int_A dA$, $S_y = \int_A x dA$, $S_x = \int_A y dA$, $S_\omega = \int_A \omega dA$, $J_{xx} = \int_A y^2 dA$, $J_{xy} = \int_A xy dA$, $J_{yy} = \int_A x^2 dA$, $J_{\omega x} = \int_A \omega x dA$, $J_{\omega y} = \int_A \omega y dA$, $J_{\omega\omega} = \int_A \omega^2 dA$ were defined. Also, the resultant distributed forces per unit length are defined as $q_x(z) = \int_s p_x(s,z)ds$, $q_y(z) = \int_s p_y(s,z)ds$, $q_z(z) = \int_s p_z(s,z)ds$ and resultant twisting moments per unit length $m(z)$ induced by the action of the applied in-plane tractions p_x, p_y about pole $A_p(a_x, a_y)$ as $m(z) = \int_s -p_x(s,z)(y(s)-a_y) + p_y(s,z)(x(s)-a_x)ds$.

The fourteen boundary conditions associated with the above field equations naturally arise as the boundary terms from the variational principle (e.g., Chapter II in this study and Gjelsvik 1981), as

$$\left\{E(Aw'-S_y u''-S_x v''-S_\omega \phi'')-\bar{N}\right\}\delta w\Big|_0^l=0$$
$$\left\{E(S_y w''-J_{yy}u'''-J_{xy}v'''-J_{\omega x}\phi''')-\bar{V}_x+\int_s p_z\left(s,z\right)x(s)ds\right\}\delta u\Big|_0^l=0$$
$$\left\{E(S_x w''-J_{xy}u'''-J_{xx}v'''-J_{\omega y}\phi''')-\bar{V}_y+\int_s p_z\left(s,z\right)y(s)ds\right\}\delta v\Big|_0^l=0$$
$$\left\{E(S_\omega w''-J_{\omega x}u'''-J_{\omega y}v'''-J_{\omega\omega}\phi'''+GJ_d E^{-1}\phi')-\bar{T}+\int_s p_z\left(s,z\right)\omega(s)ds\right\}\delta\phi\Big|_0^l=0 \qquad \text{(IV.5)}$$
$$\left\{E(-S_y w'+J_{yy}u''+J_{xy}v''+J_{\omega x}\phi'')-\bar{M}_y\right\}\delta u'\Big|_0^l=0$$
$$\left\{E(-S_x w'+J_{xy}u''+J_{xx}v''+J_{\omega y}\phi'')-\bar{M}_x\right\}\delta v'\Big|_0^l=0$$
$$\left\{E(-S_\omega w'+J_{\omega x}u''+J_{\omega y}v''+J_{\omega\omega}\phi'')-\bar{B}\right\}\delta\phi'\Big|_0^l=0$$

In Equation (5) the energy conjugate stress resultants

$$\bar{N}(0)=\int_A\bar{\sigma}_0 dA,\quad \bar{M}_y(0)=-\int_A\bar{\sigma}_0 x(s)dA,\quad \bar{M}_x(0)=-\int_A\bar{\sigma}_0 y(s)dA,\quad \bar{B}(0)=-\int_A\bar{\sigma}_0\omega(s)dA,$$
$$\bar{V}_x(0)=\int_A\bar{\tau}_0\cos\alpha\left(s\right)dA,\qquad \bar{V}_y(0)=\int_A\bar{\tau}_0\sin\alpha\left(s\right)dA,$$
$$\bar{T}(0)=\int_A\left\{-\bar{\tau}_0(s,z,r)\cos\alpha\left(s\right)\left[y(s)-a_y\right]+\bar{\tau}_0(s,z,r)\sin\alpha\left(s\right)\left[x(s)-a_x\right]\right\}dA$$

$$\bar{N}(l)=\int_A\bar{\sigma}_l dA,\quad \bar{M}_y(l)=-\int_A\bar{\sigma}_l x(s)dA,\quad \bar{M}_x(l)=-\int_A\bar{\sigma}_l y(s)dA,\quad \bar{B}(l)=-\int_A\bar{\sigma}_l\omega(s)dA,$$
$\bar{V}_x(l)=\int_A\bar{\tau}_l\cos\alpha\left(s\right)dA$, $\bar{V}_y(l)=\int_A\bar{\tau}_l\sin\alpha\left(s\right)dA$, and
$$\bar{T}(l)=\int_A\left\{-\bar{\tau}_l(s,z,r)\cos\alpha\left(s\right)\left[y(s)-a_y\right]+\bar{\tau}_l(s,z,r)\sin\alpha\left(s\right)\left[x(s)-a_x\right]\right\}dA \qquad \text{(IV.6)}$$

are defined. The conjugate stress resultants defined in Eqs. (IV.6) have a general significance in the sense that they are applicable to any non-orthogonal coordinate system. Specifically, the moment terms $\bar{M}_y(0)=-\int_A\bar{\sigma}_0 x(s)dA$, $\bar{M}_x(0)=-\int_A\bar{\sigma}_0 y(s)dA$, $\bar{M}_y(l)=-\int_A\bar{\sigma}_l x(s)dA$, and $\bar{M}_x(l)=-\int_A\bar{\sigma}_l y(s)dA$ are those about an origin which does not necessarily coincide with the centroidal axis of the tractions acting normal to the cross-sections $z=0$ and $z=l$. In conventional solutions, orthogonal systems of coordinates are adopted and the above moment terms revert to the conventional moment definitions about the centroidal axis. Also, the bimoment terms $\overline{B}(0) = -\int_A \overline{\sigma}_0 \omega(s) dA$ and $\overline{B}(l) = -\int_A \overline{\sigma}_l \omega(s) dA$ are related to a sectorial origin which does not necessarily coincide with the principal sectorial origin as defined by the orthogonal condition $S_\omega = 0$ commonly enforced in conventional solutions. Finally, the twisting moments $\overline{T}(0)$ and $\overline{T}(l)$ are the moments of the tractions tangent to the end cross-sections $z = 0$ and $z = l$ about a pole (a_x, a_y) which does not necessarily coincide with the section shear centre. Again, in conventional solutions, the pole (a_x, a_y) is selected to coincide with the shear centre defined by the orthogonality conditions $J_{\omega x} = J_{\omega y} = 0$, and the twisting moment definitions in Eq. (IV.6) become those about the shear centre.

Review of Solutions Schemes

Various solution schemes for the system of equations (IV.4) subject to the boundary conditions (IV.5) are available in the literature. These are categorized in the following four groups

Scheme 1- Solution of equilibrium equations under orthogonal coordinates:

The conventional approach (e.g., Vlasov 1961, Murray 1984) directly solves of the equilibrium equation (IV.4) subject to the boundary conditions (IV.5) under an orthogonal coordinate system which meets the conditions $S_x = S_y = S_\omega = J_{xy} = J_{\omega x} = J_{\omega y} = 0$. This approach has the advantage of uncoupling the equilibrium equations. Also, in a number of applications, the resulting boundary conditions may be uncoupled. When this is the case, this approach becomes relatively simple to implement and is suitable for hand calculations.

Scheme 2- Finite element solutions under orthogonal coordinates:

This is a numeric alternative to the direct solution of the uncoupled equilibrium equations in Scheme 1. Again, a coordinate system which satisfies the orthogonality conditions $S_x = S_y = S_\omega = J_{xy} = J_{\omega x} = J_{\omega y} = 0$ is adopted. In a finite element context, these conditions uncouple the longitudinal, transverse and rotational degrees of freedom. As a result the element stiffness matrix becomes relatively simple. Various researchers have developed finite elements based on orthogonal coordinate systems. This includes the works Krajcinovic (1969), Barsoum and Gallagher (1970), and Batoz and Dhatt (1970). This type of solution has the typical finite element advantage of handling multiple spans and complex loads with ease and flexibility when compared to Scheme 1.

Scheme 3- Solution of equilibrium equations under a non-orthogonal coordinate system:

In certain classes of problems, the adoption of an orthogonal coordinate system can result in modeling complications. This is particularly the case for members exhibiting stepwise cross-sectional changes (e.g., Erkmen and Mohareb 2006 a and Gjelsvik 1981). In these instances, it becomes more expedient to solve the system of equations (IV.4) under a non orthogonal coordinate system on some segments of the structure. This type of solution involves tedious hand computations and is outlined in Gjelsvik (1981).

Scheme 4- Finite Element Solutions under a non orthogonal coordinate system:

A family of finite elements based on a non-orthogonal coordinate system has recently been developed in Erkmen and Mohareb (2006 a), which are able to handle the solutions for the Classes of problems handled by Scheme 3 while circumventing the tedious mathematical manipulations encountered. For example, by using the stiffness matrix $\mathbf{K}_{e14\times14}$ and the energy equivalent load vector $\mathbf{R}_{14\times1}$ for element NOVEE14 (Non-Orthogonal Vlasov Element based on Exact shape functions with 14 Degrees of freedoms) which relate the nodal displacement vector $\mathbf{U}_{N14\times1}$ to the nodal force vector $\mathbf{P}_{14\times1}$ through the relation $\mathbf{P}_{14\times1} = \mathbf{K}_{e14\times14}\mathbf{U}_{N14\times1} - \mathbf{R}_{14\times1}$, one can obtain the nodal unknowns, without introducing any discretization errors.

Normal stresses

Expressions for normal stresses applicable for the solution scheme 4 are not available in the literature. In this context, this paper focuses on developing a stress computation scheme suitable for finite element solutions based on a non-orthogonal coordinate system.

Expressions for Normal stresses

The longitudinal strains are expressed by taking the derivative of Equation (IV.3) yielding $\varepsilon_{zz}(s,z) = \mathbf{x}^{\mathbf{T}}_{1\times4}\,\mathbf{u}(z)_{4\times1}$ in which the vector of coordinates $\mathbf{x}^{\mathbf{T}}_{1\times4} = \langle 1 \quad -x(s) \quad -y(s) \quad -\omega(s) \rangle$ and the vector of displacement derivatives $\mathbf{u(z)}^{\mathbf{T}}_{1\times4} = \langle w'(z) \quad u''(z) \quad v''(z) \quad \phi''(z) \rangle$ have been defined. By substituting into the constitutive relation $\sigma_{zz} \approx E\varepsilon_{zz}$, the longitudinal stresses σ_{zz} are obtained as

$$\sigma_{zz}(z,s) = E\left[w'(z) - x(s)u''(z) - y(s)v''(z) - \omega(s)\phi''(z)\right] \tag{IV.7}$$

Equation (IV.7) would suffice to compute the normal stresses if the functions $w(z), u(z), v(z), \text{and}\, \phi(z)$ are known. This will be the case when the field equations (IV.4) are directly solved subject to the boundary conditions (Solution schemes 1 and 3)

Relating normal stresses to internal forces

The boundary terms in Eqs. (IV.5) can be generalized to an arbitrary section along the member (identified by the longitudinal coordinate z). Thus, the internal force expressions $N(z) = \int_A \sigma_{zz}(z)dA$, $M_x(z) = -\int_A \sigma_{zz}(z)y(s)dA$, $M_y(z) = -\int_A \sigma_{zz}(z)x(s)dA$, and $B(z) = -\int_A \sigma_{zz}(z)\omega(s)dA$ are written. The expression of the longitudinal stress σ_{zz} obtained in Eq. (IV.7) is substituted into the above expressions yielding a set of relationships relating the internal forces and the displacement derivatives.

$$N(z) = E\left[Aw'(z) - S_y u''(z) - S_x v''(z) - S_\omega \phi''(z)\right] \tag{IV.8}$$

$$M_x(z) = -E\left[S_y w'(z) - J_{xy}(s)u''(z) - J_{xx}(s)v''(z) - J_{y\omega}(s)\phi''(z)\right] \tag{IV.9}$$

$$M_y(z) = -E\left[S_y w'(z) - J_{yy}(s)u''(z) - J_{xy}(s)v''(z) - J_{y\omega}(s)\phi''(z)\right] \tag{IV.10}$$

$$B(z) = -E\left[S_\omega w'(z) - J_{\omega x}(s)u''(z) - J_{\omega y}(s)v''(z) - J_{\omega\omega}(s)\phi''(z)\right] \tag{IV.11}$$

Eqs. (IV.8) through (IV.11) are arranged in a matrix form and the resulting system of equations is inverted to recover expressions for the vector of displacement derivatives $\mathbf{u(z)}^{\mathbf{T}}_{\mathbf{1\times4}} = \langle w'(z) \quad u''(z) \quad v''(z) \quad \phi''(z)\rangle$ in terms of the internal forces

$$\mathbf{u(z)}_{\mathbf{4\times1}} = \frac{1}{E}\mathbf{D}^{-1}\begin{Bmatrix} N(z) \\ M_y(z) \\ M_x(z) \\ B(z) \end{Bmatrix} = \frac{1}{E}\begin{bmatrix} A & -S_y & -S_x & -S_\omega \\ -S_y & J_{yy} & J_{xy} & J_{\omega x} \\ -S_x & J_{xy} & J_{xx} & J_{\omega y} \\ -S_\omega & J_{\omega x} & J_{\omega y} & J_{\omega\omega} \end{bmatrix}^{-1}\begin{Bmatrix} N(z) \\ M_y(z) \\ M_x(z) \\ B(z) \end{Bmatrix} \tag{IV.12}$$

From Eq. (IV.12), by substituting into Eq. (IV.7), a general expression for normal stresses in a non-orthogonal coordinate system is obtained as

$$\sigma_{zz}(s,z) = \langle 1 \quad -x(s) \quad -y(s) \quad -\omega(s) \rangle \mathbf{D}^{-1} \begin{Bmatrix} N(z) \\ M_y(z) \\ M_x(z) \\ B(z) \end{Bmatrix} \tag{IV.13}$$

Under Solution scheme 4, once the computation $\mathbf{P}_{14\times1} = \mathbf{K}_{e14\times14}\mathbf{U}_{N14\times1} - \mathbf{R}_{14\times1}$ is performed at the element level, the relevant nodal internal forces can be obtained and the vector $\langle N(z) \quad M_y(z) \quad M_x(z) \quad B(z) \rangle^{T}$ which appears in the right hand side of Equation (IV.13) can be fully evaluated at the nodal points $z = 0, l$, yielding stress values at these sections.

Special cases

It is of interest to note that for the case of an orthogonal system of coordinates, the off-diagonal terms in matrix $\mathbf{D}^{-1}$ in Eq. (IV.12) vanish and the stress expression simplifies to

$$\sigma_{zz}(s,z) = \frac{N(z)}{A} - \frac{M_y(z)}{J_{yy}} x(s) - \frac{M_x(z)}{J_{xx}} y(s) - \frac{B(z)}{J_{\omega\omega}} \omega(s) \tag{IV.14}$$

which coincides with the stress equation reported in Vlasov (1961) and Seaburg and Carter (1997). Equation (IV.14) is useable for solution scheme 2, but not for scheme 4. Also, for the special case of zero bimoments $B(z) = 0$, the well known stress equation for centroidal ($S_x = S_y = 0$) non-principal axes ($J_{xy} \neq 0$), (e.g., Boresi and Sidebottom 1985) are recovered as a special case from Eq. (IV.13).

$$\sigma_{zz}(s,z)=\frac{N(z)}{A}-\frac{M_y(z)}{J_{xx}J_{yy}-J_{xy}^2}\left(J_{xx}x-J_{xy}y\right)-\frac{M_x(z)}{J_{xx}J_{yy}-J_{xy}^2}\left(J_{yy}y-J_{xy}x\right) \qquad \text{(IV.15)}$$

Shear stresses in terms of stress resultants

Expression for shear stress

In line with the Vlasov theory (Vlasov 1961), the shearing stress $\tau_{zs}(s,z,r)$ is considered to consist of two components: 1) a shearing stress $\tau_c(s,z)$, which is constant across the cross-section thickness; and 2) a skew symmetric shearing stress $\tau_{sv}(z,r)=T(z)r/J_d$ due to the St. Venant torsion, i.e., $\tau_{zs}(s,z,r)=\tau_c(s,z)+\tau_{sv}(z,r)$ (Fig. IV.3).

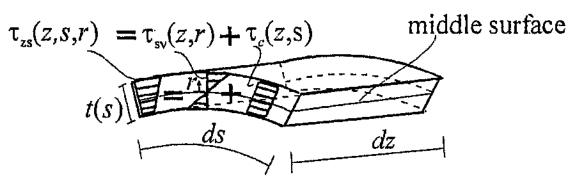

Fig. IV. 3- Shearing Stresses

It is recognized that, from a fundamental viewpoint, a non-vanishing shear stress distribution at the mid-surface is in contradiction with Vlasov's second assumption which postulates a zero value for the associated shear strain. Nevertheless, non-vanishing shear stresses arise at the mid-surface when enforcing the local equilibrium condition. By formulating equilibrium condition for a differential element *tdzds* taken from a thin-walled beam (Fig. IV.4) in the longitudinal direction, one obtains

$$\frac{\partial}{\partial z}\left[\sigma(s,z)t(s)\right]+\frac{\partial}{\partial s}\left\{\int_{-t(s)/2}^{t(s)/2}\left[\tau_c(s,z)+\tau_{sv}(z,r)\right]dr\right\}=0 \qquad \text{(IV.16)}$$

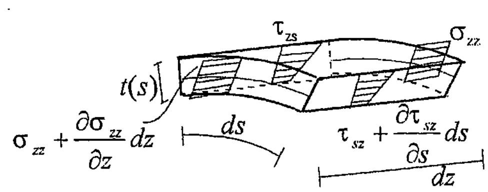

Fig. IV.4- Free body diagram of an infinitesimal thin-walled segment

The integral terms in Eq. (IV.16) simplify to $\int_{-t(s)/2}^{t(s)/2} \tau_c(s,z)dr = \tau_c(s,z)t(s)$, $\int_{-t(s)/2}^{t(s)/2} \tau_{sv}(z,r)dr = 0$. In Equation (IV.16), the longitudinal traction $p_z(s,z)$ has been assumed to vanish. Thus, the local effect of the longitudinal traction on the shear stress distribution is not considered. Within the formulation developed in this paper, the effect of longitudinal tractions $p_z(s,z)$ is modeled only in an average integral sense through the integral terms $q_z(z) = \int_S p_z(s,z)\,ds$, $\int_S x\,\partial p_z/\partial z\,ds$, $\int_S y\,\partial p_z/\partial z\,ds$ and $\int_S \omega\,\partial p_z/\partial z\,ds$ appearing in the equilibrium equation. Thus, in problems with non-vanishing longitudinal tractions, the warping shear expressions developed in this section will provide only an approximate solution.

Figure IV.5a depicts a general open thin-walled section consisting of seven plate segments ($n = 7$) and eight joints. In open sections, the number of joints always exceeds the number of plate segments by one. The numbers in square brackets denote segment numbering and the circled numbers denote joint numbering. Each segment c is defined by a beginning joint $b(c)$ and an end joint $e(c)$. For example, segment 3 has the beginning joint $b(3) = 2$ and the end joint $e(3) = 4$. The cross-section sectorial origin S_0 has been assumed to be located along plate 3. The whole cross-section has the area properties A, S_y, S_x, S_ω, J_{xy}, J_{yy}, $J_{x\omega}$, $J_{y\omega}$ while each segment c ($c = 1$ to n) has the properties A^c, S_y^c, S_x^c, S_ω^c, J_{xy}^c, J_{yy}^c, $J_{x\omega}^c$, $J_{y\omega}^c$.

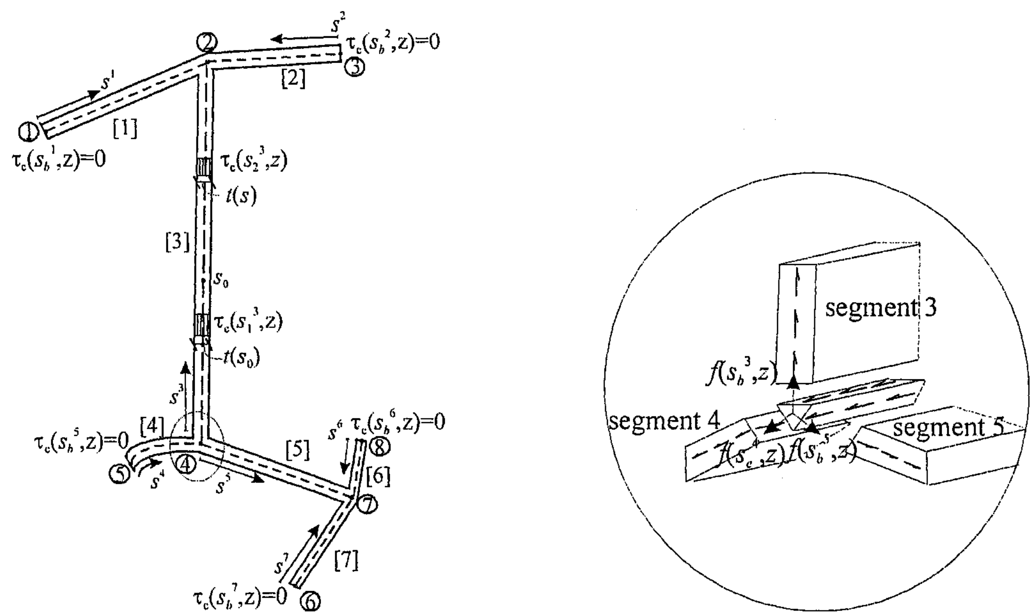

Fig. IV. 5 General cross-section (a) Geometry (b) Shear flow continuity at joint 4

Each segment c can be conceived to provide the internal shear force contributions V_x^c, V_y^c and the warping torsion contribution T_w^c. The overall section properties, internal and external forces acting on the cross-section are expressed in terms of the individual segmental contributions as

$$A=\sum_{c=1}^{n} A^c,\quad S_y=\sum_{c=1}^{n} S_y^c,\quad S_x=\sum_{c=1}^{n} S_x^c,\quad S_\omega=\sum_{c=1}^{n} S_\omega^c,\quad J_{xy}=\sum_{c=1}^{n} J_{xy}^c,\quad J_{yy}=\sum_{c=1}^{n} J_{yy}^c,$$
$$J_{x\omega}=\sum_{c=1}^{n} J_{x\omega}^c,\ J_{y\omega}=\sum_{c=1}^{n} J_{y\omega}^c,\ V_x=\sum_{c=1}^{n} V_x^c,\ V_y=\sum_{c=1}^{n} V_y^c,\ \text{and } T_w=\sum_{c=1}^{n} T_w^c \tag{IV.17}$$

In the following, it is assumed that the constant component of shearing stress $\tau_c(s_1^c, z)$ is known at a point located on cross-section z with coordinate s_1^c along segment c. It is required to find an expression for the constant component of shearing stress $\tau_c(s_2^c, z)$ at an adjacent point defined by coordinate s_2^c on the same cross-section z and segment c. By substituting Eq. (IV.7) into Eq. (IV.16) and integrating with respect to coordinate s between the limits s_1^c and s_2^c, one obtains

$$\tau_c(s_2^c,z)t(s_2^c)=\tau_c(s_1^c,z)t(s_1^c)$$
$$-E\left[w''(z)\overline{A}(s_1^c,s_2^c)-u'''(z)\overline{S}_y(s_1^c,s_2^c)-v'''(z)\overline{S}_x(s_1^c,s_2^c)-\phi'''(z)\overline{S}_\omega(s_0,s_1^c,s_2^c)\right] \quad \text{(IV.18)}$$

In Eq. (IV.18), the functions

$$\overline{A}(s_1^c,s_2^c)=\int_{s_1^c}^{s_2^c} dA\,,\ \overline{S}_y(s_1^c,s_2^c)=\int_{s_1^c}^{s_2^c} xdA\,,\ \overline{S}_x(s_1^c,s_2^c)=\int_{s_1^c}^{s_2^c} ydA\,,\ \overline{S}_\omega(s_0,s_1^c,s_2^c)=\int_{s_1^c}^{s_2^c} \omega^c(s_0,s)dA \quad \text{(IV.19)}$$

were defined. By selecting the integration limits for segment c to coincide with the joints at the beginning and end of the segment (i.e., by setting $s_1^c=s_b^c$ and $s_2^c=s_e^c$), one obtains

$$f(s_e^c,z)=f(s_b^c,z)$$
$$-E\left[w''(z)\overline{A}(s_b^c,s_e^c)-u'''(z)\overline{S}_y(s_b^c,s_e^c)-v'''(z)\overline{S}_x(s_b^c,s_e^c)-\phi'''(z)\overline{S}_\omega(s_0,s_b^c,s_e^c)\right] \quad \text{(IV.20)}$$

In Eq. (IV.17), a shear flow function $f(s,z)=\tau_c(s,z)t(s)$ has been defined.

Shear flow continuity

By writing the equilibrium condition in the longitudinal direction for a general joint j of length dz at which multiple segments intersect, a generic shear flow continuity condition is obtained

$$\sum_{c=1}^{n}\gamma(c,j)f\left(s_b^c,z\right)-\beta(c,j)f\left(s_e^c,z\right)=0 \quad \text{(IV.21)}$$

in which $\gamma(c,j)=1.0$ when the beginning joint of member c coincides with joint j (i.e., as $b(c)=j$) and $\gamma(c,j)=0.0$ otherwise. In a similar manner, one has $\beta(c,j)=1.0$ when $e(c)=j$ and $\beta(c,j)=0.0$ otherwise. For example, for the cross-section depicted in Fig. IV.5 a, by applying Eq. (IV.21) at joint 4 i.e., by setting $(j=4)$, the shear flow continuity condition takes the form $f(s_b^3,z)+f(s_e^4,z)+f(s_b^5,z)=0$ (Fig.

IV.5 b). Also, by applying Eq. (IV.21) at joint 1, at which only a single plate is connected, the shear flow boundary condition $f(s_b^1,z)=0$ is recovered. In general, for a cross-section with $n+1$ joints, $n+1$ shear flow continuity /shear flow boundary conditions can be written. The unknowns in these equations are the shear flow values at both ends of each segment. For n segments, the number of unknowns is $2n$. By expressing the shear flow conditions in a matrix form, one obtains

$$\begin{bmatrix}\boldsymbol{\gamma}_{(n+1)\times n} & \boldsymbol{\beta}_{(n+1)\times n}\end{bmatrix}\begin{Bmatrix}\mathbf{f}_{\mathbf{b}_{n\times1}} \\ \mathbf{f}_{\mathbf{e}_{n\times1}}\end{Bmatrix}=\mathbf{0}_{(n+1)\times1} \tag{IV.22}$$

in which matrices $\boldsymbol{\gamma}$, $\boldsymbol{\beta}$ consist of the entry of the shear flow continuity coefficients $\gamma(c,j)$ and $\beta(c,j)$, respectively. Vectors $\mathbf{f}_\mathbf{b}$ and $\mathbf{f}_\mathbf{e}$ consist of the shear flow unknowns at the ends of the segments. These are defined as

$$\begin{aligned}\mathbf{f}^{\mathrm{T}}{}_{\mathbf{b}}&=\left\langle f\left(s_b^1,z\right) \quad f\left(s_b^2,z\right) \quad \cdots \quad f\left(s_b^n,z\right)\right\rangle \\ \mathbf{f}^{\mathrm{T}}{}_{\mathbf{e}}&=\left\langle f\left(s_e^1,z\right) \quad f\left(s_e^2,z\right) \quad \cdots \quad f\left(s_e^n,z\right)\right\rangle\end{aligned} \tag{IV.23}$$

Using Eq. (IV.20), vector $\mathbf{f}_{\mathbf{en\times1}}$ can be expressed in terms of vector $\mathbf{f}_{\mathbf{bn\times1}}$ as

$$\mathbf{f}_{\mathbf{en\times1}}=\mathbf{f}_{\mathbf{bn\times1}}+\mathbf{v}_{\mathbf{n\times1}} \tag{IV.24}$$

in which the c_{th} member of vector $\mathbf{v}_{\mathbf{n\times1}}$ is given by

$$v(c)=-E\left[w''(z)\overline{A}(s_b^c,s_e^c)-u'''(z)\overline{S}_y(s_b^c,s_e^c)-v'''(z)\overline{S}_x(s_b^c,s_e^c)-\phi'''(z)\overline{S}_\omega(s_0,s_b^c,s_e^c)\right] \tag{IV.25}$$

Equation (IV.24) can be substituted into Eq. (IV.22) to reduce the number of unknown shear flows to n values. As a result, one obtains $n+1$ equations in n shear flow unknowns. In the absence of longitudinal tractions, it is observed that the equations are linearly dependent, i.e., one of the equations can always be expressed as a linear combination of the remaining n equations. This is a direct outcome of satisfying the global longitudinal equilibrium condition of the section (the first equation of the system given in Eq. IV.4) a-priori. Thus, a linearly independent subset of n equations can be selected among the complete set of equations given in Eq. (IV.22), and expressed as

$$\begin{bmatrix} \boldsymbol{\gamma}^*_{n\times n} & \boldsymbol{\beta}^*_{n\times n} \end{bmatrix} \begin{Bmatrix} \mathbf{f}_{\mathbf{b}_{n\times 1}} \\ \mathbf{f}_{\mathbf{b}_{n\times 1}} + \mathbf{f}_{n\times 1} \end{Bmatrix} = \mathbf{0}_{n\times 1} \tag{IV.26}$$

in which the entries of matrices $\boldsymbol{\gamma}^*_{n\times n}$ and $\boldsymbol{\beta}^*_{n\times n}$ correspond to the n shear flow conditions selected. By expanding Eq. (IV.26) and rearranging, an expression for the unknown shear flow values $\mathbf{f}_\mathbf{b}$ is recovered as

$$\mathbf{f}_{\mathbf{b}_{n\times 1}} = -\left(\boldsymbol{\gamma}^*_{n\times n} + \boldsymbol{\beta}^*_{n\times n}\right)^{-1} \boldsymbol{\beta}^*_{n\times n}\mathbf{f}_{n\times 1} \tag{IV.27}$$

The solution of Eq. (IV.27) provides shear flow values at the beginning joint of all n segments. Once these values are known, the constant component of shearing stresses at other intermediate points along any plate segment c can be obtained applying Eq. (IV.18) for the segment of interest.

Relating Shearing Stresses to Stress Resultants

The shear force $V_x^c(z)$ of segment c is the integral over the segment area of the shear flow component along the x direction.

$$V_x^c(z)=\int_{s=s_b^c}^{s=s_e^c}\tau_c(s,z)t(s)\cos\alpha(s)ds$$

$$=\tau_c(s_b^c,z)t(s_b^c)\int_{s=s_b^c}^{s=s_e^c}dx-E\left(\begin{array}{l}w''(z)\int_{s=s_b^c}^{s=s_e^c}\overline{A}(s_b^c,s)dx-u'''(z)\int_{s=s_b^c}^{s=s_e^c}\overline{S}_y(s_b^c,s)dx\\-v'''(z)\int_{s=s_b^c}^{s=s_e^c}\overline{S}_x(s_b^c,s)dx-\phi'''(z)\int_{s=s_b^c}^{s=s_e^c}\overline{S}_\omega(s_0,s_b^c,s)dx\end{array}\right)\qquad\text{(IV.28)}$$

in which the relation $dx=ds\cos\alpha(s)$ is used. The integral terms in Eq. (IV.28) can be expressed as

$$\tau_c(s_b^c,z)t(s_b^c)\int_{s=s_b^c}^{s=s_e^c}dx=\tau_c(s_b^c,z)t(s_b^c)\left(x_e^c-x_b^c\right)\qquad\text{(IV.29)}$$

$$\int_{s=s_b^c}^{s=s_e^c}\overline{A}(s_b^c,s)dx=\overline{A}(s_b^c,s_e^c)x\left(s_e^c\right)-S_y^c\qquad\text{(IV.30)}$$

$$\int_{s=s_b^c}^{s=s_e^c}\overline{S}_y(s_b^c,s)dx=\overline{S}_y(s_b^c,s_e^c)x\left(s_e^c\right)-J_{yy}^c\qquad\text{(IV.31)}$$

$$\int_{s=s_b^c}^{s=s_e^c}\overline{S}_x(s_b^c,s)dx=\overline{S}_x(s_b^c,s_e^c)x\left(s_e^c\right)-J_{xy}^c\qquad\text{(IV.32)}$$

$$\int_{s=s_b^c}^{s=s_e^c}\overline{S}_\omega(s_0,s_b^c,s)dx=\overline{S}_\omega(s_0,s_b^c,s_e^c)x\left(s_e^c\right)-J_{x\omega}^c\qquad\text{(IV.33)}$$

From Eqs. (IV.29) through (IV.33), by substituting into Eq. (IV.28) and using Eq. (IV.20), shear force $V_x^c(z)$ of segment c simplifies to

$$V_x^c(z)=(S_y^cw''-J_{yy}^cu'''-J_{xy}^cv'''-J_{\omega x}^c\phi''')-f\left(s_b^c,z\right)x_b^c+f\left(s_e^c,z\right)x_e^c\qquad\text{(IV.34)}$$

By using the summations defined in Eqs. (IV.17) and recalling that the sum of shear flows at each joint of the cross section must vanish (Eq. (IV.21)), one obtains

$$V_x(z)=\sum_{c=1}^{n}V_x^c(z)=E(S_y w''-J_{yy}u'''-J_{xy}v'''-J_{\omega x}\phi''') \tag{IV.35}$$

It is of interest to note that by setting $z=0$ or $z=l$ in Eq. (IV.35), the second natural boundary condition in Eq. (IV.4) is recovered for the case of vanishing longitudinal traction. A similar treatment leads to

$$V_y(z)=E(S_x w''-J_{xy}u'''-J_{yy}v'''-J_{\omega y}\phi''') \tag{IV.36}$$

$$T_w(z)=E(S_\omega w''-J_{\omega x}u'''-J_{\omega y}v'''-J_{\omega\omega}\phi''') \tag{IV.37}$$

By differentiating Eq. (IV.8) and noting that, in the absence of longitudinal tractions, the condition $N'(z)=0$ is satisfied, the result is arranged along with Eqs. (IV.35), (IV.36) and (IV.37) in a matrix form as

$$\begin{Bmatrix} 0 \\ V_x \\ V_y \\ T_w \end{Bmatrix} = -E\mathbf{D}\begin{Bmatrix} w'' \\ u''' \\ v''' \\ \phi''' \end{Bmatrix} \tag{IV.38}$$

By solving Eq. (IV.38) for vector $\langle w'' \quad u''' \quad v''' \quad \phi''' \rangle$ and substituting into Eq. (IV.18), the constant component of shearing stresses are expressed in terms of stress resultants as

$$\tau_c(s_2^c,z)t(s_2^c)=\tau_c(s_1^c,z)t(s_1^c)$$
$$+\langle \bar{A}(s_1^c,s_2^c) \quad -\bar{S}_y(s_1^c,s_2^c) \quad -\bar{S}_x(s_1^c,s_2^c) \quad -\bar{S}_\omega(s_0,s_1^c,s_2^c)\rangle \mathbf{D}^{-1}\begin{Bmatrix} 0 \\ V_x \\ V_y \\ T_w \end{Bmatrix} \tag{IV.39}$$

Equation (IV.39) allows the calculation of the constant component of shearing stress at point s_2^c in terms of the stress resultants V_x, V_y, and T_w. In general, the shear flow will be known at the beginning joint of the segment as a result of the solution of Eq. (IV.27).

Thus, by setting $\tau_c(s_1^c,z)t(s_1^c)=\tau_c(s_e^c,z)t(s_e^c)=f(s_e^c,z)$ into Eq. (IV.39), the shear stress at any point s_2^c on plate c is determined. For an orthogonal coordinate system, Eq. (IV.39) takes a simpler form coinciding with the one reported in Vlasov (1961).

$$\tau_c(s_2^c,z)t(s_2^c)=\tau_c(s_1^c,z)t(s_1^c)-\frac{\overline{S}_y(s_1^c,s_2^c)}{J_{yy}}V_x(z)-\frac{\overline{S}_x(s_1^c,s_2^c)}{J_{xx}}V_y(z)-\frac{\overline{S}_\omega(s_0,s_1^c,s_2^c)}{J_{\omega\omega}}T_w(z) \quad \text{(IV.40)}$$

General Interaction Requirement based on Elastic Resistance

In structural steel design codes, sections under combined internal forces are normally required to meet certain interaction equations which relate the internal forces acting on the section. Depending on section slenderness, they can attain their fully plastic resistance (for compact sections) or their elastic resistance (for non-compact sections). Under combined internal forces, these resistance requirements are mathematically described by code interaction relations. The stress expressions in the previous two sections can be combined to form a general interaction equation for any non-compact open thin-walled section. When this interaction requirement is met, the section is judged to remain in the elastic range.

By recalling that the total shear stress is the summation of the constant component of shearing stress $\tau_c(s,z)$ as given in Eq. (IV.39) and the shear stress due to the St. Venant torsion $\tau_{sv}(z,r)=2T_{sv}(z)r/J_d$ and by adopting the von Mises yield criterion $\sigma_{zz}^{\ 2}+3\tau_{zs}^{\ 2}\le\sigma_{yield}^{\ 2}$, Eqs. (IV.13) and (IV.39) can be combined to yield the following generalized interaction equation

$$\left\{\langle 1 \quad x(s) \quad y(s) \quad \omega(s)\rangle \mathbf{D}^{-1}\begin{Bmatrix} N(z)\\ M_y(z)\\ M_x(z)\\ B(z)\end{Bmatrix}\right\}^2 + 3\left\{\begin{bmatrix}\left(\dfrac{2T_{sv}(z)}{J_d} r\right) + \tau_c(s_b^c,z)\dfrac{t(s_b^c)}{t(s)} \\ + \dfrac{1}{t(s)}\left[\langle \bar{A}(s_b^c,s) \quad -\bar{S}_y(s_b^c,s) \quad -\bar{S}_x(s_b^c,s) \quad -\bar{S}_\omega(s_0,s_b^c,s)\rangle \mathbf{D}^{-1}\begin{Bmatrix}0\\V_x(z)\\V_y(z)\\T_w(z)\end{Bmatrix}\right]\end{bmatrix}^2\right\} \le \sigma_{yield}^{2} \tag{IV.41}$$

Example IV.1: Beam with coped flange

A four meter span beam is fully fixed at both ends. The beam is made of a built up wide flange steel section and subject to a torque T=30 kNm and a vertical force F=200 kN acting at mid span (Fig. IV. 6.a). The steel material has a Modulus of Elasticity E=200,000 MPa, Poisson's ratio $\nu = 0.3$ and a yield stress $\sigma_{yield} = 300\text{MPa}$. The cross-sectional geometries are given in Fig. IV. 6.b. Two cases are considered: Case a) the beam cross section is prismatic throughout the whole span AC, and Case b) Span AB remains identical to Case-a while span BC has half of the bottom flange coped (Fig. IV.6.b). Sections immediately left and right of mid-span are referred as section at B^- and section at B^+ respectively. Thus, beam cross-sections at B^- and B^+ are identical to Sec 1-1 and Sec 2-2 respectively.

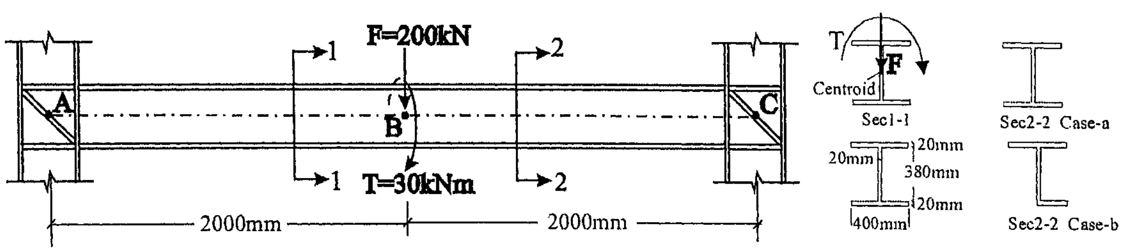

Fig. IV.6 (a) Geometry and Loading (b) Cross-section dimensions

Case-a Stress Computations

The un-coped beam in Case-a is analysed using two different coordinate systems: Case a.1) Based on Orthogonal coordinates. In this case, the origin O, the sectorial origin S_0, and the pole A_p, coincide at the section centroid as shown in Fig. IV.7.a, and Case a.2) Based on Non-orthogonal coordinates as shown in Fig. IV.7.b.

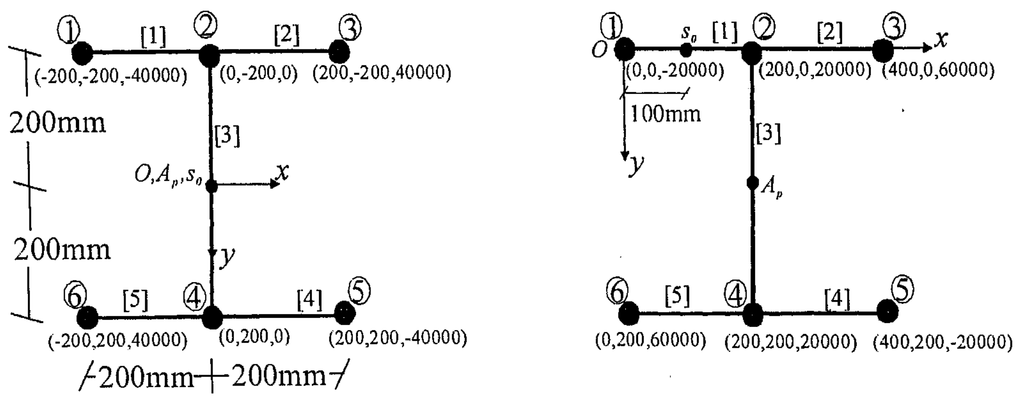

Fig IV.7. (a) Orthogonal Coordinates (b) Non-Orthogonal Coordinates

In Figure IV.7, joint numbers are circled and plate numbers are bracketed. The cross-sectional properties based on solutions schemes a.1 and a.2 are shown in Table IV.1 The algorithm to compute sectional properties are summarized in Appendix IV.A.

Table IV.1-Cross-sectional properties

Solution Scheme	A $\times10^3$ mm^2	S_x $\times10^6$ mm^3	S_y $\times10^6$ mm^3	S_ω $\times10^8$ mm^4	J_{xx} $\times10^9$ mm^4	J_{yy} $\times10^9$ mm^4	J_{xy} $\times10^8$ mm^4	$J_{\omega x}$ $\times10^{10}$ mm^4	$J_{\omega y}$ $\times10^{10}$ mm^4	$J_{\omega\omega}$ $\times10^{13}$ mm^6	J_d $\times10^6$ mm^4
a.1	24.0	0.00	0.00	0.0	0.75	0.21	0.00	0.00	0.00	0.85	3.20
a.2	24.0	4.80	4.80	4.80	1.71	1.17	9.60	9.60	9.60	1.81	3.20

Under both solution schemes the applied vertical force F is acting at the shear center since it coincides with the selected pole A_p shown in Fig. IV.7 (Murray 1984). By using element NOVEE14 (Erkmen and Mohareb 2006 a) in finite element solution scheme, and modeling the structure as assemblage of two elements (i.e., one element for each span AB and BC), exact displacements are obtained at mid-span. By using the element stiffness matrix $\mathbf{K}_{e14\times14}$, the energy equivalent load vector due to member loads $\mathbf{R}_{14\times1}$ (zero in this case) and element nodal displacement vector $\mathbf{U}_{N14\times1}$, in the relation $\mathbf{P}_{14\times1} = \mathbf{K}_{e14\times14}\mathbf{U}_{N14\times1} - \mathbf{R}_{14\times1}$, one obtains the nodal force $\mathbf{P}_{14\times1}$ vector of each element. From the nodal force vector $\mathbf{P}_{14\times1}$, one obtains the internal nodal forces at midspan. The internal forces are identical along the beam in both cases a.1 and a.2 and the maximum absolute values for all the internal forces are at the mid span. The internal forces at B^- are shown in Table IV.2.

Table IV.2-Stress Resultants at mid-span in Case-b

Section	N (kN)	V_x (kN)	V_y (kN)	M_x (kNm)	M_y (kNm)	T_w (kNm)	T_{sv} (kNm)	B (kNm^2)
B^-	0.00	0.00	100	-100	0.00	15.0	0.00	14.3

The computation of the stresses at point 2 located at section B are performed based on two solution schemes (based on orthogonal and non-orthogonal coordinates). Coordinates of joint 2 based on solution scheme a.1 and a.2 are shown in Fig. IV. 7a and Fig. IV. 7b respectively. The functions $\bar{A}, \bar{S}_y$, $\bar{S}_x$ and $\bar{S}_\omega$ that are used in shear stress calculations based on solution scheme a.1 and a.2 are provided in Tables IV.3 and IV.4 respectively.

Table IV.3-Functions $\bar{A}, \bar{S}_y$, $\bar{S}_x$ and $\bar{S}_\omega$ based on orthogonal Coordinates

Location	$\bar{A}$ x10^{3}mm^2	$\bar{S}_y$x10^{5}mm^3	$\bar{S}_x$x10^{5}mm^3	$\bar{S}_\omega$x10^{7}mm^4
joint2 of segment 1	4	-4	-8	-8
joint2 of segment 2	4	4	-8	8

Table IV.4-Functions $\bar{A}, \bar{S}_y$, $\bar{S}_x$ and $\bar{S}_\omega$ based on Non-orthogonal Coordinates

Location	$\bar{A}$ x10^{3}mm^2	$\bar{S}_y$x10^{5}mm^3	$\bar{S}_x$x10^{5}mm^3	$\bar{S}_\omega$x10^{7}mm^4
joint2 of segment 1	4	4	0	0
joint2 of segment 2	4	12	0	16

Based on the solution scheme a.1, by using the coordinates at joint 2 (i.e., $x=0$, $y=-200\text{mm}$ and $\omega=0$), the cross-sectional properties in Table IV.1 a.1, and the internal forces N_{B^-}=0, M_{yB^-}=0, M_{xB^-}=–100kNm and B_{B^-}=–14.3kNm^2 (Table IV.2) in Eq. (IV.14), one obtains the normal stress as $\sigma_{zz}=-26.8\text{MPa}$. By using the functions at joint 2 of segment 1 (i.e., $\bar{A}(s_1^1,s_2^1)=4\times10^3\text{mm}^2$, $\bar{S}_y(s_1^1,s_2^1)=-4\times10^5\text{mm}^3$, $\bar{S}_x(s_1^1,s_2^1)=-8\times10^5\text{mm}^3$ and $\bar{S}_\omega(s_0,s_1^1,s_2^1)=-8\times10^7\text{mm}^4$) while imposing the boundary condition $f(s_1^1,z)=0$, the cross-sectional properties in Table IV.1 a.1, and the internal forces $V_{xB^-}=0$, $V_{yB^-}=100\text{kN}$ and $T_{wB^-}=15\text{kNm}$ (Table IV.2) in Eq. (IV.40), one obtains the constant component of shear stress as $\tau_c=12.4\text{MPa}$. Identical values for normal and shear stresses are obtained based on the solution scheme a.2 by substituting the coordinates at joint 2 ($x=200\text{mm}$, $y=0$ and $\omega=2\times10^4\text{mm}^2$) into Eqs. (IV.13) and the functions at joint 2 of segment 1 (i.e., $\bar{A}(s_1^1,s_2^1)=4\times10^3\text{mm}^2$, $\bar{S}_y(s_1^1,s_2^1)=4\times10^5\text{mm}^3$, $\bar{S}_x(s_1^1,s_2^1)=0$ and $\bar{S}_\omega(s_0,s_1^1,s_2^1)=0$) into Eq. (IV.39), respectively along with the cross-sectional properties shown in Tables IV.1 a.2 and the identical internal forces used for solution scheme a.1 (Table IV.2).

The shear stress at joint 2 of segment 2 can be obtained from the functions $\bar{A}(s_1^1,s_2^1)$=$4\times10^3\text{mm}^2$, $\bar{S}_y(s_1^1,s_2^1)$=$4\times10^5\text{mm}^3$, $\bar{S}_x(s_3^2,s_2^2)$=$-8\times10^5\text{mm}^3$ and $\bar{S}_\omega(s_0,s_3^2,s_2^2)$=$8\times10^7\text{mm}^4$ based on the solution scheme a.1 or from the functions $\bar{A}(s_3^2,s_2^2)$=$4\times10^3\text{mm}^2$, $\bar{S}_y(s_3^2,s_2^2)$=$12\times10^5\text{mm}^3$, $\bar{S}_x$=0 and $\bar{S}_\omega(s_0,s_3^2,s_2^2)$=$16\times10^7\text{mm}^4$ based on the solution scheme a.2 as $\tau_c=-1.67\text{MPa}$. From the shear flow continuity condition at node 2 i.e., $f(s_2^1,z)+f(s_2^2,z)+f(s_2^3,z)=0$, one obtains the shear stress at joint 2 of segment 3 as $\tau_c = 10.7\text{MPa}$. By pursuing the same solution procedure for the rest of the joints one obtains the normal stress and the constant component of shear stress diagrams as shown in Figs. IV.8 a and b respectively. Based on the normal stress values obtained at the joints, normal stresses in between joints are obtained by considering the linear distribution of normal stresses at each segment and shearing stresses in between joints can be obtained by using Eq. (IV.39) at any point. Thus, in the middle of segment 3, one obtains $\tau_c = 13.4\text{MPa}$.

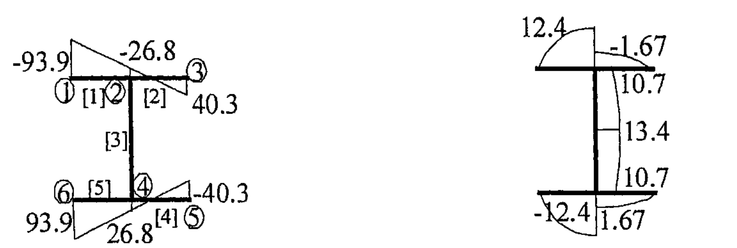

Fig IV.8.Case-a (a) Normal stress (MPa) (b) Shear stress (MPa)

Note that the boundary condition $f(s_6^5,z)=0$ is redundant, since the shear stress at joint 6 can be obtained by using the condition $\tau(s_4^5,z)=-12.4\text{MPa}$ in Eq. (IV.39). Hence the equations are linearly dependent. The shear stress due to St.Venant torsion $\tau_{sv}(z,r)=2T_{sv}(z)r/J_d$ is zero since the St. Venant torsion vanishes at mid-span (Table IV.2).

Case-b Stress Computations

Since the orthogonal axis of the coped and un-coped beams for segments AB and BC are offset in Case-b, some difficulties arise in solving the problem under a conventional technique based on orthogonal coordinates. A non-orthogonal formulation provides a convenient means of avoiding these complications and will lead to simplifications in finite element modeling and data interpretation (Chapter III). The coped beam in Case-b is modeled by selecting the origin, the sectorial origin and the pole coincide at the centroid of the un-coped section. Thus the axial force, shear forces and bending moments are defined with respect to the centroid of the un-coped section (Murray 1984). The selected system of coordinates is the orthogonal coordinates for the un-coped section along segment AB as in Case-a, in contrast to non-orthogonal coordinates for the coped section along segment BC. Cross-sectional properties of the coped section are provided in Table IV.5.

Table IV.5-Cross-sectional properties of the coped section in Case-b

A $\times 10^3$ mm^2	S_x $\times 10^6$ mm^3	S_y $\times 10^6$ mm^3	S_ω $\times 10^8$ mm^4	J_{xx} $\times 10^9$ mm^4	J_{yy} $\times 10^9$ mm^4	J_{xy} $\times 10^8$ mm^4	$J_{\omega x}$ $\times 10^{10}$ mm^4	$J_{\omega y}$ $\times 10^{10}$ mm^4	$J_{\omega\omega}$ $\times 10^{13}$ mm^6	J_d $\times 10^6$ mm^4
20	-0.80	0.40	-0.80	0.59	0.16	0.80	1.07	-1.60	0.64	2.67

By using the finite element solution scheme in a similar fashion to Case-a, one obtains exact displacements at mid-span. By using the relation $\mathbf{P}_{14\times1} = \mathbf{K}_{e14\times14}\mathbf{U}_{N14\times1} - \mathbf{R}_{14\times1}$ one obtains the nodal force vectors $\mathbf{P}_{14\times1}$ and the relevant internal forces at sections B^- and B^+. These are listed in Table IV.6.

Table IV.6-Stress Resultants at mid-span in Case-b

Section	N (kN)	V_x (kN)	V_y (kN)	M_x (kNm)	M_y (kNm)	T_w (kNm)	T_{sv} (kNm)	B (kNm^2)
B^-	-48.6	-10.2	117.6	-90.3	-5.86	16.32	0.91	12.7
B^+	-48.6	-10.2	-82.4	-90.3	-5.86	-13.53	0.76	12.7

By substituting the internal forces at section B^- and the sectional properties of the un-coped cross-section (Table IV.1 a.1) into Eqs. (IV.14) and (IV.40), one obtains the normal and the constant component of shear stresses respectively as presented in Figs.

IV.9 a. By using the internal forces at section B^+ and the sectional properties of the coped cross-section (Table IV.5) into Eqs. (IV.13) and (IV.39) one obtains the normal and the constant component of shear stresses depicted in Figs. IV. 9 b.

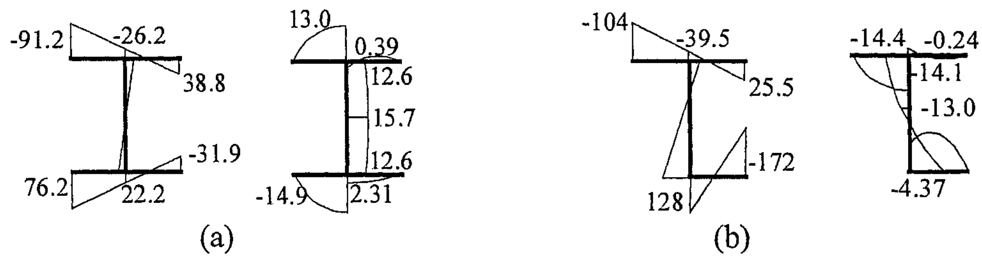

Fig IV.9. a) Normal and Shear stresses (MPa) at B^-
b) Normal and Shear stresses (MPa) at B^+

The maximum shearing stresses due to St. Venant torsion on both sides of the mid-span can be calculated for $r = 10\text{mm}$ as $\tau_{sv} = 5.74\text{MPa}$. Based on the stresses at joint 5 on the coped section and the maximum shear stress due to St. Venant torsion, one can verify that the elastic interaction criterion (in Eq. (IV.41)) is met for point 5 (i.e., $\sigma_{zz}^2 + 3\tau_{zs}^2 \le \sigma_{yield}^2$) as $172.3 < \sigma_{yield}$.

Summary and Conclusions

Expressions for normal and shear stresses in terms of stress resultants have been developed for general open thin-walled section based on non-orthogonal coordinate system. A general elastic interaction equation for general open thin-walled section has been derived. The interaction equation relates the normal force, biaxial bending, biaxial shear, St. Venant and warping torsion, and bimoments. Validity of the proposed solution scheme based on non-orthogonal coordinates is demonstrated through an example. The applicability of the new solution to a complex case which is difficult to handle using orthogonal coordinates is also illustrated. The proposed method can easily be automated and efficiently used in finite element context.

Appendix IV.A - Computation of Sectional Properties and Shear Stresses

The computations needed to perform the area integrals appearing in Eq. (IV.4) can be an onerous task to conduct by hand for a complex structure consisting of multiple asymmetric sections. A computer algorithm to automate similar tasks was developed by Heins and Wang (1978). The algorithm was later revised by Coyette (1987) who improved its computational efficiency. Prokic (2000) presented an algorithm to minimize the input data and evaluate the sectional properties of arbitrary open and closed sections corresponding to a principal coordinate system. In this study, a computer program for the calculation of cross-sectional properties for general open sections was implemented. Since non-orthogonal coordinates are used, unlike in previous works, the computations for the coordinates of centroid, shear center and the principal sectorial origin are not necessary.

The main idea of the algorithm is to define an open section using a number of user defined joints (each joint having a designation number, and two Cartesian coordinates x and y) and subdividing the cross-section into a number of plate segments (each segment being defined by a start and an end joint using a connectivity matrix similar to that used in finite element formulations). The coordinates a_x and a_y of the pole (an arbitrary point), sectorial origin S_0 (an arbitrary point located on the cross-section mid-surface) and the plate segment number on which the sectorial origin is located are also specified by the user.

Sectorial coordinates ω of joints are to be computed in two steps. In the first step, the area of the triangle between beginning joint $b(c)$ and end joint $e(c)$ of each plate segment c and pole A_p is computed with the determinant formula i.e.,

$$Area(b(c), e(c), A_p) = Det \begin{bmatrix} 1 & x_{e(c)} & y_{e(c)} \\ 1 & x_{b(c)} & y_{b(c)} \\ 1 & a_x & a_y \end{bmatrix} = \omega^c\left(b(c), A_p, e(c)\right)$$

In which $\omega^c\left(b(c), A_p, e(c)\right)$ is the sectorial area coordinates at joint $e(c)$ of segment c based on a sectorial origin located at joint $b(c)$. For the particular cross-section in Fig. IV.A.1, the beginning and end joints of segments are shown in Table IV.A.1. Sectorial area coordinate $\omega^c\left(b(c), A_p, s(x,y)\right)$ of a point on segment c can be obtained from the sectorial area coordinates at joint $e(c)$ by using linear interpolation. The sectorial are coordinate distribution on the cross-section, based on sectorial origins located at beginning joints of each segment, is shown in Fig. IV.A.1a.

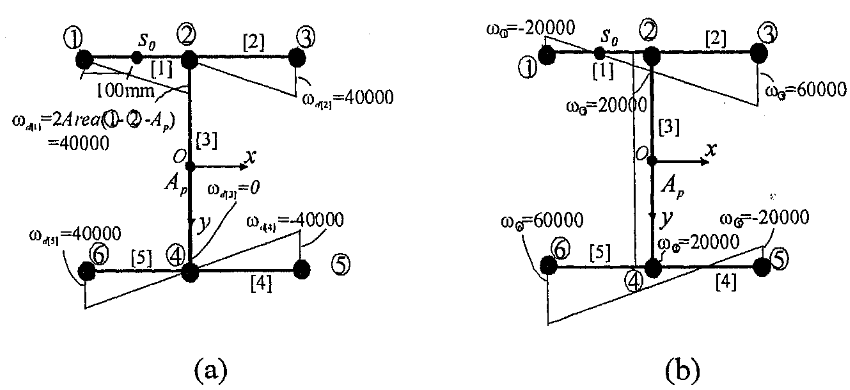

Fig. IV.A.1. (a) Sectorial are coordinates based on the sectorial origins located at the beginning joints of each segment (b) Sectorial coordinates based on the selected sectorial origin

Table IV.A.1 Beginning end joints of segments

Segment Number	[1]	[2]	[3]	[4]	[5]
Beginning joint	1	2	2	4	4
End joint	2	3	4	5	6

In the second step, by using Eq. IV.A(1), the sectorial area coordinates based on the sectorial origin located at the beginning joint of a segment c is transformed to the sectorial area coordinates based on the selected sectorial origin S_0.

$$\omega\left(S_0, A_p, s(x,y)\right) = \omega\left(S_0, A_p, b(c)\right) + \omega^c\left(b(c), A_p, s(x,y)\right) \qquad \text{IV.A(1)}$$

The sectorial are coordinate distribution on the cross-section based on the selected sectorial origin is shown in Fig. IV.A.1b.

Sectional Properties

For a segment c of start joint b(c) and end joint e(c), the properties A^c, S_y^c, S_x^c, S_ω^c, J_{xy}^c, J_{yy}^c, $J_{x\omega}^c$, and $J_{y\omega}^c$ for that segment are computed by using Eq. IV.A(2)(a-j) (Fig. IV.A.2).

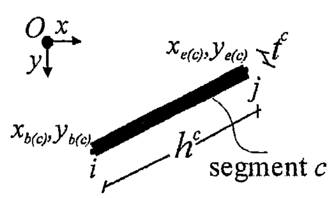

Fig. IV.A.2 x and y coordinate of end joints of a segment c

$$h^c = \sqrt{\left(x_{e(c)} - x_{b(c)}\right)^2 + \left(y_{e(c)} - y_{b(c)}\right)^2}, \qquad A^c = h^c t^c, \qquad S_y^c = \frac{1}{2} h^c t^c \left(x_{e(c)} + x_{b(c)}\right),$$

$$S_x^c = \frac{1}{2} h^c t^c \left(y_{e(c)} + y_{b(c)}\right), \qquad S_\omega^c = \frac{1}{2} h^c t^c \left(\omega_{e(c)} + \omega_{b(c)}\right),$$

$$J_{xx}^c = h^c t^c \left[\frac{1}{4}\left(y_{e(c)} + y_{b(c)}\right)^2 + \frac{1}{12}\left(y_{e(c)} - y_{b(c)}\right)^2\right],$$

$$J_{yy}^c = h^c t^c \left[\frac{1}{4}\left(x_{e(c)} + x_{b(c)}\right)^2 + \frac{1}{12}\left(x_{e(c)} - x_{b(c)}\right)^2 \right],$$
$$J_{xy}^c = h^c t^c \left[\frac{1}{4}\left(y_{e(c)} + y_{b(c)}\right)\left(x_{e(c)} + x_{b(c)}\right) + \frac{1}{12}\left(y_{e(c)} - y_{b(c)}\right)\left(x_{e(c)} - x_{b(c)}\right) \right],$$
$$J_{\omega\omega}^c = h^c t^c \left[\frac{1}{4}\left(\omega_{e(c)} + \omega_{b(c)}\right)^2 + \frac{1}{12}\left(\omega_{e(c)} - \omega_{b(c)}\right)^2 \right],$$
$$J_{\omega x}^c = h^c t^c \left[\frac{1}{4}\left(\omega_{e(c)} + \omega_{b(c)}\right)\left(x_{e(c)} + x_{b(c)}\right) + \frac{1}{12}\left(\omega_{e(c)} - \omega_{b(c)}\right)\left(x_{e(c)} - x_{b(c)}\right) \right],$$
$$J_{\omega y}^c = h^c t^c \left[\frac{1}{4}\left(\omega_{e(c)} + \omega_{b(c)}\right)\left(y_{e(c)} + y_{b(c)}\right) + \frac{1}{12}\left(\omega_{e(c)} - \omega_{b(c)}\right)\left(y_{e(c)} - y_{b(c)}\right) \right] \qquad \text{IV.A(2)(a-j)}$$

The individual contributions for all segments $(c = 1,..,n)$ are then summed up to yield the total section property required (Eq. IV.A(3) a-i).

$$A = \sum_{c=1}^{n} A^c,\quad S_y = \sum_{c=1}^{n} S_y^c,\quad S_x = \sum_{c=1}^{n} S_x^c,\quad S_\omega = \sum_{c=1}^{n} S_\omega^c,\quad J_{xx} = \sum_{c=1}^{n} J_{xx}^c,\quad J_{xy} = \sum_{c=1}^{n} J_{xy}^c,$$
$$J_{yy} = \sum_{c=1}^{n} J_{yy}^c,\ J_{\omega x} = \sum_{c=1}^{n} J_{\omega x}^c,\ J_{\omega y} = \sum_{c=1}^{n} J_{\omega y}^c,\ J_{\omega\omega} = \sum_{c=1}^{n} J_{\omega\omega}^c \qquad \text{IVA.(3)(a-i)}$$

Normal Stresses

From Eq. (IV.13), normal stress distribution in a general non-orthogonal coordinate system is obtained as

$$\sigma_{zz}(s,z) = \langle 1 \quad -x(s) \quad -y(s) \quad -\omega(s) \rangle \mathbf{D}^{-1} \begin{Bmatrix} N(z) \\ M_y(z) \\ M_x(z) \\ B(z) \end{Bmatrix}$$

in which, nodal internal forces $\langle N(z) \quad M_y(z) \quad M_x(z) \quad B(z) \rangle^{\mathrm{T}}$ and the sectional property matrix $\mathbf{D}$ are constant for every point on the cross-section. Thus, the parameters varying from point to point in a cross-section are the coordinates x, y and ω. The x and y coordinates of a point on a segment c can be obtained from the beginning $x_{b(c)}, y_{b(c)}$ and end joint coordinates $x_{e(c)}, y_{e(c)}$ by using linear interpolation (e.g., Fig. IV.A.3). Note that the sectorial area coordinate were obtained in Eq. IVA(1) (e.g., Fig. IV.A.1b).

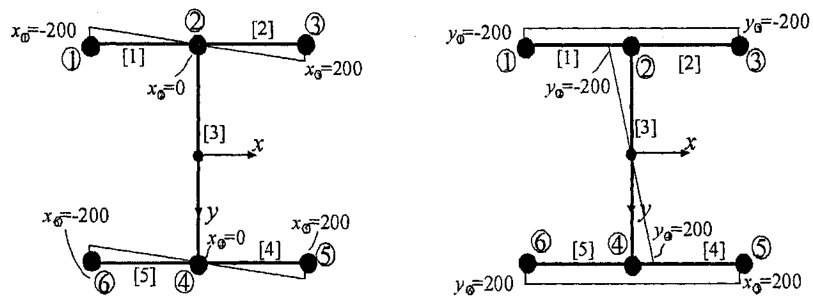

Fig. IV.A.3. (a) x coordinates (b) y coordinates

Shear Stresses

From Eq. (IV.9), constant component of shear stress distribution in a general non-orthogonal coordinate system is obtained as

$$\tau_c(s_2^c,z)t(s_2^c) = \tau_c(s_1^c,z)t(s_1^c) + \left\langle \bar{A}(s_1^c,s_2^c) \quad -\bar{S}_y(s_1^c,s_2^c) \quad -\bar{S}_x(s_1^c,s_2^c) \quad -\bar{S}_\omega(s_0,s_1^c,s_2^c) \right\rangle \mathbf{D}^{-1} \begin{Bmatrix} 0 \\ V_x \\ V_y \\ T_w \end{Bmatrix}$$

in which, the parameters that are varying from point to point on the cross section are $,\bar{A}(s_1^c,s_2^c)$, $\bar{S}_y(s_1^c,s_2^c)$, $\bar{S}_x(s_1^c,s_2^c)$, and $\bar{S}_\omega(s_0,s_1^c,s_2^c)$. The shear flow $\tau_c(s_2^c,z)t(s_2^c)$ at a point s_2^c of segment c can only be determined from the relations $\bar{A}(s_1^c,s_2^c) = \int_{s_1^c}^{s_2^c} dA$, $\bar{S}_y(s_1^c,s_2^c) = \int_{s_1^c}^{s_2^c} x dA$, $\bar{S}_x(s_1^c,s_2^c) = \int_{s_1^c}^{s_2^c} y dA$, and $\bar{S}_\omega(s_0,s_1^c,s_2^c) = \int_{s_1^c}^{s_2^c} \omega(s_0,s) dA$, when the shear flow $\tau_c(s_1^c,z)t(s_1^c)$ is given at a point s_1^c of segment c. Thus, the shear flow at least at one point of the segment should be given to obtain the shear stress distribution on the segment.

Since the shearing stresses at the edges vanish, the edge points are selected as the starting point. Thus for a segment c which has a free joint (e.g., segments 1, 2, 4 and 5 in Fig. IV.A.1), by setting $s_1^c = s_b^c$, the shear stress distributions as well as the shear stresses at the other joint of the segments can be calculated.

From the flow continuity condition at joints by using the previously obtained shear flows at the end joints of external segments one obtains the shear flow at the beginning joint of a neighboring segment (e.g., $f(s_e^1, z)+f(s_b^2, z)+f(s_b^3, z)=0$ at joint 2). The joint stresses can be obtained in an order such that the flow continuity equations will contain only one unknown at a time.

Thus an algorithm to obtain shear stress distribution involves the following steps;

- Based on the input data the external plate segments which are free at one of its end joints are determined.
- The shear stress distribution is calculated for external segments by using the vanishing condition of the shear flow at the free joints.
- The segments which are connected only to external segments are determined.
- -Shear flow continuity condition is at the end joints of the segments which are connected only to external segments, and the shear flow at one of the end joints of these segments are obtained.
- -By using the shear flow at the end joint, the shear stress distribution can be obtained.

For most open cross-sections used in practice these five steps will be enough to determine the shear stress distribution, since the cross-section is composed of external segments and segments connected to external segments. However, the computation can be pursued for more complex cross-sections by classifying its segment in a hierarchical order similar to what was explained above.

Chapter IV References

[IV.1] Barsoum. R. S. and Gallagher, R. H. 1970. Finite Element Analysis of Torsional and Torsional-Flexural Stability Problems. International Journal for Numerical Methods in Engineering, Vol. 2, 335-352.

[IV.2] Batoz, J. L. and Dhatt, G. 1990. *Modélisation des structures par éléments finis [Modelling of structures using finite elements]*, 2 Hermes Edition, Paris (in French).

[IV.3] Boresi, A.P. and Sidebottom, O.M. 1985. Advanced Mechanics of Materials, Fourth Edition, John Wiley & Sons, New York, USA.

[IV.4] Coyette, J.P. 1987. An improved subroutine for the estimation of torsional properties of thin-walled open section, Engineering Computations: International Journal for Computer-Aided Engineering, Vol. 4, pp.240-242,

[IV.5] Erkmen, R.E. and Mohareb, M. 2006. Non-orthogonal solution for thin-walled beams – A Finite Element Formulation, Canadian Journal of Civil Engineering, Vol.33, No.4, 421-439.

[IV.6] Erkmen, R.E. and Mohareb, M. 2006. Non-orthogonal solution for thin-walled beams – Applications and Modelling considerations, Canadian Journal of Civil Engineering, Vol.33, No.4, 440-450.

[IV.7] Gjelsvik, A. 1981. The theory of thin walled bars, John Wiley and Sons, New York, U.S.A.

[IV.8] Heins, C. P. and Wang, R. C. 1978. Torsional properties of open cross-sections, Computers & Structures, Vol. 9, 495-500.

[IV.9] Murray, N. W. 1984. Introduction to the theory of thin-walled structures. Claredon Press, Oxford, United Kingdom.

[IV.10] Krajcinovic, D. 1969. A Consistent Discrete Element Technique for Thin Wall Assemblages, International Journal for Solids and Structures, 5, 639-662.

[IV.11] Prokic, A. 2000. Computer Program for determination of geometrical properties of thin-walled beams with open-closed section Computers & Structures, Vol. 74, 705-715.

[IV.12] Seaburg, P.A. and Carter, C. J. 1997. Torsional Analysis of Structural Steel Members, American Institute of Steel Construction, Chicago, IL, USA.

[IV.13] Vlasov, V. Z. 1961. Thin Walled Elastic Beams, Second Edition, Israel Program for Scientific Translations, Jerusalem, Israel.

Chapter IV List of symbols

A	=	cross-sectional area (Fig. IV.1);
A_p	=	arbitrary pole (Fig. IV.1);
a_x, a_y	=	coordinates of arbitrary pole A_p (Figs. IV.1, IV.2);
b_c	=	width of the of c^{th} thin-wall segment;
B	=	bimoments;
C_w	=	warping constant;
E	=	modulus of elasticity;
$f(s,z)$	=	a shear flow function;
$\mathbf{F}_{14\times1}$	=	load vector due to end tractions;
G	=	shear modulus;
$h(s)$	=	normal distance between pole and the tangent to mid-surface;
$J_{xx}, J_{yy}, J_{xy}, J_{\omega x}, J_{\omega y}$	=	section moments of inertia and products of inertia;
J_d	=	St. Venant's torsional constant;
$J_{\omega\omega}$	=	second moment of the sectorial coordinate;
$J_{xx}^c, J_{yy}^c, J_{xy}^c, J_{\omega x}^c, J_{\omega y}^c$	=	Contribution of c^{th} segment of the cross section to the relevant moments and products of inertia;
$\mathbf{K}_{\mathbf{e}14\times14}$	=	stiffness matrix of NOVEE14 element;
l	=	length of finite element;
$m(z)$	=	twisting moments per unit length about polar axis;

M_x, M_y = bending moments;

$\overline{M}_x, \overline{M}_y$ = end bending moments induced by tractions about the polar

axis (Fig. IV.2);

n = number of segments defining a cross-section;

N = axial stress resultant;

$\overline{N}$ = axial force at the end of the beam;

$\mathbf{N}(z)^{\mathbf{T}}_{1\times 4}$ = cubic shape function vector;

NOVEE14 = Non-Orthogonal Vlasov Element based on Exact shape functions with 14 degrees of freedom

$\mathbf{p}(s,z)_{3\times 1}$ = member traction vector acting on member mid-surface (Fig. IV.2) in force per unit area;

$\mathbf{P}_{14\times 1}$ = nodal force vector due to externally applied tractions at member ends;

q_x, q_y, q_z = resultant of traction vector (force per unit length);

$\mathbf{R}_{14\times 1}$ = energy equivalent nodal force vector due to member loads;

r = coordinate normal to the section mid surface (Fig. IV.2);

S_x, S_y, S_ω = first moments of area of coordinates *x, y,* and ω;

S_0 = sectorial origin (Figs. IV.1, IV.2);

s = curvilinear coordinate along mid surface (Fig. IV.1, Fig.IV.2);

s_1^c = s coordinate of a point located on the c^{th} segment where shear stresses are assumed to be known;

s_2^c = s coordinate of a point located on the c^{th} segment where shear stresses are to be determined;

s_b^c = s coordinate at the beginning of c^{th} segment;

s_e^c = s coordinate at the end of c^{th} segment;

t_c = thickness of c^{th} thin-wall segment;

T_{sv} = St.Venant torsion (Fig. IV.2);

T_w = warping torsion (Fig. IV.2);

T = total twisting moment;

$\overline{T}$ = end twisting moments about the polar axis (Fig. IV.2);

$\mathbf{U_N}$ = nodal displacement vector for the homogeneous case;

$u(z), v(z)$ = displacements along x, y directions of arbitrary pole (Fig. IV.1);

$u_s(s,z), v_s(s,z)$ = horizontal and vertical displacements of arbitrary point B_p located on section mid-surface (Fig. IV.1);

V_x, V_y = shear stress resultants;

$\overline{V}_x, \overline{V}_y$ = shear stress resultants at the end of the beam (Fig. IV.2);

$w(z)$ = function related to the longitudinal displacement of the section

$w_s(s,z)$ = longitudinal displacement of arbitrary point B_p on the mid-surface (Fig. IV.2);

x, y, z = coordinates of arbitrary point B_p (Figs. IV.1, IV.2);

$\beta(c,j)$, $\gamma(c,j)$ = coefficients for shear flow continuity for joint j;

$\phi(z)$ = angle of twist about the longitudinal axis;

$\boldsymbol{\varphi}_{N4\times1}, \mathbf{u}_{N4\times1}, \mathbf{v}_{N4\times1}, \mathbf{w}_{N2\times1}$	=	nodal displacement vectors;
σ_{zz}	=	longitudinal stress;
$\bar{\sigma}, \bar{\tau}$	=	externally applied tractions at the ends of the element;
ω	=	sectorial area;

Chapter IV List of Tables

Chapter IV List of Figures

Chapter V

Torsion Analysis of Thin-Walled Beams Including Shear Deformation Effects

Abstract

The first part of this chapter develops a theory for the torsional analysis of open thin-walled beams of general cross-sections. The theory accounts for shear deformation effects. Statically admissible stress fields are postulated in agreement with those resulting from the Vlasov thin-walled beam theory. The principle of stationary complementary energy is then adopted to formulate the governing field compatibility condition under the stress fields postulated. The naturally arising boundary terms are found to relate the warping deformations to the internal force fields. A torsion beam example is solved using the new theory in order to illustrate its applicability to practical problems. The second part of the chapter implements the solution numerically in a force-based finite element context. Two finite elements are developed by assuming linear and hyperbolic bimoment fields. The FEA solutions are shown to provide lower bound representations of the stiffness when compared to those based on conventional beam theories founded on postulated kinematic assumptions.

Keywords: torsion, warping, thin-walled beams, shear deformation, finite element, complementary energy.

Introduction

Open thin walled steel sections subjected to twisting moments are generally prone to large warping stresses and excessive angles of twist. It is therefore common practice to avoid twisting moments in steel assemblies consisting of open steel sections whenever possible. However, in a number of practical applications, twisting cannot be avoided and the designer is compelled to count on the torsional resistance of these members. The classical formulation for open thin-walled sections subjected to non-uniform torsion was developed by Vlasov (1961). The Vlasov formulation is based on two fundamental kinematic assumptions. These are: a) In-plane deformations of the section are negligible, and b) Shear strains along the section mid-surface are negligible.

Closed-form solutions for the torsional analysis of thin-walled beams under various loads and boundary conditions were presented in a number of texts e.g., Heins and Seaburg (1963) and Seaburg and Carter (1997). Barsoum (1970) and Barsoum and Gallagher (1970) modeled warping torsion of open steel sections using two finite element formulations featuring C1 and C2 continuity of the twisting angle, respectively. The solutions were based on cubic and fifth order Hermitian polynomial interpolations. The solution based on cubic Hermitian polynomials is found to yield results close to those based on closed-form solutions only when a sufficiently large number of elements are used (McGuire et al. 2000).

Krajcinovic derived a displacement based finite element formulation (1969) and a force based finite element formulation (1970) for the torsional analysis of thin-walled sections based on hyperbolic interpolation functions. A finite element for the analysis of open and closed thin-walled sections was developed by Gunnlaugson and Pedersen (1981). The finite element in Krajcinovic (1969) was successfully employed to the approximate analysis of curved beams by Dvorkin et al. (1989). Batoz and Dhatt (1990) developed a generalized 14 DOF thin-walled beam element based on an orthogonal system of coordinates. Mohareb and Nowzartash (2003) demonstrated the exactness of the solution of Krajcinovic (1969) for the case of non-vanishing member loads. Erkmen and Mohareb (2006) extended the formulation to thin-walled beams using non-orthogonal coordinate systems. A common feature in the above formulations is the omission of the effect of shear deformations in line with the second assumption of the Vlasov theory.

Several beam finite elements were developed according to the Timoshenko beam model for solid beams which account for shear deformation effects due to non-uniform bending. This includes the work of Mucichescu (1984), Friedman and Kostmatka (1993), and Nowzartash and Mohareb (2005). Displacement based formulations incorporating shear deformation effects for thin-walled beams were developed by Chen and Blandford (1989) and Back and Will (1998). Shakourzadeh et al. (1995) derived a finite element based on the thin walled beam theory of Benscoter (1954), which incorporates the effect of shear deformation effects due to warping torsion. The formulations in Mucichescu (1984), Friedman and Kostmatka (1993), Nowzartash and Mohareb (2005), Chen and Blandford (1989), Back and Will (1998), Shakourzadeh et al. (1995), and Benscoter (1954) have the commonality of starting with kinematic assumptions and formulating the governing equilibrium equations by employing the principle of minimum potential energy or the principle of virtual work, and thus provide an upper bound representation of the structure stiffness in the sense that under given loads, the internal strain energy is smaller than that based on a 3D theory of elasticity solution (Synge 1957). Based on more elaborate kinematic assumptions, advanced beam theories accounting for the cross-section warping were developed by several authors e.g., Levinson (1981), Bickford (1982), and Heyliger and Reddy (1988).

A hybrid stress formulation including shear deformations due to warping was developed by Tralli (1985). Gendy et al. (1990) developed hybrid strain formulations for the flexural torsional analysis of thin-walled beams. Schulz and Filippou (1998) developed a finite element for torsional-flexural analysis of thin-walled and moderately thick-walled beams by assuming that the transverse normal stresses are negligible.

The idea of this paper is to develop an approach which incorporates shear deformation effects due to warping by assuming statically admissible stress fields in conjunction with the principle of stationary complementary energy. Stress resultant interpolation functions are subsequently assumed to formulate a flexibility matrix which is then inverted to yield to the element stiffness matrix. Since the proposed solution satisfies the Vlasov beam equilibrium condition in a point-wise sense while generally satisfying compatibility only in an average integral sense, it leads to an under-prediction of the structure stiffness, a feature that is desirable to designers when compared to solutions leading to over-prediction of the structure stiffness.

Assumptions

The formulation is restricted to the torsional analysis of prismatic beams with open sections. The material is assumed to remain elastic throughout deformation. This assumption is justified in a large number of applications by the fact that, due to the weak torsional stiffness of open sections, they frequently attain excessive angles of twist, a serviceability limit state, prior to undergoing any plastic deformations. The normal stresses along the tangential direction of cross-section profile are assumed negligible, in line with most beam theories.

Assumed Stress Fields

As a starting point, statically admissible stress fields (i.e., stresses exactly satisfying the equilibrium conditions in a point-wise sense) are postulated. The normal and shearing stress fields analogous to those based on the Vlasov thin-walled beam theory (Vlasov 1961) are selected. These are:

$$\sigma(s,z)=\frac{B(z)\omega(s)}{C_w} \tag{V.1}$$

$$\tau_w(s,z)=-\frac{T_w(z)\bar{S}_\omega(s)}{C_w t(s)} \tag{V.2}$$

$$\tau_{sv}(z,r)=\frac{T_{sv}(z)}{J_d}r \tag{V.3}$$

in which $\sigma(s,z)$ and $\tau_w(s,z)$ are the longitudinal and shearing stress fields, respectively, which are induced by bimoment $B(z)$ and warping torsion $T_w(z)$. These stress fields are assumed to be functions of the longitudinal coordinate z and the circumferential coordinate s, measured from the principal sectorial origin S_0 (Fig. V.1). Coordinate s identifies the coordinates $[x(s), y(s)]$ of any point P on the middle surface (Fig. V.2). The shearing stress $\tau_{sv}(s,r)$ is induced by the St. Venant torsion $T_{sv}(z)$ and has a linear distribution across the thickness. Hence it is a function of coordinate r which is the normal distance from the mid-surface in the plane of cross-section. Symbol $t(s)$ denotes the thickness of the section as a function of the coordinate s (Fig. V.2).

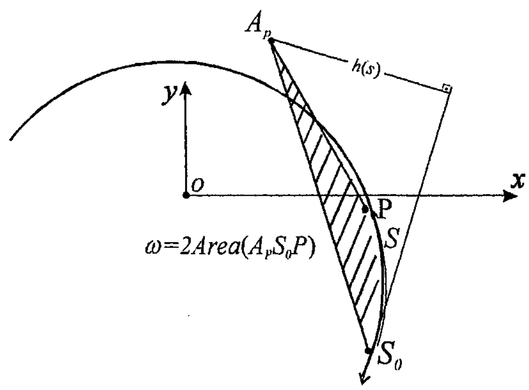

Fig. V.1- Coordinates and Sectorial Area

In order to eliminate the coupling between torsional response and flexural deformations, origin O (Figure V.1) is selected to coincide with the section centroid while the pole A_p is selected to coincide with the section shear center (Vlasov 1961). The above selections allow the stresses and deformations obtained from a torsional analysis to be additive to those based on conventional flexural analysis (Erkmen and Mohareb 2006). In line with the Vlasov theory, coordinate $\omega(s)=\int_{s_0}^{s} h(s)ds$ is the sectorial coordinate measured from the principal sectorial origin s_0 where $h(s)$ is the distance from the section shear centre to the tangent of the profile at coordinate s (Fig. V.1). The function $\overline{S}_{\omega}(s)=\int_{s_1}^{s}\omega(\varsigma)t(\varsigma)d\varsigma$ is the sectorial static moment, in which the lower integration limit s_1 is chosen such that the corresponding warping shear stress $\tau_w(s_1,z)$ vanishes (e.g., at an edge of the cross-section with zero external tractions).

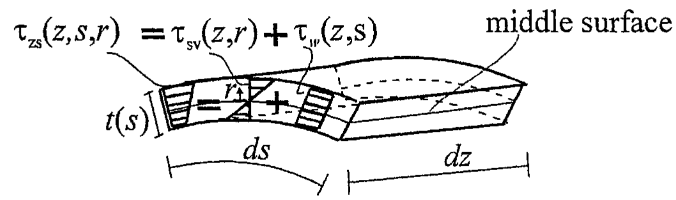

Fig. V.2-Shearing stresses

Symbol C_w is the warping constant and is defined by the integration of the square of sectorial coordinate over the cross-sectional area *i.e.*, $C_w = \int_A \omega^2 dA$. Symbol J_d is the St. Venant torsional constant. For a cross-section consisting of n thin-walled rectangular pieces of constant thickness t_i and width b_i, the St. Venant torsional constant is obtained by the formula $J_d \approx \sum_{i=1}^{n} 1/3 b_i t_i^3$ (Boresi and Sidebottom 1985) when $b_i/t_i \geq 10$. Functions $B(z)$, $T_w(z)$, and $T_{sv}(z)$ are to be determined based on equilibrium conditions, and possibly on compatibility considerations. In force-based finite element formulations such as the one sought in this paper, satisfying the compatibility requirement in a strict point-wise sense is not necessary, although it will be shown that meeting this condition provides superior solutions compared to other force formulations which violate this requirement.

First Equilibrium Requirement

As shown in Figure V.2, the total shear stress $\tau_{zs}(s,z,r)$ can be expressed as the sum of the constant component due to warping $\tau_w(s,z)$ and the component due to St.Venant torsion $\tau_{sv}(s,r)$. By writing the equilibrium condition in the longitudinal direction for a differential piece taken from a thin-walled beam in the absence of externally applied longitudinal tractions (Fig. V.3), one obtains

$$\frac{\partial}{\partial z}\left[\sigma(s,z)t(s)\right] + \frac{\partial}{\partial s}\left[\int_{-t(s)/2}^{t(s)/2} \tau_w(s,z)dr + \int_{-t(s)/2}^{t(s)/2} \tau_{sv}(s,r)dr\right] = 0 \qquad \text{(V.4)}$$

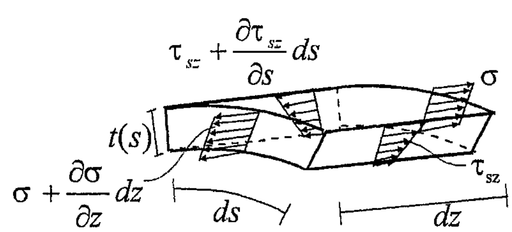

Fig. V.3- Longitudinal Equilibrium of an infinitesimal element

From Equations (V.1), (V.2) and (V.3) by substituting into Eq. (V.4) and noting that due to linear distribution of shear stresses induced by the St. Venant torsion, their integration along the thickness vanishes i.e., $\int_{-t(s)/2}^{t(s)/2} \tau_{sv}(z,r)dr = 0$, the following relationship between function $B(z)$ and $T_w(z)$ is established

$$B'(z) = T_w(z) \tag{V.5}$$

In Equation (V.5) and the following equations, all primes denote differentiation with respect to longitudinal coordinate *z*.

Second Equilibrium Requirement

Under externally applied distributed twisting moment per unit length $t(z)$ (Fig. V.4), the torsional equilibrium condition for an infinitesimal element of length *dz* can be expressed as

$$T'(z) = T_w'(z) + T_{sv}'(z) = -t(z) \tag{V.6}$$

in which the total twisting moment $T(z)$ is the sum of the warping torsion $T_w(z)$ and the St. Venant torsion $T_{sv}(z)$. By integrating Eq. (V.6) from *z* to *l*, one obtains

$$\left[T_{sv}(l) + T_w(l)\right] - \left[T_{sv}(z) + T_w(z)\right] = -\int_z^l t(\eta)d\eta \tag{V.7}$$

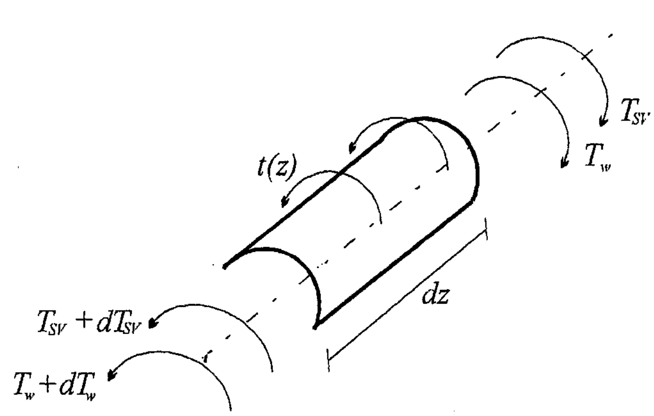

Fig. V.4- Torsional equilibrium of a beam segment

Equation (V.7) will be used to express the St. Venant torsion in terms of the warping torsion. By setting $z=0$ in Eq. (V.7), one obtains

$$T_l - T_0 = \left[T_{sv}(l) + T_w(l)\right] - \left[T_{sv}(0) + T_w(0)\right] = -\int_0^l t(z)dz \tag{V.8}$$

Equation (V.8) establishes the relation between the end twisting moments and will subsequently be used in expressing the load potential.

Variational Formulation

The total complementary energy π^* can be expressed as

$$\pi^* = U^* + V^* \tag{V.9}$$

in which U^* is the complementary strain energy and V^* is the potential of the generalized forces. The complementary strain energy U^* has three components. These are due to: a) the normal stresses induced by bimoments, b) the shearing stresses induced by warping torsion, and c) the shearing stresses induced by St.Venant torsion. The complementary strain energy U^* is expressed as

$$U^*\left(\sigma, \tau_w, T_{sv}\right) = \frac{1}{2E}\int_V \sigma^2 dV + \frac{1}{2G}\int_V \tau_w{}^2 dV + \frac{1}{2GJ_d}\int_0^l T_{sv}{}^2 dz \tag{V.10}$$

The external load potential has two contributions. These are due to: a) the external member loads, and b) the end forces. It is expressed as

$$V^*\left(B_0,B_l,T_l,T_0\right)=-\int_0^l \phi(z)t(z)dz-T_l\phi_l-B_l\theta_l+B_0\theta_0+T_0\phi_0 \qquad \text{(V.11)}$$

in which T_0, T_l, B_0 and B_l are the twisting moments and bimoments at ends $z=0$ and $z=l$ respectively (Fig. V.5). At $z=l$, the direction of the end rotation is identical to the end twisting moment and the direction of the warping deformation is identical to the end bimoment. Thus the sign of the second and third terms is negative. Conversely, at $z=0$, the positive signs in the last two terms of Eq. (V.11) are due to the fact that the directions of the assumed generalized displacements ϕ_0 and θ_0 are defined opposite to the directions of T_0 and B_0 (Fig. V.4). From Eqs. (V.1) and (V.2), by substituting into Eq. (V.10), the complementary strain energy U^* can be expressed in terms of the stress resultants as

$$U^*\left(B,T_w,T_{sv}\right)$$
$$=\frac{1}{2E}\int_0^l\left[\frac{B(z)}{C_w}\right]^2\int_A[\omega(s)]^2dAdz+\frac{1}{2G}\int_0^l\left[\frac{T_w(z)}{C_w}\right]^2\int_A\left[\frac{\bar{S}_\omega(s)}{t(s)}\right]^2dAdz+\frac{1}{2GJ_d}\int_0^l[T_{sv}(z)]^2dz$$

(V.12)

Equations (V.5) and (V.7) are used to express the warping and St. Venant torsion functions $T_w(z)$ and $T_{sv}(z)$ in terms of functions $B'(z)$ and $t(z)$ and then substituted into Eq. (V.12) yielding,

$$U^*\left(B,B',T_l\right)=\frac{1}{2EC_w}\int_0^l[B(z)]^2dz+\frac{1}{2GJ_{r\omega}}\int_0^l[B'(z)]^2dz+\frac{1}{2GJ_d}\int_0^l\left[T_l-B'(z)+\int_z^l t(\eta)d\eta\right]^2dz$$

(V.13)

in which $J_{r\omega}$ is a newly arising cross-sectional property associated with the distribution of shear stresses over the cross-section and is calculated from

$$J_{r\omega} = \frac{C_w^{\;2}}{\int_A \left[\frac{\bar{S}_\omega(s)}{t(s)}\right]^2 dA} \tag{V.14}$$

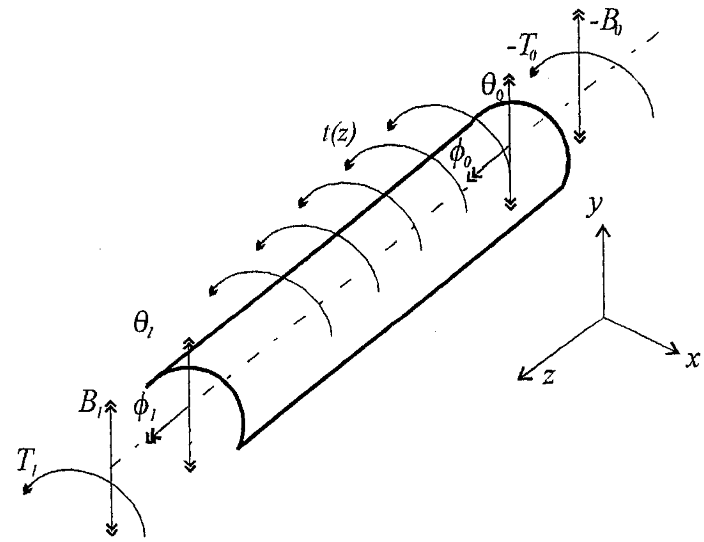

Fig. V.5 Sign Convention for Nodal forces and displacements

From Eqs. (V.11) and (V.13), by substituting into Eq. (V.9), using the equilibrium relation provided in Eq. (V.8), and taking the variation of the resulting total complementary energy expression, one obtains,

$$\begin{aligned}\delta\pi^* = {} & \frac{1}{EC_w}\int_0^l B\delta B dz + \int_0^l \left[\left(\frac{1}{GJ_{r\omega}} + \frac{1}{GJ_d}\right)B' - \frac{1}{GJ_d}\int_z^l t(\eta)d\eta - \frac{T_l}{GJ_d}\right]\delta B' dz \\ & -\delta T_l\left(\phi_l - \phi_0\right) - \delta B_l\theta_l + \delta B_0\theta_0\end{aligned} \tag{V.15}$$

In obtaining Eq. (V.15), the variation of the load potential due to the external twisting moment vanishes since the applied twisting moments $t(z)$ are specified quantities. By integrating Eq. (V.15) by parts, one obtains

$$\delta\pi^*(B,B',T_l)$$

$$= \int_0^l \left[\frac{B}{EC_w} - \left(\frac{1}{GJ_{r\omega}} + \frac{1}{GJ_d} \right) B'' - \frac{t(z)}{GJ_d} \right] \delta B dz$$

$$+ \left[\left(\frac{1}{GJ_{r\omega}} + \frac{1}{GJ_d} \right) B_l' - \theta_l - \frac{T_l}{GJ_d} \right] \delta B_l - \left[\left(\frac{1}{GJ_{r\omega}} + \frac{1}{GJ_d} \right) B_0' - \theta_0 - \frac{T_0}{GJ_d} \right] \delta B_0 \quad \text{(V.16)}$$

$$-[\phi_l - \phi_0]\delta T_l$$

In the boundary terms of Eq.(V.16), either B_0, B_l and T_l are specified or the corresponding bracketed terms vanish. In the integral term of Eq. (V.16), since δB is an arbitrary function, its coefficient must vanish for the condition $\delta\pi^* = 0$ to be realized. Thus, the following field equation is recovered

$$k^2 B - B'' = \left(\frac{J_{r\omega}}{J_d + J_{r\omega}} \right) t(z) \quad \text{(V.17)}$$

in which the parameter $k = \sqrt{\dfrac{GJ_d J_{r\omega}}{EC_w(J_d + J_{r\omega})}}$ is defined. Equation (V.17) can be regarded as a compatibility condition under the assumed statically admissible stress fields postulated in Eq. (V.1) through (V.3). The boundary terms arising in Eq. (V.16) lead to the following boundary relations

$$\theta_0 = \left(\frac{1}{GJ_{r\omega}} + \frac{1}{GJ_d} \right) B_0' - \frac{T_0}{GJ_d} \quad \text{or } B_0 = specified \quad \text{(V.18)}$$

and

$$\theta_l = \left(\frac{1}{GJ_{r\omega}} + \frac{1}{GJ_d} \right) B_l' - \frac{T_l}{GJ_d} \quad \text{or } B_l = specified \quad \text{(V.19)}$$

and either

$$\phi_l - \phi_0 = 0 \qquad \text{or } T_l = specified \quad \text{(V.20)}$$

Equation (V.20) signifies that either the beam exhibits rigid body rotation or the twisting moment applied to the end of the beam is specified. Note that Eq. (V.8), relates the twisting moment at end $z = 0$ to that at $z = l$.

Stress resultants for the Case of no member loads

The homogenous form of the compatibility equation is obtained by setting $t(z) = 0$ in Eq. (V.17), i.e., $k^2 B - B'' = 0$ which has the following solution

$$B(z) = c_1 \cosh kz + c_2 \sinh kz \tag{V.21}$$

From Eq. (V.5), by taking the derivative of Eq. (V.21) with respect to longitudinal coordinate z, the following expression for warping torsion is obtained.

$$T_w(z) = c_1 k \sinh kz + c_2 k \cosh kz \tag{V.22}$$

The St. Venant torsion is then obtained by substituting Eq. (V.22) into Eq. (V.7) yielding

$$T_{sv}(z) = -c_1 k \sinh kz - c_2 k \cosh kz + T_l \tag{V.23}$$

Generalized Displacements for the Case of no member loads

From Eq. (V.23), and the relation between the St. Venant torsion and the derivative of the angle of twist $T_{sv}(z) = GJ_d \phi'(z)$, the angle of twist $\phi(z)$ can be expressed as

$$\phi(z) = \left\langle -\frac{1}{GJ_d} \cosh kz \quad -\frac{1}{GJ_d} \sinh kz \quad \frac{1}{GJ_d} z \quad 1 \right\rangle \begin{Bmatrix} c_1 k \\ c_2 k \\ T_l \\ c_3 \end{Bmatrix} \tag{V.24}$$

In Eq. (V.24), c_3 is the integration constant to be determined from the displacement boundary conditions of the problem. Noting that the compatibility requirement is to be satisfied for any segment of beam of length z, one can set l=z in Eq. (V.16) leading to the following relation

$$\theta(z)=\left(\frac{1}{GJ_{r\omega}}+\frac{1}{GJ_{d}}\right)B'(z)-\frac{T(z)}{GJ_{d}} \tag{V.25}$$

By considering $T(z)=T_l$ for the case of no member loads, using the derivative of Eq. (V.21) and substituting into Eq.(V.25), one obtains

$$\theta(z)=\left\langle \left(\frac{1}{GJ_{r\omega}}+\frac{1}{GJ_{d}}\right)k\sinh kz \quad \left(\frac{1}{GJ_{r\omega}}+\frac{1}{GJ_{d}}\right)k\cosh kz \quad \frac{-1}{GJ_{d}} \quad 0\right\rangle \begin{Bmatrix} c_1 k \\ c_2 k \\ T_l \\ c_3 \end{Bmatrix} \tag{V.26}$$

From Equations (V.24) and (V.26), one can obtain the end displacements as

$$\{u\}_{4\times 1}=[S]_{4\times 4}\{c\}_{4\times 1} \tag{V.27}$$

in which $\langle u\rangle^{T}_{1\times 4}=\langle \phi_0 \quad \theta_0 \quad \phi_l \quad \theta_l\rangle$, $\langle c\rangle^{T}_{1\times 4}=\langle c_1 k \quad c_2 k \quad T_l \quad c_3\rangle$ and

$$[S]_{4\times 4}=\begin{bmatrix} -\frac{1}{GJ_d} & 0 & 0 & 1 \\ 0 & \left(\frac{1}{GJ_{r\omega}}+\frac{1}{GJ_{d}}\right)k & \frac{-1}{GJ_d} & 0 \\ -\frac{\cosh kl}{GJ_d} & -\frac{\sinh kl}{GJ_d} & \frac{l}{GJ_d} & 1 \\ \left(\frac{1}{GJ_{r\omega}}+\frac{1}{GJ_{d}}\right)k\sinh kl & \left(\frac{1}{GJ_{r\omega}}+\frac{1}{GJ_{d}}\right)k\cosh kl & \frac{-1}{GJ_d} & 0 \end{bmatrix}$$

By inverting Eq. (V.27) and substituting into Eqs. (V.24) and (V.26), the angle of rotation and warping deformation are obtained in terms of the end displacements as

$$\phi(z)=\left\langle -\frac{1}{GJ_d}\cosh kz \quad -\frac{1}{GJ_d}\sinh kz \quad \frac{1}{GJ_d}z \quad 1\right\rangle [S]^{-1}_{4\times 4}\{u\}_{4\times 1} \tag{V.28}$$

$$\theta(z)=\left\langle \left(\frac{1}{GJ_{r\omega}}+\frac{1}{GJ_{d}}\right)k\sinh kz \quad \left(\frac{1}{GJ_{r\omega}}+\frac{1}{GJ_{d}}\right)k\cosh kz \quad \frac{-1}{GJ_{d}} \quad 0\right\rangle [S]^{-1}_{4\times 4}\{u\}_{4\times 1} \tag{V.29}$$

Example V.1- Closed Form Solution

The objective of this example is to illustrate the use of the field and boundary equations developed in the previous section in a practical problem. A W200x59 simply supported beam (section dimensions are shown in Figure V.6, and section properties are $C_w = 1.87 \times 10^{11} mm^6$, $J_d = 3.90 \times 10^6 mm^4$, $J_{r\omega} = 4.89 \times 10^7 mm^4$, and $k = 0.89 \times 10^{-3}$) is spanning three meters $L = 3,000mm$. It is subject to concentrated twisting moment $T_{ex} = 10kNm$ acting at $L_1 = 2,000mm$ from the left support as illustrated in Figure V.6. It is required to determine the angle of twist at the point of application of the load. Material is structural steel $E = 200,000MPa, G = 77,000MPa$. From Eq. (V.21), the bimoment field equations can be written as $B_1(z) = c_1 \cosh kz + c_2 \sinh kz$ for $0 \le z \le L_1$, and $B_2(z) = d_1 \cosh kz + d_2 \sinh kz$ for $L_1 \le z \le L$. For all field terms in this example, subscript 1 denotes the left span $0 \le z \le L_1$ and subscript 2 denotes the right span $L_1 \le z \le L$. By writing the torsion equilibrium condition of the intermediate joint $T_1(L_1) - T_2(L_1) = T_{ex}$ while enforcing the continuity condition of the warping deformation at that joint $\theta_1(L_1) = \theta_2(L_1)$ and using Eq. (V.25), one obtains $(1 + J_d/J_{rw})[B_1'(L_1) - B_2'(L_1)] = T_{ex} = 10 \times 10^6 Nmm$. Also, by using the force boundary conditions $B_1(0) = 0$, $B_2(L) = 0$ and the bimoment equilibrium condition for the intermediate joint, $B_1(L_1) - B_2(L_1) = B_{ext} = 0$, one obtains the four conditions necessary to determine the integration constants c_1, c_2, d_1 and d_2. These are found to be $c_1 = 0$, c_2=$1.56 \times 10^9 Nmm^2$, $d_1 = 3.22 \times 10^{10} Nmm^2$, and $d_2 = -3.25 \times 10^{10} Nmm^2$. From Eq. (V.24) the angle of twist field can be expressed as $\phi_1(z) = [T_1 z - B_1(z)]/GJ_d + c_3$ for $0 \le z \le L_1$

and $\phi_2(z)=[T_2 z-B_2(z)]/GJ_d+d_3$ for $L_1<z\le L$. By using the boundary conditions $\phi_1(0)=0$, $\phi_1(L_1)=\phi_2(L_1)$, $\phi_2(L)=0$ and $T_1(L_1)-T_2(L_1)=T_{ex}$ together with $B_1(0)=0$, $B_1(L_1)=B_2(L_1)$ and $B_2(L)=0$, one obtains the constants $c_3=0$, $d_3=0.666$ *rad*, $T_1(\mathrm{L}_1)$=$3.33\times10^6 Nmm$ and $T_2(\mathrm{L}_1)$=$-6.67\times10^6 Nmm$. Based on the obtained constants, the angle of twist at the point of load application is found as ϕ=0.0717 *rad.* This value compares with $\phi=0.0705$ *rad* as predicted by the Vlasov theory (Closed form expressions for the angle of twist based on the Vlasov theory are provided in Heins and Seaburg 1963 for the given problem). In the given example, the Vlasov theory which neglects shear deformation effects, underestimates the angle of twist as predicted by the current theory by nearly 2%. Other quantities of interest at $z=L_1$ are found to be $\theta(L_1)=3.219\times10^{-5}mm^{-1}$ and $B(L_1)=0.45\times10^{10}Nmm^2$ which corresponds to a maximum normal stress $\sigma_{\max}=243Mpa$ and a maximum warping shearing stress $\tau_{w\max}=14.9MPa$. The new theory has the obvious advantage of capturing shear deformation effect.

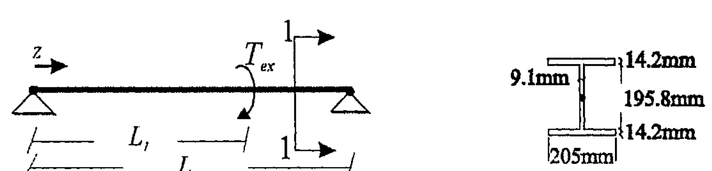

Sec1-1

Fig. V.6- Simply supported beam with singular Twisting moment

In principle, the field and boundary conditions developed can accommodate other practical problems involving loading schemes and boundary conditions. However, a more systematic approach for computer implementation is developed in the following sections by adapting the above theory in a finite element context.

Finite Element Formulations

Element based on Linear Interpolation of the Bimoment Field

In order to formulate a force-based finite element formulation, one must select force field functions satisfying the equilibrium equations and force boundary conditions. While equilibrium equations (V.5) and (6) relate the warping and St. Venant torsional functions to the bimoment function, they do not assign any constraints on the selection of the self-equilibrating bimoment field function. A linear interpolation scheme for the bimoments field is selected to relate the bimoment field to its nodal values B_0 at end *z=0* to B_l at end *z=l* (Fig. V.5). The resulting element will be referred to as TLE4 (Torsional Linear Element with 4 degrees of freedom)

$$B(z) = B_0\left(1-\frac{z}{L}\right)+B_l\left(\frac{z}{L}\right) \tag{V.30}$$

From the first equilibrium requirement in Eq. (V.5), by taking the derivative of Eq. (V.30) with respect to longitudinal coordinate *z*, an expression for the warping torsion is obtained.

$$T_w(z) = -B_0/l + B_l/l \tag{V.31}$$

The St. Venant torsion is then obtained by substituting Eq. (V.31) into the equilibrium condition in Eq. (V.7) yielding

$$T_{sv}(z) = B_0/l - B_l/l + T_l + \int_z^l t(\eta)d\eta \tag{V.32}$$

Equations (V.30) through (V.32) are arranged in matrix form, yielding

$$\begin{Bmatrix} B(z) \\ T_w(z) \\ T_{sv}(z) \end{Bmatrix}_{3\times1} = \begin{bmatrix} \langle L^T(z) \rangle_{1\times3} \\ \langle L'^T(z) \rangle_{1\times3} \\ \langle M^T(z) \rangle_{1\times3} \end{bmatrix} [H_a]_{3\times3} \{P\}_{3\times1} + \begin{Bmatrix} 0 \\ 0 \\ \Gamma(z) \end{Bmatrix} \tag{V.33}$$

In Equation (V.33), $\Gamma(z) = \int_z^l t(\eta)d\eta$ and $\langle P \rangle^T{}_{1\times3} = \langle -B_0 \quad T_l \quad B_l \rangle$ in which the first term is assigned a negative sign to conform to the end stress resultants sign convention previously defined in Fig. V.5, and

$$[H_a]_{3\times3} = \begin{bmatrix} -1 & 0 & 0 \\ 0 & 1 & 0 \\ 0 & 0 & 1 \end{bmatrix} \tag{V.34}$$

In Eq. (V.33), the matrix of interpolation functions can be explicitly expressed as

$$\begin{Bmatrix} \langle L^T(z) \rangle_{1\times3} \\ \langle L'^T(z) \rangle_{1\times3} \\ \langle M^T(z) \rangle_{1\times3} \end{Bmatrix} = \begin{bmatrix} (1-z/l) & 0 & (z/l) \\ (-1/l) & 0 & (1/l) \\ (1/l) & 1 & (-1/l) \end{bmatrix}_{3\times3} \tag{V.35}$$

By substituting Eq. (V.33) into Eq. (V.13), one obtains

$$\begin{aligned} \pi^* = {} & \frac{1}{2EC_w} \int_0^l \left[\langle P \rangle^T{}_{1\times3} [H_a]_{3\times3} \{L(z)\}_{3\times1} \langle L(z) \rangle^T{}_{1\times3} [H_a]_{3\times3} \{P\}_{3\times1} \right] dz \\ & + \frac{1}{2GJ_{r\omega}} \int_0^l \left[\langle P \rangle^T{}_{1\times3} [H_a]_{3\times3} \{L'(z)\}_{3\times1} \langle L'(z) \rangle^T{}_{1\times3} [H_a]_{3\times3} \{P\}_{3\times1} \right] dz \\ & + \frac{1}{2GJ_d} \int_0^l \left[\left(\langle P \rangle^T{}_{1\times3} [H_a]_{3\times3} \{M(z)\}_{3\times1} + \Gamma(z) \right) \left(\langle M(z) \rangle_{1\times3} [H_a]_{3\times3} \{P\}_{3\times1} + \Gamma(z) \right) \right] dz \\ & - \langle d \rangle^T{}_{1\times3} \{P\}_{3\times1} - \int_0^l \phi(z) t(z) dz \end{aligned} \tag{V.36}$$

In Equation (V.36), the reduced nodal displacement vector $\langle d \rangle^T{}_{1\times3} = \langle \theta_0 \quad (\phi_l - \phi_0) \quad \theta_l \rangle$ has been defined. By evoking the stationarity conditions of the complementary energy,

$\partial\pi^*/\partial\{P\}_{3\times1}=\{0\}_{3\times1}$, one obtains the compatibility relations based on the assumed interpolation field

$$[F]_{3\times3}\{P\}_{3\times1}=\{d\}_{3\times1}-\{\psi\}_{3\times1} \tag{V.37}$$

In Equations (V.37), $[F]_{3\times3}$ is the flexibility matrix given by

$$[F]_{3\times3}=[H_a]_{3\times3}\int_0^l\left[\frac{\{L(z)\}_{3\times1}\langle L(z)\rangle_{1\times3}}{EC_w}+\frac{\{L'(z)\}_{3\times1}\langle L'(z)\rangle_{1\times3}}{GJ_{r\omega}}+\frac{\{M(z)\}_{3\times1}\langle M(z)\rangle_{1\times3}}{GJ_d}\right]dz\,[H_a]_{3\times3} \tag{V.38}$$

and $\{\psi\}_{3\times1}$ is the displacement vector due to member loads given by

$$\{\psi\}_{3\times1}=[H_a]_{3\times3}\int_0^l\left[\frac{\{M(z)\}_{3\times1}\Gamma(z)}{GJ_d}\right]dz \tag{V.39}$$

By solving Equation 36 for the nodal force vector $\{P\}_{3\times1}$, one obtains

$$\{P\}_{3\times1}=[F]_{3\times3}^{-1}\{d\}_{3\times1}-[F]_{3\times3}^{-1}\{\psi\}_{3\times1} \tag{V.40}$$

Displacement vector $\{d\}_{3\times1}$ can be expressed in terms of the full nodal displacement vector $\langle d_f\rangle^T_{1\times4}=\langle\phi_0\quad\theta_0\quad\phi_l\quad\theta_l\rangle$ through

$$\{d\}_{3\times1}=\left[\{p\}_{3\times1}\;\vdots\;[I]_{3\times3}\right][H_b]_{4\times4}\{d_f\}_{4\times1} \tag{V.41}$$

In Equation (V.41), vector $\langle p\rangle^T_{1\times3}=\langle 0\quad 1\quad 0\rangle$, and the unit matrix $[I]_{3\times3}$ have been defined and matrix $[H_b]_{4\times4}$ is defined as

$$[H_b]_{4\times4}=\begin{bmatrix}-1&0&0&0\\0&1&0&0\\0&0&1&0\\0&0&0&1\end{bmatrix} \tag{V.42}$$

From Eq. (V.41) by substituting into Eq. (V.40) one obtains,

$$\{P\}_{3\times1} = \left[[F]^{-1}_{3\times3}\{p\}_{3\times1} \;\vdots\; [F]^{-1}_{3\times3}[I]_{3\times3}\right][H_b]_{4\times4}\{d_f\}_{4\times1} - [F]^{-1}_{3\times3}\{\psi\}_{3\times1} \tag{V.43}$$

From Eq. (V.43), by substituting into Eq. (V.8), one obtains

$$T_0 = \langle p\rangle^T_{1\times3}\left[[F]^{-1}_{3\times3}\{p\}_{3\times1} \;\vdots\; [F]^{-1}_{3\times3}[I]_{3\times3}\right][H_b]_{4\times4}\{d_f\}_{4\times1} - \langle p\rangle^T_{1\times3}[F]^{-1}_{3\times3}\{\psi\}_{3\times1} + \int_0^l t(z)dz \tag{V.44}$$

Equations (V.43) and (V.44) are consolidated into a single matrix equation as

$$[H_b]_{4\times4}\{P_f\}_{4\times1} = \left[\begin{array}{c|c} \langle p\rangle^T_{1\times3}[F]^{-1}_{3\times3}\{p\}_{3\times1} & \langle p\rangle^T_{1\times3}[F]^{-1}_{3\times3} \\ \hline [F]^{-1}_{3\times3}\{p\}_{3\times1} & [F]^{-1}_{3\times3} \end{array}\right][H_b]_{4\times4}\{d_f\}_{4\times1}$$
$$-\left(\left\{\begin{array}{c} \langle p\rangle^T_{1\times3}[F]^{-1}_{3\times3} \\ \hline [F]^{-1}_{3\times3} \end{array}\right\}_{4\times3}\{\psi\}_{3\times1} - \left\{\begin{array}{c} \int_0^l t(z)dz \\ \hline \{0\}_{3\times1} \end{array}\right\}_{4\times1}\right) \tag{V.45}$$

In Equation (V.45), the full nodal force vector is defined as

$\langle P_f\rangle^T_{1\times4} = \langle -T_0 \quad -B_0 \quad T_l \quad B_l\rangle$. By pre-multiplying both sides of Eq. (V.45) by matrix

$[H_b]_{4\times4}$, one obtains

$$\{P_f\}_{4\times1} = [K_f]_{4\times4}\{d_f\}_{4\times1} - \{\Lambda_f\}_{4\times1} \tag{V.46}$$

in which the full stiffness matrix $[K_f]_{4\times4}$ is given by

$$[K_f]_{4\times4} = [H_b]_{4\times4}\left[\begin{array}{c|c} \langle p\rangle^T_{1\times3}[F]^{-1}_{3\times3}\{p\}_{3\times1} & \langle p\rangle^T_{1\times3}[F]^{-1}_{3\times3} \\ \hline [F]^{-1}_{3\times3}\{p\}_{3\times1} & [F]^{-1}_{3\times3} \end{array}\right][H_b]_{4\times4} \tag{V.47}$$

and the energy equivalent nodal force vector is

$$\{\Lambda_f\}_{4\times1} = [H_b]_{4\times4}\left(\left\{\begin{array}{c} \langle p\rangle^T_{1\times3}[F]^{-1}_{3\times3} \\ \hline [F]^{-1}_{3\times3} \end{array}\right\}_{4\times3}\{\psi\}_{3\times1} - \left\{\begin{array}{c} \int_0^l t(z)dz \\ \hline \{0\}_{3\times1} \end{array}\right\}_{4\times1}\right) \tag{V.48}$$

The explicit form of the stiffness matrix $\left[K_f\right]_{4\times4}$ and the energy equivalent member load vector $\left\{\Lambda_f\right\}_{4\times1}$ for the special case of a linearly distributed twisting moment for element is given in Appendix V.A.

Element based on Hyperbolic Interpolation of the Bimoment Field

The objective of this section is to formulate a finite element with superior convergence characteristics to that formulated in the previous section. Towards this goal, in lieu of adopting linear interpolation bimoment functions, bimoments fields which satisfy the compatibility condition in Eq. (V.17) for the case of no member loads $t(z)=0$ are postulated instead. The resulting element will subsequently be termed as THE4 (Torsional Hyperbolic Element with 4 degrees of freedom). Equation (V.21) provides the solution for the bimoment function under zero member loads. By enforcing the force boundary conditions through the relations $B(0)=B_0$, and $B(l)=B_l$, one obtains $c_1=B_0$ and $c_2=\left(B_l-B_0\cosh kl\right)/\sinh kl$ and the bimoment field can be interpolated through the following functions

$$B(z)=\left\langle L_h\right\rangle_{1\times2}^{T}\begin{Bmatrix}B_0\\B_l\end{Bmatrix}_{2\times2}=\left\langle\left(\cosh kz-\frac{\cosh kl}{\sinh kl}\sinh kz\right)\quad\left(\frac{\sinh kz}{\sinh kl}\right)\right\rangle\begin{Bmatrix}B_0\\B_l\end{Bmatrix}\qquad\text{(V.49)}$$

in which $\left\langle L_h\right\rangle_{1\times2}^{T}$ is the vector of hyperbolic interpolation functions. By using the bimoment field in Eq. (V.49), and satisfying the equilibrium equations in (V.5) and (V.7), one can relate the internal forces to the nodal internal force values through

$$\begin{Bmatrix} B(z) \\ T_w(z) \\ T_{sv}(z) \end{Bmatrix}_{3\times1} = \begin{Bmatrix} \langle L_h(z)\rangle_{1\times3} \\ \langle L_h'(z)\rangle_{1\times3} \\ \langle M_h(z)\rangle_{1\times3} \end{Bmatrix} [H_a]_{3\times3}\{P\}_{3\times1}$$

$$= \begin{bmatrix} \left(\cosh kz - \dfrac{\cosh kl}{\sinh kl}\sinh kz\right) & 0 & \left(\dfrac{\sinh kz}{\sinh kl}\right) \\ \left(k\sinh kz - k\dfrac{\cosh kl}{\sinh kl}\cosh kz\right) & 0 & \left(k\dfrac{\cosh kz}{\sinh kl}\right) \\ \left(-k\sinh kz + k\dfrac{\cosh kl}{\sinh kl}\cosh kz\right) & 1 & \left(-k\dfrac{\cosh kz}{\sinh kl}\right) \end{bmatrix}_{3\times3} [H_a]_{3\times3}\{P\}_{3\times1} \tag{V.50}$$

By replacing $\langle L(z)\rangle^T$ and $\langle M(z)\rangle^T$ in Eq. (V.36) by $\langle L_h(z)\rangle^T$ and $\langle M_h(z)\rangle^T$ as defined in Eq. (V.50), and following a procedure similar to the one followed through Eq. (V.39), a new flexibility matrix $[F_h]_{3\times3}$ and associate energy equivalent vector $\{\psi_h\}_{3\times1}$ for linearly distributed twisting moment is obtained. These are provided in Appendix V.B. Also, by following the procedure similar to that described in Eq. (V.38) through Eq. (V.48), one numerically obtains the full stiffness matrix $\left[K_{hf}\right]_{4\times4}$ based on hyperbolic interpolation functions and the corresponding energy equivalent member load vector $\{\Lambda_{hf}\}_{4\times1}$ for the case of linearly distributed member load. Conceptually, since element THE4 satisfies the field compatibility condition for the case of zero member loads it is expected, at least for problems not involving distributed member loads, to converge to the solution based on the exact solution of the differential equation, while using a small number of elements than those based on element TLE4. This observation will be confirmed in the following example.

Example V.2 – Finite Element Solution

A cantilever beam with a channel section is illustrated in Figure V.7. The cantilever has a four meter span with material properties $E = 200,000MPa$ and $G = 77,000MPa$, and cross-sectional properties $C_w = 5.18 \times 10^{15} mm^6$, $J_d = 4.10 \times 10^9 mm^4$, $J_{rw} = 4.57 \times 10^{10} mm^4$, and $k = 0.53 \times 10^{-3}$. The problem is identical to the example presented in Shakourzadeh et al. (1995) for the sake of comparison of the results based on THE4 and TLE4 elements with those based on the Vlasov and Benscoter theories as reported in Shakourzadeh et al. (1995). Unlike the present theory which is based on postulated stress fields, the Benscoter theory is based on postulated kinematic assumptions allowing for deformation effects. Five solutions are provided. These are based on the Vlasov theory, the Benscoter theory, a THE4 solution with a single element, a TLE4 solution with four elements, and a TLE4 solution with eight elements. The table provides values of the angle of twist, warping deformation at cantilever tip and the bimoments at cantilever root. The percentage differences with the Vlasov solution are also given. It is clear that the Vlasov solution provides the stiffest representation of the structure, since it neglects shear deformation effects, in contrast to the remaining solutions. The Benscoter solution, provides a lower bound estimate of the deformation (including shear deformation effects) as evidenced by the magnitude of the angle of twist which is only 1.2% higher than the Vlasov solution. The THE4 element provides an upper bound for the angle of twist (8% higher than the one based on the Vlasov theory). By providing multiple THE4 elements, the same results were exactly obtained. This is a natural outcome of the fact that interpolation functions of element THE4 exactly satisfy the homogenous form of the compatibility equation in (V.17), which will be shown to eliminate any discretization error in obtaining the nodal variables. This is not the case for element TLE4 where it is shown that an eight element solution provides a better solution than a four element solution. It is of interest to note that, unlike displacement based finite element formulations which tend to underestimate the deformation, the present THE4 and TLE4 consistently overestimate the deformations. This leads to an error on the conservative side, a feature that is welcome from a design viewpoint. The cantilever span is reduced to three meters as illustrated in Figure V.7 and the results based on Vlasov theory and THE4 and the differences between two theories are presented in Table V.2. As expected, the difference in angle of twist at cantilever tip between the Vlasov solution and THE4 solution for three meter cantilever span increases to around 12%.

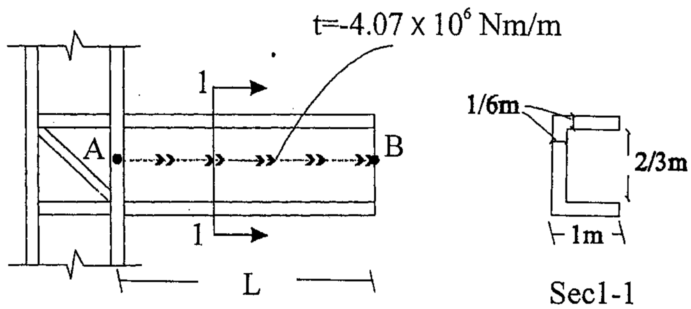

Fig. V.7 Cantilever beam under concentrated twisting moment

Table V.1 Results for Example V.2 (cantilever span = 4m)

Solution type	Angle of twist at cantilever tip (rad)	Percentage difference from Vlasov Theory	Warping deformation at cantilever tip (rad m^{-1})	Percentage difference from Vlasov Theory	Bimoment at cantilever root (10^6N m^2)	Percentage difference from Vlasov Theory
Vlasov	0.04503		0.01160		18.33	
Benscoter	0.04557	1.2 %	0.01157	0.3 %	18.17	0.9 %
THE4	0.04842	7.5 %	0.01141	1.6 %	17.26	5.8 %
TLE4-8 elements	0.04870	8.1 %	0.01156	0.3 %	17.17	6.3 %
TLE4-4 elements	0.04954	10.0 %	0.01202	3.6 %	16.91	7.7 %

Table V.2 Results for Example V.2 (cantilever span = 3m)

Solution type	Angle of twist at tip (rad)	Warping at tip (rad m^{-1})	Bimoment at root ($\times 10^6$N m^2)
Vlasov	0.0196	0.00746	12.13
THE4	0.0220 (+12.2%)	0.00722 (+3.2%)	11.37 (+6.3 %)

Convergence Characteristics of Element TLE4

By adopting the dimensionless coordinate $\xi = z/l$, the homogenous compatibility differential equation in Eq. (V.17) takes the form $(kl)^2 B - d^2B/d\xi^2 = 0$ for the case of zero member loads. The corresponding solution is $B(z) = c_1 \cosh kz + c_2 \sinh kz$ which was used to formulate element THE4. For an element with short span, $kl \to 0$, and the differential equation of compatibility approaches the condition $d^2B/d\xi^2 = 0$. The corresponding solution takes the linear form $B(z) = c_1 + c_2 z$ which was adopted to formulate element TLE4. The above demonstrates that as a mesh is refined for a given problem, the behavior of element TLE4 will approach that of element THE4. This is also consistent with the observations made in Example V.2, in which the eight TLE4 element solution is found to be closer to that based on the THE4 element, than the four TLE4 element solution. For the eight element solution the kl value is closer to zero than in the case of the four element solution. Thus, the adoption of a linear approximation of the bimoment field in that case is more accurate than in the latter.

Exactness of THE4 Solution for the Case of Non-vanishing member loads

The formulation of element THE4 was based on satisfying the homogeneous form of the compatibility condition. In contrast to element TLE4, the nodal values predicted based on element THE4 were shown not to cause any discretization errors for the case involving zero member loads $t(z)=0$. A question arises regarding the exactness of the nodal values predicted by element THE4 for the non-homogeneous case $t(z)\neq 0$. In the following, a proof is provided that, indeed, the nodal values based on element THE4 are exact for the non-homogeneous case.

For the case of non-vanishing twisting moments $t(z)\neq 0$, the general solution of the bimoment field $\overline{B}(z)$ is the sum of the homogenous solution $B_h(z)$ and the particular solution $B_p(z)$ i.e., $\overline{B}(z)=B_h(z)+B_p(z)$. The homogenous solution $B_h(z)$ is

$$B_h(z)=c_{h1}\cosh kz+c_{h2}\sinh kz \tag{V.51}$$

and the particular solution $B_p(z)$ can be expressed as

$$B_p(z)=c_{p1}\cosh kz+c_{p2}\sinh kz+\beta(z) \tag{V.52}$$

in which function $\beta(z)$ is dependent upon the member loads $t(z)$ through the relation

$$k^2\beta(z)-\beta(z)''=\left(\frac{J_{r\omega}}{J_d+J_{r\omega}}\right)t(z) \tag{V.53}$$

By using Eqs. (V.21) through (V.33), $B_h(z)$ and $B_p(z)$ can be expressed as

$$B_h(z)=\langle L_h(z)\rangle^T_{1\times 3}[H_a]_{3\times 3}\{P_h\}_{3\times 1} \tag{V.54}$$

In Equation (V.54), vector $\langle P_h\rangle^T_{1\times 3}=\langle -B_{h0} \quad T_{hl} \quad B_{hl}\rangle$ is defined. The component T_{hl} can be selected such that $T_{hl}=T_l$. Also,

$$B_p(z)=\langle L_h(z)\rangle^T_{1\times 3}[H_a]_{3\times 3}\{P_p\}_{3\times 1}+\beta(z) \tag{V.55}$$

In Equation (V.55), vector $\langle P_p\rangle^T_{1\times3}=\langle -B_{p0}\quad T_{pl}\quad B_{pl}\rangle$ is defined. Vector $\langle P_p\rangle_{1\times3}$ can be selected such that $B_p(l)=0$, $B_p(0)=0$ and $T_{pl}=0$. By substituting Eq. (V.54) into the expression $\overline{B}(z)=B_h(z)+B_p(z)$, one obtains

$$\overline{B}(z)=\langle L_h(z)\rangle^T_{1\times3}[H_a]_{3\times3}\{P_h\}_{3\times1}+B_p(z) \tag{V.56}$$

From Eq. (V.56), by substituting into Eqs. (V.5) and (V.7) one obtains expressions for the warping and St. Venant twisting moments for the case $t(z)\neq 0$

$$\overline{T_w}(z)=\langle L_h'(z)\rangle^T_{1\times3}[H_a]_{3\times3}\{P_h\}_{3\times1}+B_p'(z) \tag{V.57}$$

$$\overline{T_{sv}}(z)=\langle M_h(z)\rangle^T_{1\times3}[H_a]_{3\times3}\{P_h\}_{3\times1}-B_p'(z)+\Gamma(z) \tag{V.58}$$

By substituting Eqs. (V.56), (V.57) and (V.58) in Eq. (V.13), one obtains

$$\begin{aligned}\pi^*=&\frac{1}{2EC_w}\int_0^l\Big[\Big(\langle P_h\rangle^T_{1\times3}[H_a]_{3\times3}\{L_h(z)\}_{3\times1}+B_p(z)\Big)\Big(\langle L_h(z)\rangle^T_{1\times3}[H_a]_{3\times3}\{P_h\}_{3\times1}+B_p(z)\Big)\Big]dz\\&+\frac{1}{2GJ_{r\omega}}\int_0^l\Big[\Big(\langle P_h\rangle^T_{1\times3}[H_a]_{3\times3}\{L_h'(z)\}_{3\times1}+B_p'(z)\Big)\Big(\langle L_h'(z)\rangle^T_{1\times3}[H_a]_{3\times3}\{P_h\}_{3\times1}+B_p'(z)\Big)\Big]dz\\&+\frac{1}{2GJ_d}\int_0^l\Big[\Big(\langle P_h\rangle^T_{1\times3}[H_a]_{3\times3}\{M_h(z)\}_{3\times1}-B_p'(z)+\Gamma(z)\Big)\Big(\langle M_h(z)\rangle^T_{1\times3}[H_a]_{3\times3}\{P_h\}_{3\times1}-B_p'(z)+\Gamma(z)\Big)\Big]dz\\&-\langle d\rangle^T_{1\times3}\{P\}_{3\times1}-\int_0^l\phi(z)t(z)dz\end{aligned} \tag{V.59}$$

In Eq. (V.59), vector $\{P\}_{3\times1}$ is identical to vector $\{P_h\}_{3\times1}$, since $B_p(l)=0$, $B_p(0)=0$ and $T_{pl}=0$. By using the stationarity conditions $\partial\pi^*/\partial\{P_h\}=\{0\}$, one obtains

$$[F_h]_{3\times3}\{P_h\}_{3\times1}=\{d\}_{3\times1}-\{\psi_h\}_{3\times1}-[H_a]_{3\times3}\{\kappa\}_{3\times1} \tag{V.60}$$

in which

$$\{\kappa\}_{3\times 1}=\int_0^l\left(\frac{\{L_h(z)\}_{3\times 1}B_p(z)}{EC_w}+\frac{\{L_h'(z)\}_{3\times 1}B_p'(z)}{GJ_{r\omega}}-\frac{\{M_h(z)\}_{3\times 1}B_p'(z)}{GJ_d}\right)dz \tag{V.61}$$

After integrating Eq. (V.61) by parts, one obtains

$$\{\kappa\}_{3\times 1}=\int_0^l\left(\frac{\{L_h(z)\}_{3\times 1}}{EC_w}-\left(\frac{1}{GJ_{r\omega}}+\frac{1}{GJ_d}\right)\{L_h''(z)\}_{3\times 1}\right)B_p(z)dz+\left(\frac{\{L_h'(z)\}_{3\times 1}}{GJ_{r\omega}}-\frac{\{M_h(z)\}_{3\times 1}}{GJ_d}\right)B_p(z)\Bigg|_0^l$$

Since $\{L_h''(z)\}_{3\times 1}=-\{M_h'(z)\}_{3\times 1}$ and $\frac{1}{EC_w}\{L_h\}-\left(\frac{1}{GJ_{r\omega}}+\frac{1}{GJ_d}\right)\{L_h''\}=\{0\}$ with

$B_p(l)=B_p(0)=0$, vector $\{\kappa\}_{3\times 1}$ can be shown to vanish.

Equation (V.60) signifies that for a member subjected to distributed member loads $t(z)$, the product of the flexibility matrix $[F_h]_{3\times 3}$ formulated based on a bimoment field which satisfies the homogeneous form of the compatibility condition by the exact nodal force vector $\{P_h\}_{3\times 1}$ is equal to the vector of nodal displacements $\{d\}_{3\times 1}$ minus the displacement vector due to member loads $\{\psi_h\}_{3\times 1}$ based on a bimoment field which satisfy the homogeneous form of the compatibility condition. The proof extends the exactness of the nodal displacement/force values based on element THE4 to cases of non-vanishing member twisting moments $t(z)\neq 0$. In contrast element TLE4 leads to discritization errors both for the homogenous and non-homogenous loading conditions.

Summary and Conclusions

The field equation and boundary conditions for the torsional analysis of thin-walled structures including shear deformation effects due to warping torsion are developed. The formulation is based on postulated statically admissible stress fields in conjunction with the complementary energy functional. The theory developed is used to solve a problem to illustrate its applicability using closed form solution. The approach is then extended to formulate two finite elements which capture shear deformation effects. Element (TLE4) demonstrates more flexible behavior than the second element (THE4) and converges to the THE4 results when a refined mesh is adopted. Element THE4 yields nodal displacements in exact agreement with those based on a closed form solution of the differential equation of compatibility, for the case of zero and non-zero member loads. The formulation based on element THE4 allows the use of a minimal number of finite elements. For squat beams, shear deformation effects are shown to gain significance. The angle of twist based on the new formulation is larger than that predicted by conventional theories which neglect shear deformation effects.

Appendix V.A– Stiffness Matrix for Element TLE4 and corresponding Energy Equivalent Member Load Vector

The elements of the stiffness matrix for Element TLE4 are

$$K_{f11} = \left(12G\chi EJ_d + 12EC_w + GJ_dL^2\right)/\left(12E\chi L + GL^3\right) \qquad \text{V.A(1)}$$

$$K_{f12} = -\left(6GEC_w\right)/\left(12E\chi + GL^2\right) \qquad \text{V.A(2)}$$

$$K_{f22} = \left(12\chi E^2C_w + 4GEL^2C_w\right)/\left(12E\chi L + GL^3\right) \qquad \text{V.A(3)}$$

$$K_{f24} = \left(2L^2GEC_w - 12\chi E^2C_w\right)/\left(12E\chi L + GL^3\right) \qquad \text{V.A(4)}$$

$$K_{f21} = K_{f12} = K_{f14} = K_{f41} = -K_{f23} = -K_{f32} = -K_{f34} = -K_{f43} \qquad \text{V.A(5)}$$

$$K_{f33} = K_{f11} = -K_{f13} = -K_{f31} \qquad \text{V.A(6)}$$

In Equations V.A(1) to VA(6) $\chi = C_w/J_{r\omega}$ is used. Member load is assumed to be a linear function i.e., $t(z) = Az + B$. The elements of the corresponding load vector are

$$\Lambda_{f1} = -\left(4AL + 3B\right)L/6 + \left(AL^2 + BL\right) \qquad \text{V.A(7)}$$

$$\Lambda_{f2} = 0 \qquad \text{V.A(8)}$$

$$\Lambda_{f3} = \left(4AL + 3B\right)L/6 \qquad \text{V.A(9)}$$

$$\Lambda_{f4} = 0 \qquad \text{V.A(10)}$$

Appendix V.B–Flexibility Matrix and Energy Vector due to Member Load for Element THE4

The elements of the flexibility matrix for Element THE4 are

$$F_{h11} = \Phi\left(J_{rw}EC_w k^2 \cosh kL \sinh kL + J_{rw}EC_w k^3 L + k^2 J_d EC_w \cosh kL \sinh kL \right. \\ \left. -GJ_d J_{rw} Lk + GJ_d J_{rw} \cosh kL \sinh kL + k^3 J_d EC_w L\right) \quad \text{V.B(1)}$$

$$F_{h12} = -\Phi\left[-2J_{rw}EC_w k + 2J_{rw}EC_w k\left(\cosh kL\right)^2\right] \quad \text{V.B(2)}$$

$$F_{h13} = -\Phi\left(-J_{rw}EC_w k^2 \sinh kL - k^3 J_d EC_w L \cosh kL - k^2 J_d EC_w \sinh kL \right. \\ \left. -J_{rw}EC_w k^3 L \cosh kL + GJ_d J_{rw} kL \cosh kL - GJ_d J_{rw} \sinh kL\right) \quad \text{V.B(3)}$$

$$F_{h21} = -1/GJ_d \quad \text{V.B(4)}$$

$$F_{h22} = L/GJ_d \quad \text{V.B(5)}$$

$$F_{h23} = -1/GJ_d \quad \text{V.B(6)}$$

$$F_{h31} = \Phi\left(-GJ_d J_{rw} Lk \cosh kL + k^2 EC_w J_d \sinh kL + GJ_{rw} J_d \sinh kL \right. \\ \left. +k^3 J_d EC_w L + J_{rw}EC_w k^2 \sinh kL + J_{rw}EC_w k^3 L \cosh kL\right) \quad \text{V.B(7)}$$

$$F_{h32} = -\Phi\left[-2J_{rw}EC_w k + 2J_{rw}EC_w k\left(\cosh kL\right)^2\right] \quad \text{V.B(8)}$$

$$F_{h33} = -\Phi\left(+GJ_{rw} J_d kL - k^3 J_d EC_w L - GJ_d J_{rw} \cosh kL \sinh kL \right. \\ \left. - EC_w J_{rw} k^2 \cosh kL \sinh kL - EC_w J_{rw} k^3 L - EC_w J_d k^2 L \cosh kL \sinh kL\right) \quad \text{V.B(9)}$$

In Equations V.B(1) to V.B(9) $\Phi = 1/\left(2GJ_d(\sinh kL)^2 J_{rw}EC_w k\right)$ is used. Member load is assumed to be a linear function i.e., $t(z) = Az + B$. The elements of the load vector are

$$\psi_{h1} = \left.\begin{matrix} -\left(2ALk + Bk - 2A\sinh kL + BLk^2 \sinh kL \right. \\ \left. + AL^2k^2 \sinh kL - Bk \cosh kL\right) \end{matrix}\right/ \left(GJ_d k^2 \sinh kL\right) \quad \text{V.B(10)}$$

$$\psi_2 = \left(4AL + 3B\right)L^2/\left(6GJ_d\right) \quad \text{V.B(11)}$$

$$\psi_3 = \left(2A\sinh kL - 2ALk\cosh kL + Bk - Bk\cosh kL\right)/\left(GJ_d k^2 \sinh kL\right) \quad \text{V.B(12)}$$

Chapter V References

[V.1] Back, S.Y., and Will, K.M. 1998. A shear-flexible element with warping for thin-walled open beams. International Journal for Numerical Methods in Engineering, 43 (7): 1173-1191.

[V.2] Barsoum, R.S., 1970. A finite element formulation for the general stability analysis of thin walled members. Ph. D. thesis, Cornell University, Ithaca, New York, USA

[V.3] Barsoum, R.S., Gallagher, R.H., 1970. Finite element analysis of torsional and torsional-flexural stability problems. International Journal for Numerical Methods in Engineering, 2, 335-352.

[V.4] Batoz, J.L., and Dhatt, G., 1990. Modélisation des structures par éléments finis. Vol. 2, poutres et plaques. (Modeling of structures with finite elements, Vol. 2, Beams and plates). Hermes edition, Paris. (in French).

[V.5] Benscoter, S.U. 1954. A theory of torsion bending for multicell beams. Journal of Applied Mechanics, 53: 25-34.

[V.6] Bickford W.B. 1982. A consistent higher order theory. Develop. Theor. Appl Mech., 11,137-150.

[V.7] Boresi, A.P., Sidebottom, O.M., 1985. Advanced Mechanics of Materials. Fourth Edition, John Wiley & Sons, New York, USA.

[V.8] Chen, H., Blandford, G.E., 1989. A C^0 finite element formulation for thin-walled beams. International Journal for Numerical Methods in Engineering, 20(10): 2239-2255.

[V.9] Dvorkin, E.N., Celentano, D., Cuitino, A., and Gioia, G., 1989. A Vlassov beam element. Computers and Structures, 33(1): 187-196.

[V.10] Erkmen, R.E. and Mohareb, M. 2006. Non-orthogonal solution for thin-walled beams – A Finite Element Formulation, Canadian Journal of Civil Engineering, Vol.33, No.4, 421-439.

[V.11] Friedman, Z. and Kosmatka, J. B. 1993, An Improved Two-node Timoshenko Beam Finite Element, Computers & Structures Vol.47,No.3, pp.473-481

[V.12] Gendy, A.S., Saleeb, A.F., and Chang, T.Y.P., 1992. Generalized thin-walled beam models for flexural-torsional analysis. Computers and Structures, 42(4): 531-550.

[V.13] Gunnlaugsson, G.A., and Pedersen, P.T., 1982. A finite element formulation for beams with thin walled cross-sections. Computers and Structures, 15(6): 691-699.

[V.14] Heins, C.P. and Seaburg, P.A. 1963, Torsion Analysis of Rolled Steel Sections, Bethlehem Steel Company, PA, USA

[V.15] Heyliger P.R. and Reddy J.N. 1988. A higher order beam finite element for bending and vibration problems. J. Sound Vib., 126(2),309-326.

[V.16] Krajcinovic, D., 1969. A consistent discrete elements technique for thin wall assemblages. International Journal for Solids and Structures, 5: 639-662.

[V.17] Krajcinovic, D., 1970. Matrix force analysis of thin-walled structures. Journal of Structural Engineering, ASCE, 96(1): 107-120.

[V.18] Levinson M. 1981. A new rectangular beam theory. J Sound Vib., 74(1), 81-87.

[V.19] McGuire, W. M., Gallagher H. G., Ziemian, R.D. 2000, Matrix Structural Analysis. Second Edition. John Wiley & Sons, Inc., NY, USA.

[V.20] Mohareb, M., and Nowzartash, F., 2003. Exact finite element for warping torsion of open sections. Journal of Structural Engineering, ASCE. 129(2): 215-223.

[V.21] Mucichescu, D. T., 1984 Bounds for Stiffness of Prismatic Beams, J. Struct. Eng., 110(6), 1410-1414

[V.22] Nowzartash F, Mohareb M. 2005. Planar Bending of Sandwich Beams with Transverse Loads off the centroidal axis. J. Eng. Mech., 4, 385-396.

[V.23] Schulz, M., Filippou, F.C. 1998. Generalized Warping Torsion Formulation. Journal of Engineering Mechanics, ASCE, 124(3): 339-347.

[V.24] Seaburg, P. A. and Carter, C. J. 1997, Torsional Analysis of Structural Steel Members, American Institute of Steel Construction, Chicago, IL

[V.25] Shakourzadeh, H., Guo, Y.Ch., and Batoz, J.L., 1995. A torsional bending element for thin-walled beams with open and closed cross sections. Computers and Structures, 55(6): 1045-1054.

[V.26] Synge J.L. 1957. The Hypercircle in Mathematical Physics. Cambridge University Press.

[V.27] Tralli, A., 1986. A Simple Hybrid Model for Torsion and Flexure of Thin-Walled Beams. Computers and Structures, 22(4): 649-658.

[V.28] Vlasov, V.Z., 1961. Thin Walled Elastic Beams. Second Edition, Israel Program for Scientific Translations, Jerusalem, Israel.

Chapter V List of Symbols

A	=	cross-sectional area;
A_p	=	pole (Fig. V.1);
b_i	=	width of the of i^{th} thin-wall segment;
B	=	bimoments;
$\overline{B}(z)$	=	general solution of the bimoment field;
$B_h(z)$	=	homogenous solution of the bimoment field;
$B_p(z)$	=	particular solution of the bimoment field;
c_1, c_2, c_3	=	integration constants;
$\langle c \rangle^T_{1\times4}$	=	vector of constants c_1, c_2, c_3;
C_w	=	warping constant;
$\langle d \rangle^T_{1\times3}$	=	reduced nodal displacement vector;
$\langle d_f \rangle^T_{1\times4}$	=	full nodal displacement vector;
E	=	modulus of elasticity;
$[F]_{3\times3}$	=	flexibility matrix based on linear interpolation;
$[F_h]_{3\times3}$	=	flexibility matrix based on hyperbolic interpolation;
G	=	shear modulus;
$h(s)$	=	normal distance between pole and the tangent to mid-surface at point s;
$[H_a]_{3\times3}$	=	matrix introduced to alter signs of reduced nodal force

vector;

$[H_b]_{4\times4}$ = matrix introduced to alter signs of full nodal force vector;

$[I]_{3\times3}$ = unit matrix;

J_d = St. Venant's torsional constant;

$J_{r\omega}$ = new cross-sectional property associated with the distribution of shear stresses;

k = constant $\sqrt{GJ_d J_{r\omega} / EC_w (J_d + J_{r\omega})}$

$[K_f]_{4\times4}$ = full stiffness matrix based on linear interpolation;

$[K_{hf}]_{4\times4}$ = full stiffness matrix based on hyperbolic interpolation;

l = length of finite element;

$\langle L(z)\rangle_{1\times3}$ = vector of linear interpolation functions;

$\langle L_h(z)\rangle_{1\times3}$ = vector of hyperbolic interpolation functions;

$\langle M(z)\rangle_{1\times3}$ = vector of interpolation functions relating the St. Venant torsion to nodal forces associated with linear bimoment interpolation functions

$\langle M_h(z)\rangle_{1\times3}$ = vector of interpolation functions relating the St. Venant torsion to nodal forces associated with hyperbolic bimoment interpolation functions

n = number of segments defining a cross-section;

$\langle p \rangle^{T}_{1\times 3}$	= vector relating the full nodal displacement vector to reduced displacement vector;
$\langle P \rangle^{T}_{1\times 3}$	= reduced nodal force vector;
$\langle P_h \rangle^{T}_{1\times 3}$	= reduced nodal force vector based on homogenous solution;
$\langle P_p \rangle^{T}_{1\times 3}$	= reduced nodal force vector based on particular solution;
$\langle P_f \rangle^{T}_{1\times 4}$	= full nodal force vector;
r	= coordinate normal to the section mid surface (Fig. V.2);
s	= curvilinear coordinate along mid surface (Fig. V.1, Fig.V.2);
$[\mathbf{S}]_{4\times 4}$	= matrix relating nodal displacements to displacement functions;
S_0	= sectorial origin (Figs. V.1);
$\overline{S}_{\omega}$	= sectorial static moment
$t(s)$	= thickness of the thin-wall segment (Fig.V.2);
$t(z)$	= twisting moments per unit length (Fig.V.5);
T	= total twisting moment;
TLE4	= Torsional Linear Element with 4 degrees of freedom;
THE4	= Torsional Hyperbolic Element with four degrees of freedom;
T_{sv}	= St.Venant torsion (Fig. V.4);
T_{w}	= warping torsion (Fig. V.4);

$\langle u \rangle_{1\times 4}^{T}$	=	vector of nodal displacements;
U^*	=	complementary strain energy;
V^*	=	potential of the generalized forces;
V	=	volume of element;
x, y, z	=	coordinates of any point P on mid-surface (Figs. V.1);
$\beta(z)$	=	function dependent upon member loads;
$\phi(z)$	=	angle of twist;
$\Gamma(z)$	=	function of member loads;
$\{\kappa\}_{3\times 1}$	=	nodal displacement vector associated with particular solution;
$\{\Lambda_f\}_{4\times 1}$	=	energy equivalent member load vector based on linear interpolation;
$\{\Lambda_{hf}\}_{4\times 1}$	=	energy equivalent member load vector based on hyperbolic interpolation;
$\theta(z)$	=	warping function;
π^*	=	total complementary energy;
σ	=	longitudinal stress (Fig. V.3);
τ_{sv}	=	shear stress due to St.Venant torsion (Fig. V.2);
τ_w	=	shear stress due to warping (Fig. V.2);
ω	=	sectorial area (Fig. V.1);
ξ	=	dimensionless longitudinal coordinate;
$\{\psi\}_{3\times 1}$	=	displacement vector due to member loads based on linear

interpolation;

$\{\psi_h\}_{3\times1}$ = displacement vector due to member loads based on hyperbolic interpolation;

Chapter V List of Tables

Chapter V List of Figures

Chapter VI

Buckling analysis of Thin-walled open members based on Complementary Energy functional

Abstract

The first part of this chapter develops a formulation for the buckling analysis of thin-walled members based on the principle of stationary complementary energy. Some of the aspects of the Vlasov beam theory are used to describe the behavior of members under buckling deformation. Koiter's formulation based on the polar decomposition theory in finite elasticity is used in formulating the complementary energy expression, equilibrium equations, and the associated neutral stability conditions in which the rotation fields appear explicitly. Statically admissible stress fields based on the Vlasov theory are used in conjunction with the Koiter's variational formulation to yield the buckling solution of open thin-walled members. The formulation incorporates shear deformation effects. In the second part of the chapter, a finite element formulation is developed for the buckling of thin-walled beams based on the principle of stationary complementary energy. A series of examples demonstrate the validity of the finite elements formulated and their applicability to a wide variety of buckling problems, involving column flexural and torsional buckling, lateral torsional buckling of beams, moment gradient effects, beams with mono-symmetric sections, and the effect of the load position relative to the shear centre.

Keywords

Thin-walled members, finite element, complementary energy, column-buckling, lateral torsional buckling.

Introduction and Literature Review

Stability Analysis of Thin-Walled members

The equilibrium equations for flexural, torsional and lateral buckling for general thin-walled open sections under compression and bending were first derived by Timoshenko (1945). Chajes and Winter (1965) developed the equilibrium equations for the flexural torsional buckling of singly-symmetric thin-walled sections. Krajcinovic (1969) used the principle of virtual work to obtain the elastic and the geometric stiffness matrices for thin-walled members. By using the principle of stationary potential energy, Bazant and Nimeri (1973) developed solutions for large deflection and post-buckling of thin-walled straight and curved beams. Yoo (1980) obtained the elastic and geometric stiffness matrices for asymmetric thin-walled members. Hancock et. al. (1980) investigated the flexural torsional buckling of I-section beams by adopting more refined kinematic assumptions than those based on the Vlasov theory in which the effect of web distortion was incorporated. Roberts and Azizan (1983) investigated the effect of pre-buckling deformations on flexural torsional bucking of thin walled beams. Trahair and Bild (1990) derived the energy expressions for lateral torsional buckling of mono-symmetric thin-walled beams. Pi and Trahair (1992 a, b) provided a comparison between bucking solutions incorporating pre-buckling deformation effects to those excluding these effects. Later on, Trahair and Pi (1997) developed solutions incorporating the second order effect due to axial shortening under twist deformations, commonly known as the Wagner strain, and the associated stress resultant. Kim et al. (2003) incorporated shear deformation effects in formulating buckling solutions for thin-walled beams. In their solution, they modified the Vlasov theory by relaxing the condition equating the generalized rotation fields to the derivatives of the associated generalized displacements. Mohareb and

Dabbas (2003) developed a finite element model to predict lateral buckling resistance of T-shaped frames consisting of wide flange sections. In their analysis, by neglecting shear deformation effects, the buckling load predictions for short cantilevers were significantly higher than those predicted based on the ABAQUS S4R shell element model which includes shear deformation effects. This observation has suggested the need to develop a buckling solution which incorporates the effect of shear deformation.

Stability Analyses based on Complementary Energy Variational Principles

Westergaard (1941) was possibly the first to adopt the complementary energy for the buckling analysis of members. His research focused on statically determinate Euler-Bernoulli beam-column problems. His formulation was found to coincide with the one obtained by Timoshenko (1913) which was based on the principle of stationary potential energy method while imposing the equilibrium conditions a priori. Oran (1967) applied the complementary energy principle for the buckling analysis of statically indeterminate columns. He formulated a quadratic complementary energy expression for the linearized pre-buckling state and adopted it in deriving the stability criterion. However, for statically indeterminate structures, a strict force based complementary energy formulation appeared to involve some difficulties in determining the buckling loads. He also proposed a modified method, in which the internal force field is indirectly interpolated by assuming a deflected shape. The modified principle did not suffer from the drawbacks of the strict force based method which can be regarded as a generalization of Timoshenko's method for estimating buckling loads for statically indeterminate columns. Schreyer-Shih (1973) and Popelar (1974) circumvented the difficulties of the Oran's strict force based method by enforcing certain conditions a-posteriori in order to select the buckling load that is in agreement with the actual boundary conditions. The conditions imposed can be conceived to enforce the proper geometric boundary conditions of the problem. Shih and Schreyer (1973) and Popelar (1974) illustrated the superiority of complementary energy principle over the total potential energy principle in predicting the buckling loads of columns for a given set of approximate displacement fields. Murakawa et al. (1981) applied the complementary energy principle for the stability and post buckling analysis of columns. Other buckling solutions based on the stationary complementary energy principle include the work of Oran (1968), Koiter (1976) and Tabarrok and Simpson (1977).

Masur and Popelar (1976) derived a complementary energy expression in terms of generalized stresses, in which the constitutive relations between the generalized stresses and generalized strains assumed invertible. They applied the stationary complementary energy principle for a lateral torsional buckling problem of a symmetric thin-walled beam by expressing the generalized stress field in terms of the stress resultants of Vlasov theory in orthogonal coordinates (i.e., the origin coincides with the section centroid, the pole is located at the shear center and the sectorial origin is located at a principal sectorial origin). Lateral torsional buckling analysis of thin-walled beams based on the stationary complementary energy principle is also reported in Elias (1986). Like Masur and Popelar (1976), Elias' analysis is also based on orthogonal system of coordinates.

In this context, the present study aims at developing a general buckling solution for thin-walled beams based on the principle of stationary complementary energy principle able to capture lateral torsional buckling effects. The current study differs from the ones available in the literature in several respects. These are: a) Material, stress and strain measures of finite elasticity are adopted, thus the formulation is developed in a more general finite elasticity context b) equilibrium equations are satisfied at the stress level c) a general non-orthogonal coordinate system is adopted. This feature allows the modeling of transverse loads which are offset from the shear centre d) it incorporates shear deformation effects, and e) it develops a general purpose finite element solution applicable to a wide variety of problems and boundary conditions.

Generalized Hooke's material for 3D Finite Elasticity

John (1960) introduced the concept of harmonic material in finite elasticity problems, in which the strain energy density is a function only of the principal extensions. He identified the principal extensions as the principal values of the right extensional strain ε_{ij} of the polar decomposition theory (de Veubeke 1972), e.g., $\varepsilon_{11} = (dl_1 - dL_1)/dL_1$, where dL_1 and dl_1 are the un-deformed and deformed lengths respectively for an infinitesimal element along the principal strain direction. He demonstrated that the proposed harmonic type material definition coincides with the well known elastic Hooke material for the limiting case of infinitesimal deformations. Lur'e (1968) formulated the internal strain energy density expression for harmonic material in terms of the first invariant of the linear strain and its square in i.e., $W_i(\varepsilon) = G\left[\left(\varepsilon_{11}{}^2 + \varepsilon_{22}{}^2 + \varepsilon_{33}{}^2\right) + \nu I_{\varepsilon 1}{}^2/(1-2\nu)\right]$, in which ε_{11}, ε_{22} and ε_{33} are the principal right extensional strains and $I_{\varepsilon 1} = \varepsilon_{11} + \varepsilon_{22} + \varepsilon_{33}$, G is the shear modulus and ν is the Poisson's ratio. He termed such a material as "semilinear". Koiter (1976) pointed out that the semilinear isotropic material assumption can be considered as an acceptable generalization of Hooke's law in geometrically non-linear elasticity. He adopted the semilinear material concept into buckling analysis of plate problems.

Stress and Strain Measures in Finite Elasticity

Several stress and strain measures for the geometric nonlinear analysis of structures are established in literature. Levinson (1965) and Zubov (1970) showed that a strict complementary energy expression in finite elasticity can be formulated based on the first Piola-Kirchoff stress tensor. However, the first Piola-Kirchoff stress-deformation gradient pair of tensors was shown to be non-objective, i.e., they are not invariant under rigid body rotation (Bathe 1982, Pai and Nayfeh 1994). Novozhilov (1961) has shown that the constitutive relations relating these stresses and associated deformation gradient measures can be used in a displacement based solution. However, they cannot be employed in a force based formulation since the nine stress fields become inter-related in order to satisfy the moment equilibrium equations, a necessary requirement in a force based formulation. Thus only six out of the nine stress fields become independent, which would have to be related to the nine independent components of the deformation gradient. Thus in a force based formulation, it becomes impossible to express the nine deformation gradient components in terms of the six independent stress tensor components. This handicap was pointed out by several authors including de Veubeke (1972), Koiter (1973), Dill (1977) and Ogden (1977).

The second Piola-Kirchoff stress tensor and the associated energy conjugate Green-Lagrange strain tensor are commonly used in finite elasticity (Washizu 1982 and Bathe-1982) since they can be demonstrated to be objective (Pai and Nayfeh 1994). Under these stress and strain tensors, while the constitutive relations are able to predict the stresses corresponding to a certain state of strains, the inverse relation is difficult to formulate. This makes them suitable measures to adopt under displacement based finite element formulations (Bathe 1982), but impractical to use in a force based solution (de Veubeke 1972) such as the one sought in this work. Another difficulty which arises when adopting the Second Piola-Kirchoff stress tensor (and stress resultants based upon them) is the fact that they have no apparent directions. Hence, they are difficult to adopt when describing the force boundary conditions (Pai and Nayfeh 1994), a key issue in buckling formulations.

De Veubeke (1972) adopted the Jaumann stress tensor and the conjugate right extensional strain tensor in finite elasticity solutions based on the principle of stationary complementary energy. Koiter (1976) obtained the complementary energy expression for semilinear material, the equations of neutral equilibrium and formulated a general stability criterion in terms of the Jaumann stress tensor and rigid body rotation tensor under the assumptions of small strains, moderately small rotations, and a linearized pre-buckling state (an initially straight column with no volume change and cross-sectional change under pre-buckling load). Pai and Nayfeh (1994) demonstrated that Jaumann stresses and their energy conjugate right extensional strains are objective. They also showed that under the simplifying assumption of the Euler-Bernoulli beam theory; a) plane section remains plane, and; b) beam axis stays perpendicular to cross-section plane, the Jaumann stresses have the same directions across any given cross-section, and their stress resultants are physically measurable and have physically identifiable directions. In buckling problems, this characteristic makes the Jaumann stress tensor a more suitable stress measure to adopt than the second Piola Kirchoff tensor, as it is able to represent the force boundary conditions of the problem. According to Pai and Palazotto (1995) and Pai et al. (1998), the Jaumann stresses can be related to the right extensional strains through the constitutive relations of linear elasticity.

Assumptions

The assumptions made in the formulation are as follows:

- Strains are assumed to be small and the rotations are assumed moderate. Thus, in the Euler-Rodrigues expression, (which relates the rotation tensor to the three mutually independent rotation vectors) the rotation terms higher than second order are neglected. The Euler-Rodrigues formula was adopted by several researchers for the buckling analysis of thin-walled beams including Elias (1986), Chen and Blandford (1991), Kim (1996), Kim and Kim (2000), McGuire et.al. (2000) and Souza (2000).
- The second order terms in the equations relating the rotation vector components and displacement derivatives are neglected.
- The cross-section remains rigid under deformation, in agreement with the first Vlasov assumption.
- Stress distributions and stress resultant-stress relations are postulated to be in agreement with those based on the Vlasov theory.
- Deformations prior buckling are neglected.
- The material is assumed to be of semilinear type, which is defined by replacing the engineering stress-strain pair in linear elasticity with the Jaumann stress and right extensional strain pair in Hooke's constitutive relations.

- The inextensional buckling assumption (Trahair 1993) is adopted, thus the normal force remains constant throughout buckling.

Deformation and Rotation

Two coordinate systems are adopted. The fixed XYZ (spatial) Cartesian coordinate system (Fig. VI.1) has the Z axis oriented along the axial direction (in the un-deformed configuration) of the beam while axes X-Y are parallel to the plane of the cross-section. The *xyz* (material) curvilinear coordinate system (Fig.VI.1) is altering with the deformation of the structure so that *x*, *y* and *z* coordinates of a point on the beam after deformation will be identical of those before deformation (Novozhilov 1961). The material coordinate system coincides with the spatial coordinate system only for the undeformed beam.

The deformation gradient tensor F_{ij}, is the partial differentiation of the current position vector X_i with respect to the material coordinate x_j i.e., $F_{ij} = \partial X_i / \partial x_j$. Throughout the text X_1, X_2 and X_3 indicate X, Y, Z, and x_1, x_2 and x_3 indicate *x*, *y*, *z* respectively. Based on the polar decomposition theory, deformation gradient tensor F_{ij} can be expressed in terms of the rigid body rotation tensor R_{ik}, and the symmetric right extensional strain tensor ε_{kj} as $F_{ij} = R_{ik}\left(\varepsilon_{kj} + \delta_{kj}\right)$, in which δ_{kj} is the Kronecker's delta and throughout the text repeated index summation convention is adopted for indices *i*, *j* and *k*. The infinitesimal parallelepiped in Fig. VI.1 is deformed under the successive application of stretch, rotation and rigid translation described by the displacement fields u_s, v_s and w_s along the X, Y and Z directions respectively. In Fig. IV.1, the unit vectors of the triad $\vec{e}_0$ are defined along the principal strain directions of the *un-deformed* parallelepiped while the unit vectors of the triad $\vec{e}$ are defined along the principal strain directions of the *deformed* parallelepiped. Note that the directions of coordinate axis XYZ and *xyz* are not necessarily oriented along the principal directions.

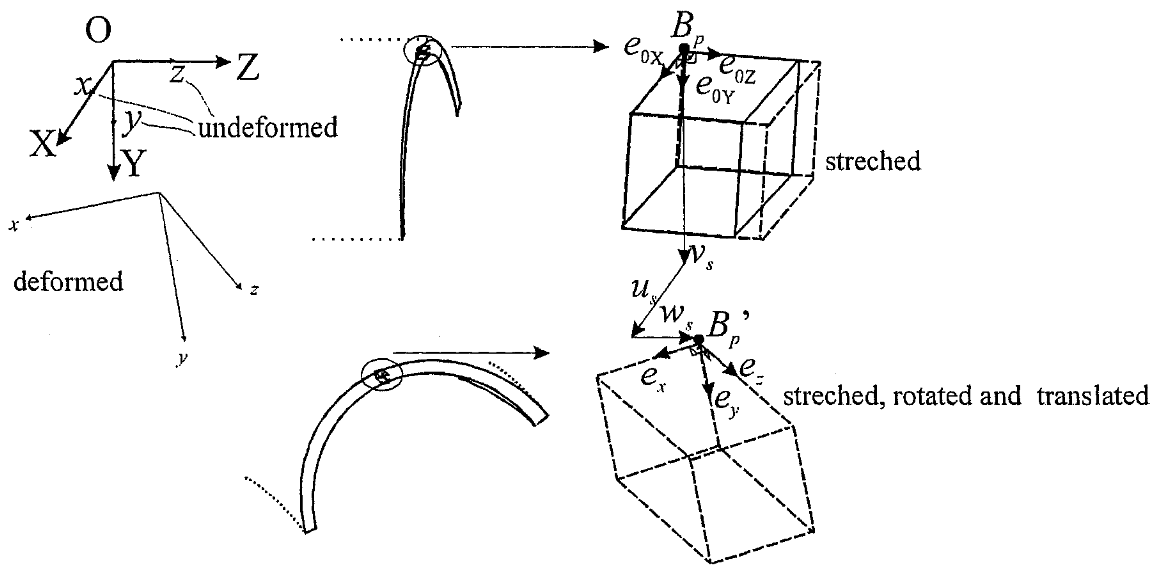

Fig. VI.1. Deformations of an infinitesimal element of volume along principal directions observed from spatial coordinates

Rotation Tensor

Rotation tensor R_{ij} determines the orientation of triad $\vec{e}$ with respect to the triad $\vec{e}_0$ (Fig. VI.1) i.e., $e_i = R_{ij}e_{0j}$. Six of the nine components of the rotation tensor are linearly dependent given the orthogonality property $R_{ij}R_{mj} = \delta_{im}$. By using the Euler-Rodrigues formula (Koiter 1976), the rotation tensor can be expressed in terms of three independent rotation vector components ϕ_1, ϕ_2 and ϕ_3 about the X, Y and Z direction respectively as

$$R_{ij} = \delta_{ij}(1-\frac{1}{2}\phi_k\phi_k) + \varepsilon_{ikj}\phi_k + \frac{1}{2}\phi_i\phi_j + o\left(|\phi|^3\right) \tag{VI.1}$$

In Eq. (VI.1), ε_{imj} is the permutation symbol and $o\left(|\phi|^3\right)$ represents rotation vector terms higher than the second order. Throughout the text the indices 1, 2, 3 for ϕ_i indicate X, Y, Z respectively.

The deformation of the beam axis passing through point B_p and the projections of the deformed axis to Y-Z plane and X-Z plane are illustrated in Figs. VI.2a-c respectively. Based on the right hand rule sign convention, the direction of the rotation vector with component ϕ_X is opposite to the direction which provides a positive displacement derivative v_s' (Fig. VI.2b) (primes denote differentiation with respect to longitudinal coordinate z) whereas the direction of the rotation vector with component ϕ_Y is identical to the direction which provides positive displacement derivative u_s' (Fig. VI.2c). Thus, one has $\phi_X = -v'_s$ and $\phi_Y = u'_s$. Also, by neglecting the rotation terms higher than second order, the rotation tensor can be expressed in matrix form as (Kim 1996, McGuire et al. 2000)

$$R_{ij} \approx \begin{bmatrix} 1 & -\phi_Z & u_s' \\ \phi_Z & 1 & v_s' \\ -u_s' & -v_s' & 1 \end{bmatrix} + \frac{1}{2}\begin{bmatrix} -\left(\phi_Z^2 + u_s'^2\right) & -v_s'u_s' & -\phi_Z v_s' \\ -v_s'u_s' & -\left(\phi_Z^2 + v_s'^2\right) & \phi_Z u_s' \\ -\phi_Z v_s' & \phi_Z u_s' & -\left(v_s'^2 + u_s'^2\right) \end{bmatrix} \tag{VI.2}$$

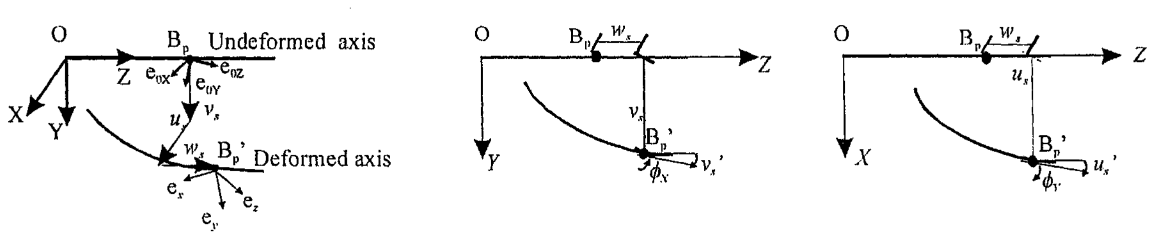

(a) Thee Dimensional view (b) Projection in YZ plane (c) Projection in XZ plane

Fig. VI.2 Deformation of beam axis observed from spatial coordinates

Stress Definitions

In Fig. VI.3, an initially un-deformed parallelepiped has the dimensions dx, dy and dz which stays constant in the material coordinates throughout deformation. On the other hand, the dimensions of the deformed parallelepiped are measure in terms of dX, dY and dZ in spatial coordinates. The forces f_X, f_Y and f_Z are acting on the surfaces which were initially perpendicular to X, Y and Z axes respectively. In general, forces f_X, f_Y and f_Z do not act along the directions of the normal to the surfaces n_X, n_Y and n_Z. The components i_{0X}, i_{0Y} and i_{0Z} of triad $\vec{i}_0$ (Fig. VI.3) are unit vectors along X, Y and Z directions respectively.

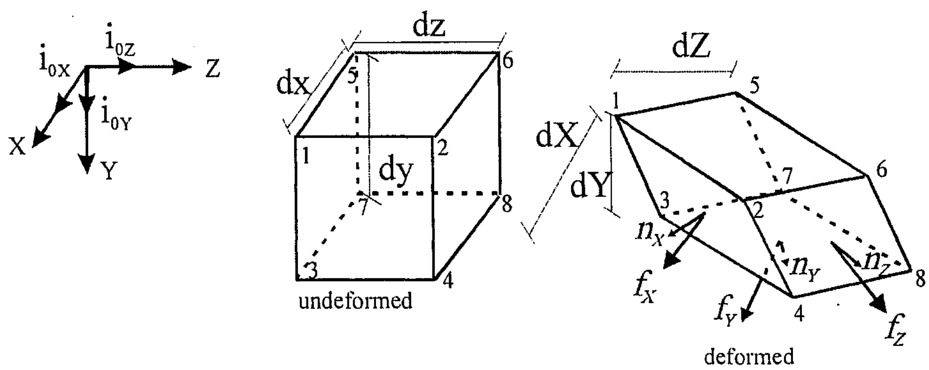

Fig. VI.3 Forces acting on the deformed shape observed from spatial coordinates XYZ

The first Piola-Kirchoff stresses D_{ij} are defined as the forces acting along X, Y and Z axes per unit of initial <u>un-deformed</u> area i.e., $D_{jk} = \left[f_j / \left(dx_p dx_q \right) \right] i_{0k}$, in which $j \neq p \neq q$ (i.e., p and q are not free indices and are determined by index j in order to refer to the un-deformed areas on which the forces f_j are acting, Pai et al. 1998). Indices 1, 2, 3 for D_{ij}, f_j and i_{0k} indicate X, Y, Z respectively. Note that the triad $\vec{i}_0$ in Fig. VI.3 is fixed with the spatial coordinate system while the triad $\vec{e}_0$ in Fig. VI.1 is oriented along the principal directions and varies from point to point within the volume of the element. For isotropic materials, the Jaumann stresses σ_{ik} can be expressed in terms of the first Piola-Kirchoff stress tensor D_{ij} and the rigid body rotation tensor R_{jk} as $\sigma_{ik} = D_{ij}R_{jk}$ (Koiter 1976). Note that indices 1, 2, 3 for σ_{ik} indicate x, y, z respectively. Since the direction of Jaumann stress components change throughout deformation, the Jaumann stresses are referred to the material coordinate system. Physical interpretations of the Jaumann stress are provided in the works of Bufler (1982), Reissner (1985) and Pai et al (1994), and in Appendix VI.A .

The Vlasov beam theory

As a result of the first Vlasov assumption, in-plane cross-sectional distortions throughout deformation are assumed negligible, the in-plane buckling displacements $u_s(s,z)$ and $v_s(s,z)$ of a point B_p (Fig. VI.4) located on the section mid-surface can be expressed in terms of the in-plane displacement components $u(z)$ and $v(z)$ of an arbitrarily located pole $A_p(a_x,a_y)$ located in the plane of the cross-section and the angle of twist of the cross-section $\phi_Z(z)$ (Fig. VI.4a). Coordinate s, measured from an arbitrary sectorial origin S_0 located on the section profile, and oriented according to the right hand rule about axis z, identifies material coordinates $[x(s), y(s)]$ of point B_p with respect to the material coordinate system. Thus, one has

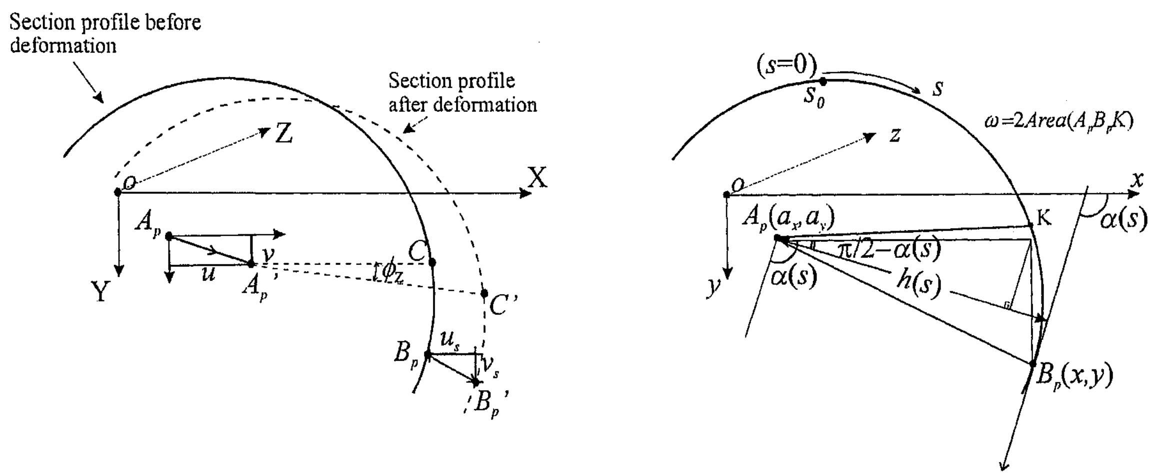

(a) Cross-section Displacements
in spatial coordinates

(b) Sectorial Area definition
in material coordinates

Fig. VI.4 Displacements and coordinates of a thin-walled section

$$u_s(s,z) = u(z) - \left[y(s) - a_y\right]\sin\phi_Z(z) \approx u(z) - \left[y(s) - a_y\right]\phi_Z(z) \tag{VI.3}$$

$$v_s(s,z) = v(z) + \left[x(s) - a_x\right]\sin\phi_Z(z) \approx v(z) + \left[x(s) - a_x\right]\phi_Z(z) \tag{VI.4}$$

In Eqs. (VI.3) and (VI.4) all $\phi_Z(z)$ terms up to second order in Taylor series expansion (i.e., $\sin\phi_Z(z) = \phi_Z(z) + o\left(|\phi_Z|^3\right)$) are retained in line with the moderate rotations assumption. From Eqs. (VI.3) and (VI.4), by taking the derivatives with respect to the longitudinal coordinate z, one obtains the cross-section rotation fields consistent with a Vlasov beam as

$$\phi_X(z,x) = -v'(z) - \left(x - a_x\right)\phi_Z' \tag{VI.5}$$

and

$$\phi_Y(z,y) = u'(z) - \left(y - a_y\right)\phi_Z' \tag{VI.6}$$

In line with the Vlasov theory, the stress components $\sigma_{xx}, \sigma_{yy}, \sigma_{xy}, D_{XX}, D_{YX}, D_{XY}, D_{YY}$ are neglected throughout the analysis i.e., and the stress resultant functions are defined as

$$(a)\, N(z)=\int_A \sigma_{zz}(z,s)dA, \quad (b)\, M_x(z)=\int_A \sigma_{zz}(z,s)y(s)dA, \quad (c)\, V_y(z)=\int_A \sigma_{zy}(z,s,r)dA,$$

$$(d)\, M_y(z)=-\int_A \sigma_{zz}(z,s)x(s)dA, \ (e)\, B(z)=\int_A \sigma_{zz}(z,s)\omega(s)dA, \ (f)\, V_x(z)=\int_A \sigma_{zx}(z,s,r)dA,$$

$$(g)\, T(z)=\int_A \left\{-\sigma_{zx}(z,s,r)\left[y(s)-r\cos\alpha-a_y\right]+\sigma_{zy}(z,s,r)\left[x(s)+r\sin\alpha-a_x\right]\right\}dA$$

$$(h)\, T_w(z)=\int_A \left\{-\sigma_{zx}(z,s,r)\left[y(s)-a_y\right]+\sigma_{zy}(z,s,r)\left[x(s)-a_x\right]\right\}dA \qquad \text{(VI.7)}$$

In Equation (VI.7) $\omega(s)=\int_{S_0}^{s} h(\xi)d\xi$ and $h(s)=(x-a_x)\sin\alpha(s)-(y-a_y)\cos\alpha(s)$ (Fig. VI.4b), coordinate r is the normal distance from the mid-surface, $dA=drds$ is an element of cross-section area in the material coordinates, $\int_A dA=\int_S\left(\int_{-t(s)/2}^{t(s)/2} dr\right)ds$, symbols $\int_A$ and $\int_S$ are due to the integration over the total area and perimeter of the cross-section respectively and $t(s)$ is the plate thickness (Fig. VI.5). The stress expressions in terms of stress resultants functions in a non-orthogonal coordinate system are adopted from Chapter IV Eq. (IV. 13)[1].

$$\sigma_{zz}=\langle 1 \quad -x(s) \quad -y(s) \quad -\omega(s)\rangle \mathbf{D}_{4\times4}^{-1}\begin{Bmatrix} N \\ M_y \\ -M_x \\ -B \end{Bmatrix} \qquad \text{(VI.8)}$$

in which matrix $\mathbf{D}_{4\times4}$ is given by

[1]Note that the stress resultants defined in Chapter IV are based on the definitions $M_x(z)=-\int_A \sigma_{zz}(z,s)y(s)dA$ and $B(z)=-\int_A \sigma_{zz}(z,s)\omega(s)dA$. In contrast, the stress resultants $M_x(z)$ and $B(z)$ in this chapter are consistent with the Eqs. (VI.7) b and e. Thus, Eq. (VI.8) differs from its counterpart in Chapter IV by a minus sign in front of the stress resultants $M_x(z)$ and $B(z)$.

$$\mathbf{D}_{4\times4} = \begin{bmatrix} A & -S_y & -S_x & -S_\omega \\ -S_y & J_{yy} & J_{xy} & J_{\omega x} \\ -S_x & J_{xy} & J_{xx} & J_{\omega y} \\ -S_\omega & J_{\omega x} & J_{\omega y} & J_{\omega\omega} \end{bmatrix} \qquad \text{(VI.9)}$$

and the section constants $A = \int_A dA$, $S_y = \int_A x dA$, $S_x = \int_A y dA$, $S_\omega = \int_A \omega dA$, $J_{xx} = \int_A y^2 dA$, $J_{xy} = \int_A xy dA$, $J_{yy} = \int_A x^2 dA$, $J_{\omega x} = \int_A \omega x dA$, $J_{\omega y} = \int_A \omega y dA$, $J_{\omega\omega} = \int_A \omega^2 dA$ are defined.

In line with the Vlasov theory, the Jaumann stress components σ_{zx} and σ_{zy} are expressed in terms of a stress component σ_{zs} generalized for finite deformations which is acting in the direction tangent to the section contour line for small deformations (Fig. VI.5a) i.e., $\sigma_{zy} = \sigma_{zs} \sin\alpha$ and $\sigma_{zx} = \sigma_{zs} \cos\alpha$. The magnitude of this component can be expressed as the resultant of the components σ_{zy} and σ_{zx} through $\sigma_{zs}{}^2 = \sigma_{zx}{}^2 + \sigma_{zy}{}^2$. Also, it is noted that the stress component σ_{zr} which is in the direction normal to the tangent to the profile for small deformations vanishes (Fig. VI.5a) i.e.,

$$\sigma_{zr} = \sigma_{zx} \sin\alpha - \sigma_{zy} \cos\alpha = 0 \qquad \text{(VI.10)}$$

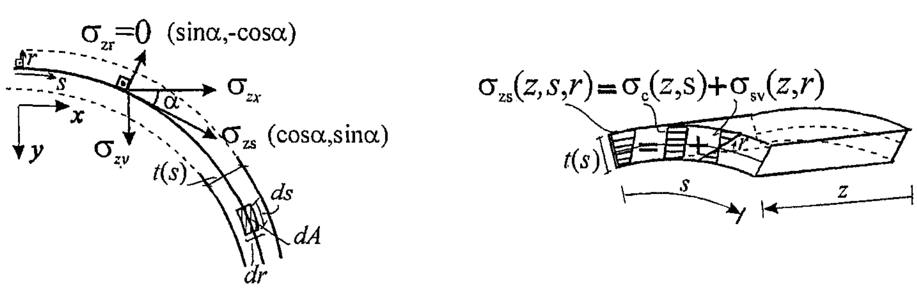

(a) Stress components on the section contour line

(b) Linear and constant stress components across the thickness

Fig. VI.5- Components of the Jaumann stresses for small deformations in line with the Vlasov theory

The stress component σ_{zs} consists of two components: a component constant across the thickness (due to the combination of warping torsion and biaxial shear forces) and a component with a linear variation along thickness due to the St. Venant torsion. Thus, the Jaumann stress component σ_{zs} is assumed to have a linear distribution across the thickness taking the form $\sigma_{zs}(z,s,r) = \sigma_c(z,s) + \sigma_{sv}(z,r)$ in which $\sigma_c(z,s)$ is the constant component across the thickness and $\sigma_{sv}(z,r)$ has linear variation throughout thickness. For small deformation the distribution of the Jaumann stress component σ_{zs} across thickness is illustrated in Fig. VI.5b. The constant stress component can be expressed in terms of the stress resultant functions as (Chapter IV Eq. IV.39)

$$\sigma_c(z,s) = \frac{1}{t(s)} \left\langle \bar{A}(s) \quad -\bar{S}_y(s) \quad -\bar{S}_x(s) \quad -\bar{S}_\omega(s) \right\rangle \mathbf{D}_{4\times4}^{-1} \begin{Bmatrix} 0 \\ V_x \\ V_y \\ T_w \end{Bmatrix} \qquad \text{(VI.11)}$$

In Eq. (VI.11), the functions $\bar{A}(s) = \int_{s_b}^{s} dA$, $\bar{S}_y(s) = \int_{s_b}^{s} x dA$, $\bar{S}_x(s) = \int_{s_b}^{s} y dA$ and $\bar{S}_\omega(s_0, s) = \int_{s_b}^{s} \omega(s_0, s) dA$ are defined, in which s_b is the coordinate s of the one of the edges of the cross-section at which Jaumann stress component $\sigma_c(z,s)$ vanishes i.e., $\sigma_c(z, s_b) = 0$.

The stress component due to St. Venant torsion (which is linear across the thickness) is

$$\sigma_{sv}(z,r) = \frac{2r}{J_d} T_{sv}(z) \qquad \text{(VI.12)}$$

Notation for Pre-buckling and Buckling Stress Rotation and Displacement Fields

A thin-walled beam is brought from the un-deformed state to a deformed state under a reference pre-buckling load. Under the reference load, the structure will undergo a rotation tensor R_{ij}^{p} and will be subjected to the Piola-Kirchoff stress fields D_{ij}^{p}, and Jauman Stress tensor σ_{ij}^{p}. As a general notation convention, all field variables with a superscript p will relate to the pre-buckled configuration under the reference load (Fig. VI.6).

The reference load is then increased by a scalar multiplier value λ so that the structure attains the state of onset of buckling. At that state, the corresponding rotation tensor, first Piola-Kirchoff stress, and Jauman stress tensors become $\lambda R_{ij}^{p}, \lambda D_{ij}^{p}, \lambda\sigma_{ij}^{p}$, respectively.

In the final buckled configuration, the final rotation tensor, first Piola-Kirchoff stress, and Jauman stress tensors become $R_{ij}^{*}, D_{ij}^{*}, \sigma_{ij}^{*}$. As a general notation convention, variables with a superscript * will relate to the final buckled configuration.

In going from the point of onset of buckling to the final buckled configuration, the change in rotation tensor, first Piola-Kirchoff stress, and Jauman stress tensors are noted as ΔR_{ij}, $\Delta D_{ij}, \Delta\sigma_{ij}$ respectively. The above three sets of rotation and stress fields are related through $R_{ij}^{*} = \lambda R_{ij}^{p} + \Delta R_{ij}$, $D_{ij}^{*} = \lambda D_{ij}^{p} + \Delta D_{ij}$, and $\sigma_{ik}^{*} = \lambda\sigma_{ik}^{p} + \Delta\sigma_{ik}$.

Finally, all field variables without a superscript * or p and those which are not preceded by Δ are generic in nature and can be applied to the pre-buckling state, to the onset of buckling, or to the final buckled configuration by changing symbols, as needed. This has been the case for all field variables appearing in Equations (VI.1) through (VI.12). For instance, by adding a * superscript to all field variables in Eq.(VI.1), one recovers an expression for the rotation tensor in the final buckled configuration i.e., $R^*_{ij}=\delta_{ij}(1-\frac{1}{2}\phi^*_k\phi^*_k)+\varepsilon_{ikj}\phi^*_k+\frac{1}{2}\phi^*_i\phi^*_j$.

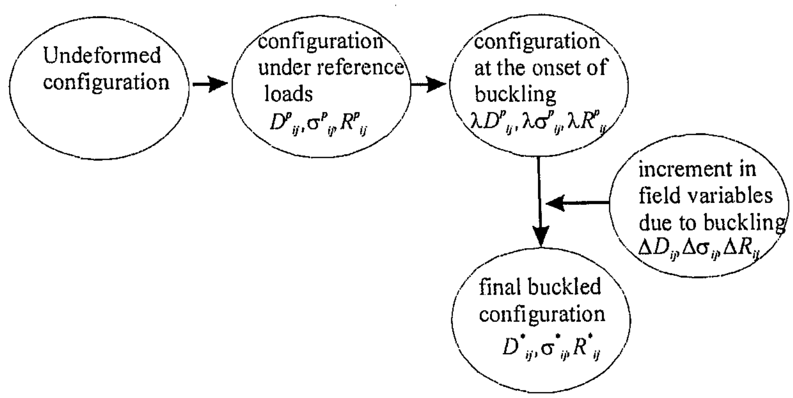

Fig. VI.6 Notation and Definitions of Field Variables

By neglecting the pre-buckling rotations (i.e., $\lambda R^p_{ij}=\delta_{ij}$ and $\phi^*_i=\lambda\phi^p_i+\Delta\phi_i\approx\Delta\phi_i$), the rotation tensor in the final buckled configuration R^*_{ij} can be expressed in terms of the buckling rotation vector components in going from the state of onset of buckling to the final buckled configuration $\Delta\phi_i$ as

$$R^*_{ij}=\delta_{ij}(1-\frac{1}{2}\Delta\phi_k\Delta\phi_k)+\varepsilon_{ikj}\Delta\phi_k+\frac{1}{2}\Delta\phi_i\Delta\phi_j \qquad \text{(VI.13)}$$

Equilibrium Conditions

Translational equilibrium can be easily expressed in terms of first Piola-Kirchoff stress tensor D_{ij} since its components have constant directions along the Z, X and Y axes throughout the volume. In the absence of body forces, the pre-buckling translational equilibrium equations under reference loads are expressed as

$$\partial D_{ij}^p / \partial x_i = 0 \tag{VI.14}$$

Also, the translational equilibrium equations in the final buckled configuration are expressed as

$$\lambda \, \partial D_{ij}^p / \partial x_i + \Delta D_{ij} / \partial x_i = 0 \tag{VI.15}$$

From Eq. (VI.14), by substituting into Eq. (VI.15), one obtains

$$\Delta D_{ij} / \partial x_i = 0 \tag{VI.16}$$

Since the pre-buckling rotations are negligible i.e., $\phi_i^p = 0$ and $\lambda R_{ij}^p \approx \delta_{ij}$, the Jaumann stress tensor is found to coincide with the first Piola-Kirchoff stress tensor through the relation

$$\sigma_{ik}^p = D_{ij}^p R_{jk}^p \approx D_{ij}^p \delta_{jk} = D_{ik}^p \tag{VI.17}$$

The equilibrium of angular momentum can be reduced to the symmetry condition of the Jaumann stress tensor i.e., $\varepsilon_{rik} \sigma_{ik}^* = \varepsilon_{rik} D_{ij}^* R_{jk}^* = 0$, from which one obtains

$$\left(\lambda D_{ij}^p + \Delta D_{ij}\right) = \left(\lambda \sigma_{ik}^p + \Delta \sigma_{ik}\right) R_{jk}^* \tag{VI.18}$$

From Eq. (VI.17), by substituting into Eq. (VI.18), and neglecting the second order small terms in the resulting expressions (Koiter 1976), the angular equilibrium equations simplify to

$$\Delta D_{ik} = \Delta \sigma_{ik} + \lambda \sigma_{ij}^p \varepsilon_{jmk} \Delta \phi_m \tag{VI.19}$$

By expanding Eq. (VI.16) while eliminating the vanishing stresses, the translational equilibrium equations along the Z, X and Y directions are expressed respectively as

$$\frac{\partial(\Delta D_{ZZ})}{\partial z}+\frac{\partial(\Delta D_{XZ})}{\partial x}+\frac{\partial(\Delta D_{YZ})}{\partial y}=0 \tag{VI.20}$$

$$\frac{\partial(\Delta D_{ZX})}{\partial z}=0 \tag{VI.21}$$

$$\frac{\partial(\Delta D_{ZY})}{\partial z}=0 \tag{VI.22}$$

Also, by eliminating the vanishing stresses for the Vlasov beam, the nine angular equilibrium equations obtained from Eq. (VI.19), simplify to

$$\lambda\sigma_{xz}^{p}\Delta\phi_{X}=0, \qquad \lambda\sigma_{xz}^{p}\Delta\phi_{Y}=0, \qquad \lambda\sigma_{yz}^{p}\Delta\phi_{X}=0, \qquad \lambda\sigma_{yz}^{p}\Delta\phi_{Y}=0 \quad \text{(VI.23) (a-d)}$$

and

$$\Delta D_{ZZ}=\Delta\sigma_{zz}, \qquad \Delta D_{ZX}=\Delta\sigma_{zx}-\lambda\left(\sigma_{zz}^{p}\Delta\phi_{Y}-\sigma_{zy}^{p}\Delta\phi_{Z}\right),$$

$$\Delta D_{ZY}=\Delta\sigma_{zy}-\lambda\sigma_{zx}^{p}\Delta\phi_{Z}+\lambda\sigma_{zz}^{p}\Delta\phi_{X}, \qquad \Delta D_{XZ}=\Delta\sigma_{xz}, \qquad \Delta D_{YZ}=\Delta\sigma_{yz} \quad \text{(VI.24) (a-e)}$$

From Eqs. (VI.24) a, d and e, by substituting into Eqs. (VI.20), and using the relations

$$\left[\partial(\Delta\sigma_{sz})/\partial s\right]ds=\left[\partial(\Delta\sigma_{sz})/\partial x\right]dx+\left[\partial(\Delta\sigma_{sz})/\partial y\right]dy, \quad dx=ds\cos\alpha, \quad dy=ds\sin\alpha,$$

and $\Delta\sigma_{xz}=\Delta\sigma_{sz}\cos\alpha$ and $\Delta\sigma_{yz}=\Delta\sigma_{sz}\sin\alpha$ one obtains the equilibrium condition along the Z direction in terms of Jaumann stresses due to buckling as

$$\frac{\partial(\Delta\sigma_{zz})}{\partial z}+\frac{\partial(\Delta\sigma_{sz})}{\partial s}=0 \tag{VI.25}$$

Statement of the Problem and Scope

Lateral torsional buckling phenomena occur when a member is subjected to loads which induce combinations of axial forces, bending about the section major principal axis and the associate shear forces. The limiting condition corresponding to the buckling state under such loads is obtained through a bifurcation analysis. The presence of lateral forces inducing bending about the minor axis and the associated shear, torsion, or bimoments, would transform the problem into a non-linear force-deformation analysis. In the buckling analysis sought in the current study, such effects do not appear. Thus, the beam is subjected to axial forces, bending moments acting about the major centroidal axis and in-plane vertical forces, which do not cause any pre-buckling shear forces V_x^p and associated bending moments M_y^p, twisting moments due to warping T_w^p, St. Venant torsion T_{sv}^p, nor bimoments B^p throughout the beam. In all subsequent formulations, the beam axes x and y are selected to be parallel to the major and minor axis respectively (Fig. VI.7a-d).

Throughout buckling, the displacements in vertical direction, moments about the major axis, associated shear force acting along the minor axis, and increment in axial force all vanish i.e., $\Delta v = \Delta M_x = \Delta V_y = \Delta N = 0$. The later condition is consistent with the inextensional buckling assumption (Trahair 1993).

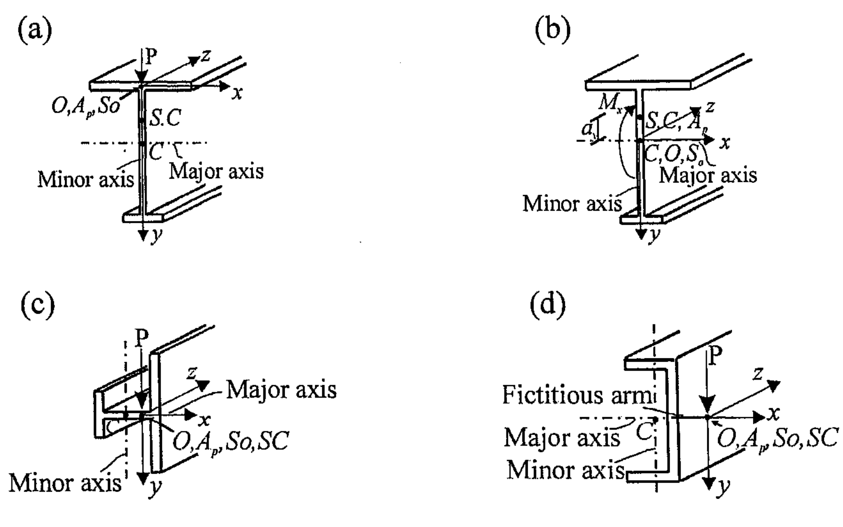

Fig. VI.7 (a)Vertical force applied to a mono-symmetric section at top flange (non-orthogonal coordinates) (b) Moment about the major centroidal axis applied to a mono-symmetric section in orthogonal coordinates (c) Vertical force applied to a mono-symmetric section (non-orthogonal coordinates) (d) Vertical force applied to Channel section (non-orthogonal coordinates)

Formulation

The formulation provides modeling flexibility by selecting non-orthogonal as well as orthogonal systems of coordinates. By selecting the origin O, pole A_p, sectorial origin S_o to coincide with the point of application of the external load P, one can pursue a buckling analysis in which the effect of the transverse load position is considered (e.g., Fig. VI.7 a illustrates a case where top flange loading is applied to a mono-symmetric section).

By using the relations in Eq. (VI.7) for pre-buckled and buckled configurations, and using the relation $\sigma_{ik}^{*} = \lambda_b \sigma_{ik} + \Delta\sigma_{ik}$ one obtains

$$N^p(z) = \int_A \sigma_{zz}^p(z,s)dA, \qquad M_x^p(z) = \int_A \sigma_{zz}^p(z,s)y(s)dA, \quad V_y^p(z) = \int_A \sigma_{zy}^p dA \qquad \text{(VI.26) (a-c)}$$

and

$$\Delta M_y(z) = -\int_A \Delta\sigma_{zz}(z,s)x(s)dA, \ \Delta B(z) = \int_A \Delta\sigma_{zz}(z,s)\omega(s)dA, \ \Delta V_x(z) = \int_A \Delta\sigma_{zx} dA,$$

$$\Delta T(z) = \int_A \left\{-\Delta\sigma_{zx}\left[y(s)-a_y - r\cos\alpha\right] + \Delta\sigma_{zy}\left[x(s)-a_x + r\sin\alpha\right]\right\} dA$$

$$\Delta T_w(z) = \int_A \left\{-\Delta\sigma_{zx}\left[y(s)-a_y\right] + \Delta\sigma_{zy}\left[x(s)-a_x\right]\right\} dA \qquad \text{(VI.27) (a-e)}$$

By using Eqs. (VI.8), (VI.11) and (VI.12) for pre-buckled and buckled final configuration, and the relations $\sigma_{ik}^{*} = \lambda\sigma_{ik} + \Delta\sigma_{ik}$, $\Delta M_x = \Delta V_y = \Delta N = 0$ and $V_x^p = M_y^p = T_w^p = T_{sv}^p = B^p = 0$, one obtains

$$\sigma_{zz}^p = \langle 1 \quad -x(s) \quad -y(s) \quad -\omega(s) \rangle \mathbf{D}_{4\times4}^{-1} \begin{Bmatrix} N^p \\ 0 \\ -M_x^p \\ 0 \end{Bmatrix} \qquad \text{(VI.28)}$$

$$\Delta\sigma_{zz} = \langle 1 \quad -x(s) \quad -y(s) \quad -\omega(s) \rangle \mathbf{D}_{4\times4}^{-1} \begin{Bmatrix} 0 \\ \Delta M_y \\ 0 \\ -\Delta B \end{Bmatrix} \tag{VI.29}$$

$$\Delta\sigma_c(z,s) = \frac{1}{t(s)} \langle \bar{A}(s) \quad \bar{S}_y(s) \quad \bar{S}_x(s) \quad \bar{S}_\omega(s) \rangle \mathbf{D}_{4\times4}^{-1} \begin{Bmatrix} 0 \\ \Delta V_x \\ 0 \\ \Delta T_w \end{Bmatrix} \tag{VI.30}$$

and

$$\Delta\sigma_{sv}(z,r) = \frac{2r\Delta T_{sv}(z)}{J_d} \tag{VI.31}$$

Equilibrium Equations in Terms of Stress Resultants

Translational Equilibrium in the transverse direction

By substituting Eqs. (VI.24)-b into Eq. (VI.21) and integrating over the cross-section area one obtains

$$\int_A \frac{\partial}{\partial z}\left[\Delta\sigma_{zx} - \lambda\left(\sigma_{zz}^p \Delta\phi_Y - \sigma_{zy}^p \Delta\phi_Z\right)\right] dA = 0 \tag{VI.32}$$

Equation (VI.6) is applied for the buckling deformation i.e., $\Delta\phi_Y(z,y) = \Delta u'(z) - \left(y - a_y\right)\Delta\phi_Z'$ and then substituted into Eq. (VI.32) . By using the expression for the pre-buckling stress resultants (Eqs. (VI.26) a-c) and Equation (VI.27)-c for the buckling stresses and integrating with respect to coordinate *z*, one obtains

$$\Delta V_x = \Delta V_{x\alpha} + \lambda\left(N^p \Delta u' - M_x^p \Delta\phi_Z' - V_y^p \Delta\phi_Z + a_y N^p \Delta\phi_Z'\right) = 0 \tag{VI.33}$$

in which constant $\Delta V_{x\alpha}$ appears when integrating Eq. (VI.32) with respect to coordinate *z*.

Torsional Equilibrium

By multiplying Eq. (VI.21) by $a_y - y(s) + r\cos\alpha$ and Eq. (VI.22) by $x(s) - a_x + r\sin\alpha$, summing both equations, integrating over the cross-section area and using the moment equilibrium equations (VI.24) b-c, one obtains

$$\begin{aligned}&\int_A \left\{\frac{\partial}{\partial z}\left[\Delta\sigma_{zx} - \lambda\left(\sigma_{zz}^p \Delta\phi_Y - \sigma_{zy}^p \Delta\phi_Z\right)\right]\right\}\left(a_y - y + r\cos\alpha\right)\\ &+\left\{\frac{\partial}{\partial z}\left[\Delta\sigma_{zy} - \lambda\sigma_{zx}^p \Delta\phi_Z + \lambda\sigma_{zz}^p \Delta\phi_X\right]\right\}\left(x - a_x + r\sin\alpha\right)dA = 0\end{aligned} \tag{VI.34}$$

By substituting Eqs. (VI.6) into Eq. (VI.34), and using the stress resultant expressions (VI.26) a, b for pre-buckling stresses and Equation (VI.27) d , one obtains

$$\begin{aligned}&\Delta T' - \lambda\Big\{N^p a_y \Delta u' - M_x^p \Delta u' - 2M_x^p a_y \Delta\phi_Z' + N^p\left(a_y^{\,2} + a_x^{\,2}\right)\Delta\phi_Z' + W\Delta\phi_Z'\\ &+\int_A \sigma_{zz}^p \left\{\left[\Delta u' - \left(y - a_y\right)\Delta\phi_Z'\right]\cos\alpha + \left[\left(x - a_x\right)\Delta\phi_Z' + \Delta v'\right]\sin\alpha\right\} r\,dA\\ &+\Delta\phi_Z \int_A \left[\sigma_{zy}^p\left(y - r\cos\alpha - a_y\right) + \sigma_{zx}^p\left(x - a_x + r\sin\alpha\right)\right]dA\Big\}' = 0\end{aligned} \tag{VI.35}$$

By noting that for any function $f(s,z)$, $\int_A f(s,z) r\,dA = \int_S f(s,z)\left(\int_{-t(s)/2}^{t(s)/2} r\,dr\right)ds$ and $\int_{-t(s)/2}^{t(s)/2} r\,dr = 0$, the first integral term appearing in Eq. (VI.35) can be shown to vanish. By using Eq. (VI.10) and from the relations $x - a_x = h\sin\alpha$, $y - a_y = -h\cos\alpha$, $\sigma_{zx}^p = \sigma_{zs}^p \cos\alpha$ and $\sigma_{zy}^p = \sigma_{zs}^p \sin\alpha$, the last integral term appearing in Eq. (VI.35) can also be shown to vanish. In Eq. (VI.35), W is the Wagner stress resultant $W = \int_A \sigma_{zz}^p (x^2 + y^2) dA$ (Trahair 1993). By using Eq. (VI.28) for the pre-buckling state, one obtains.

$$W = \langle I_p \quad -I_{py} \quad -I_{px} \quad -I_{p\omega} \rangle \mathbf{D}_{4\times4}^{-1} \begin{Bmatrix} N^p \\ 0 \\ -M_x^p \\ 0 \end{Bmatrix} \tag{VI.36}$$

In Eq. (VI.36), the sectional properties $I_p = \int_A (x^2+y^2)dA$, $I_{py} = \int_A x(x^2+y^2)dA$, $I_{px} = \int_A y(x^2+y^2)dA$ and $I_{p\omega} = \int_A \omega(x^2+y^2)dA$ reported in Timoshenko (1945) appear naturally. By defining constants

$$r_{N0}^2 = \langle I_p \quad -I_{py} \quad -I_{px} \quad -I_{p\omega} \rangle \mathbf{D}_{4\times4}^{-1} \begin{Bmatrix} 1 \\ 0 \\ 0 \\ 0 \end{Bmatrix}$$

and

$$\beta_{Nx} = \langle I_p \quad -I_{py} \quad -I_{px} \quad -I_{p\omega} \rangle \mathbf{D}_{4\times4}^{-1} \begin{Bmatrix} 0 \\ 0 \\ -1 \\ 0 \end{Bmatrix} - 2a_y,$$

one can express the Wagner stress resultant for mono-symmetric sections in terms of the pre-buckling stress resultants as $W = N^p r_{N0}^2 + M_x^p \left(\beta_{Nx} + 2a_y\right)$. It is noted that the new expressions for r_{N0}^2 and β_{Nx} in non-orthogonal coordinate systems revert to the well known expressions $r_0^2 = I_p / A$ and $\beta_x = I_{px}/I_x - 2a_y$ for an orthogonal coordinate system which are reported in Timoshenko (1945) and Trahair (1993). It can be verified that the mono-symmetry property $\beta_x = I_{px}/I_x - 2a_y$ vanishes for all sections symmetric about x axis. Thus by integrating Eq. (VI.35) with respect to z one obtains

$$\Delta T = \Delta T_\alpha + \lambda \left[N^p a_y \Delta u' - M_x^p \Delta u' + \beta_{Nx} M_x^p \Delta\phi_Z' + N^p \left({r_{N0}}^2 + {a_y}^2 + {a_x}^2 \right) \Delta\phi_Z' \right] \tag{VI.37}$$

in which symbol ΔT_α appears when integrating Eq.(VI.35) with respect to coordinate z

Moment equilibrium about y axis

By multiplying Eq. (VI.25) by $x(s)$, integrating over the cross-section area, and using the relation $dA = t(s)ds$ one obtains

$$\int_A \left[\frac{\partial(\Delta\sigma_{zz})}{\partial z} + \frac{\partial(\Delta\sigma_{sz})}{\partial s} \right] x dA = \int_A \frac{\partial \Delta\sigma_{zz}}{\partial z} x dA + \Delta\sigma_{sz} x(s) t(s)\big|_S - \int_A \Delta\sigma_{sz} \frac{\partial x}{\partial s} dA = 0 \qquad \text{(VI.38)}$$

In Eq. (VI.38) symbol $\big|_S$ denotes the integration over the perimeter of the cross-section. Thus, the second term on the right hand side vanishes since the stresses due to buckling vanish at the boundaries of the cross-section i.e., $\Delta\sigma_{sz}\big|_S = 0$. By substituting the relations $\partial x/\partial s = \cos\alpha$ and $\Delta\sigma_{xz} = \Delta\sigma_{sz}\cos\alpha$ into Eq. (VI.38), one obtains

$$\int_A \frac{\partial \Delta\sigma_{zz}}{\partial z} x dA - \int_A \Delta\sigma_{zx} dA = 0 \qquad \text{(VI.39)}$$

Also, by substituting Eq. (VI.6) into Eq. (VI.39), and using Eqs. (VI.27) a-c, one obtains

$$-\Delta M_y{}' - \Delta V_x = 0 \qquad \text{(VI.40)}$$

From Eq. (VI.33), by substituting into Eq. (VI.40) and integrating with respect to *z*, one obtains

$$\Delta M_y = \Delta M_{y\alpha} - \Delta V_{x\alpha} z - \lambda \int \left(N^P \Delta u' - M_x^P \Delta\phi_Z' - V_y^P \Delta\phi_Z + a_y N^P \Delta\phi_Z' \right) dz \qquad \text{(VI.41)}$$

in which symbol $\Delta M_{y\alpha}$ appears when integrating Eq. (VI.40) with respect to coordinate z.

Bimoment Equilibrium

By multiplying Eq. (VI.25) by $\omega(s)$, integrating over the cross-section area and using the relation $dA = t(s)ds$ one obtains

$$\int_A \left[\frac{\partial(\Delta\sigma_{zz})}{\partial z}+\frac{\partial(\Delta\sigma_{sz})}{\partial s}\right]\omega(s)dA = \int_A \frac{\partial\Delta\sigma_{zz}}{\partial z}\omega dA + \Delta\sigma_{sz}\omega(s)t(s)\big|_S - \int_A \Delta\sigma_{sz}\frac{\partial\omega}{\partial s}dA = 0 \quad \text{(VI.42)}$$

The second term on the right hand side of Eq. (VI.42) vanishes since the stresses due to buckling vanish at the boundaries of the cross-section i.e., $\Delta\sigma_{sz}\big|_S = 0$. By using the relations $\partial\omega/\partial s = h(s)$, $\Delta\sigma_{xz} = \Delta\sigma_{sz}\cos\alpha$ and $\Delta\sigma_{yz} = \Delta\sigma_{sz}\sin\alpha$ in Eq. (VI.38), one obtains

$$\int_A \frac{\partial\Delta\sigma_{zz}}{\partial z}\omega dA - \int_A \left[-\Delta\sigma_{zx}\left(y(s)-a_y\right)+\Delta\sigma_{zy}\left(x(s)-a_x\right)\right]dA = 0 \quad \text{(VI.43)}$$

From Eqs. (VI.27) b and e by substituting into Eq. (VI.43) one obtains $\Delta B' - \Delta T_w = 0$. By using the relation $\Delta T = \Delta T_w + \Delta T_{sv}$, one obtains

$$\Delta B' - \Delta T + \Delta T_{sv} = 0 \quad \text{(VI.44)}$$

From Eq. (VI.37), by substituting into Eq. (VI.44) and integrating with respect to coordinate z one obtains

$$\Delta B = \Delta B_\alpha + \Delta T_\alpha z + \lambda \int \left[N^P a_y \Delta u' - M_x^P \Delta u' + \beta_x M_x^P \Delta\phi_Z' + N^P\left(r_{N0}{}^2 + a_y{}^2 + a_x{}^2\right)\Delta\phi_Z'\right]dz - \int \Delta T_{sv} dz \quad \text{(VI.45)}$$

in which symbol ΔB_α appears when integrating Eq. (VI.45) with respect to coordinate z.

Complementary Energy Expression and Buckling Formulation based on the Principle of Stationary Complementary Energy

Similar to the Trefftz stability criterion for total potential energy i.e., $\delta\left(\frac{1}{2}\delta^2\pi\right) = 0$, one can express the stability criterion based on the complementary energy as provided by Koiter (1976) and Oran (1967) i.e., $\delta\left(\frac{1}{2}\delta^2\pi^*\right) = 0$. The complementary energy expression for semilinear material under finite deformations is provided by Koiter (1976) as

$$\pi^*(R_{ij}^*, \sigma_{ij}^*) = \int_{V_0} \left[\frac{1}{4G} \left(\sigma_{ij}^* \sigma_{ij}^* - \frac{\nu}{1+\nu} \sigma_{ii}^{*2} \right) + \sigma_{ii}^* - R_{ij}^* \sigma_{ji}^* \right] dV \qquad \text{(VI.46)}$$

In Eq. (VI.46), G is the shear modulus, ν is the Poisson's ratio and V_0 is the volume of the un-deformed body. By expanding the complementary energy functional in the neighborhood of the buckling configuration using Taylor series, neglecting the terms higher than the second order and considering the fact that the first variation vanishes $\delta\pi^* = 0$, one obtains the second variation of complementary energy expression (Appendix VI.B) as

$$\delta^2 \pi^* = \int_{V_0} \left\{ \left(\lambda \sigma_{ii}^p \Delta\phi_m \Delta\phi_m - \lambda \sigma_{ij}^p \Delta\phi_j \Delta\phi_i \right) + \frac{1}{2G} \left[\Delta\sigma_{ij} \Delta\sigma_{ij} - \frac{\nu}{(1+\nu)} \left(\Delta\sigma_{ii} \right)^2 \right] \right\} dV \qquad \text{(VI.47)}$$

Second variation of Complementary Energy

By omitting the vanishing stress fields i.e., $\Delta\sigma_{xx} = \Delta\sigma_{yy} = \Delta\sigma_{xy} = \sigma_{xx}^p = \sigma_{yy}^p = \sigma_{xy}^p = 0$, the second variation of complementary energy simplifies to

$$\delta^2 \pi^* = \int_V \left[\begin{array}{l} \lambda \left[\Delta\phi_Y{}^2 \sigma_{zz}^p + \Delta\phi_X{}^2 \sigma_{zz}^p - \Delta\phi_Z \Delta\phi_Y (\sigma_{yz}^p + \sigma_{zy}^p) - \Delta\phi_Z \Delta\phi_X (\sigma_{xz}^p + \sigma_{zx}^p) \right] \\ + \frac{1}{E} \left(\Delta\sigma_{zz} \right)^2 + \frac{1}{2G} \left(\Delta\sigma_{xz}{}^2 + \Delta\sigma_{zx}{}^2 \right) + \frac{1}{2G} \left(\Delta\sigma_{yz}{}^2 + \Delta\sigma_{zy}{}^2 \right) \end{array} \right] dV \qquad \text{(VI.48)}$$

In Eq. (VI.48), the relation $E = 2G(1+\nu)$ was used. By substituting Eqs. (VI.5) and (VI.6) into Eq. (VI.48), integrating the term $\Delta\phi_Y{}^2 \sigma_{zz}^p + \Delta\phi_X{}^2 \sigma_{zz}^p - \Delta\phi_Z \Delta\phi_Y (\sigma_{yz}^p + \sigma_{zy}^p) - \Delta\phi_Z \Delta\phi_X (\sigma_{xz}^p + \sigma_{zx}^p)$ over the cross-sectional area and using Eqs. (VI.23) a and d, i.e., $\lambda \sigma_{xz}^p \Delta\phi_X = \lambda \sigma_{yz}^p \Delta\phi_Y = 0$, one obtains

$$\delta^2\pi^* = \lambda \int_L \left\{ \int_A \left[\left(\Delta u' - \left(y-a_y\right)\Delta\phi_Z'\right)^2 \sigma_{zz}^p + \left(\left(x-a_x\right)\Delta\phi_Z'\right)^2 \sigma_{zz}^p \right] dA \right\} dz$$
$$+ \int_V \left[\frac{1}{E}\left(\Delta\sigma_{zz}\right)^2 + \frac{1}{G}\left(\Delta\sigma_{xz}\right)^2 + \frac{1}{G}\left(\Delta\sigma_{yz}\right)^2 \right] dV \qquad \text{(VI.49)}$$

In Eq. (VI.49), by performing the integration over the cross-sectional area and using the relation $W = \int_A \sigma_{zz}^p \left(y^2 + x^2\right) dA = N^P r_{N0}^2 + M_x^P \left(\beta_{Nx} + 2a_y\right)$ one obtains

$$\delta^2\pi^* = \lambda \int_L \left[\Delta u'^2 N + 2\Delta u' \Delta\phi_Z' \left(-M_x^P + a_y N^P\right) + \Delta\phi_Z'^2 \left(r_{No}^2 + a_y^2 + a_x^2\right) N^P + \Delta\phi_Z'^2 \beta_{Nx} M_x^P \right] dz$$
$$+ \int_V \left[\frac{1}{E}\left(\Delta\sigma_{zz}\right)^2 + \frac{1}{G}\left(\Delta\sigma_{xz}\right)^2 + \frac{1}{G}\left(\Delta\sigma_{yz}\right)^2 \right] dV \qquad \text{(VI.50)}$$

By using the relations $\Delta\sigma_{zx} = \Delta\sigma_{zs}\cos\alpha$, $\Delta\sigma_{zy} = \Delta\sigma_{zs}\sin\alpha$ and $\Delta\sigma_{zs} = \Delta\sigma_c + \Delta\sigma_{sv}$, the last two terms in Eq. (VI.50) can be expressed as $\int_{V_0} \frac{1}{G}\left[\left(\Delta\sigma_{zx}\right)^2 + \left(\Delta\sigma_{zy}\right)^2\right] dV = \int_{V_0} \frac{1}{G}\left(\Delta\sigma_{zs}\right)^2 dV = \int_{V_0} \frac{1}{G}\left(\Delta\sigma_c + \Delta\sigma_{sv}\right)^2 dV$. Since the integration across the thickness of the linear stresses due to St. Venant torsion vanish i.e., $\int_{-t(s)/2}^{t(s)/2} \Delta\sigma_{sv} dr = 0$, one obtains

$$\int_{V_0} \frac{1}{G}\left[\left(\Delta\sigma_{zx}\right)^2 + \left(\Delta\sigma_{zy}\right)^2\right] dV = \int_{V_0} \frac{1}{G}\left[\left(\Delta\sigma_c\right)^2 + \left(\Delta\sigma_{sv}\right)^2\right] dV \qquad \text{(VI.51)}$$

From Eqs. (VI.30) and (VI.31), by substitution into Eq. (VI.51), one obtains

$$\int_{V_0} \frac{1}{G}\left[\left(\Delta\sigma_c\right)^2 + \left(\Delta\sigma_{sv}\right)^2\right] dV = \int_L \frac{1}{G} \langle \Delta V_x \quad \Delta T_w \rangle \chi_{2\times 2}^{-1} \begin{Bmatrix} \Delta V_x \\ \Delta T_w \end{Bmatrix} + \frac{\Delta T_{sv}^{\ 2}}{GJ_d} dz \qquad \text{(VI.52)}$$

In Eq. (VI.52), matrix $\chi_{2\times 2}^{-1}$ is defined as

$$\chi_{2\times2}^{-1}=\begin{bmatrix}0&1&0&0\\0&0&0&1\end{bmatrix}\mathbf{D}_{4\times4}^{-1}\int_A\frac{1}{t^2}\begin{bmatrix}\overline{A}^2&-\overline{A}\overline{S}_y&-\overline{A}\overline{S}_x&-\overline{A}\overline{S}_\omega\\-\overline{A}\overline{S}_y&\overline{S}_y^{\,2}&\overline{S}_y\overline{S}_x&\overline{S}_y\overline{S}_\omega\\-\overline{A}\overline{S}_x&\overline{S}_y\overline{S}_x&\overline{S}_x^{\,2}&\overline{S}_x\overline{S}_\omega\\-\overline{A}\overline{S}_\omega&\overline{S}_y\overline{S}_\omega&\overline{S}_x\overline{S}_\omega&\overline{S}_\omega^{\,2}\end{bmatrix}dA\mathbf{D}_{4\times4}^{-1}\begin{bmatrix}0&0\\1&0\\0&0\\0&1\end{bmatrix}\qquad\text{(VI.53)}$$

From Eqs. (VI.29) by substituting into Eq. (VI.50), the second variation of the complementary energy can be expressed in terms of the stress resultants as

$$\begin{aligned}\delta^2\pi^*=\lambda\int_L&\left[\Delta u'^2N^p+2\Delta u'\Delta\phi_Z'\left(-M_x^p+a_yN^p\right)+\Delta\phi_Z'^2\left(r_{N0}^{\;2}+a_y^{\;2}+a_x^{\;2}\right)N^p+\Delta\phi_Z'^2\beta_{Nx}M_x^p\right]dz\\&+\int_L\left\{\frac{1}{E}\left\langle\Delta M_y\quad\Delta B\right\rangle\mathbf{D}_{r2\times2}^{-1}\begin{Bmatrix}\Delta M_y\\\Delta B\end{Bmatrix}+\frac{1}{G}\left\langle\Delta V_x\quad\Delta T_w\right\rangle\chi_{2\times2}^{-1}\begin{Bmatrix}\Delta V_x\\\Delta T_w\end{Bmatrix}+\frac{\Delta T_{sv}^{\;2}}{GJ_d}\right\}dz\end{aligned}\qquad\text{(VI.54)}$$

In Eq. (VI.54), matrix $\left[D_r\right]_{2\times2}^{-1}$ is defined as

$$\mathbf{D}_{r2\times2}^{-1}=\begin{bmatrix}0&1&0&0\\0&0&0&-1\end{bmatrix}\mathbf{D}_{4\times4}^{-1}\begin{bmatrix}0&0\\1&0\\0&0\\0&-1\end{bmatrix}\qquad\text{(VI.55)}$$

Field Equations and Boundary Conditions

From Equations (VI.33) and (VI.37), one can express the functions $\Delta u'$, $\Delta\phi'$ as

$$\begin{Bmatrix}\Delta u'\\\Delta\phi_Z'\end{Bmatrix}=\frac{1}{\lambda}\mathbf{C}_{2\times2}^{-1}\begin{Bmatrix}\Delta V_x-\Delta V_{x\alpha}+\lambda V_y^p\Delta\phi_Z\\\Delta T-\Delta T_\alpha\end{Bmatrix}\qquad\text{(VI.56)}$$

in which matrix $\mathbf{C}_{2\times2}$ is defined as

$$\mathbf{C}_{2\times2}=\begin{bmatrix}N^p&\left(a_yN^p-M_x^p\right)\\\left(a_yN^p-M_x^p\right)&\left[\beta_{Nx}M_x^p+\left(r_{N0}^{\;2}+a_y^{\;2}+a_x^{\;2}\right)N^p\right]\end{bmatrix}$$

From Equations (VI.33), (VI.37), (VI.40), (VI.44), (VI.56) and the relation $M_x^{p\,\prime}=V_y^p$ one can express Eq. (VI.54) as

$$\delta^2\pi^*$$

$$=\frac{1}{\lambda}\int_L\left[\left\langle\left(-\Delta M_y'-\Delta V_{x\alpha}+\lambda V_y^p\Delta\phi_Z\right)\quad\left(\Delta B'+\Delta T_{sv}-\Delta T_\alpha\right)\right\rangle\mathbf{C}_{2\times2}^{-1}\begin{Bmatrix}\left(-\Delta M_y'-\Delta V_{x\alpha}+\lambda V_y^p\Delta\phi_Z\right)\\\left(\Delta B'+\Delta T_{sv}-\Delta T_\alpha\right)\end{Bmatrix}\right]dz \quad \text{(VI.57)}$$

$$+\int_L\left\{\frac{1}{E}\left\langle\Delta M_y\quad\Delta B\right\rangle\mathbf{D}_{\mathrm{r}2\times2}^{-1}\begin{Bmatrix}\Delta M_y\\\Delta B\end{Bmatrix}+\frac{1}{G}\left\langle-\Delta M_y'\quad\Delta B'\right\rangle\chi_{2\times2}^{-1}\begin{Bmatrix}-\Delta M_y'\\\Delta B'\end{Bmatrix}+\frac{\Delta T_{sv}^{\ 2}}{GJ_d}\right\}dz$$

Note that Eq. (VI.57) contains force parameters only when there is no moment gradient i.e., $V_y^p=0$. Since the variation of the second variation of the complementary energy vanishes for the condition of neutral stability, i.e., $\delta\left(\frac{1}{2}\delta^2\pi^*\right)=0$, by substituting Eq. (VI.57) into the variation of Eq. (VI.57) and using integration by parts one obtains (Appendix VI.C)

$$\frac{1}{2}\delta\left(\delta^2\pi^*\right)=$$

$$\int_L\delta\left(\Delta M_y\right)\left[\Delta u''+\frac{1}{E}\left\langle\Delta M_y\quad\Delta B\right\rangle\mathbf{D}_{\mathrm{r}2\times2}^{-1}\begin{Bmatrix}1\\0\end{Bmatrix}+\frac{1}{G}\left\langle-\Delta M_y''\quad\Delta B''\right\rangle\chi_{2\times2}^{-1}\begin{Bmatrix}1\\0\end{Bmatrix}\right]dz$$

$$+\int_L\delta\left(\Delta B\right)\left[-\Delta\phi_Z''+\frac{1}{E}\left\langle\Delta M_y\quad\Delta B\right\rangle\mathbf{D}_{\mathrm{r}2\times2}^{-1}\begin{Bmatrix}0\\1\end{Bmatrix}-\frac{1}{G}\left\langle-\Delta M_y''\quad\Delta B''\right\rangle\chi_{2\times2}^{-1}\begin{Bmatrix}0\\1\end{Bmatrix}\right]dz$$

$$+\int_L\delta\left(\Delta T_{sv}\right)\left[\Delta\phi_Z'+\frac{\Delta T_{sv}}{GJ_d}\right]dz+\int_L\lambda V_y^p\Delta u'\delta\left(\Delta\phi_Z\right)dz$$

$$+\left[\delta\Delta M_y\left(-\Delta u'+\frac{1}{G}\left\langle-\Delta M_y'\quad\Delta B'\right\rangle\chi_{2\times2}^{-1}\begin{Bmatrix}-1\\0\end{Bmatrix}\right)\right]_0^L$$

$$+\left[\delta\Delta B\left(\Delta\phi_Z'+\frac{1}{G}\left\langle-\Delta M_y'\quad\Delta B'\right\rangle\chi_{2\times2}^{-1}\begin{Bmatrix}0\\1\end{Bmatrix}\right)\right]_0^L$$

$$-\left[\delta\left(\Delta V_{x\alpha}\right)\Delta u\right]_0^L-\left[\delta\left(\Delta T_\alpha\right)\Delta\phi_Z\right]_0^L=0 \quad \text{(VI.58)}$$

In Eq. (VI.58), it can be demonstrated that the term $\lambda V_y^p\Delta u'=0$ under the assumption made in the formulation (Appendix VI.C) which vanishes the last field term. From the first three integral terms in Eq. (VI.58), one obtains the compatibility conditions at neutral equilibrium. The boundary conditions are obtained from the remaining terms.

Simplification under Orthogonal Coordinates

From Equation (VI.58) by adopting orthogonal coordinates i.e., $S_x = S_y = J_{xy} = J_{\omega x} = J_{\omega y} = 0$, one obtains

$$\frac{1}{2}\delta\left(\delta^2\pi^*\right)=$$

$$\int_L\left[\delta\Delta M_y\left(\Delta u''+\frac{\Delta M_y}{EJ_{yy}}-\frac{\Delta M_y''}{G\chi_{11}}\right)+\delta\Delta B\left(-\Delta\phi_Z''+\frac{\Delta B}{EJ_{\omega\omega}}-\frac{\Delta B''}{G\chi_{22}}\right)+\delta\Delta T_{sv}\left(\Delta\phi_Z'+\frac{\Delta T_{sv}}{GJ_d}\right)\right]dz \quad \text{(VI.59)}$$

$$+\delta\Delta M_y\left[-\Delta u'+\frac{\Delta M_y'}{G\chi_{11}}\right]_0^L+\delta\Delta B\left[\Delta\phi_Z'+\frac{\Delta B'}{G\chi_{22}}\right]_0^L-\delta\Delta V_{x\alpha}\left[\Delta u\right]_0^L-\delta\Delta T_\alpha\left[\Delta\phi_z\right]_0^L$$

In Eq. (VI.59), χ_{11} and χ_{22} are the first and second diagonal terms of matrix $\chi_{2\times 2}$.

Flexural buckling of columns

For the column in-plane flexural buckling, the terms related to torsion vanish i.e., $\Delta B = \Delta T_{sv} = \Delta T_\alpha = \phi_Z = 0$, reducing Eq. (VI.59) to

$$\frac{1}{2}\delta\left(\delta^2\pi^*\right)=\int_L\delta\Delta M_y\left(\Delta u''+\frac{\Delta M_y}{EJ_{yy}}-\frac{\Delta M_y''}{G\chi_{11}}\right)dz+\delta\Delta M_y\left[-\Delta u'+\frac{\Delta M_y'}{G\chi_{11}}\right]_0^L-\delta\Delta V_{x\alpha}\left[\Delta u\right]_0^L \quad \text{(VI.60)}$$

In Eq. (VI.60), the first integral provides the compatibility equations at neutral equilibrium, whereas the second and third terms are the boundary conditions. By neglecting the contribution of shear deformation in Eq. (VI.60) i.e., $\Delta M_y''/G\chi_{11} \approx 0$ and $\Delta M_y'/G\chi_{11} \approx 0$, one obtains the compatibility equations and boundary conditions reported in Oran (1961). We note that the constant $\Delta V_{x\alpha}$ appearing in this formulation (Fig. VI.8) coincides with the internal vertical force reported in Oran's derivations.

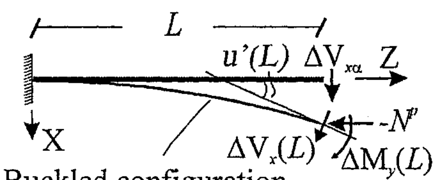

Fig. VI.8 Flexural buckling of a cantilever without shear deformation

Torsional Buckling of columns

For pure torsional buckling of columns, the terms related to bending vanish i.e., $M_x^p = V_y^p = \Delta M_y = \Delta V_{x\alpha} = 0$, reducing Eq. (VI.59) to

$$\frac{1}{2}\delta\left(\delta^2\pi^*\right) =$$
$$\int_L \left\{ \delta\Delta B\left(-\Delta\phi_Z'' + \frac{\Delta B}{EJ_{\omega\omega}} - \frac{\Delta B''}{G\chi_{22}}\right) + \delta\Delta T_{sv}\left(\Delta\phi_Z' + \frac{\Delta T_{sv}}{GJ_d}\right)\right\} dz + \delta\Delta B\left[\Delta\phi_Z' + \frac{\Delta B'}{G\chi_{22}}\right]_0^L - \delta\Delta T_\alpha\left[\Delta\phi_Z\right]_0^L$$

(VI.61)

In equation (VI.61), the first and the second integrals provide the compatibility equations at neutral stability, whereas the remaining terms provide the boundary conditions.

Finite Element Formulation

Interpolation of Buckling Displacement Fields

By adopting the Hermitian polynomials to interpolate for the lateral displacement and rotation fields of element i one obtains

$$\Delta u^{(i)}(z) = \mathbf{H}(z)_{1\times4}^T \Delta\mathbf{u}_{\mathrm{N}\,4\times1}^{(i)} \qquad \text{(VI.62)}$$

$$\Delta\phi_Z^{(i)}(z) = \mathbf{H}(z)_{1\times4}^T \Delta\boldsymbol{\varphi}_{\mathrm{N}\,4\times1}^{(i)} \qquad \text{(VI.63)}$$

In Eq. (VI.62) and (VI.63), vector $\mathbf{H}(z)_{1\times4}^T$ contains the Hermitian polynomials

$$\mathbf{H}(z)_{1\times4}^T = \left\langle \left(1 - \frac{3z^2}{L^2} + \frac{2z^3}{L^3}\right) \left(z - \frac{2z^2}{L} + \frac{z^3}{L^2}\right) \left(\frac{3z^2}{L^2} - \frac{2z^3}{L^3}\right) \left(-\frac{z^2}{L} + \frac{z^3}{L^2}\right) \right\rangle \qquad \text{(VI.64)}$$

and $\mathbf{\Delta u}^{(i)}_{\mathrm{N}\,4\times1}$ and $\mathbf{\Delta \varphi}^{(i)}_{\mathrm{N}\,4\times1}$ are the element end displacement and rotation vectors due to buckling

$$\mathbf{\Delta u}^{(i)T}_{\mathrm{N}\,1\times4} = \left\langle \Delta u^{(i)}_1 \quad \Delta u'^{(i)}_1 \quad \Delta u^{(i)}_2 \quad \Delta u'^{(i)}_2 \right\rangle \tag{VI.65}$$

$$\mathbf{\Delta \varphi}^{(i)T}_{\mathrm{N}\,1\times4} = \left\langle \Delta \phi^{(i)}_{Z1} \quad \Delta \phi'^{(i)}_{Z1} \quad \Delta \phi^{(i)}_{Z2} \quad \Delta \phi'^{(i)}_{Z2} \right\rangle \tag{VI.66}$$

Superscripts to the right of a symbol denote the element number. Subscripts 1 and 2 to denote the first and second nodes of the element (Fig. VI.9).

Interpolation of the pre-buckling Stress Resultant Fields

The pre-buckling internal stress resultant fields for an element i are limited to cases of constant normal force and linear bending moment distributions (Fig. VI.9).

$$N^{p(i)}(z) = N^{p(i)} \tag{VI.67}$$

$$M^{p(i)}_x(z) = M^{p(i)}_{x1}\left(1 - z/L\right) + M^{p(i)}_{x2}\left(z/L\right) \tag{VI.68}$$

$$V^{p(i)}_y = \frac{M^{p(i)}_{x2} - M^{p(i)}_{x1}}{L} \tag{VI.69}$$

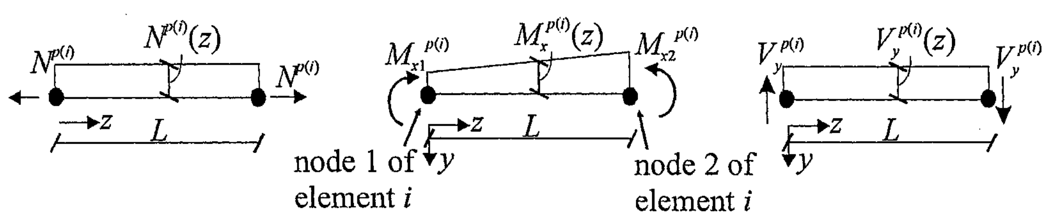

Fig. VI.9- Pre-buckling internal stress resultant distribution

In Eq. (VI.68), $M^{p(i)}_{x1}$ and $M^{p(i)}_{x2}$ represent the pre-buckling bending moments about the x axis at the first and second nodes of element i.

Stress Resultants throughout Buckling

By substituting Eqs. (VI.62) through (VI.69) into the equilibrium equations in Eqs. (VI.33), (VI.37), (VI.41) and (VI.45), one obtains the internal stress resultants due to buckling of element i as

$$\Delta V_x^{(i)}(z)=\Delta V_{x\alpha}^{(i)}+\lambda\left\{N^{p(i)}\mathbf{H}'(z)_{1\times4}^T\Delta\mathbf{u}_{\mathrm{N}\,4\times1}^{(i)}-\left[\left(M_x^{p(i)}(z)-a_yN^{p(i)}\right)\mathbf{H}'(z)_{1\times4}^T+V_y^{p(i)}\mathbf{H}(z)_{1\times4}^T\right]\Delta\boldsymbol{\varphi}_{\mathrm{N}\,4\times1}^{(i)}\right\} \tag{VI.70}$$

$$\Delta T^{(i)}(z)=\Delta T_\alpha^{(i)}+\lambda\left[-\left(M_x^{p(i)}(z)-a_yN^{p(i)}\right)\mathbf{H}'(z)_{1\times4}^T\Delta\mathbf{u}_{\mathrm{N}\,4\times1}^{(i)}+Q^{p(i)}(z)\mathbf{H}'(z)_{1\times4}^T\Delta\boldsymbol{\varphi}_{\mathrm{N}\,4\times1}^{(i)}\right] \tag{VI.71}$$

$$\Delta M_y^{(i)}(z)=\Delta M_{y\alpha}^{(i)}-\Delta V_{x\alpha}^{(i)}z-\lambda\left[N^{p(i)}\mathbf{H}(z)_{1\times4}^T\Delta\mathbf{u}_{\mathrm{N}\,4\times1}^{(i)}-\left(M_x^{p(i)}(z)-a_yN^{p(i)}\right)\mathbf{H}(z)_{1\times4}^T\Delta\boldsymbol{\varphi}_{\mathrm{N}\,4\times1}^{(i)}\right] \tag{VI.72}$$

$$\begin{aligned}\Delta B^{(i)}(z)=\Delta B_\alpha^{(i)}+\Delta T_\alpha^{(i)}z+\lambda&\left\{\left[-\left(M_x^{p(i)}(z)-a_yN^{p(i)}\right)\mathbf{H}(z)_{1\times4}^T+V_y^{p(i)}\mathbf{G}(z)_{1\times4}^T\right]\Delta\mathbf{u}_{\mathrm{N}\,4\times1}^{(i)}\right.\\&\left.+\left[Q^{p(i)}(z)\mathbf{H}(z)_{1\times4}^T-V_y^{p(i)}\beta_{Nx}\mathbf{G}(z)_{1\times4}^T\right]\Delta\boldsymbol{\varphi}_{\mathrm{N}\,4\times1}^{(i)}\right\}-\int\Delta T_{sv}^{(i)}dz\end{aligned} \tag{VI.73}$$

In Eq (VI.73), the definitions $Q^{p(i)}(z)=N^{p(i)}\left(r_{N0}^2+a_x^{\,2}+a_y^{\,2}\right)+M_x^{p(i)}(z)\beta_{Nx}$ and $\mathbf{G}(z)_{1\times4}^T=\int\mathbf{H}(z)_{1\times4}^T dz$ were used. Superscripts to the right of a symbol denote the element number.

Additionally, it will be assumed that the St. Venant twisting moment field throughout buckling ΔT_{sv}^i to have a constant distribution along the element.

Joint Equilibrium for Collinear Elements

From Eqs. (VI.70) through (VI.73), by using the relations $\Delta V_{x2}^{(i)}=\Delta V_x^{(i)}(L^{(i)})$, $\Delta T_2^{(i)}=\Delta T^{(i)}(L^{(i)})$, $\Delta M_{y2}^{(i)}=\Delta M_y^{(i)}(L^{(i)})$ and $\Delta B_2^{(i)}=\Delta B^{(i)}(L^{(i)})$, one obtains the stress resultants due to buckling at node k of element i (Fig. VI.10) as

$$\Delta V_{x2}^{(i)} = \Delta V_{x\alpha}{}^{(i)} + \lambda\left\{N^{p(i)}\Delta u_2'^{(i)} - \left[\left(M_{x2}^{p(i)} - a_y N^{p(i)}\right)\Delta\phi_{Z2}'^{(i)} + V_y^{p(i)}\Delta\phi_{Z2}^{(i)}\right]\right\} \tag{VI.74}$$

$$\Delta T_2^{(i)} = \Delta T_\alpha^{(i)} + \lambda\left\{-\left(M_{x2}^{pv} - a_y N^{p(i)}\right)\Delta u_2'^{(i)} + Q_2^{p(i)}\Delta\phi_{Z2}'^{(i)}\right\} \tag{VI.75}$$

$$\Delta M_{y2}^{(i)} = \Delta M_{y\alpha}^{(i)} - \Delta V_{x\alpha}^{(i)} L^{(i)} - \lambda\left\{N^{p(i)}\Delta u_2^{(i)} - \left(M_{x2}^{p(i)} - a_y N^{p(i)}\right)\Delta\phi_{Z2}^{(i)}\right\} \tag{VI.76}$$

$$\begin{aligned}\Delta B_2^{(i)} = \Delta B_\alpha^{(i)} + \Delta T_\alpha^{(i)} L^{(i)} - \Delta T_{sv}^{(i)} L^{(i)} + \lambda\Big\{&\left[-\left(M_{x2}^{p(i)} - a_y N^{p(i)}\right)\Delta u_2^{(i)} + V_y^{p(i)}\mathbf{G}(L^{(i)})_{1\times4}^T \mathbf{\Delta u}_{\mathrm{N}\,4\times1}^{(i)}\right] \\ &+ \left[Q_2^{p(i)}\Delta\phi_{Z2}^{(i)} - V_y^{p(i)}\beta_{Nx}\mathbf{G}(L^{(i)})_{1\times4}^T \mathbf{\Delta\varphi}_{\mathrm{N}\,4\times1}^{(i)}\right]\Big\}\end{aligned} \tag{VI.77}$$

Subscript 2 to the right of all symbols in Eqs. (VI.74) through (VI.77) denotes the second joint of the element as shown in Fig. VI.10. From Eqs. (VI.70) through (VI.73), by using the nodal equilibrium conditions $\Delta V_{x1}^{(i+1)} = \Delta V_x^{(i+1)}(0)$, $\Delta T_1^{(i+1)} = \Delta T^{(i+1)}(0)$, $\Delta M_{y1}^{(i+1)} = \Delta M_y^{(i+1)}(0)$ and $\Delta B_1^{(i+1)} = \Delta B^{(i+1)}(0)$, one obtains the stress resultants due to buckling at node k for element i+1 (Fig. VI.10) as

$$\Delta V_{x1}^{(i+1)} = \Delta V_{x\alpha}^{(i+1)} + \lambda\left\{N^{p(i+1)}\Delta u_1'^{(i+1)} - \left[\left(M_{x1}^{p(i+1)} - a_y N^{p(i+1)}\right)\Delta\phi_1'^{(i+1)} + V_y^{p(i+1)}\Delta\phi_{Z1}^{(i+1)}\right]\right\} \tag{VI.78}$$

$$\Delta T_1^{(i+1)} = \Delta T_\alpha^{(i+1)} + \lambda\left[-\left(M_{x1}^{p(i+1)} - a_y N^{p(i+1)}\right)\Delta u_1'^{(i+1)} + Q_1^{p(i+1)}\Delta\phi_{Z1}'^{(i+1)}\right] \tag{VI.79}$$

$$\Delta M_{y1}^{(i+1)} = \Delta M_{y\alpha}^{(i+1)} - \lambda\left[N^{p(i+1)}\Delta u_1^{(i+1)} - \left(M_{x1}^{p(i+1)} - a_y N^{p(i+1)}\right)\Delta\phi_{Z1}^{(i+1)}\right] \tag{VI.80}$$

$$\Delta B_1^{(i+1)} = \Delta B_\alpha^{(i+1)} + \lambda\left[-\left(M_{x1}^{p(i+1)} - a_y N^{p(i+1)}\right)\Delta u_1^{(i+1)} + Q_1^{p(i+1)}\Delta\phi_{Z1}^{(i+1)}\right] \tag{VI.81}$$

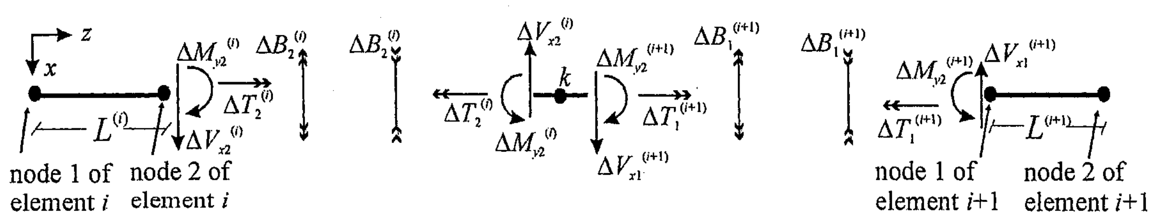

Fig. VI.10 Stress resultants due to buckling for two adjacent elements i and i+1 with a common node k

Subscript 1 to the right of all symbols in Eqs. (VI.78) through (VI.81) denotes the first joint of the element (Fig. VI.10). By applying the equilibrium conditions at node k, i.e.,

$\Delta V_{x2}^{(i)} = \Delta V_{x1}^{(i+1)}$, $\Delta T_2^{(i)} = \Delta T_1^{(i+1)}$, $\Delta M_{y2}^{(i)} = \Delta M_{y1}^{(i+1)}$, and the relation $\Delta B_2^{(i)} = \Delta B_1^{(i+1)}$, and using Eqs. (VI.74) through (VI.81) and the relations $\Delta u_2^{(i)} = \Delta u_1^{(i+1)}$, $\Delta u_2'^{(i)} = \Delta u_1'^{(i+1)}$, $\Delta\phi_{Z2}^{(i)} = \Delta\phi_{Z1}^{(i+1)}$, $\Delta\phi'^{(i)}_{Z2} = \Delta\phi'^{(i+1)}_{Z1}$, $M_{x2}^{p(i)} = M_{x1}^{p(i+1)}$, $N^{p(i)} = N^{p(i+1)}$, $V_y^{p(i)} = V_y^{p(i+1)}$ one obtains

$$\Delta V_{x\alpha}^{(i+1)} = \Delta V_{x\alpha}^{(i)} \tag{VI.82}$$

$$\Delta T_{\alpha}^{(i+1)} = \Delta T_{\alpha}^{(i)} \tag{VI.83}$$

$$\Delta M_{y\alpha}^{(i+1)} = \Delta M_{y\alpha}^{(i)} - \Delta V_{x\alpha}^{(i)} L^{(i)} \tag{VI.84}$$

$$\Delta B_{\alpha}^{(i+1)} = \Delta B_{\alpha}^{(i)} + \Delta T_{\alpha}^{(i)} L^{(i)} + \lambda\left(V_y^{p(i)} \mathbf{G}(L^{(i)})_{1\times4}^T \Delta\mathbf{u}_{\mathrm{N}\,4\times1}^{(i)} - V_y^{p(i)} \beta_{Nx} \mathbf{G}(L^{(i)})_{1\times4}^T \Delta\boldsymbol{\varphi}_{\mathrm{N}\,4\times1}^{(i)}\right) - \Delta T_{sv}^{(i)} L^{(i)} \tag{VI.85}$$

It is noted that since the bimoment is a self equilibrating stress resultant, the condition $\Delta B_2^{(i)} = \Delta B_1^{(i+1)}$ does not stand for the equilibrium at node. However, since the local bimoment effect caused by external loading is excluded from the analysis, the bimoment due to buckling is postulated to be continuous at the nodes. From Eqs. (VI.84) and (VI.85) one obtains

$$\Delta V_{x\alpha}^{(i)} = \frac{\Delta M_{y\alpha}^{(i)} - \Delta M_{y\alpha}^{(i+1)}}{L^{(i)}} \tag{VI.86}$$

$$\Delta T_{\alpha}^{(i)} = -\frac{\Delta B_{\alpha}^{(i)} - \Delta B_{\alpha}^{(i+1)} + \lambda\left(V_y^{p(i)} \mathbf{G}(L^{(i)})_{1\times4}^T \Delta\mathbf{u}_{\mathrm{N}\,4\times1}^{(i)} - V_y^{p(i)} \beta_{Nx} \mathbf{G}(L^{(i)})_{1\times4}^T \Delta\boldsymbol{\varphi}_{\mathrm{N}\,4\times1}^{(i)}\right)}{L^{(i)}} + \Delta T_{sv}^{i} \tag{VI.87}$$

Equations (VI.86) and (VI.87) are used to eliminate $\Delta V_{x\alpha}^{(i)}$ and $\Delta T_{\alpha}^{(i)}$ from Eqs. (VI.70) through (VI.73). Thus, the internal stress resultant fields due to buckling for element i can be expressed as

$$\begin{aligned} \Delta V_x^{(i)}(z) = {} & \frac{\Delta M_{y\alpha}^{(i)} - \Delta M_{y\alpha}^{(i+1)}}{L^{(i)}} + \\ & \lambda\left\{N^{p(i)} \mathbf{H}'(z)_{1\times4}^T \Delta\mathbf{u}_{\mathrm{N}\,4\times1}^{(i)} - \left[\left(M_x^{p(i)}(z) - a_y N^{p(i)}\right) \mathbf{H}'(z)_{1\times4}^T + V_y^{p(i)} \mathbf{H}(z)_{1\times4}^T\right] \Delta\boldsymbol{\varphi}_{\mathrm{N}\,4\times1}^{(i)}\right\} \end{aligned} \tag{VI.88}$$

$$\Delta T^{(i)}(z) = -\frac{\Delta B_{\alpha}^{(i)} - \Delta B_{\alpha}^{(i+1)}}{L^{(i)}} + \Delta T_{sv}^{(i)} + \lambda \left\{ \left[-\left(M_x^{p(i)}(z) - a_y N^{p(i)}\right) \mathbf{H'}(z)_{1\times 4}^T - \frac{V_y^{p(i)}}{L^{(i)}} \mathbf{G}(L^{(i)})_{1\times 4}^T \right] \Delta \mathbf{u}_{\mathrm{N}\,4\times 1}^{(i)} + \left[Q^{p(i)} \mathbf{H'}(z)_{1\times 4}^T + \frac{V_y^{p(i)} \beta_{Nx}}{L^{(i)}} \mathbf{G}(L^{(i)})_{1\times 4}^T \right] \Delta \boldsymbol{\varphi}_{\mathrm{N}\,4\times 1}^{(i)} \right\} \tag{VI.89}$$

$$\Delta M_y^{(i)}(z) = \Delta M_{y\alpha}^{(i)}\left(1 - \frac{z}{L^{(i)}}\right) + \Delta M_{y\alpha}^{(i+1)} \frac{z}{L^{(i)}} - \lambda \left\{ N^{p(i)} \mathbf{H}(z)_{1\times 4}^T \Delta \mathbf{u}_{\mathrm{N}\,4\times 1}^{(i)} - \left(M_x^{pi}(z) - a_y N^{p(i)}\right) \mathbf{H}(z)_{1\times 4}^T \Delta \boldsymbol{\varphi}_{\mathrm{N}\,4\times 1}^{(i)} \right\} \tag{VI.90}$$

$$\Delta B^{(i)}(z) = \Delta B_{\alpha}^{(i)}\left(1 - \frac{z}{L^{(i)}}\right) + \Delta B_{\alpha}^{(i+1)} \frac{z}{L^{(i)}} + \lambda \left\{ \left[-\left(M_x^{p(i)}(z) - a_y N^{p(i)}\right) \mathbf{H}(z)_{1\times 4}^T + V_y^{p(i)} \mathbf{G}(z)_{1\times 4}^T - V_y^{p(i)} \mathbf{G}(L^{(i)})_{1\times 4}^T \frac{z}{L^{i}} \right] \Delta \mathbf{u}_{\mathrm{N}\,4\times 1}^{(i)} + \left[Q^{p(i)} \mathbf{H}(z)_{1\times 4}^T - V_y^{p(i)} \beta_{Nx} \mathbf{G}(z)_{1\times 4}^T + V_y^{p(i)} \beta_{Nx} \mathbf{G}(L^{(i)})_{1\times 4}^T \frac{z}{L^{(i)}} \right] \Delta \boldsymbol{\varphi}_{\mathrm{N}\,4\times 1}^{(i)} \right\} \tag{VI.91}$$

By considering the relation $\Delta T_w = \Delta T - \Delta T_{sv}$, the warping torsion due to buckling ΔT_w for element i can be expressed as

$$\Delta T_w^{(i)}(z) = -\frac{\Delta B_{\alpha}^{(i)} - \Delta B_{\alpha}^{(i+1)}}{L^{(i)}} + \lambda \left\{ \left[-\left(M_x^{p(i)}(z) - a_y N^{p(i)}\right) \mathbf{H'}(z)_{1\times 4}^T - \frac{V_y^{p(i)}}{L^{(i)}} \mathbf{G}(L^{(i)})_{1\times 4}^T \right] \Delta \mathbf{u}_{\mathrm{N}\,4\times 1}^{(i)} + \left[Q^{p(i)} \mathbf{H'}(z)_{1\times 4}^T + \frac{V_y^{p(i)} \beta_{Nx}}{L^{(i)}} \mathbf{G}(L^{(i)})_{1\times 4}^T \right] \Delta \boldsymbol{\varphi}_{\mathrm{N}\,4\times 1}^{(i)} \right\} \tag{VI.92}$$

Also, from Eq. (VI.87), the St.Venant torsion ΔT_{sv} due to buckling for element i can be written as

$$\Delta T_{sv}^{(i)} = \Delta T_{\alpha}^{(i)} + \frac{B_{\alpha}^{(i)} - \Delta B_{\alpha}^{(i+1)}}{L^{(i)}} + \frac{\lambda}{L^{(i)}} \left(V_y^{p(i)} \mathbf{G}(L^{(i)})_{1\times 4}^T \Delta \mathbf{u}_{\mathrm{N}\,4\times 1}^{(i)} - V_y^{p(i)} \beta_{Nx} \mathbf{G}(L^{(i)})_{1\times 4}^T \Delta \boldsymbol{\varphi}_{\mathrm{N}\,4\times 1}^{(i)} \right) \tag{VI.93}$$

From Eq. (VI.62) and (VI.63), by substituting into Eq. (VI.54) and using the relation $M_x^{p(i)}(z) = M_{x0}^{p(i)} + V_y^{p(i)} z$, one obtains the second variation of complementary energy for element i as

$$\delta^2\pi^{*(i)} = \lambda\Big\{ N\Delta\mathbf{u}^{(i)T}_{\mathrm{N}\,1\times4}\mathbf{K}^{(i)}_{\mathrm{g1}\,4\times4}\Delta\mathbf{u}^{(i)}_{\mathrm{N}\,4\times1} - 2\Delta\mathbf{u}^{(i)T}_{\mathrm{N}\,1\times4}\Big[\Big(M^{p(i)}_{x0} - a_y N\Big)\mathbf{K}^{(i)}_{\mathrm{g1}\,4\times4} + V^{p(i)}_y\mathbf{K}^{(i)}_{\mathrm{g2}\,4\times4}\Big]\Delta\boldsymbol{\varphi}^{(i)}_{\mathrm{N}\,4\times1}$$

$$+\Delta\boldsymbol{\varphi}^{(i)T}_{\mathrm{N}\,1\times4}\Big\{\Big[N\Big(r_{N0}^{\ 2} + a_y^{\ 2} + a_x^{\ 2}\Big) + \beta_{Nx}M^{p(i)}_{x0}\Big]\mathbf{K}^{(i)}_{\mathrm{g1}\,4\times4} + \beta_{Nx}V^{p(i)}_y\mathbf{K}^{(i)}_{\mathrm{g2}\,4\times4}\Big\}_{4\times4}\Delta\boldsymbol{\varphi}^{(i)}_{\mathrm{N}\,4\times1}\Big\} \qquad \text{(VI.94)}$$

$$+\int_L\left\{\frac{1}{E}\left\langle \Delta M^{(i)}_y \quad \Delta B^{(i)}\right\rangle \mathbf{D}^{-1}_{\mathrm{r}2\times2}\begin{Bmatrix}\Delta M^{(i)}_y\\ \Delta B^{(i)}\end{Bmatrix} + \frac{1}{G}\left\langle \Delta V^{(i)}_x \quad \Delta T^{(i)}_w\right\rangle \boldsymbol{\chi}^{-1}_{2\times2}\begin{Bmatrix}\Delta V^{(i)}_x\\ \Delta T^{(i)}_w\end{Bmatrix} + \frac{\Delta T^{(i)2}_{sv}}{GJ_d}\right\}dz$$

in which, $\mathbf{K}^{(i)}_{\mathrm{g1}\,4\times4} = \int_{L^{(i)}}\mathbf{H}'(z)_{4\times1}\mathbf{H}'(z)^T_{1\times4}\,dz$, and $\mathbf{K}^{(i)}_{\mathrm{g2}\,4\times4} = \int_{L^{(i)}}\mathbf{H}'(z)_{4\times1}\mathbf{H}'(z)^T_{1\times4}\,z\,dz$ were used.

Matrices $\mathbf{K}^{(i)}_{\mathrm{g1}\,4\times4}$ and $\mathbf{K}^{(i)}_{\mathrm{g2}\,4\times4}$ are explicitly given in Appendix VI.D. From Eqs. (VI.88) through (VI.93), by substituting into Eq. (VI.94), one obtains the second variation of complementary energy for element i as

$$\delta^2\pi^{*(i)} = \lambda\Delta\mathbf{d}^{(i)T}_{\mathrm{N}\,1\times8}\mathbf{K}^{(i)}_{\mathrm{g}\ 8\times8}\Delta\mathbf{d}^{(i)}_{\mathrm{N}\,8\times1} + \lambda^2\left\langle \Delta\mathbf{t}^{(i)}_{1\times1} \;\middle|\; \Delta\mathbf{f}^{(i)T}_{\mathrm{N}\ 1\times4} \;\middle|\; \Delta\mathbf{d}^{(i)T}_{\mathrm{N}\,1\times8}\right\rangle \mathbf{B}^{(i)}{}_{13\times13}\begin{Bmatrix}\Delta\mathbf{t}^{(i)}_{1\times1}\\ \hline \Delta\mathbf{f}^{(i)}_{\mathrm{N}\ 4\times1}\\ \hline \Delta\mathbf{d}^{(i)}_{\mathrm{N}\ 8\times1}\end{Bmatrix} \qquad \text{(VI.95)}$$

In Eq. (VI.95), the following definitions were used;

$$\Delta\mathbf{t}^{(i)}_{1\times1} = \Delta T^{(i)}_{\alpha}/\lambda \qquad \text{(VI.96)}$$

$$\Delta\mathbf{f}^{(i)T}_{\mathrm{N}\ 1\times4} = 1/\lambda\left\langle \Delta M^{(i)}_{y\alpha} \quad \Delta M^{(i+1)}_{y\alpha} \;\middle|\; \Delta B^{(i)}_{\alpha} \quad \Delta B^{(i+1)}_{\alpha}\right\rangle \qquad \text{(VI.97)}$$

$$\Delta\mathbf{d}^{(i)T}_{\mathrm{N}\,1\times8} = 1/\lambda\left\langle \Delta\mathbf{u}^{(i)T}_{\mathrm{N}\,1\times4} \;\middle|\; \Delta\boldsymbol{\varphi}^{(i)T}_{\mathrm{N}\,1\times4}\right\rangle \qquad \text{(VI.98)}$$

In Eq. (VI.95), matrix $\mathbf{K}^{(i)}_{\mathrm{g}\ 8\times8}$, multiplied by λ, is the geometric matrix of the element which takes the form

$$\mathbf{K}^{(i)}_{\mathrm{g}\ 8\times8} = \left[\begin{array}{c|c} N\mathbf{K}^{(i)}_{\mathrm{g1}\,4\times4} & -\Big\{\Big(M^{p(i)}_{x0} - a_y N^{p(i)}\Big)\mathbf{K}^{(i)}_{\mathrm{g1}\,4\times4} + V^{p(i)}_y\mathbf{K}^{(i)}_{\mathrm{g2}\,4\times4}\Big\} \\ \hline -\Big\{\Big(M^{p(i)}_{x0} - a_y N^{p(i)}\Big)\mathbf{K}^{(i)T}_{\mathrm{g1}\,4\times4} + V^{p(i)}_y\mathbf{K}^{(i)T}_{\mathrm{g2}\,4\times4}\Big\} & \Big\{\Big[N^{p(i)}\Big(r_{N0}^{\ 2} + a_y^{\ 2} + a_x^{\ 2}\Big) + \beta_{Nx}M^{p(i)}_{x0}\Big]\mathbf{K}^{(i)}_{\mathrm{g1}\,4\times4} + V^{p(i)}_y\beta_{Nx}\mathbf{K}^{(i)}_{\mathrm{g2}\,4\times4}\Big\} \end{array}\right]$$

(VI.99)

where matrices $\mathbf{K}^{(i)}_{\mathrm{g1}\,4\times4}$ and $\mathbf{K}^{(i)}_{\mathrm{g2}\,4\times4}$ are given in Appendix VI.D. Also in Eq. VI.95, matrix $\mathbf{B}^{(i)}{}_{13\times13}$, multiplied by λ^2, leads to the structure elastic stiffness matrix after a) matrices

$\mathbf{B}^{(i)}{}_{13\times13}$ are assembled for the whole structure, (b) joint equilibrium conditions for all nodes are enforced and (c) the nodal forces have been eliminated through a process of static condensation. Matrix $\mathbf{B}^{(i)}{}_{13\times13}$ can be expressed in a partitioned form as

$$\mathbf{B}^{(i)}{}_{13\times13} = \left[\begin{array}{c|c|c} \mathbf{B}^{(i)}_{\mathbf{t}\ 1\times1} & \mathbf{B}^{(i)}_{\mathbf{tf}\ 1\times4} & \mathbf{B}^{(i)}_{\mathbf{td}\ 1\times8} \\ \hline \mathbf{B}^{(i)T}_{\mathbf{tf}\ 4\times1} & \mathbf{B}^{(i)}_{\mathbf{f}\ 4\times4} & \mathbf{B}^{(i)}_{\mathbf{fd}\ 4\times8} \\ \hline \mathbf{B}^{(i)T}_{\mathbf{td}\ 8\times1} & \mathbf{B}^{(i)T}_{\mathbf{fd}\ 8\times4} & \mathbf{B}^{(i)}_{\mathbf{d}\ 8\times8} \end{array}\right] \tag{VI.100}$$

The expression for sub-matrices $\mathbf{B}^{(i)}_{\mathbf{t}\ 1\times1}$, $\mathbf{B}^{(i)}_{\mathbf{tf}\ 1\times4}$, $\mathbf{B}^{(i)}_{\mathbf{td}\ 1\times8}$, $\mathbf{B}^{(i)}_{\mathbf{f}\ 4\times4}$, $\mathbf{B}^{(i)}_{\mathbf{fd}\ 4\times8}$ and $\mathbf{B}^{(i)}_{\mathbf{d}\ 8\times8}$ are given in Appendix VI.D.

The Assembly Process

For a co-linear structure consisting of N nodes and N-1 elements by using Eq. (VI.95), one obtains the second variation of complementary energy of the structure $\delta^2\pi^*$ as the summation of the second variation of the complementary energy for individual elements $\delta^2\pi^{*(i)}$ i.e.,

$$\delta^2\pi^* = \lambda\sum_{i=1}^{N-1}\Delta\mathbf{d}^{(i)T}_{\mathrm{N}\ 1\times8}\mathbf{K}^{(i)}_{\mathbf{g}\ 8\times8}\Delta\mathbf{d}^{(i)}_{\mathrm{N}\ 8\times1}+\lambda^2\sum_{i=1}^{N-1}\left\langle\Delta\mathbf{t}^{(i)}_{1\times1}\ \vdots\ \Delta\mathbf{f}^{(i)T}_{\mathrm{N}\ 1\times4}\ \vdots\ \Delta\mathbf{d}^{(i)T}_{\mathrm{N}\ 1\times8}\right\rangle\mathbf{B}^{(i)}{}_{13\times13}\left\{\begin{array}{c}\Delta\mathbf{t}^{(i)}_{1\times1}\\ \hline \Delta\mathbf{f}^{(i)}_{\mathrm{N}\ 4\times1}\\ \hline \Delta\mathbf{d}^{(i)}_{\mathrm{N}\ 8\times1}\end{array}\right\} \tag{VI.101}$$

Inter-element displacement continuity C^1 is satisfied. Thus, element end displacements and their derivatives can be replaced with nodal displacements and their derivatives as $\Delta u_2^{(i)}=\Delta u_1^{(i+1)}=\Delta u_{i+1}$, $\Delta u'^{(i)}_2=\Delta u'^{(i+1)}_1=\Delta u'_{i+1}$, $\Delta\phi^{(i)}_{Z2}=\Delta\phi^{(i+1)}_{Z1}=\Delta\phi_{Zi+1}$, and $\Delta\phi'^{(i)}_{Z2}=\Delta\phi'^{(i+1)}_{Z1}=\Delta\phi'_{Zi+1}$.

The global vector of nodal displacements $\Delta\mathbf{d}_{\mathrm{NG}4N\times1}$ can be written as $\Delta\mathbf{d}^T_{\mathrm{NG}1\times4N}=\frac{1}{\lambda}\left\langle\Delta u_1\ \ \Delta u'_1\ \ \Delta\phi_{Z1}\ \ \Delta\phi'_{Z1}\ \vdots\ \Delta u_2\ \ \Delta u'_2\ \ \Delta\phi_{Z2}\ \ \Delta\phi'_{Z2}\ \vdots\ ..\ \vdots\ \Delta u_N\ \ \Delta u'_N\ \ \Delta\phi_{ZN}\ \ \Delta\phi'_{ZN}\right\rangle$.

Since there are four displacement degrees of freedom at each node, the size of vector is $\Delta\mathbf{d}_{\mathrm{NG}4N\times1}$ is $4N\times1$. By assembling the element geometric stiffness matrices $\mathbf{K}^{(i)}_{\mathrm{g}\ 8\times8}$, one obtains the structure geometric stiffness matrix $\mathbf{K}_{\mathrm{G}4N\times4N}$ as

$$\Delta\mathbf{d}_{\mathrm{NG}1\times4N}^{T}\mathbf{K}_{\mathrm{G}4N\times4N}\Delta\mathbf{d}_{\mathrm{NG}4N\times1}=\sum_{i=1}^{N-1}\Delta\mathbf{d}^{(i)T}_{\mathrm{N}\ 1\times8}\mathbf{K}^{(i)}_{\mathrm{g}\ 8\times8}\Delta\mathbf{d}^{(i)}_{\mathrm{N}\ 8\times1} \tag{VI.102}$$

The technique in assembling the global geometric stiffness matrix $\mathbf{K}_{\mathrm{G}4N\times4N}$ from the element geometric stiffness matrices $\mathbf{K}^{(i)}_{\mathrm{g}\ 8\times8}$ is identical to that commonly used in displacement based finite element formulations (e.g., Bathe 1982).

The inter-element equilibrium conditions have to be satisfied prior to imposing the stability criterion i.e., $\delta\left\{\frac{1}{2}\delta^2\pi^*\right\}=0$.

Inter-element Moment and Bimoment Continuity

Because of the inter-element moment and bimoment continuity conditions (i.e., $\Delta M^{(i)}_{y2}=\Delta M^{(i+1)}_{y1}$, and $\Delta B^{(i)}_{2}=\Delta B^{(i+1)}_{1}$), vectors $\Delta\mathbf{f}^{(i)T}_{\mathrm{N}\ 1\times4}$ and $\Delta\mathbf{f}^{(i+1)T}_{\mathrm{N}\ 1\times4}$ of two adjacent elements have the two common integration constants $\Delta M^{(i+1)}_{y\alpha}$ and $\Delta B^{(i+1)}_{\alpha}$. Thus, these constants can be conceived as stress resultant values at nodes. For the whole structure, a global generalized force vector can be defined as $\Delta\mathbf{f}_{\mathrm{NG}1\times2N}^{T}=1/\lambda\left\langle\Delta M^{(1)}_{y\alpha}\quad\Delta B^{(1)}_{\alpha}\;\vdots\;\Delta M^{(2)}_{y\alpha}\quad\Delta B^{(2)}_{\alpha}\;\vdots\;\ldots\quad\ldots\;\vdots\;\Delta M^{(N)}_{y\alpha}\quad\Delta B^{(N)}_{\alpha}\right\rangle$. Since there are two integration constants corresponding to each node, the size of this vector is $1\times2N$.

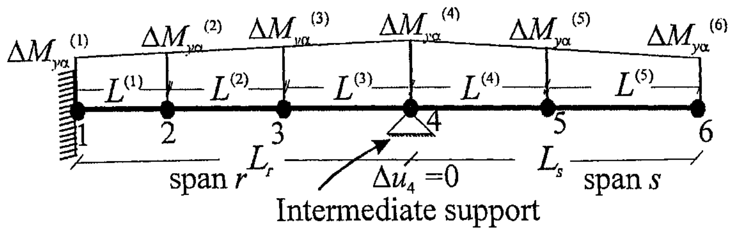

Fig.VI.11 Distribution of integration constants $\Delta M_{y\alpha}^{(i)}$ on a beam with intermediate support

Since the inter-element torsional equilibrium conditions are not imposed at this stage, the torsional integration constants ΔT_α^i are considered independent for each element. Thus, one may express the vector of torsional integration constants as $\mathbf{\Delta t}_{\mathrm{NG}1\times(N-1)}^{T} = 1/\lambda\left\langle \Delta T_\alpha^{(1)} \quad \Delta T_\alpha^{(2)} \quad \ldots \quad \Delta T_\alpha^{(N-1)} \right\rangle$. Since there are N-1 elements for a beam having N nodes and since there is a single torsional integration constant ΔT_α^i for each element i, the dimension of the vector $\mathbf{\Delta t}_{\mathrm{NG}1\times(N-1)}^{T}$ is $1\times(N-1)$. By imposing the inter-element C^1 continuity for displacements, as well as moment and bimoment continuity conditions, one obtains the matrix $\mathbf{B}_{\mathrm{G}(7N-1)\times(7N-1)}$ such that

$$\left\langle \mathbf{\Delta t}_{\mathrm{NG}1\times(N-1)}^{T} \,\vdots\, \mathbf{\Delta f}_{\mathrm{NG}1\times 2N}^{T} \,\vdots\, \mathbf{\Delta d}_{\mathrm{NG}1\times 4N}^{T} \right\rangle \mathbf{B}_{\mathrm{G}(7N-1)\times(7N-1)} \begin{Bmatrix} \mathbf{\Delta t}_{\mathrm{NG}(N-1)\times 1} \\ \hline \mathbf{\Delta f}_{\mathrm{NG}2N\times 1} \\ \hline \mathbf{\Delta d}_{\mathrm{NG}4N\times 1} \end{Bmatrix}$$
$$= \sum_{i=1}^{N-1} \left\langle \mathbf{\Delta t}_{1\times 1}^{(i)} \,\vdots\, \mathbf{\Delta f}_{\mathrm{N}\ 1\times 4}^{(i)T} \,\vdots\, \left\langle \mathbf{\Delta d}_{\mathrm{N}}^{(i)} \right\rangle_{1\times 8}^{T} \right\rangle \mathbf{B}^{(i)}{}_{13\times 13} \begin{Bmatrix} \mathbf{\Delta t}_{1\times 1}^{(i)} \\ \hline \mathbf{\Delta f}_{\mathrm{N}\ 4\times 1}^{(i)} \\ \hline \mathbf{\Delta d}_{\mathrm{N}\ 8\times 1}^{(i)} \end{Bmatrix} \qquad \text{(VI.103)}$$

In which matrix $\mathbf{B}_{\mathrm{G}}$ can be expressed in a partitioned form as

$$\mathbf{B}_{\mathrm{G}(7N-1)\times(7N-1)}=\left[\begin{array}{c|c|c}\mathbf{B}^{\mathrm{G}}_{\mathrm{t}\,(N-1)\times(N-1)} & \mathbf{B}^{\mathrm{G}}_{\mathrm{tf}(N-1)\times 2N} & \mathbf{B}^{\mathrm{G}}_{\mathrm{td}(N-1)\times 4N}\\ \hline \mathbf{B}^{\mathrm{G}T}_{\mathrm{tf}\,2N\times(N-1)} & \mathbf{B}^{\mathrm{G}}_{\mathrm{f}\;2N\times 2N} & \mathbf{B}^{\mathrm{G}}_{\mathrm{fd}2N\times 4N}\\ \hline \mathbf{B}^{\mathrm{G}T}_{\mathrm{td}4N\times(N-1)} & \mathbf{B}^{\mathrm{G}T}_{\mathrm{fd}4N\times 2N} & \mathbf{B}^{\mathrm{G}}_{\mathrm{d}\;4N\times 4N}\end{array}\right] \tag{VI.104}$$

Inter-element Twisting Moment Continuity

Continuity of the twisting moment field may be interrupted by intermediate supports which restrain the angle of twist (e.g., Fig. VI.12). For each span in which the twisting moment ΔT is continuous i.e., $\Delta T_2^{(i)} = \Delta T_1^{(i+1)}$, the inter-element equilibrium condition in Eq. (VI.83) is imposed. Hence constants $\Delta T_\alpha^{(i)}$ can be expressed in terms of a single constant per span.

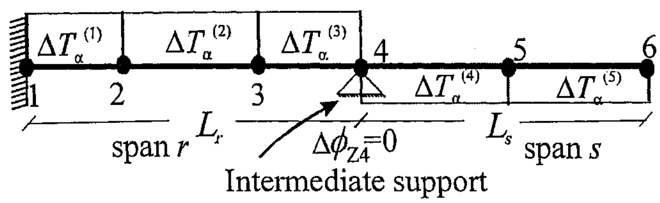

Fig.VI.12 Distribution of torsional integration constant $\Delta T_\alpha^{(i)}$ on a beam with middle support

For the beam in Fig. VI.12, the twisting moment field due to buckling can be expressed in terms of the constants $\Delta T_\alpha^{(r)}$ for span r and $\Delta T_\alpha^{(s)}$ for span s i.e., $\Delta T_\alpha^{(r)} = \Delta T_\alpha^{(i)}$ in which $(i = 1,2,3)$ and $\Delta T_\alpha^{(s)} = \Delta T_\alpha^{(i)}$ in which $(i = 4,5)$, by imposing the twisting moment continuity condition, the vector of independent torsional constants can be written as $\Delta\mathbf{t}_{\mathrm{r}1\times 2}^{T} = 1/\lambda\left\langle \Delta T_\alpha^{(r)} \quad \Delta T_\alpha^{(s)}\right\rangle$. The vector of torsional constants $\Delta\mathbf{t}_{\mathrm{NG}1\times 5}^{T} = 1/\lambda\left\langle \Delta T_\alpha^{(1)} \quad \Delta T_\alpha^{(2)} \quad \Delta T_\alpha^{(3)} \quad \Delta T_\alpha^{(4)} \quad \Delta T_\alpha^{(5)}\right\rangle$ can be expressed in terms of the vector of independent torsional constants $\Delta\mathbf{t}_{\mathrm{r}1\times 2}^{T}$ as

$$\begin{Bmatrix} \Delta T_{\alpha}^{(1)} \\ \Delta T_{\alpha}^{(2)} \\ \Delta T_{\alpha}^{(3)} \\ \hdashline \Delta T_{\alpha}^{(4)} \\ \Delta T_{\alpha}^{(5)} \end{Bmatrix} = \begin{bmatrix} 1 & 0 \\ 1 & 0 \\ 1 & 0 \\ \hdashline 0 & 1 \\ 0 & 1 \end{bmatrix} \begin{Bmatrix} \Delta T_{\alpha}^{(r)} \\ \Delta T_{\alpha}^{(s)} \end{Bmatrix}$$

In general, dimension of $\mathbf{\Delta t}_{\mathrm{r}1\times a}^{T}$ will be $1\times a$ in which a is equal to the number of spans in which twisting moment due to buckling is continuous. By establishing a matrix $\mathbf{c}_{1(N-1)\times a}$ to impose torsional continuity condition, one can express vector $\mathbf{\Delta t}_{\mathrm{NG}(N-1)\times 1}$ in terms of vector $\mathbf{\Delta t}_{\mathrm{r}a\times 1}$ as

$$\mathbf{\Delta t}_{\mathrm{NG}(N-1)\times 1} = \mathbf{c}_{1(N-1)\times a}\mathbf{\Delta t}_{\mathrm{r}a\times 1} \tag{VI.105}$$

Inter-element Shear Force Continuity

Continuity of the shear force field is interrupted by intermediate supports which prevent lateral displacements (e.g., Fig. VI.11). For each span with continuous shear force ΔV_x, the condition in Eq. (VI.82) is satisfied. Thus, the integration constants $\Delta V_{x\alpha}{}^{(i)}$ can be expressed in terms of a single constant per span (e.g., $\Delta V_{x\alpha}^{(r)} = \Delta V_{x\alpha}^{(i)}$ for elements $i=1,2,3$ and $\Delta V_{x\alpha}^{(s)} = \Delta V_{x\alpha}^{(i)}$ for elements $i=4,5$). For span r, by applying Eq. (VI.84) for elements 1 through j-1 ($j=1,2,3,4$) and summing all j-1 equations one obtains

$$\Delta M_{y\alpha}^{(j)} = \Delta M_{y\alpha}^{(1)} - \Delta V_{x\alpha}^{(r)} \sum_{i=1}^{j-1} L^{(i)} \tag{VI.106}$$

By following a similar procedure for all of the three elements of span r one obtains

$$\Delta V_{x\alpha}^{(r)} L_r = \Delta M_{y\alpha}^{(1)} - \Delta M_{y\alpha}^{(4)} \tag{VI.107}$$

In Equation (VI.107), L_r is the length of span r. From Eq. (VI.107), by substituting into Eq. (VI.106) one obtains $\Delta M_{y\alpha}^{(j)}$ in terms of the constants $\Delta M_{y\alpha}^{(1)}$ and $\Delta M_{y\alpha}^{(4)}$ as $\Delta M_{y\alpha}^{(j)}{=}\Delta M_{y\alpha}^{(1)}\left(L_r-\sum_{i=1}^{j-1}L^{(i)}\Big/L_r\right)+\Delta M_{y\alpha}^{(4)}\left(\sum_{i=1}^{j-1}L^{(i)}\Big/L_r\right)$. Similar relations can be written for span s as $\Delta M_{y\alpha}^{(j)}{=}\Delta M_{y\alpha}^{(4)}\left(L_r-\sum_{i=1}^{j-1}L^{(i)}\Big/L_s\right)+\Delta M_{y\alpha}^{(6)}\left(\sum_{i=1}^{j-1}L^{(i)}\Big/L_s\right)$ in which $(j=4,5,6)$, and L_s is the length of span s. Thus in general, based on shear force continuity, the moment integration constants at the nodes can be expressed in terms of the moment integration constants at the ends of the spans. This relation can be written as

$$\Delta M_{y\alpha}^{(j)}=\frac{\Delta M_{y\alpha}^{(k)}}{L_{sp}}\left(L_{sp}-\sum_{i=k}^{j-1}L^{(i)}\right)+\frac{\Delta M_{y\alpha}^{(N)}}{L_{sp}}\left(\sum_{i=k}^{j-1}L^{(i)}\right) \tag{VI.108}$$

In Eq. (VI.108), k and N represent the end nodes of the span (i.e., $j=k,..,N$) and L_{sp} is the length of span. For the structure in Fig. VI.11, the moment field can be expressed in terms of the constants $\Delta M_{y\alpha}^{(1)}$, $\Delta M_{y\alpha}^{(4)}$ and $\Delta M_{y\alpha}^{(6)}$ and the vector of independent moment and bimoment integration constants can be written as $\Delta\mathbf{f}_{\mathrm{Nr1\times9}}^{T}{=}1/\lambda\left\langle\Delta M_{y\alpha}^{(1)}\quad\Delta B_{\alpha}^{(1)}\;\vdots\;\Delta B_{\alpha}^{(2)}\;\vdots\;\Delta B_{\alpha}^{(3)}\;\vdots\;\Delta M_{y\alpha}^{(4)}\quad\Delta B_{\alpha}^{(4)}\;\vdots\;\Delta B_{\alpha}^{(5)}\;\vdots\;\Delta M_{y\alpha}^{(6)}\quad\Delta B_{\alpha}^{(6)}\right\rangle$. The vector of moment and bimoment integration constants $\Delta\mathbf{f}_{\mathrm{NG1\times12}}^{T}{=}1/\lambda\left\langle\Delta M_{y\alpha}^{(1)}\quad\Delta B_{\alpha}^{(1)}\;\vdots\;\Delta M_{y\alpha}^{(2)}\quad\Delta B_{\alpha}^{(2)}\;\vdots\;\ldots\quad\ldots\;\vdots\;\Delta M_{y\alpha}^{(6)}\quad\Delta B_{\alpha}^{(6)}\right\rangle$ can be expressed in terms of the vector $\Delta\mathbf{f}_{\mathrm{Nr1\times9}}^{T}$ as

$$
\begin{Bmatrix} \Delta M_{ya}^{(1)} \\ \Delta B_{\alpha}^{(1)} \\ \Delta M_{ya}^{(2)} \\ \Delta B_{\alpha}^{(2)} \\ \Delta M_{ya}^{(3)} \\ \Delta B_{\alpha}^{(3)} \\ \Delta M_{ya}^{(4)} \\ \Delta B_{\alpha}^{(4)} \\ \Delta M_{ya}^{(5)} \\ \Delta B_{\alpha}^{(5)} \\ \Delta M_{ya}^{(6)} \\ \Delta B_{\alpha}^{(6)} \end{Bmatrix}
=
\begin{bmatrix}
1 & 0 & 0 & 0 & 0 & 0 & 0 & 0 & 0 \\
0 & 1 & 0 & 0 & 0 & 0 & 0 & 0 & 0 \\
\dfrac{L^{(2)}+L^{(3)}}{L^{(1)}+L^{(2)}+L^{(3)}} & 0 & 0 & 0 & \dfrac{L^{(1)}}{L^{(1)}+L^{(2)}+L^{(3)}} & 0 & 0 & 0 & 0 \\
0 & 0 & 1 & 0 & 0 & 0 & 0 & 0 & 0 \\
\dfrac{L^{(3)}}{L^{(1)}+L^{(2)}+L^{(3)}} & 0 & 0 & 0 & \dfrac{L^{(1)}+L^{(2)}}{L^{(1)}+L^{(2)}+L^{(3)}} & 0 & 0 & 0 & 0 \\
0 & 0 & 0 & 1 & 0 & 0 & 0 & 0 & 0 \\
0 & 0 & 0 & 0 & 1 & 0 & 0 & 0 & 0 \\
0 & 0 & 0 & 0 & 0 & 1 & 0 & 0 & 0 \\
0 & 0 & 0 & 0 & \dfrac{L^{(5)}}{L^{(4)}+L^{(5)}} & 0 & 0 & \dfrac{L^{(4)}}{L^{(4)}+L^{(5)}} & 0 \\
0 & 0 & 0 & 0 & 0 & 0 & 1 & 0 & 0 \\
0 & 0 & 0 & 0 & 0 & 0 & 0 & 1 & 0 \\
0 & 0 & 0 & 0 & 0 & 0 & 0 & 0 & 1
\end{bmatrix}
\begin{Bmatrix} \Delta M_{ya}^{(1)} \\ \Delta B_{\alpha}^{(1)} \\ \Delta B_{\alpha}^{(2)} \\ \Delta B_{\alpha}^{(3)} \\ \Delta M_{ya}^{(4)} \\ \Delta B_{\alpha}^{(4)} \\ \Delta B_{\alpha}^{(5)} \\ \Delta M_{ya}^{(6)} \\ \Delta B_{\alpha}^{(6)} \end{Bmatrix}
$$

In general, the dimension of $\Delta\mathbf{f}_{\mathrm{Nr}1\times b}^{T}$ will be $1\times b$ in which b depends on the number of spans in which shear force due to buckling is continuous i.e., b= number of spans + N+1. By establishing a matrix to impose shear force continuity condition $\mathbf{c}_{2\ 2N\times b}$, one can express vector $\Delta\mathbf{f}_{\mathrm{NG}2N\times 1}$ in terms of vector $\Delta\mathbf{f}_{\mathrm{Nr}b\times 1}$ i.e.,

$$\Delta\mathbf{f}_{\mathrm{NG}2N\times 1} = \mathbf{c}_{2\ 2N\times b}\Delta\mathbf{f}_{\mathrm{Nr}b\times 1} \tag{VI.109}$$

Enforcing Force Boundary Conditions

Member End free to rotate and warp

Force boundary conditions should be specified at a joint unless the conjugate displacements are restrained. For instance, for the beam in Fig. VI.13, element five is free to rotate and warp at $z=L^{(5)}$. Thus, the force boundary conditions based on Eq. (VI.58) are $\Delta M_{y2}^{(5)}=\Delta B_{2}^{(5)}=0$. By inserting these conditions into Eqs. (VI.90) and (VI.91), and setting $z = L^{(5)}$ one obtains the integration constants $\Delta M_{y\alpha}^{(6)}$ and $\Delta B_{\alpha}^{(6)}$ in terms of the nodal displacements Δu_6 and $\Delta\phi_6$ as

$$\Delta M_{y\alpha}^{(6)} = -\lambda\left[-N^{p(5)}\Delta u_6 + \left(M_{x2}^{p(5)} - a_y N^{p(5)}\right)\Delta\phi_{Z6}\right] \tag{VI.110}$$

$$\Delta B_{\alpha}^{(6)} = -\lambda\left[\left(M_{x2}^{p(5)} - a_y N^{p(5)}\right)\Delta u_6 + Q^{p(5)}\Delta\phi_{Z6}\right] \tag{VI.111}$$

After eliminating the integration constants $\Delta M_{y\alpha}^{(6)}$ and $\Delta B_{\alpha}^{(6)}$, the vector of independent moment and bimoment integration constants can be written as $\mathbf{\Delta f}_{\mathrm{Nm}1\times7}^{T} = 1/\lambda\left\langle \Delta M_{y\alpha}^{(1)} \quad \Delta B_{\alpha}^{(1)} \mid \Delta B_{\alpha}^{(2)} \mid \Delta B_{\alpha}^{(3)} \mid \Delta M_{y\alpha}^{(4)} \quad \Delta B_{\alpha}^{(4)} \mid \Delta B_{\alpha}^{(5)} \right\rangle$. By using Eqs. (VI.110) and (VI.111), the vector of moment and bimoment integration constants $\mathbf{\Delta f}_{\mathrm{Nr}1\times9}^{T}$ can be expressed in terms of the nodal displacement vector $\mathbf{\Delta d}_{\mathrm{NG}\,24\times1}$ and the vector of independent moment and bimoment integration constants $\mathbf{\Delta f}_{\mathrm{Nm}1\times7}^{T}$ as

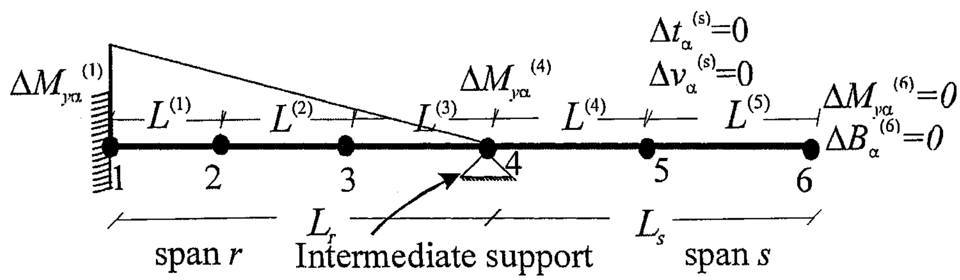

Fig. VI.13 – Force boundary conditions for the cantilever with intermediate support

$$\begin{Bmatrix} \Delta M_{y\alpha}^{(1)} \\ \Delta B_{\alpha}^{(1)} \\ \hdashline \Delta B_{\alpha}^{(2)} \\ \hdashline \Delta B_{\alpha}^{(3)} \\ \hdashline \Delta M_{y\alpha}^{(4)} \\ \Delta B_{\alpha}^{(4)} \\ \hdashline \Delta B_{\alpha}^{(5)} \\ \hdashline \Delta M_{y\alpha}^{(6)} \\ \Delta B_{\alpha}^{(6)} \end{Bmatrix} = \left[\begin{array}{cc:c:c:cc:c} 1 & 0 & 0 & 0 & 0 & 0 & 0 \\ 0 & 1 & 0 & 0 & 0 & 0 & 0 \\ \hdashline 0 & 0 & 1 & 0 & 0 & 0 & 0 \\ \hdashline 0 & 0 & 0 & 1 & 0 & 0 & 0 \\ \hdashline 0 & 0 & 0 & 0 & 1 & 0 & 0 \\ 0 & 0 & 0 & 0 & 0 & 1 & 0 \\ \hdashline 0 & 0 & 0 & 0 & 0 & 0 & 1 \\ \hdashline 0 & 0 & 0 & 0 & 0 & 0 & 0 \\ 0 & 0 & 0 & 0 & 0 & 0 & 0 \end{array}\right] \begin{Bmatrix} \Delta M_{y\alpha}^{(1)} \\ \Delta B_{\alpha}^{(1)} \\ \hdashline \Delta B_{\alpha}^{(2)} \\ \hdashline \Delta B_{\alpha}^{(3)} \\ \hdashline \Delta M_{y\alpha}^{(4)} \\ \Delta B_{\alpha}^{(4)} \\ \hdashline \Delta B_{\alpha}^{(5)} \end{Bmatrix}$$

$$+ \begin{array}{c} \\ 7\left\{\begin{matrix} \\ \\ \\ \\ \end{matrix}\right. \\ \\ \\ \end{array} \left[\begin{array}{c:cccc} \multicolumn{5}{c}{\overbrace{\hspace{20em}}^{24}} \\ 0\ldots0 & 0 & 0 & 0 & 0 \\ \cdot & \cdot & \cdot & \cdot & \cdot \\ \cdot & \cdot & \cdot & \cdot & \cdot \\ 0\ldots0 & 0 & 0 & 0 & 0 \\ \hdashline 0\ldots0 & N^{p(5)} & 0 & -\left(M_{xl}^{p(5)} - a_y N^{p(5)}\right) & 0 \\ 0\ldots0 & -\left(M_{xl}^{p(5)} - a_y N^{p(5)}\right) & 0 & -\left(N^{p(5)}\left(r_{N0}{}^2 + a_y{}^2 + a_x{}^2\right) + M_{xl}^{p(5)} \beta_{Nx}\right) & 0 \end{array}\right] \begin{Bmatrix} \Delta u_1 \\ \Delta u'_1 \\ \Delta \phi_{Z1} \\ \Delta \phi'_{Z1} \\ \hdashline \cdot \\ \cdot \\ \cdot \\ \hdashline \Delta u_6 \\ \Delta u'_6 \\ \Delta \phi_{Z6} \\ \Delta \phi'_{Z6} \end{Bmatrix}_{24\times1}$$

In general, dimension s of vector $\mathbf{\Delta f}_{\mathrm{Nm}1\times s}^{T}$ depends on the number of boundary conditions related to nodes free to rotate and warp i.e., s=b-num. of force B.C on moments and bimoments. By establishing matrices $\mathbf{c}_{3b\times s}$ and $\mathbf{c}_{4b\times 4N}$ to impose the force boundary conditions the vector of moment and bimoment integration constants $\mathbf{\Delta f}_{\mathrm{Nr}b\times1}$ can be written in terms of the nodal displacement vector $\mathbf{\Delta d}_{\mathrm{NG}4N\times1}$ and a vector of independent moment and bimoment integration constants $\mathbf{\Delta f}_{\mathrm{Nm}s\times1}$ in which the integration constants $\Delta M_{y\alpha}^{(N)}$ and $\Delta B_{\alpha}^{(N)}$ are eliminated i.e.,

$$\Delta\mathbf{f}_{\mathrm{Nr}b\times1} = \left[\mathbf{c}_{3b\times s} \;\vdots\; \mathbf{c}_{4b\times4N}\right]\left\{\frac{\Delta\mathbf{f}_{\mathrm{Nm}s\times1}}{\Delta\mathbf{d}_{\mathrm{NG}4N\times1}}\right\} \tag{VI.112}$$

Note that the moment integration constant $\Delta M_{y\alpha}^{(N)}$, which is eliminated when imposing free rotation condition, always explicitly appear in vector $\Delta\mathbf{f}_{\mathrm{Nr}b\times1}$. This is because moment integration constant $\Delta M_{y\alpha}^{(N)}$ is always at the end of the span and is not eliminated due to shear continuity condition in previous step.

Member End free to translate

From the boundary condition in Eq. (VI.58), the shear force integration constant can be specified at the boundaries unless it is prevented against lateral translation. For instance for the beam in Fig.VI.15, element (5) is free to translate at $z = L^{(5)}$ (i.e., $\Delta u_6 \neq 0$). Thus, one obtains $\Delta V_{x\alpha}^{(5)} = \Delta V_{x\alpha}^{(s)} = 0$. By using the relation $\Delta M_{y\alpha}^{(6)} = \Delta M_{y\alpha}^{(4)} - \Delta V_{x\alpha}^{(s)} L_s$, one obtains $\Delta M_{y\alpha}^{(4)} = \Delta M_{y\alpha}^{(6)}$. Since the element (5) is also free to rotate at $z = L^{(5)}$, the constant $\Delta M_{y\alpha}^{(6)}$ is eliminated in the previous step. Thus, the vector of independent moment and bimoment integration constants can be written as $\Delta\mathbf{f}_{\mathrm{Nt}1\times6}^{T} = 1/\lambda\left\langle \Delta M_{y\alpha}^{(1)} \quad \Delta B_{\alpha}^{(1)} \;\vdots\; \Delta B_{\alpha}^{(2)} \;\vdots\; \Delta B_{\alpha}^{(3)} \;\vdots\; \Delta B_{\alpha}^{(4)} \;\vdots\; \Delta B_{\alpha}^{(5)} \right\rangle$. By substituting the relation $\Delta M_{y\alpha}^{(4)} = \Delta M_{y\alpha}^{(6)}$ into the force boundary condition in Eq. (VI.110) one obtains

$$\Delta M_{y\alpha}^{(4)} = -\lambda\left[-N^{p(5)}\Delta u_6(L^{(5)}) + \left(M_{xl}^{p(5)} - a_y N^{p(5)}\right)\Delta\phi_{Z6}(L^{(5)})\right] \tag{VI.113}$$

By using Eq. (VI.113), the vector of moment and bimoment integration constants $\Delta\mathbf{f}_{\mathrm{Nm}1\times7}^{T}$ can be expressed in terms of the nodal displacement vector $\Delta\mathbf{d}_{\mathrm{NG}24\times1}$ and the vector of independent moment and bimoment integration constants $\Delta\mathbf{f}_{\mathrm{Nt}1\times6}^{T}$ as

$$
\begin{Bmatrix} \Delta M_{y\alpha}^{(1)} \\ \Delta B_{\alpha}^{(1)} \\ \hdashline \Delta B_{\alpha}^{(2)} \\ \hdashline \Delta B_{\alpha}^{(3)} \\ \hdashline \Delta M_{y\alpha}^{(4)} \\ \Delta B_{\alpha}^{(4)} \\ \hdashline \Delta B_{\alpha}^{(5)} \end{Bmatrix}
=
\begin{bmatrix} 1 & 0 & 0 & 0 & 0 & 0 \\ 0 & 1 & 0 & 0 & 0 & 0 \\ 0 & 0 & 1 & 0 & 0 & 0 \\ 0 & 0 & 0 & 1 & 0 & 0 \\ 0 & 0 & 0 & 0 & 0 & 0 \\ 0 & 0 & 0 & 0 & 1 & 0 \\ 0 & 0 & 0 & 0 & 0 & 1 \end{bmatrix}
\begin{Bmatrix} \Delta M_{y\alpha}^{(1)} \\ \Delta B_{\alpha}^{(1)} \\ \hdashline \Delta B_{\alpha}^{(2)} \\ \hdashline \Delta B_{\alpha}^{(3)} \\ \hdashline \Delta B_{\alpha}^{(4)} \\ \hdashline \Delta B_{\alpha}^{(5)} \end{Bmatrix}
+
\left[\begin{array}{c:cccc} & \multicolumn{4}{c}{\overbrace{\hphantom{N^{p(5)} \quad 0 \quad -\left(M_{xl}^{p(5)}-a_y N^{p(5)}\right) \quad 0}}^{24}} \\ 0\ldots0 & & 0 & 0 & 0 \\ 0\ldots0 & & 0 & 0 & 0 \\ 0\ldots0 & & 0 & 0 & 0 \\ 0\ldots0 & & 0 & 0 & 0 \\ \hdashline 0\ldots0 & N^{p(5)} & 0 & -\left(M_{xl}^{p(5)}-a_y N^{p(5)}\right) & 0 \\ \hdashline 0\ldots0 & 0 & 0 & 0 & 0 \\ 0\ldots0 & 0 & 0 & 0 & 0 \end{array}\right]
\begin{Bmatrix} \Delta u_1 \\ \Delta u'_1 \\ \Delta \phi_{Z1} \\ \Delta \phi'_{Z1} \\ \hdashline . \\ . \\ . \\ \hdashline \Delta u_6 \\ \Delta u'_6 \\ \Delta \phi_{Z6} \\ \Delta \phi'_{Z6} \end{Bmatrix}
$$

In general dimension sh of vector $\mathbf{\Delta f}^{T}_{\mathrm{Nt}1\times sh}$ depends on the number of force boundary conditions i.e., sh=s-num. of force B.C on shear force. By defining matrices $\mathbf{c}_{5s\times sh}$ and $\mathbf{c}_{6s\times 4N}$ to impose the force boundary condition, the vector of moment and bimoment integration constants $\mathbf{\Delta f}_{\mathrm{Nm}\,s\times 1}$ can be written in terms of the nodal displacement vector $\mathbf{\Delta d}_{\mathrm{NG}\,4N\times 1}$ and the vector of independent moment and bimoment integration constants $\mathbf{\Delta f}_{\mathrm{Nt}\,sh\times 1}$ as

$$
\mathbf{\Delta f}_{\mathrm{Nm}\,s\times 1} = \left[\mathbf{c}_{5s\times sh} \;\vdots\; \mathbf{c}_{6s\times 4N}\right] \begin{Bmatrix} \mathbf{\Delta f}_{\mathrm{Nt}\,sh\times 1} \\ \hdashline \mathbf{\Delta d}_{\mathrm{NG}\,4N\times 1} \end{Bmatrix} \qquad \text{(VI.114)}
$$

Member End free to twist

From the boundary condition in Eq. (VI.58), the torsional integration constant can be specified at the boundaries unless it is prevented against angle of twist. For instance for the beam in Fig.VI.13, element (5) is free to twist at $z = L^{(5)}$. Thus, one has $\Delta T_{\alpha}^{(5)} = \Delta T_{\alpha}^{(s)} = 0$. The vector of independent torsional integration constants can be written as $\mathbf{\Delta t}_{\mathrm{b}1\times 1} = 1/\lambda \left\{\Delta T_{\alpha}^{(r)}\right\}$. The vector of torsional constants

$\mathbf{\Delta t}_{\mathrm{r}1\times2}^{T} = 1/\lambda\langle \Delta T_{\alpha}^{(r)} \quad \Delta T_{\alpha}^{(s)} \rangle$ can be expressed in terms of the vector of independent torsional constants $\mathbf{\Delta t}_{\mathrm{b}1\times1}^{T}$ as

$$\begin{Bmatrix} \Delta T_{\alpha}^{(r)} \\ \Delta T_{\alpha}^{(s)} \end{Bmatrix} = \begin{bmatrix} 1 \\ 0 \end{bmatrix} \left\{ \Delta T_{\alpha}^{(r)} \right\}$$

In general, the dimension tb of vector $\mathbf{\Delta t}_{\mathrm{b}1\times tb}^{T}$ depends on the number of force boundary conditions related to ends free to twist i.e., tb=a-num. of force B.C on torsion. By establishing matrix $\mathbf{c}_{7a\times tb}$ to impose the force boundary condition, the vector of torsional integration constants $\mathbf{\Delta t}_{\mathrm{r}a\times1}$ is written in terms of the vector of independent torsional constants $\mathbf{\Delta t}_{\mathrm{b}tb\times1}$ as

$$\mathbf{\Delta t}_{\mathrm{r}a\times1} = \mathbf{c}_{7a\times tb}\mathbf{\Delta t}_{\mathrm{b}tb\times1} \tag{VI.115}$$

By imposing the inter-element twisting moment continuity, shear force continuity, force boundary conditions, one obtains the elastic matrix $\mathbf{B}_{\mathrm{G2}}$ such that

$$\begin{aligned} &\left\langle \mathbf{\Delta t}_{\mathrm{b}1\times tb}^{T} \;\vdots\; \mathbf{\Delta f}_{\mathrm{Nt}1\times sh}^{T} \;\vdots\; \mathbf{\Delta d}_{\mathrm{NG}1\times 4N}^{T} \right\rangle \mathbf{B}_{\mathrm{G2}(tb+sh+4N)\times(tb+sh+4N)} \begin{Bmatrix} \mathbf{\Delta t}_{\mathrm{b}tb\times1} \\ \hdashline \mathbf{\Delta f}_{\mathrm{Nt}sh\times1} \\ \hdashline \mathbf{\Delta d}_{\mathrm{NG}4N\times1} \end{Bmatrix} \\ &= \left\langle \mathbf{\Delta t}_{\mathrm{NG}1\times(N-1)}^{T} \;\vdots\; \mathbf{\Delta f}_{\mathrm{NG}1\times 2N}^{T} \;\vdots\; \mathbf{\Delta d}_{\mathrm{NG}1\times 4N}^{T} \right\rangle \mathbf{B}_{\mathrm{G}(7N-1)\times(7N-1)} \begin{Bmatrix} \mathbf{\Delta t}_{\mathrm{NG}(N-1)\times1} \\ \hdashline \mathbf{\Delta f}_{\mathrm{NG}2N\times1} \\ \hdashline \mathbf{\Delta d}_{\mathrm{NG}4N\times1} \end{Bmatrix} \end{aligned} \tag{VI.116}$$

Matrix $\mathbf{B}_{\mathrm{G2}(tb+sh+4N)\times(tb+sh+4N)}$ is expressed in a partitioned form as

$$\mathbf{B}_{\mathrm{G2}(tb+sh+4N)\times(tb+sh+4N)} = \left[\begin{array}{c:c:c} \mathbf{B}_{\mathrm{t}\ tb\times tb}^{\mathrm{G2}} & \mathbf{B}_{\mathrm{tf}\ tb\times sh}^{\mathrm{G2}} & \mathbf{B}_{\mathrm{td}\ tb\times 4N}^{\mathrm{G2}} \\ \hdashline \mathbf{B}_{\mathrm{tf}\ sh\times tb}^{\mathrm{G2}T} & \mathbf{B}_{\mathrm{f}\ sh\times sh}^{\mathrm{G2}} & \mathbf{B}_{\mathrm{fd}\ sh\times 4N}^{\mathrm{G2}} \\ \hdashline \mathbf{B}_{\mathrm{td}\ 4N\times tb}^{\mathrm{G2}T} & \mathbf{B}_{\mathrm{fd}\ 4N\times sh}^{\mathrm{G2}T} & \mathbf{B}_{\mathrm{d}\ 4N\times 4N}^{\mathrm{G2}} \end{array}\right] \tag{VI.117}$$

From Eqs. (VI.105), (VI.109), (VI.112), (VI.114) and (VI.115) by substituting into Eq. (VI.116), one obtains the expression of the sub-matrices in Eq. (VI.117) as

$$\mathbf{B}^{\mathbf{G2}}_{\mathbf{t}\ tb\times tb} = \mathbf{c}^{T}_{7tb\times a}\mathbf{c}^{T}_{1a\times(N-1)}\mathbf{B}^{\mathbf{G}}_{\mathbf{t}\ (N-1)\times(N-1)}\mathbf{c}_{1(N-1)\times a}\mathbf{c}_{7a\times tb} \tag{VI.118}$$

$$\mathbf{B}^{\mathbf{G2}}_{\mathbf{tf}\ tb\times sh} = \mathbf{c}^{T}_{7tb\times a}\mathbf{c}^{T}_{1a\times(N-1)}\mathbf{B}^{\mathbf{G}}_{\mathbf{tf}(N-1)\times 2N}\mathbf{c}^{T}_{22N\times b}\mathbf{c}_{3b\times s}\mathbf{c}_{5s\times sh} \tag{VI.119}$$

$$\begin{aligned}\mathbf{B}^{\mathbf{G2}}_{\mathbf{td}\ tb\times 4N} &= \mathbf{c}^{T}_{7tb\times a}\mathbf{c}^{T}_{1a\times(N-1)}\mathbf{B}^{\mathbf{G}}_{\mathbf{tf}(N-1)\times 2N}\mathbf{c}^{T}_{22N\times b}\mathbf{c}_{3b\times s}\mathbf{c}_{6s\times 4N} + \mathbf{c}^{T}_{7tb\times a}\mathbf{c}^{T}_{1a\times(N-1)}\mathbf{B}^{\mathbf{G}}_{\mathbf{td}(N-1)\times 4N} \\ &+ \mathbf{c}^{T}_{7tb\times a}\mathbf{c}^{T}_{2b\times 2N}\mathbf{B}^{\mathbf{G}}_{\mathbf{fd}2N\times 4N}\mathbf{c}_{4b\times 4N}\end{aligned} \tag{VI.120}$$

$$\mathbf{B}^{\mathbf{G2}}_{\mathbf{f}\ sh\times sh} = \mathbf{c}^{T}_{5sh\times s}\mathbf{c}^{T}_{3s\times b}\mathbf{c}^{T}_{2b\times 2N}\mathbf{B}^{\mathbf{G}}_{\mathbf{f}\ 2N\times 2N}\mathbf{c}_{22N\times b}\mathbf{c}_{3b\times s}\mathbf{c}_{5s\times sh} \tag{VI.121}$$

$$\begin{aligned}\mathbf{B}^{\mathbf{G2}}_{\mathbf{fd}\ sh\times 4N} &= \mathbf{c}^{T}_{5sh\times s}\mathbf{c}^{T}_{3s\times b}\mathbf{c}^{T}_{2b\times 2N}\mathbf{B}^{\mathbf{G}}_{\mathbf{f}\ 2N\times 2N}\mathbf{c}_{2\ 2N\times b}\mathbf{c}_{3b\times s}\mathbf{c}_{6s\times 4N} + \mathbf{c}^{T}_{5sh\times s}\mathbf{c}^{T}_{3s\times b}\mathbf{c}^{T}_{2b\times 2N}\mathbf{B}^{\mathbf{G}}_{\mathbf{fd}2N\times 4N} \\ &+ \mathbf{c}^{T}_{5sh\times s}\mathbf{c}^{T}_{3s\times b}\mathbf{c}^{T}_{2b\times 2N}\mathbf{B}^{\mathbf{G}}_{\mathbf{f}\ 2N\times 2N}\mathbf{c}_{2\ 2N\times b}\mathbf{c}_{4b\times 4N}\end{aligned} \tag{VI.122}$$

$$\begin{aligned}\mathbf{B}^{\mathbf{G2}}_{\mathbf{d}\ 4N\times 4N} &= \left(\mathbf{c}^{T}_{3s\times b}\mathbf{c}^{T}_{2b\times 2N}\mathbf{B}^{\mathbf{G}}_{\mathbf{fd}2N\times 4N} + \mathbf{c}^{T}_{3s\times b}\mathbf{c}^{T}_{2b\times 2N}\mathbf{B}^{\mathbf{G}}_{\mathbf{f}\ 2N\times 2N}\mathbf{c}_{22N\times b}\mathbf{c}_{4b\times 4N}\right)\mathbf{c}_{6s\times 4N} + \mathbf{c}^{T}_{4\ 4N\times b}\mathbf{c}^{T}_{2b\times 2N}\mathbf{B}^{\mathbf{G}}_{\mathbf{fd}2N\times 4N} \\ &+ \mathbf{c}^{T}_{2b\times 2N}\mathbf{B}^{\mathbf{G}}_{\mathbf{fd}2N\times 4N}\mathbf{c}_{4b\times 4N} + \mathbf{c}^{T}_{4\ 4N\times b}\mathbf{c}^{T}_{2b\times 2N}\mathbf{B}^{\mathbf{G}}_{\mathbf{f}\ 2N\times 2N}\mathbf{c}_{2\ 2N\times b}\mathbf{c}_{4b\times 4N} + \mathbf{B}^{\mathbf{G}}_{\mathbf{d}\ 4N\times 4N} \\ &+ \mathbf{c}^{T}_{64N\times s}\Big[\mathbf{c}^{T}_{5sh\times s}\mathbf{c}^{T}_{3s\times b}\mathbf{c}^{T}_{2b\times 2N}\mathbf{B}^{\mathbf{G}}_{\mathbf{f}\ 2N\times 2N}\mathbf{c}_{2\ 2N\times b}\mathbf{c}_{3b\times s}\mathbf{c}_{6s\times 4N} \\ &\qquad + \mathbf{c}^{T}_{5sh\times s}\left(\mathbf{c}^{T}_{3s\times b}\mathbf{c}^{T}_{2b\times 2N}\mathbf{B}^{\mathbf{G}}_{\mathbf{fd}2N\times 4N} + \mathbf{c}^{T}_{3s\times b}\mathbf{c}^{T}_{2b\times 2N}\mathbf{B}^{\mathbf{G}}_{\mathbf{f}\ 2N\times 2N}\mathbf{c}_{2\ 2N\times b}\mathbf{c}_{4b\times 4N}\right)\Big]\end{aligned} \tag{VI.123}$$

By satisfying the essential equilibrium and force boundary conditions of the variational principle as well as C^1 continuity of displacement fields, the second variation of the complementary energy functional can be written as

$$\delta^2\pi^* = \Delta\mathbf{d}^{T}_{\mathbf{NG}1\times 4N}\lambda\mathbf{K_G}\Delta\mathbf{d}_{\mathbf{NG}4N\times 1} + \lambda^2\left\langle \Delta\mathbf{t}^{T}_{\mathbf{b}1\times tb} \;\vdots\; \Delta\mathbf{f}^{T}_{\mathbf{Nt}1\times sh} \;\vdots\; \Delta\mathbf{d}^{T}_{\mathbf{NG}1\times 4N}\right\rangle \mathbf{B}_{\mathbf{G2}(tb+sh+4N)\times(tb+sh+4N)}\begin{Bmatrix}\Delta\mathbf{t}_{\mathbf{b}tb\times 1}\\ \hdashline \Delta\mathbf{f}_{\mathbf{Nt}sh\times 1}\\ \hdashline \Delta\mathbf{d}_{\mathbf{NG}4N\times 1}\end{Bmatrix} \tag{VI.124}$$

Stability Condition

By taking the variation of Eq. (VI.124), one obtains the stability condition of the beam i.e., $\delta\left\{\frac{1}{2}\delta^2\pi^*\right\} = 0$ as

$$\begin{bmatrix} 0 & 0 & 0 \\ 0 & 0 & 0 \\ 0 & 0 & \mathbf{K}_{G4N\times 4N} \end{bmatrix} \begin{Bmatrix} \Delta\mathbf{t}_{btb\times 1} \\ \Delta\mathbf{f}_{Ntsh\times 1} \\ \Delta\mathbf{d}_{NG4N\times 1} \end{Bmatrix} + \lambda \begin{bmatrix} \mathbf{B}^{G2}_{t\ tb\times tb} & \mathbf{B}^{G2}_{tf\ tb\times sh} & \mathbf{B}^{G2}_{td\ tb\times 4N} \\ \mathbf{B}^{G2T}_{tf\ sh\times tb} & \mathbf{B}^{G2}_{f\ sh\times sh} & \mathbf{B}^{G2}_{fd\ sh\times 4N} \\ \mathbf{B}^{G2T}_{td\ 4N\times tb} & \mathbf{B}^{G2T}_{fd\ 4N\times sh} & \mathbf{B}^{G2}_{d\ 4N\times 4N} \end{bmatrix} \begin{Bmatrix} \Delta\mathbf{t}_{btb\times 1} \\ \Delta\mathbf{f}_{Ntsh\times 1} \\ \Delta\mathbf{d}_{NG4N\times 1} \end{Bmatrix} = 0 \quad \text{(VI.125)}$$

In Eq. (VI.125), matrix $\mathbf{K}_G$ has no degrees of freedom corresponding to the vectors $\Delta\mathbf{t}_{btb\times 1}$ and $\Delta\mathbf{f}_{Ntsh\times 1}$. By eliminating the components in $\mathbf{B}_{G2}$ corresponding to vectors $\Delta\mathbf{t}_{btb\times 1}$ and $\Delta\mathbf{f}_{Ntsh\times 1}$ in Eq. (VI.125) through static condensation, one obtains

$$\left[\mathbf{K}_{G4N\times 4N} + \lambda\mathbf{K}_{E4N\times 4N}\right]\Delta\mathbf{d}_{NG4N\times 1} = 0 \quad \text{(VI.126)}$$

In Eq. (VI.126), matrix $\mathbf{K}_{E4N\times 4N}$ is the global elastic stiffness matrix which is expressed as

$$\mathbf{K}_{E4N\times 4N} = \mathbf{B}^{G2}_{d\ 4N\times 4N} - \mathbf{B}^{G2T}_{td\ 4N\times tb}\mathbf{B}^{G2-1}_{t\ tb\times tb}\mathbf{B}^{G2}_{td\ tb\times 4N} - \mathbf{G}^{T}_{4N\times sh}\mathbf{A}^{-1}_{sh\times sh}\mathbf{G}_{sh\times 4N} \quad \text{(VI.127)}$$

in which, $\mathbf{A}_{sh\times sh} = \mathbf{B}^{G2}_{f\ sh\times sh} - \mathbf{B}^{G2T}_{tf\ sh\times tb}\mathbf{B}^{G2-1}_{t\ tb\times tb}\mathbf{B}^{G2}_{tf\ tb\times sh}$ and $\mathbf{G}_{sh\times 4N} = \mathbf{B}^{G2}_{fd\ sh\times 4N} - \mathbf{B}^{G2T}_{tf\ sh\times tb}\mathbf{B}^{G2-1}_{t\ tb\times tb}\mathbf{B}^{G2}_{td\ tb\times 4N}$

Displacement Boundary Conditions

The support degrees of freedom can be grouped together and Eq. (VI.126) can be written as

$$\left[\begin{bmatrix} \mathbf{K}_{Gs} & \mathbf{K}_{Grs} \\ \mathbf{K}_{Gsr} & \mathbf{K}_{Gr} \end{bmatrix}_{4N\times 4N} + \lambda \begin{bmatrix} \mathbf{K}_{Es} & \mathbf{K}_{Ers} \\ \mathbf{K}_{Esr} & \mathbf{K}_{Er} \end{bmatrix}_{4N\times 4N}\right] \begin{Bmatrix} \Delta\mathbf{d}_s \\ \Delta\mathbf{d}_r \end{Bmatrix}_{4N\times 1} = 0 \quad \text{(VI.128)}$$

In Eq. (VI.128), the sub-matrices pertinent to the supports are assigned the subscripts *s* and those relating the remaining degrees of freedom have the subscripts *r*. By enforcing the condition $\Delta\mathbf{d}_s = \mathbf{0}$, one obtains

$$\left[[\mathbf{K}_{Gr}] + \lambda[\mathbf{K}_{Er}]\right]\{\Delta\mathbf{d}_r\} = 0 \quad \text{(VI.129)}$$

The eigenvalue problem in Eq. (VI.129) is solved to yield the buckling load factor $(1/\lambda)$.

Examples

General

The examples presented in this section illustrate the applicability of the proposed formulations to practical problems. The problems presented also provide an indication of the validity of the new solution in comparison to results based on shell finite element analysis solutions and other closed form or numerical solutions in literature. Steel material is used in all examples for which the Modulus of Elasticity is $E = 2\times10^5 MPa$, Poisson's Ratio is $\upsilon = 0.3$ and the corresponding Shear Modulus is $G = 77\times10^3 MPa$.

Two elements are developed in this study. In element BECE (Buckling Element based on Complementary Energy), the effect of shear deformation is omitted (i.e., $\chi^{-1}_{2\times2} \approx [0]_{2\times2}$), whereas in element BECES (Buckling Element based on Complementary Energy including Shear deformation) the effect of shear deformation is retained. For all examples except Example VI.1, sixteen beam elements (BECE or BECES, as applicable) are used to model the structures.

In addition, finite element shell models are developed under ABAQUS, a general purpose finite element program using the four nodded shell element (S4R) with reduced integration. The S4R element is efficient and reliable for large displacements, large rotations and finite membrane strains (Mohareb and Dabbas 2003). The main advantages of reduced integration are; i) it avoids shear locking that occurs in fully integrated elements and ii) it reduces the CPU time necessary for the analysis of the model and gives more accurate results for thin shells (Zinoviev and Mohareb 2004). The multiple point constraints MPC type SLIDER (Hibbit et al. 2001a,b) are adopted in order to approximately impose the first Vlasov assumption and increase the buckling loads in local buckling modes for rather short spans. This type of MPC keeps the specified node(s) on a straight line defined by two other nodes but allows the possibility of moving along the line and allows the line change in length. In all examples, the cross-section dimensions are selected to prevent local and distortional buckling modes as the first modes in ABAQUS shell models, thus the first modes obtained are global buckling modes. The mesh, boundary condition and loading details for the ABAQUS FEA models for each problem are given in Appendix E.

Alternative solution methods developed by Masur and Popelar (1976), Elias (1986) and Trahair (1993) are used for comparison. Note that these solutions do not include the effect of shear deformation in the analysis. Kutlukaya (2004) implemented a computer program based on the buckling element developed by Trahair (1993). In the buckling analysis, the element has two nodes with four degrees of freedom at each node including lateral displacement, out of plane rotation, angle of twist and warping degrees of freedom. The element can be used to obtain solutions for symmetric cross-sections based on orthogonal system of coordinates. The results obtained by using this element will be referred to as Trahair's element, which was used in Examples VI.1, VI.2, VI.3 and VI.4. Sixteen Trahair's elements are used for all examples.

In all models, pinned supports imply that both the translation and angle of twist are restrained ($\Delta u = \Delta\phi = 0$) while the first derivative of lateral displacement and warping deformation are free ($\Delta u' \neq 0, \Delta\phi' \neq 0$). Fixed supports imply that the derivative of lateral displacement and warping deformation are prevented as well as lateral displacement and angle of twist ($\Delta u = \Delta u' = \Delta\phi = \Delta\phi' = 0$). The relations $\Delta u' = \Delta\phi' = 0$ would be exact when shear deformation is neglected (element BECE) while they become approximate when shear deformation is included (element BECES) since in Eq. (VI.58), the boundary conditions for restraint warping deformation and the first derivative of lateral displacement were obtained as $-\Delta u' + \frac{1}{G}\langle -\Delta M_y' \quad \Delta B' \rangle \chi_{2\times2}^{-1} \begin{Bmatrix} -1 \\ 0 \end{Bmatrix} = 0$ and $\Delta\phi_Z' + \frac{1}{G}\langle -\Delta M_y' \quad \Delta B' \rangle \chi_{2\times2}^{-1} \begin{Bmatrix} 0 \\ 1 \end{Bmatrix} = 0$. The buckling load predictions for modes higher than the first one are given in Appendix VI.F.

Example VI.1 Flexural and Torsional Buckling of Simply-Supported column

A simply supported column (Fig. VI. 14) is made of a symmetric I section and is subject to uniform axial load. The column span L is 2,000mm and the cross-sectional dimensions are shown in Fig. VI.14. An axial load P is applied at the right end of the column at the centroid C of the cross-section (which also coincides with the shear center and the principal sectorial origin of the cross-section). In practical situations, the strength of such a short column would be governed by the yield resistance of the cross-section and the buckling strength would be of academic interest. Nevertheless, a short column was adopted in this example in order to provide a medium to illustrate shear deformation effects on the elastic buckling load. This effect will be shown to be more pronounced in other problems (Example VI.9).

The column is modeled using elements BECE and BECES by selecting the origin, pole and sectorial origin to coincide at the point of application of the external load which corresponds to an orthogonal system of coordinates. The number of elements used to model the column varied from 2 to 16 elements of equal length.

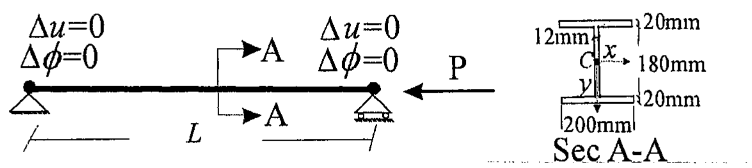

Fig. VI.14-Simply supported beam with symmetric cross-section

In Tables VI.1 and VI.2, the buckling load predictions based on BECE, BECES and Trahair's element (1993), are compared with those based on ABAQUS FEA shell element model and closed form solutions (which do not include shear deformation effects) for the first (flexural) buckling mode and the second (torsional) buckling mode.

Table VI.1-Flexural buckling (first mode)

Element Type	Number of Elements	Buckling Load P(kN)	P/P_{ABAQUS}	P/P_e
ABAQUS	6000	12,822	1	0.97439
Trahair 1993	2	13,258	1.0340	1.0075
	4	13,166	1.0268	1.0005
	8	13,160	1.0264	1.0001
	16	13,160	1.0264	1.0001
BECE	2	13,163	1.0266	1.0003
	4	13,160	1.0264	1.0001
	8	13,159	1.0263	1.0000
	16	13,159	1.0263	1.0000
BECES	2	12,830	1.0006	0.97500
	4	12,827	1.0004	0.97477
	8	12,827	1.0004	0.97477
	16	12,827	1.0004	0.97477
$P_e = \pi^2 EI/L^2$		13,159	1.02628	1

Table VI.2-Torsional buckling (second mode)

Element Type	Number of Elements	Buckling Load P (kN)	P/P_{ABAQUS}	P/P_e
ABAQUS	6000	19,019	1	0.94242
Trahair 1993	2	20,279	1.0662	1.0049
	4	20195	1.0618	1.0007
	8	20,190	1.0616	1.0004
	16	20,189	1.0615	1.0004
BECE	2	18,567	0.97623	0.92002
	4	19,763	1.0391	0.97929
	8	20,075	1.0555	0.99475
	16	20,154	1.0597	0.99866
BECES	2	18,127	0.95310	0.89822
	4	19,317	1.0157	0.95719
	8	19,629	1.0321	0.97265
	16	19,708	1.0362	0.97656
$P_e = \left(GJ_d + \pi^2 EJ_{\omega\omega}/L^2\right)/r_0^2$		20,181	1.0611	1

One can verify from Table VI.1 that Elements BECE and BECES provide upper bound predictions for the flexural buckling modes. The flexural buckling mode solution based on element BECE is analogous to the Timoshenko quotient (Westergaard 1941). Thus, the approximate buckling load prediction is always an upper bound to the exact solution.

It is observed that the inclusion of shear deformation effect provides a more flexible representation of the column stiffness and thus slightly reduces the magnitude of the buckling load. The buckling load prediction based on BECES is closer to the prediction of ABAQUS model.

On the other hand, as shown in Table VI.2, elements BECE and BECES provide a lower bound representation of the stiffness for torsional buckling since the interpolation field for St.Venant torsion was not expressed in terms of the rotation field, but interpolated independently (as a constant function). In Figures VI.15a and b, the St.Venant torsion, the function $-GJ_d\phi_z'$ and warping torsion fields based on element BECE due to buckling are shown based on the analysis with four elements and sixteen elements respectively. Since the second compatibility condition in Eq. VI.61 i.e., $\left[\phi_z' + \Delta T_{sv}/GJ_d\right] = 0$ is satisfied only in an average integral sense, the distribution of the St.Venant torsion field is improved as the number of elements increases. Hence, the buckling load predictions improve. A mathematical demonstration for the possibility of a lower bound property for element BECE is presented in Appendix VI.G.

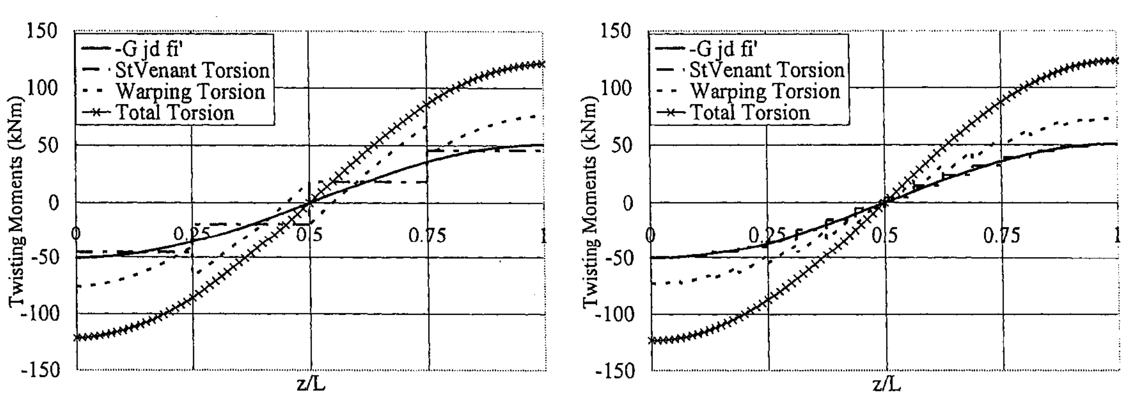

a) Based on a four element solution b) Based on a sixteen element solution

Fig. VI.15 Twisting moments

Note that, since the amplitude of buckling deformations are not unique, the normalization scheme presented in Fig. VI.15 a and Fig. VI.15 b is such that it provides the same maximum torsion.

Convergence characteristics of the solution

In Eq. VI.E.24, it is also demonstrated that when the contribution of the St.Venant torsion is omitted, element BECE provides an upper bound representation of the stiffness in comparison to the exact solution in a torsional buckling mode with omitted St.Venant torsion rigidity. This conclusion is numerically illustrated for both elements BECE and BECES in Table VI.3.

Table VI.3- Torsional buckling neglecting the contribution of St.Venant torsion

Element Type	Number of	Buckling Load P (kN)	$\frac{P}{P_e}$
BECE	2	11,938	1.0003
	4	11,935	1.0000
	8	11,935	1.0000
	16	11,935	1.0000
BECES	2	11,640	0.97528
	4	11,634	0.97478
	8	11,634	0.97478
	16	11,634	0.97478
$P_e = \pi^2 EC_w / (r_0 L)^2$		11,935	1

The predicted mode shapes based on BECE (16 elements), BECES (16 elements) and ABAQUS (6,000 elements) are presented in Figs. VI.16 a and b. The lateral displacements are provided at web mid height. The displacements and rotations based on elements BECE and BECES are scaled so that the maximum displacement based on BECE or BECES and that based on the ABAQUS model are equal. The procedure adopted to obtain the mode shapes is explained in Appendix VI.H. The mode shape predictions based on BECE and BECES are in excellent agreement with those based on the ABAQUS model.

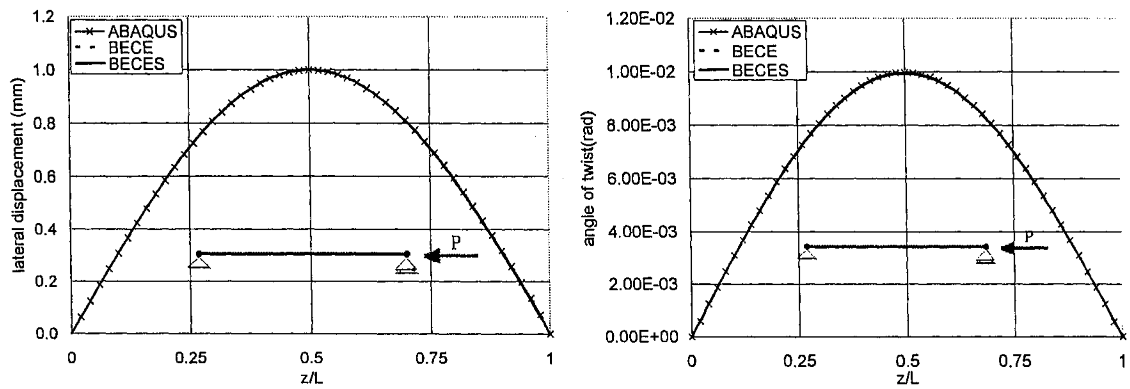

Fig. VI.16 a- Flexural buckling mode b-Torsional buckling mode

When the span L is reduced to 1,600 mm, one obtains the buckling load predictions in bending mode and torsional mode as shown in Tables VI.4 and VI.5 respectively.

Table VI.4-Flexural buckling (first mode)

Element Type	Number of Elements	Buckling Load P (kN)	$\frac{P}{P_{ABAQUS}}$	$\frac{P}{P_e}$
ABAQUS	6000	19,799	1	0.9629
Trahair 1993	2	20,716	1.0463	1.0075
	4	20,572	1.0390	1.0005
	8	20,562	1.0385	1.0000
	16	20,562	1.0385	1.0000
BECE	2	20,567	1.0388	1.0002
	4	20,562	1.0385	1.0000
	8	20,562	1.0385	1.0000
	16	20,562	1.0385	1.0000
BECES	2	19,767	0.99838	0.96134
	4	19,762	0.99813	0.96109
	8	19,762	0.99813	0.96109
	16	19,762	0.99813	0.96109
$P_e = \pi^2 EI/L^2$		20,562	1.0385	1

Table VI.5-Torsional buckling (second mode)

Element Type	Number of Elements	Buckling Load P (kN)	$\frac{P}{P_{ABAQUS}}$	$\frac{P}{P_e}$
ABAQUS	6000	25,303	1	0.94084
Trahair 1993	2	27,043	1.0688	1.0055
	4	26,912	1.0636	1.0007
	8	26,903	1.0632	1.0003
	16	26,903	1.0632	1.0003
BECE	2	25,305	1.0001	0.94092
	4	26,478	1.0464	0.98453
	8	26,789	1.0587	0.99610
	16	26,868	1.0619	0.99903
BECES	2	24,441	0.96593	0.90879
	4	25,608	1.0121	0.95218
	8	25,919	1.0243	0.96375
	16	25,998	1.0275	0.96668
$P_e = \left(GJ_d + \pi^2 EC_w/L^2\right)/r_0^2$		26,894	1.0298	1

By using a sixteen element mesh for the torsional buckling analysis of the column with a 2,000 mm span had a ratio of the St.Venant torsion to warping torsion at the root of the column (z=0) of 0.68 (Fig. VI.15b), whereas for the shorter column spanning 1,600 mm, the ratio reduces to 0.43. The St.Venant torsion is thus more dominant in longer spans. For torsional buckling, the convergence rates of elements BECE and BECES are higher for shorter spans. This suggests that for longer spans one may need to increase the number of elements in order to improve accuracy. However, buckling load predictions are always more conservative compared to those based on total potential energy formulations, an advantageous feature from an engineering point of view. By comparing the results based on BECE and BECES in Table VI.1 and VI.4, and Table VI.2 and VI.5 respectively, one can also verify that the shear deformation effect increases for columns of shorter spans.

Example VI.2 Effect of Boundary Conditions on Column Flexural Buckling

A column is spanning 8,000 mm. The cross-section is identical that of Example 1 Fig. VI.14. The buckling load of the column is investigated for two types of boundary conditions as shown in Column (1) of Table VI.6. The external load P shown in Table VI.6 is applied at the section centroid. Thus, an orthogonal system of coordinates is used in both problems. Buckling loads based on Trahair elements (sixteen elements) is provided in Column (3), while columns (4) and (5) provide the buckling loads predicted by elements BECE and BECES. Euler buckling loads are provided in Column (6). The results based on ABAQUS analysis are given in Column 2. In all examples except in Example 4 (Tables VI.8), the bracketed numbers below the critical moments are the percentage ratios of the predicted buckling moments to that predicted by the ABAQUS model.

Table VI.6-Flexural Buckling load predictions under axial load

(1)	(2)	(3)	(4)	(5)	(6)
Boundary Condition and Loading	ABAQUS (kN)	Trahair(1993) (kN)	BECE (kN)	BECES (kN)	Euler Load (kN)
 P	1667	1683 (%101)	1683 (%101)	1676 (%101)	1679 (%101)
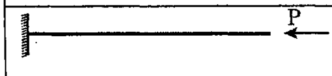 P	204	206 (%101)	206 (%101)	206 (%101)	206 (%101)

Since the column span is relatively long, the contribution of shear deformation is insignificant in buckling load predictions and the results based on BECE and BECES are in agreement within 1% (Table VI.6). The corresponding buckling mode shapes are presented in Figures VI.17 a, b respectively. The mode shape predictions based on BECE and BECES are also in excellent agreement with those based on ABAQUS model.

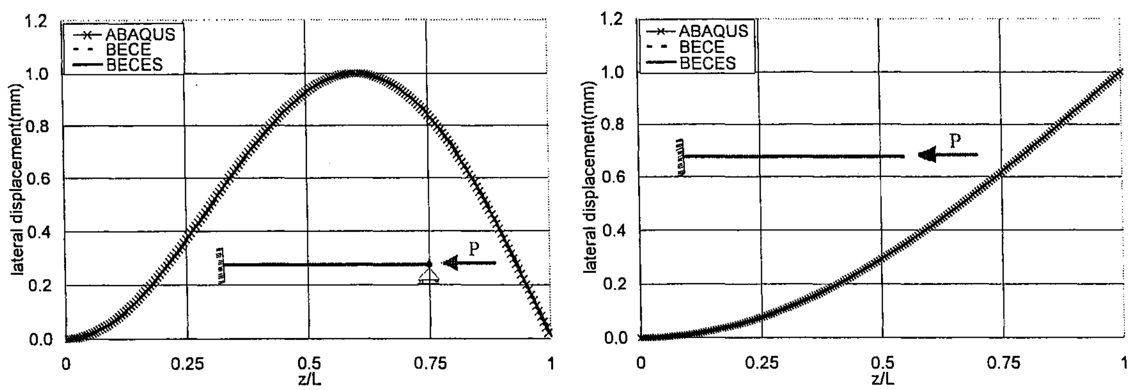

a- Fixed-pinned column b- Fixed-free column

Fig. VI.17 Buckling Modes

Example VI.3 Lateral Torsional Buckling of Beams with doubly symmetric cross-section

For the problems shown in Table VI.7, the cross-section is identical to that given in Fig. VI.14. All beams are simply supported and span 8,000 mm. The beam is subject to several linear bending moment distributions. The results based on ABAQUS FEA model is provided in Column 2. The closed form solution for the buckling moment of simply supported beam under uniform bending moment is

$M_u = (\pi/L)\sqrt{EJ_{yy}GJ_d + (\pi E/L)^2 J_{yy}J_{ww}}$. For the case of uniform moment (Case 1 in Table VI.7), this formula predicts a buckling moment of 286 kNm. For other moment gradient configurations, various codes (e.g., LRFD 1999) provide predictions of the critical moment in the form $M_{cr} = C_b M_u$ in which C_b is a constant depending on the moment gradient and ranges from unity in the case of uniform moment (case 1) to $C_b = 2.3$ for case 5. The critical moments $M_{cr} = C_b M_u$ based on the LRFD procedure are given in Column (3) of table VI.7. Also, the buckling moments based on Trahair elements (sixteen elements) is provided in Column (4), while columns (5) and (6) provide the buckling moments predicted by elements BECE and BECES.

Table VI.7- Buckling moments for simply supported beams under linear moment gradient

	(1)	(2)	(3)	(4)	(5)	(6)
	Boundary condition and Loading	ABAQUS (kNm)	LRFD (kNm)	Trahair (kNm)	BECE (kNm)	BECES (kNm)
1	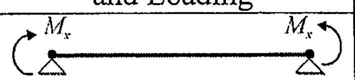	272	286 (%105)	286 (%105)	285 (%105)	283 (%104)
2	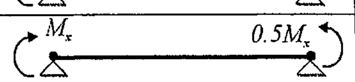	359	357 (%99.4)	376 (%105)	375 (%104)	371 (%103)
3	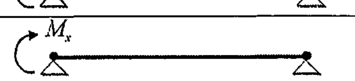	489	477 (%97.5)	513 (%105)	512 (%105)	505 (%103)
4	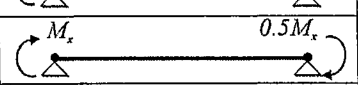	654	620 (%94.8)	691 (%106)	689 (%105)	682 (%104)
5	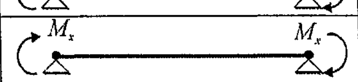	717	648 (%90.3)	754 (%105)	752 (%105)	744 (%104)

From Table VI.7, one can verify that all BECE and BECES results are in very good agreement with the results based on ABAQUS. Except Case 1 LRFD (1999) predictions are the most conservative among all while the Trahair element tends to slightly overestimate the buckling moment by 5% compared to ABAQUS results. Element BECES provides the closest predictions to ABAQUS solution. Critical moment predictions based on Element BECE are 5% higher than those predicted by ABAQUS while element BECES predictions are 3% to 4% higher than those based on ABAQUS. As expected, for the 8,000 mm span members, shear deformation effects are insignificant. Buckling mode shape comparisons for various solutions are depicted in Figures VI.18 through VI.22 and show excellent agreement between BECE, BECES, and ABAQUS. The lateral displacements are provided at web mid height.

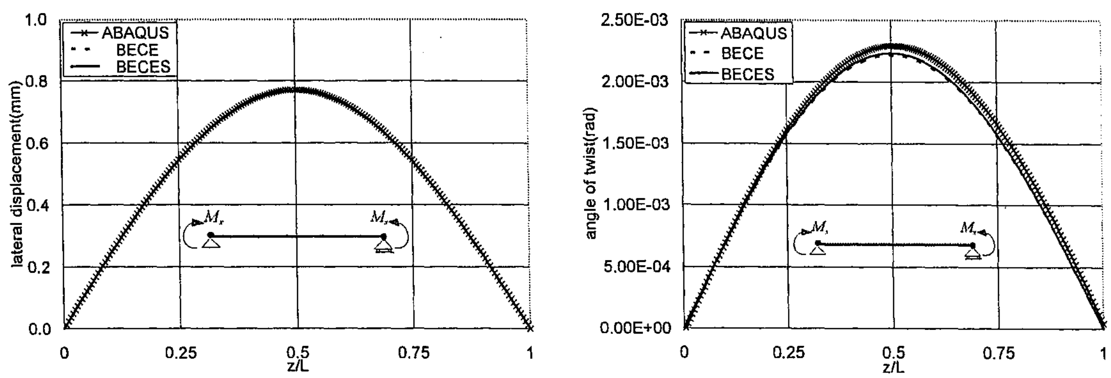

a-Lateral displacement b-Angle of twist

Fig. VI.18 Buckling Mode for Case1 in Table VI.7

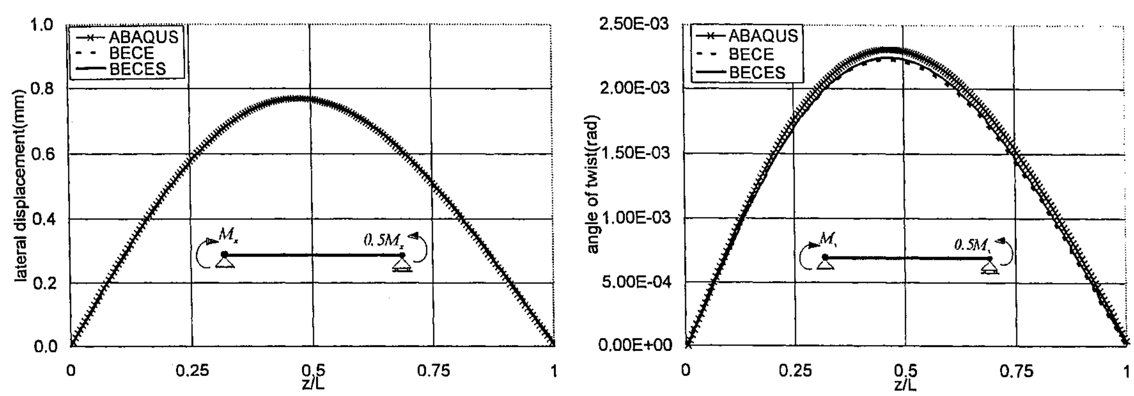

a-Lateral displacement b-Angle of twist

Fig. VI.19 Buckling Mode for Case2 in Table VI.7

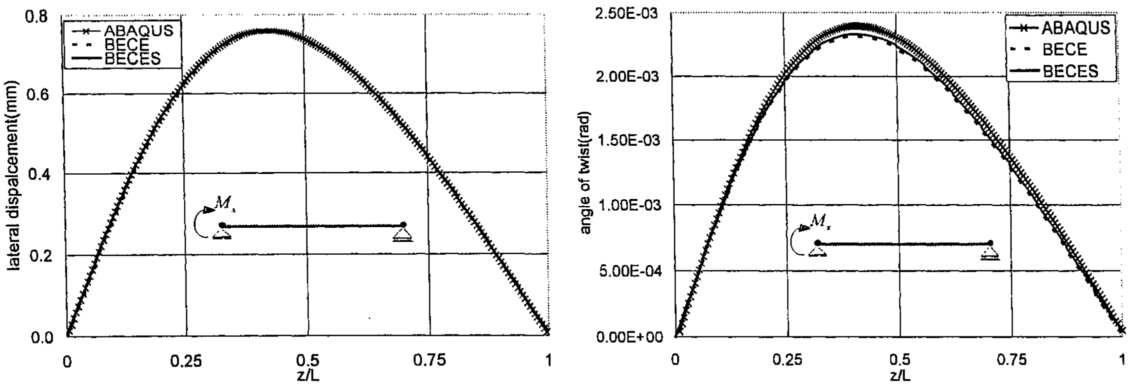

a-Lateral displacement b-Angle of twist

Fig. VI.20 Buckling Mode for Case3 problem in Table VI.7

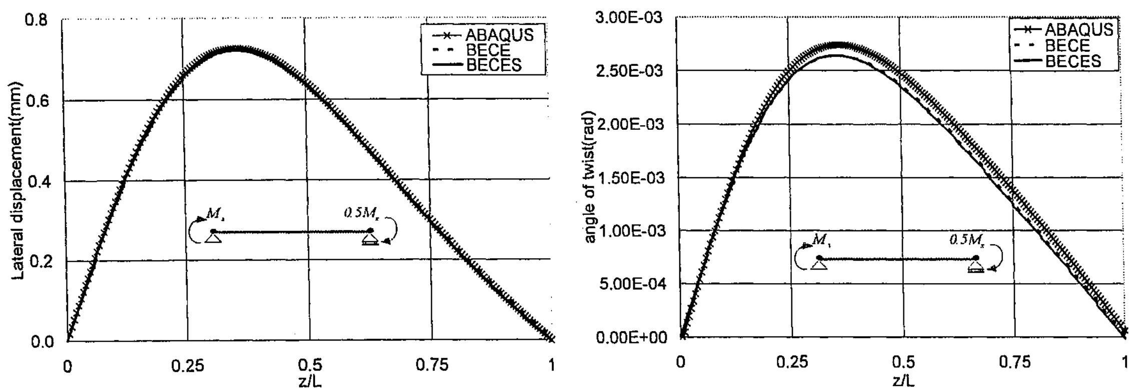

a-Lateral displacement b-Angle of twist

Fig. VI.21 Buckling Mode for Case4 in Table VI.7

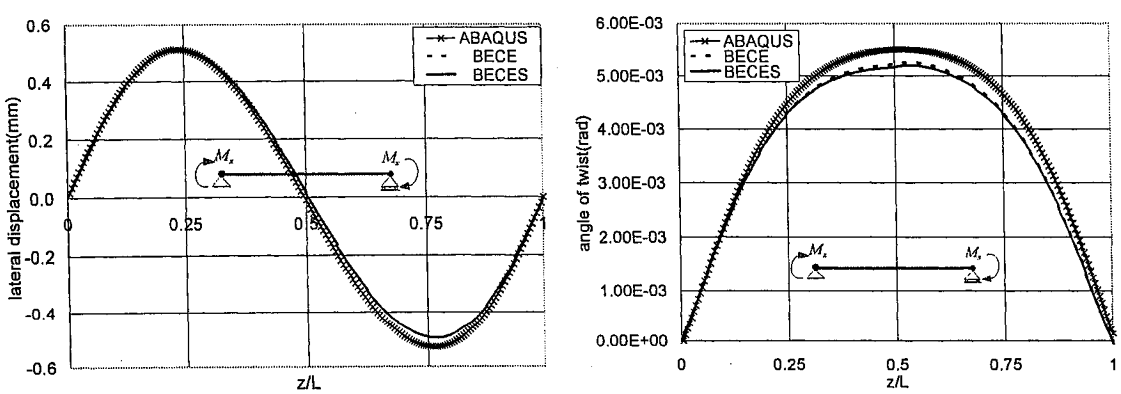

a-Lateral displacement b-Angle of twist

Fig. VI.22 Buckling Mode for Case5 in Table VI.7

Example VI.4 Lateral Torsional Buckling of a fixed-pinned beam under uniform moment

For the beam shown in Fig. VI. 23, the cross-section is identical to that given in Fig. VI.14 and the beam is investigated for a) 8,000 mm (Case 1 in Table VI. 8) and b) 4,000 mm (Case 2 in Table VI. 8) spans. From the pre-buckling analysis the beam is assumed to have uniform bending moment distribution and the boundary conditions for lateral torsional buckling analysis are assumed to be fixed at one end (z=0) while simply supported at the other end ($z=L$) as shown in Fig. VI.23. The problem is analyzed using four types of solutions: 1) Trahair's element (1993), 2) the complementary energy based method developed by Masur and Popelar (1976), 3) BECE, and 4) BECES elements developed in this study.

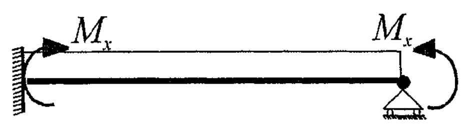

Fig. VI.23 Boundary conditions and pre-buckling loading

Masur and Popelar (1976) obtained the critical buckling moment of the given problem by using complementary energy formulation as $M_{cr} = 4.49\sqrt{1+(4.49)^2 EC_w/(L^2GJ_d)}\sqrt{EI_{yy}GJ_d}/L$. The results based on Trahair (sixteen elements), Masur and Popelar (1976), BECE and BECES are given in column (2), (3), (4) and (5) respectively. In Table VI.8, the bracketed numbers below the critical moments are the percentage ratios of the predicted buckling moments to that predicted by Trahair's element.

Table VI.8- Buckling moments for a fixed-pinned beam under uniform moment

	(1) Beam Span L (mm)	(2) Trahair (kNm)	(3) Masur and Popelar (kNm)	(4) BECE (kNm)	(5) BECES (kNm)
1	8,000	426	425 (99.8%)	424 (99.5%)	420 (98.6%)
2	4,000	1,032	1,030 (99.8%)	1,029 (99.7%)	1,013 (98.2%)

One can verify that all the results are in excellent agreement and the difference does not exceed 2%. Solutions based on Masur and Popelar (1976) and Trahair (1993) are closer to those based on BECE rather than those based on BECES, since the shear deformation effect is omitted in these solutions. BECES provides slightly more conservative buckling moment predictions due to the shear deformation effect which can be observed to increase for shorter span. The mode shape comparisons for Trahair, BECE and BECES are depicted in Figs VI. 24 and shows excellent agreement.

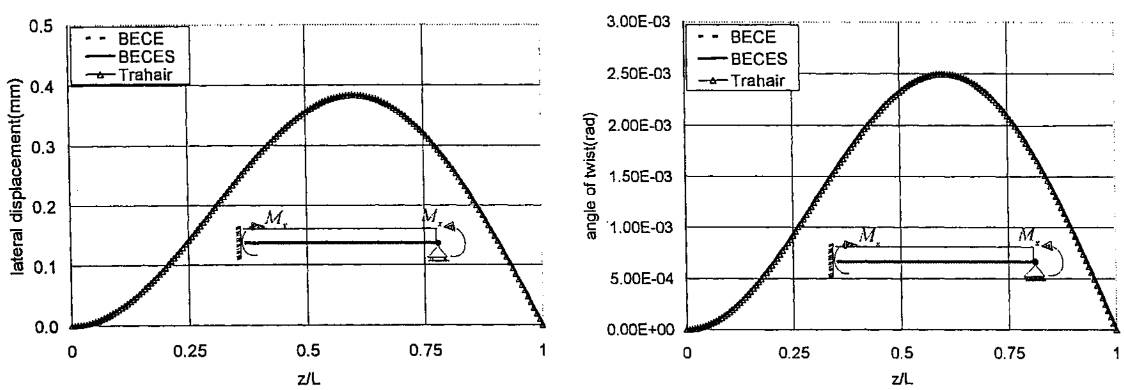

a-Lateral displacement

b-Angle of twist

Fig. VI.24 Buckling Mode

Example VI.5 Lateral Torsional Buckling of a cantilever under uniform moment

A cantilever is under uniform bending moment which is applied by a moment at the tip as shown in Fig. VI.25. The cross-sections is selected as in Fig.14 and the buckling moment of the cantilever is investigated for 4,000 mm and 8,000 mm spans. Indeed, cantilever with a tip moment rarely occurs in practice; however the buckling moment in this case is of academic interest. The problem is analyzed using four type of solutions: 1) ABAQUS (results are given in column 2 of Table VI.9), 2) Trahair's element (1993), 3) Element BECE, and 4) Element BECES both developed in this study.

Fig. VI.25 Boundary Conditions and pre-buckling loading

Trahair (1993, p.171 Eq. 9.5) developed a solution for the buckling moment resistance M_{cr} of a cantilever under uniform moment with symmetric cross-sections by using the formulation $M_{cr} = (\pi/2L)\sqrt{EI_{yy}GJ_d\left[1+\pi^2 EC_w/\left(4GJ_dL^2\right)\right]}$. Buckling moments predicted by Trahair's formulation are provided in column (3). Columns (4) and (5) provide the buckling moments predicted by elements BECE and BECES.

Table VI.9- Buckling moments for a cantilever under uniform moment

	(1)	(2)	(3)	(4)	(5)
	Beam Span L (mm)	ABAQUS (kNm)	Trahair (kNm)	BECE (kNm)	BECES (kNm)
1	8000	133	138 (104%)	138 (104%)	137 (103%)
2	4000	271	286 (106%)	285 (105%)	283 (104%)

One can verify shear deformation effects is insignificant and all results agree within 6% in this problem. ABAQUS provides the lowest buckling predictions among all solutions. The mode shapes based on BECE, BECES and ABAQUS are depicted in Figs. VI. 26 for 4,000mm span and are in excellent agreement. The lateral displacements are provided at web mid height.

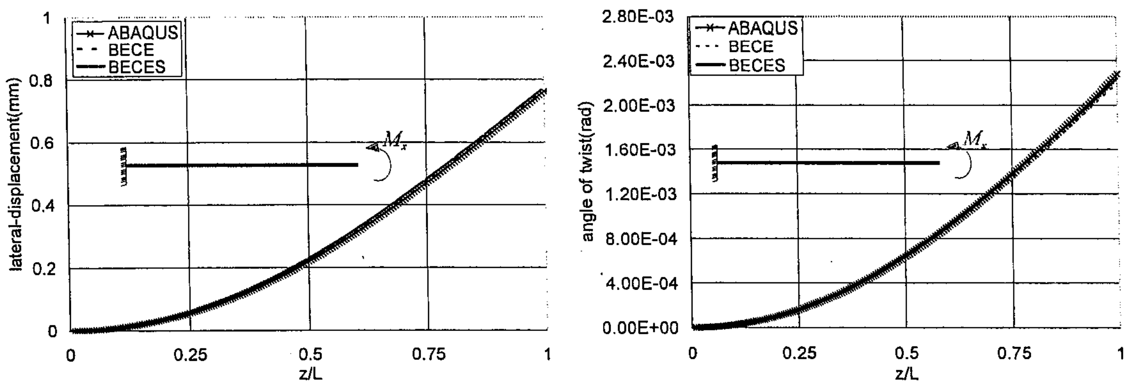

a-Lateral displacement b-Angle of twist

Fig. VI.26 Buckling Mode

Example VI.6 Load Position Effect for a Cantilever under transverse load

The buckling load for a cantilever subjected to a transverse load P at the free end is investigated for 10,000 mm and 4,000 mm beam spans. The cantilever has a C shape cross-section with the dimensions shown in Fig. VI. 27. Three cases are considered for the point of applications of the load. Load P is applied at a) 100 mm above the shear center, b) from the shear center, and c) 100 mm below the shear center (Table VI.8).

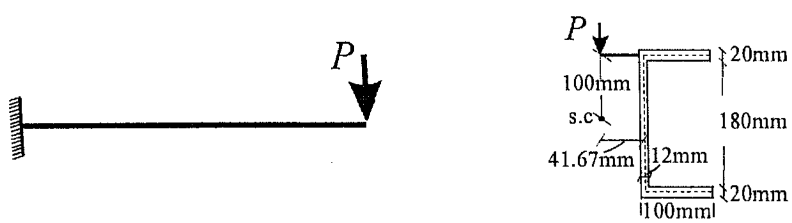

a) Boundary conditions and Loading b) dimensions of the cross-section

Fig. VI. 27 Cantilever with C-shape cross-section

The problem is analyzed using five buckling solutions: 1) Trahair's element (1993), 2) the complementary energy based solution developed by Elias (1986), 3) BECE and 4) BECES elements developed in this study, and 5) ABAQUS.

Trahair (1993, p. 174, Eq. 9.12), suggested to calculate the buckling load resistance P of a cantilever with C-shape cross-section by using

$$P_{Trahair} = \frac{\sqrt{EI_{yy}GJ_d}}{L^2}\left\{11\left[1+1.2\varepsilon\big/\sqrt{1+1.44\varepsilon^2}\right]+4(K-2)\left[1+1.2(\varepsilon-0.1)\big/\sqrt{1+1.44(\varepsilon-0.1)^2}\right]\right\}$$

, in which $\varepsilon = y_Q/L\left(\sqrt{EI_{yy}/GJ_d}\right)$ and $K=\sqrt{\pi^2 EC_w/\left(GJ_d L^2\right)}$ and y_Q is the vertical distance of the application point of the load to the shear center (e.g., $y_Q = 100mm$ for bottom flange loading).

In Elias solution, the effect of the warping stiffness EC_w is neglected relative to the St. Venant stiffness GJ_d thus, the ratio $k=\sqrt{EC_w/\left(GJ_d L^2\right)}$ is assumed negligible relative to unity. For the 10,000 mm span, the warping stiffness is indeed negligible as $k \approx 0.045 \ll 1$. Elias solution is based on orthogonal system of coordinates and provide buckling load predictions for shear center loading only. Elias (1986) suggests that the load position effect could be accounted for by using the factors developed by Timoshenko (1961), thus the buckling load prediction based on Elias can be obtained as $P_{Elias} = 4.013(1-\varepsilon)\sqrt{EI_{yy}GJ_d}\,/L^2$.

In modeling the problem using elements BECE and BECES, the origin O, pole A_p, sectorial origin S_o are selected to coincide with the point of application of load P. Thus the selected system of coordinates is non-orthogonal. Note that for case b) (shear center loading), the solutions based on BECE and BECES in orthogonal coordinates provides identical results to the those based on non-orthogonal coordinates obtained by selecting the origin O, pole A_p and sectorial origin S_o coincide at the shear center. The results based on ABAQUS, Trahair (1993), Elias (1986), BECE and BECES are provided in columns (2), (3), (4), (5) and (6), in Tables VI .10 and VI .11 for 10,000mm and 4,000mm spans respectively.

Table VI.10 Buckling load by considering load position effects for 10,000 mm span

(1)	(2)	(3)	(4)	(5)	(6)
Point for the load application	ABAQUS (kN)	Trahair (kN)	Elias (kN)	BECE (kN)	BECES (kN)
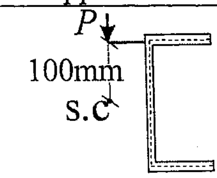	10.7	11.2 (%105)	10.1* (%94.4)	10.5 (%98.1)	10.4 (%97.2)
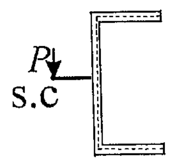	11.4	11.8 (%104)	10.7 (%93.9)	11.2 (%98.2)	11.1 (%97.4)
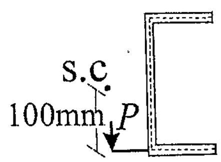	12.1	12.4 (%102)	11.2* (%92.6)	11.8 (%97.5)	11.6 (%95.9)

* The Timoshenko Load position factor has been applied

Since the beam span is relatively long, the effect of St.Venant stiffness is large relative to the warping stiffness. Thus, the results based on Elias solution agrees well with ABAQUS. Elias results range from 94.4% to 92.6% of those based on ABAQUS. Trahair results range from 105% to 113% higher than those based on ABAQUS. BECE results range from 102% to 105% of ABAQUS results, while the best agreement is obtained for BECES which range from 101% to 104%. For the shorter span of 4,000mm, the warping torsion becomes more significant i.e., $k \approx 0.112$, thus solution based on Elias diverges form others as shown in Table VI.11.

Table VI.11 Buckling loads by considering load position effects for 4,000 mm span

1	2	3	4	5	6
Point for the load application	ABAQUS (kN)	Trahair (kN)	Elias (kN)	BECE (kN)	BECES (kN)
P 100mm S.C	65.2	73.9 (%113)	57.8* (%88.7)	68.3 (%105)	67.5 (%104)
P S.C	81.7	86.3 (%106)	66.7 (%81.6)	84.5 (%103)	83.2 (%102)
S.C 100mm P	92.8	97.7 (%105)	75.6* (%81.5)	95.5 (%103)	93.8 (%101)

* The Timoshenko Load position factor has been applied

A comparison of the lateral displacement and angle of twist for 4,000 mm span is presented in Figures VI.28, VI.29 and VI.30 for all three cases. Excellent agreement with ABAQUS mode shapes is observed. The lateral displacements are given at the top flange, at the shear center and at the bottom flange in Figs. VI.28 a, b and c respectively

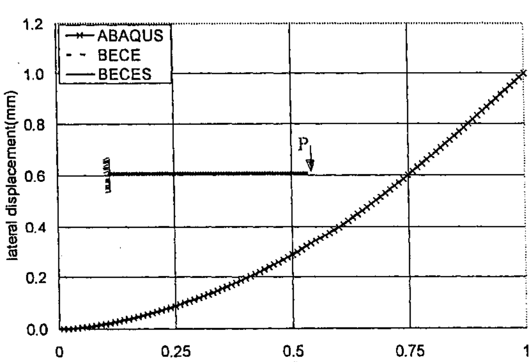

a-Lateral displacement

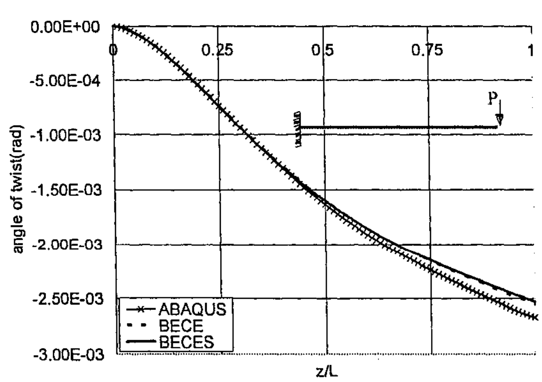

b-Angle of twist

Fig. VI.28 Buckling Mode for Top Flange Loading

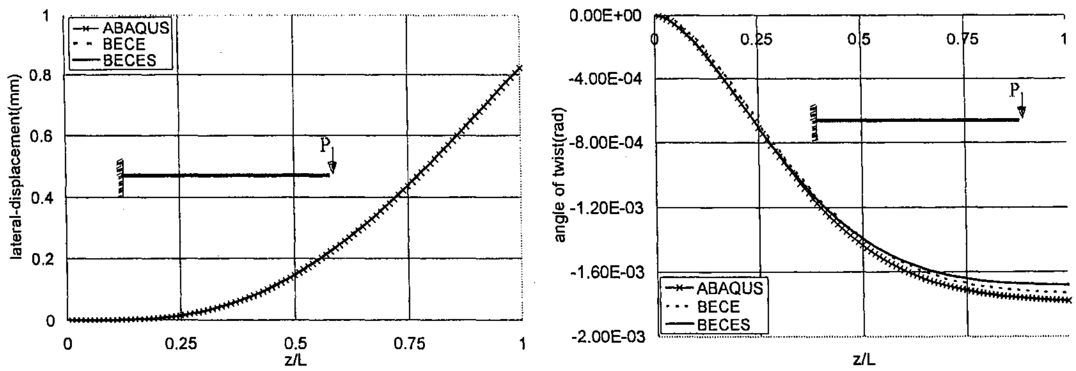

a-Lateral displacement b-Angle of twist

Fig. VI.29 Buckling Mode for Shear center Loading

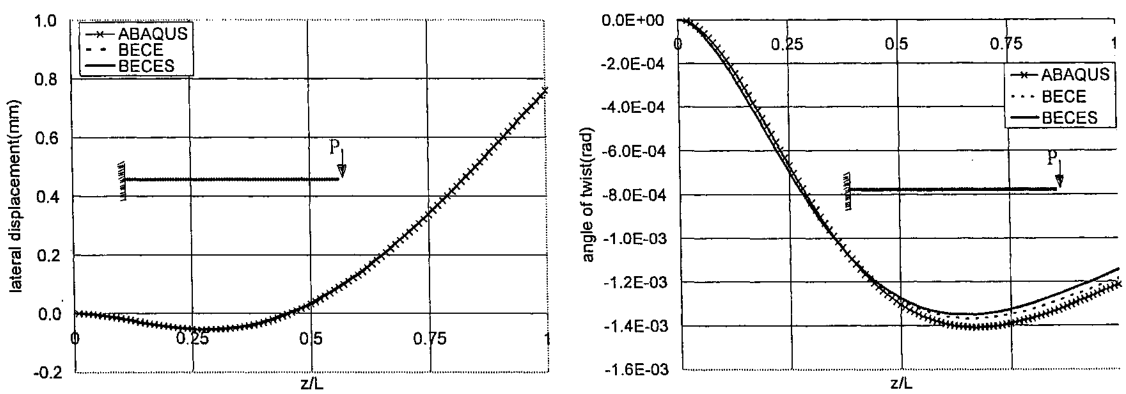

a-Lateral displacement b-Angle of twist

Fig. VI.30 Buckling Mode for Bottom Flange Loading

Example VI.7 Lateral Torsional Buckling of Mono-symmetric beams under uniform moment

A simply supported beam with mono-symmetric cross-section is subjected to uniform bending moment as shown in Fig. VI.31a. Dimensions of the cross-section are shown in Fig. VI.31b. The beam is analyzed for 8,000mm (Case 1), and 4,000mm (Case 2), spans using four type of solutions: 1) ABAQUS shell element analysis , 2) Trahair's element (1993), 3) BECE element, and 4) BECES element.

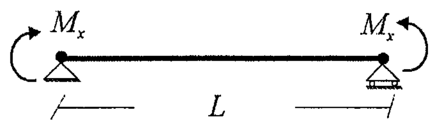

a) Boundary conditions and Loading

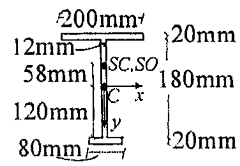

b) dimensions of the cross-section

Fig. 31 Mono-symmetric beam under uniform moment

Trahair's solution (Eq. 7.22 page 125 in Trahair 1993) for the buckling moment of mono-symmetric sections under uniform bending moment is $M = M_{yz}\left[\left(\beta_x P_y/2M_{yz}\right) \pm \sqrt{1+\left(\beta_x P_y/2M_{yz}\right)^2}\right]$, in which $P_y = \pi^2 EI_y/L^2$ and $M_{yz} = \sqrt{\left(\pi^2 EI_y/L^2\right)\left(GJ_d + \pi^2 EC_w/L^2\right)}$. Trahair's solution is based on orthogonal system of coordinates in which the shear center is offset by 58 mm from the centroid in the negative y direction as shown in Fig. VI.31. b, thus the offset value a_y is set to -58 mm. The mono-symmetric property of the cross-section is $\beta_x = \left(1/I_x\right)\int_A y\left(x^2+y^2\right)dA - 2a_y = 153.01$ mm. The results based on Trahair's analysis is provided in Column 3 in Table 12.

In BECE and BECES models, identical results are obtained based on both orthogonal coordinates and non-orthogonal coordinates in which the location of pole, centroid, and sectorial origin can be selected anywhere on the web. The results based on ABAQUS FEA model is provided in Column 2 in Table 12. The results based on BECE and BECES elements are provided in Columns 4 and 5 in Table 12 respectively

Table VI.12-Buckling moments of mono-symmetric beams under uniform moment

	(1)	(2)	(3)	(4)	(5)
	Beam Span L (mm)	ABAQUS (kNm)	Trahair (kNm)	BECE (kNm)	BECES (kNm)
1	8,000	135	141 (%104)	141 (%104)	139 (%103)
2	4,000	224	242 (%109)	241 (%108)	237 (%106)

One can verify that the results based on BECE and BECES are in very good agreement with those based on Trahair (1993) and ABAQUS. The maximum difference between ABAQUS analysis and those based on Trahair (1993) and BECE are around 9%. Buckling moment predictions based on BECES are closer to ABAQUS model solutions and the maximum difference is around 4%. The corresponding lateral displacement at the centroid of the section and angle of twist predictions for 4,000 mm span are presented in Fig. VI.32. The mode shape predictions of BECE and BECES are in very good agreement with those based on ABAQUS model. The example illustrates the ability of elements BECE and BECES to successfully capture mono-symmetry effects.

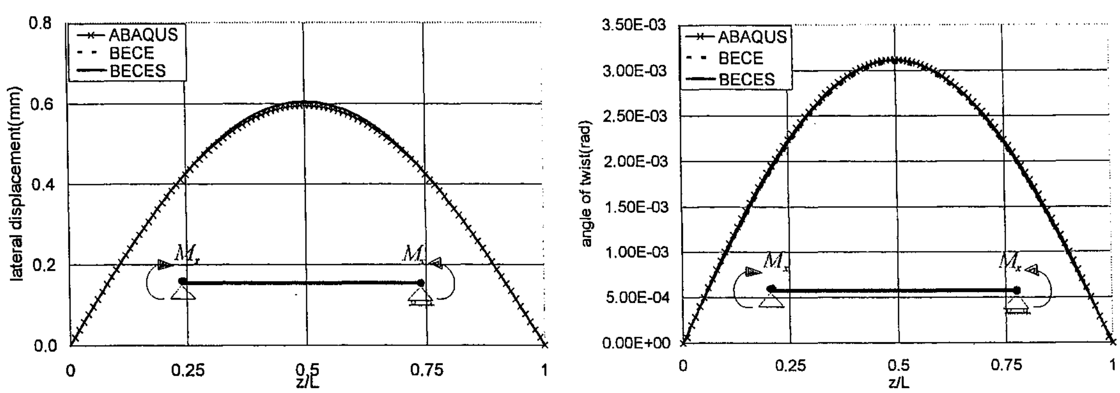

a-Lateral displacement b-Angle of twist

Fig. VI.32 Buckling Mode

Example VI.8 Lateral Torsional Buckling of Mono-symmetric beams under mid-span load

A simply supported beam with mono-symmetric cross-section is subjected to a mid-span load acting at the top flange (Fig. VI. 33). Dimensions of the cross-section are shown in

Table VI.13. The beam is analyzed for a 8,000mm span(Case 1), and 4,000mm span (Case 2), using three type of solutions: 1) ABAQUS shell element analysis, 2) BECE element, and 3) BECES element. In modeling the problem using elements BECE and BECES, the origin O, pole A_p, sectorial origin S_o are selected to coincide with the point of application of load P. Thus the selected system of coordinates is non-orthogonal. The results based on ABAQUS, BECE and BECES are provided in columns (2), (3) and (4) in Table VI.13 respectively.

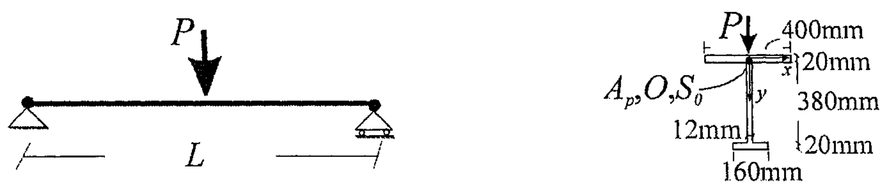

a) Boundary conditions and Loading b) dimensions of the cross-section

Fig. 33 Mono-symmetric section

Table VI.13 Buckling load predictions of a mono-symmetric beam under mid-span load

	(1)	(2)	(3)	(4)
	Beam Span L (mm)	ABAQUS (kN)	BECE (kN)	BECES (kN)
1	8,000	380.2	394.9 (%104)	360.4 (%94.8)
2	4,000	1,636	1,764 (%107)	1,561 (%95.4)

One can verify that the results are in good agreement in all solutions. The behaviour of the element BECES is slightly more flexible than that of the ABAQUS model. When the span is reduced to 4,000 mm, the difference between BECE and BECES increases up to (107%-95.4%$\approx$12%), which is due to the shear deformation effect. The corresponding lateral displacement at the centroid of the top flange and angle of twist predictions for 4,000 mm span are presented in Fig. VI.34. The mode shape predictions of BECE and BECES are in good agreement with those based on the ABAQUS model.

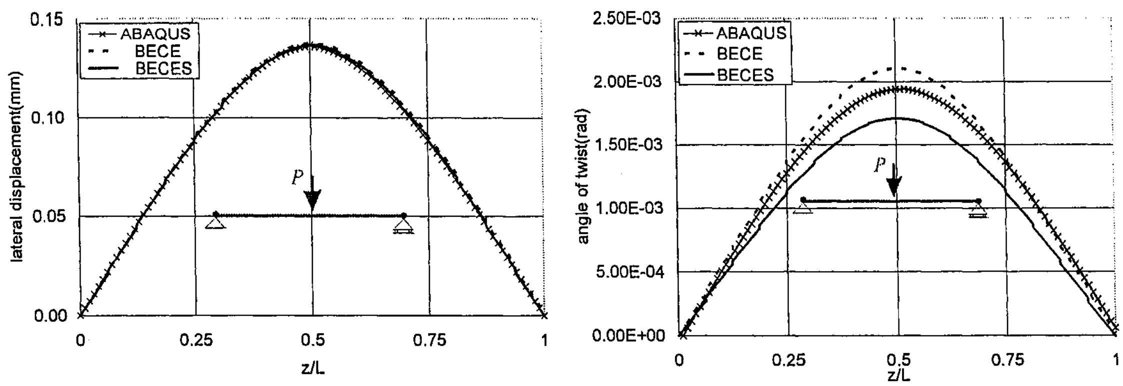

a-Lateral displacement   b-Angle of twist

Fig. VI.34 Buckling Mode

Example VI.9 Shear Deformation Effect in a Propped Cantilever with an Overhang

A propped cantilever with overhang (shown in Table VI.14) is subject to a transverse load P applied to the top flange as shown. When modeling the problem using BECE and BECES, the origin O, pole A_p, sectorial origin S_o are selected to coincide with the point of application of the external vertical load P.

Table VI.14 Buckling load predictions for a propped cantilever with an overhang

Boundary Conditions and Loading	Cross-section	ABAQUS (kN)	BECE (kN)	BECES (kN)
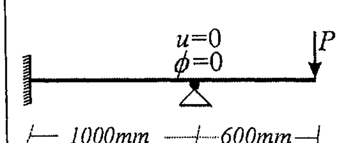	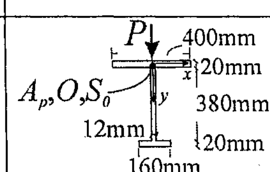	7,180	8,760 (%122)	7,630 (%106)

One can verify that the results based on BECE and BECES differ by 22 % and 6 % respectively from the buckling load predictions of ABAQUS. Buckling load predictions by neglecting the shear deformation effect significantly overestimate the buckling load. The corresponding lateral displacement at the centroid of the top flange and angle of twist predictions are presented in Fig. VI.35. The mode shape predictions of elements BECE and BECES are in good agreement with those based on ABAQUS model. The example illustrates that, in some instances, shear deformation effects are significant and should be incorporated into the analysis for a safe prediction of buckling loads.

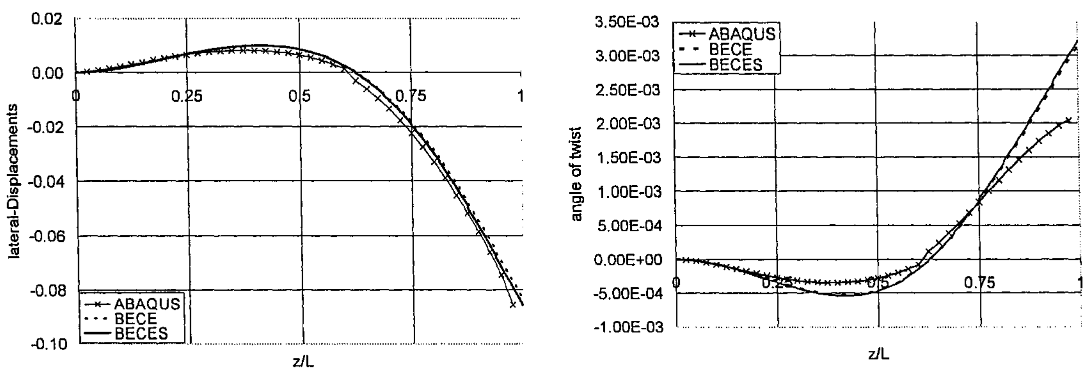

a-Lateral displacement b-Angle of twist

Fig. VI.35 Buckling Mode

Summary and Conclusions

The finite element solutions developed in this study are able to accurately predict classical solutions for column flexural buckling and torsional buckling, and beam lateral torsional buckling under uniform moments and linear moment gradients for doubly symmetric, mono-symmetric and channel sections. By adopting non-orthogonal system of coordinates, the solution is able to successfully capture load position effects relative to the shear centre. In addition to accurately predict the buckling loads corresponding to the fundamental buckling mode, the formulation was shown to accurately predict the buckling modes and higher buckling loads. In contrast to displacement based formations which tend to over-predict buckling loads, the present formulation can under-predict buckling loads. This is a desirable feature from a design viewpoint. The current formulation successfully captures shear deformation effects, a feature that is neglected in most available buckling solutions for thin-walled members. It was shown that conventional solutions which neglect shear deformation effects can overestimate the predicted buckling load in some cases.

Appendix VI.A- Geometric Interpretation of First Piola-Kirchoff and Jaumann stresses in 2D problems

The geometric interpretation of the first Piola-Kirchoff stress D_{ij} and Jaumann stress σ_{ij} components in plane deformation are illustrated (Fig. VI.A.1) for two different scenarios; a) the infinitesimal element ABCD in Fig. VI.A.1a undergoes stretching/shortening deformations along its principal directions, rigid body rotations and translations, and takes the configuration A'B'C'D' after deformation, and b) the infinitesimal element EFGH in Fig. V I.A.1b undergoes distortion deformations as well as stretching/shortening, rigid body rotations and translations, and takes the configuration E'F'G'H' after deformation. The rectangular element ABCD in Fig. VI.A.1a stays rectangular, while the angle between the perpendicular edges in Fig. VIA.1b changes after deformation. The thickness of both the un-deformed elements ABCD and EFGH is t and sides of both plates are parallel to Z and X axes (Figs. VI.A.1 a and b). Unit vectors $\vec{e}_{OZ}$ and $\vec{e}_{OX}$ are oriented along the undeformed principal directions while unit vectors $\vec{e}_z$ and $\vec{e}_x$ are oriented along the deformed principal directions in both cases (Figs. VI.A.1a and b).

The first Piola-Kirchoff stresses are defined as the forces acting on the deformed element oriented along the fixed X and Z axes per unit of initial un-deformed area. Thus, for the first Piola-Kirchoff stress components D_{ZX} and D_{ZZ}, the respective un-deformed areas are $\mathrm{BC}\times t$ in Fig. VIA.1.a and $\mathrm{FG}\times t$ in Fig. VIA.1b. Jaumann stresses are defined as the forces acting on the deformed element oriented along the rigidly rotated configuration per unit of initial un-deformed area. In Fig. VIA.1a, the direction of the Jaumann stress component σ_{zz} is determined by the rigid body rotation angle ϕ_A (i.e., $\sigma_{zz} = D_{ZX} \sin\phi_A + D_{ZZ} \cos\phi_A$) and is acting along the principal strain directions parallel to the direction of the unit vector $\vec{e}_z$ (Fig. VI.A.1a). The Jaumann stress component σ_{zx} vanishes since there is no distortion due to shear deformation between the edges A'B' and B'C'. In Fig. VI.A.1b the rigid body rotation angle between the unit vectors $\vec{e}_{OZ}$ and $\vec{e}_z$ is denoted by ϕ_Y. In Fig. VI.A.1b the angle between $\vec{e}_{OX}$ and $\vec{e}_x$ is also ϕ_Y. Thus, the orientation and magnitude of the Jaumann stress components σ_{zz} and σ_{zx} can be related to the first Piola-Kirchoff stresses D_{ZX} and D_{ZZ}, and the rigid body rotation ϕ_Y through $\sigma_{zz} = D_{ZX} \sin\phi_Y + D_{ZZ} \cos\phi_Y$ and $\sigma_{zx} = D_{ZX} \cos\phi_Y - D_{ZZ} \sin\phi_Y$. Note that these relations are independent from the angles γ_1 and γ_2 (Fig. VI.A.1b) due to shear deformation. Also note that in Fig. VI.A.1b, the Jaumann stress component σ_{zz} is not perpendicular to the edge F'G' as oppose to the Jaumann stress component σ_{zz} perpendicular to the edge B'C' in Fig. VI.A.1a.

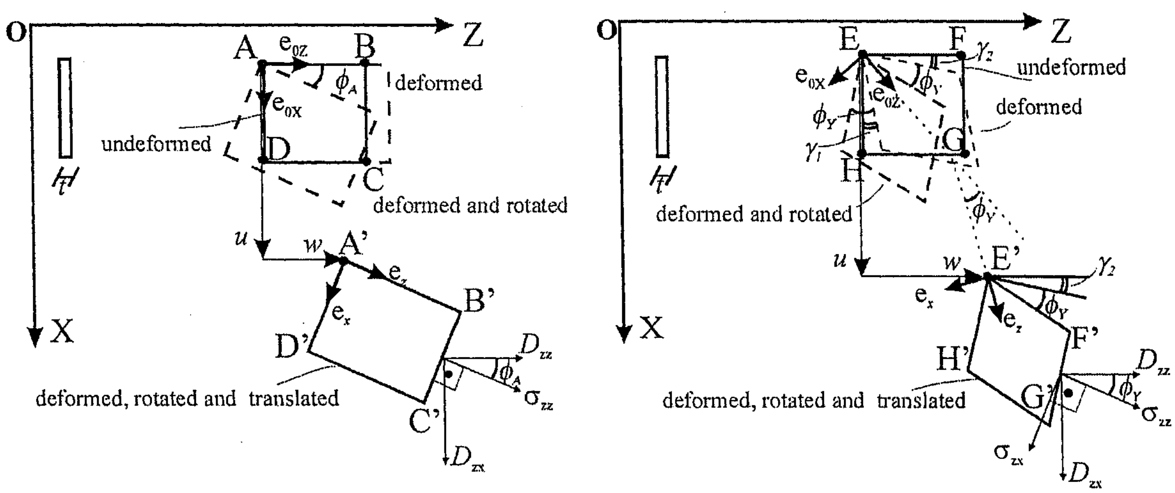

(a) stretching/shortening deformation (b) stretching/shortening and distortion

Fig. VI.A.1-Directions of First Piola-Kirchoff and Jaumann stresses

By omitting the terms higher than second order in the Taylor series expansion of trigonometric functions $\sin\phi_{\mathrm{Y}}$ and $\cos\phi_{\mathrm{Y}}$ i.e., $\sin\phi_{\mathrm{Y}} \approx \phi_{\mathrm{Y}}$, $\cos\phi_{\mathrm{Y}} \approx 1-\phi_{\mathrm{Y}}^2/2$ and using the approximation $\phi_{\mathrm{Y}} = u'_s$, one obtains the relation $\sigma_{zz} = D_{\mathrm{ZX}}R_{\mathrm{XZ}} + D_{\mathrm{ZZ}}R_{\mathrm{ZZ}}$ and $\sigma_{zx} = D_{\mathrm{ZX}}R_{\mathrm{XX}} + D_{\mathrm{ZZ}}R_{\mathrm{ZX}}$. In tensorial form, we have $\sigma_{ik} = D_{ij}R_{jk}$, $i,j,k = 1,2$, in which $R_{\mathrm{XZ}} = u'_s$, $R_{\mathrm{ZZ}} = 1-1/2(u'_s)^2$, $R_{\mathrm{ZX}} = -u'_s$ $R_{\mathrm{XX}} = 1-1/2(u'_s)^2$. The 3D form of the tensor R_{ij} is given in Eq. (VI.2).

Appendix VI.B- Formulation of Variational Expression in terms of Jaumann Stresses

The objective of this appendix is to obtain the functional to be used in the buckling analysis. The final equation is reported in Koiter (1976). However, the explicit mathematical manipulations were not given.

The complementary energy expression for semilinear material under finite deformations is given in Eq. (VI.45). The complementary energy functional is expanded according to Taylor series in the neighborhood of the configuration on set of buckling, i.e. $\sigma^*_{ik} = \lambda\sigma^p_{ik} + \Delta\sigma_{ik}$ and $R^*_{ij} = \lambda R^p_{ij} + \Delta R_{ij}$ as

$$\pi^*(\lambda\sigma^p_{ij}+\Delta\sigma_{ij}, \lambda R^p_{ij}+\Delta R_{ij}) = \pi^*(\lambda\sigma^p_{ij}, \lambda R^p_{ij}) + \delta\pi^*(\lambda\sigma^p_{ij}, \lambda R^p_{ij}) + 1/2\,\delta^2\pi^*(\lambda\sigma^p_{ij}, \lambda R^p_{ij}) + O(\Delta^3) \qquad \text{VI.B(1)}$$

In Eq. VI.B(1), λ is the buckling load factor, $O(\Delta^3)$ represents the sum of the terms higher than second order. Given that in the pre-buckling state, the stationarity condition $\delta\pi^*(\lambda\sigma^p_{ij}, \lambda R^p_{ij}) = 0$ is satisfied, Equation VI.B(1) simplifies to

$$\pi^*(\lambda\sigma^p_{ij}+\Delta\sigma_{ij}, \lambda R^p_{ij}+\Delta R_{ij}) - \pi^*(\lambda\sigma^p_{ij}, \lambda R^p_{ij}) \cong 1/2\,\delta^2\pi^*(\lambda\sigma^p_{ij}, \lambda R^p_{ij}) \qquad \text{VI.B(2)}$$

In Equation VI.B(2), the Taylor series terms beyond the second term were omitted. In a neutral equilibrium state, there exists an equilibrium and compatible state in the neighborhood of buckling load $\lambda\sigma^p_{ij}$ for which the first variation of the complementary energy vanishes. By using Eq. VI.B(2) and vanishing of the first variation of complementary energy at buckling load (Oran 1967 and Koiter 1976), we obtain the buckling criterion for complementary energy.

$$\delta\left[1/2\,\delta^2\pi^*(\lambda\sigma_{ij}^p,\lambda R_{ij}^p)\right]=0 \qquad \text{VI.B(3)}$$

When pre-buckling deformations are neglected, the rotation tensor at the onset of buckling becomes equal to the unit tensor i.e., $\lambda R_{ij}^p=\delta_{ij}$. From Eq. (VI.13), the increment in the rotation tensor can be expressed as

$$\Delta R_{ij}=\varepsilon_{imj}\Delta\phi_m+\frac{1}{2}\Delta\phi_i\Delta\phi_j-\delta_{ij}\frac{1}{2}\Delta\phi_m\Delta\phi_m \qquad \text{VI.B(4)}$$

By substituting Eqs. VI.B(4) and (VI.45) into Eq. VI.B(2), the second variation of the complementary energy is expressed as

$$\begin{aligned}
&\pi^*(\lambda R_{ij}^p+\Delta R_{ij},\lambda\sigma_{ij}^p+\Delta\sigma_{ij})-\pi^*(\lambda R_{ij}^p,\lambda\sigma_{ij}^p)\\
&=\int_{V_0}\left\{\frac{1}{4G}\left[\left(\lambda\sigma_{ij}^p+\Delta\sigma_{ij}\right)\left(\lambda\sigma_{ij}^p+\Delta\sigma_{ij}\right)-\frac{\nu}{1+\nu}\left(\lambda\sigma_{ii}^p+\Delta\sigma_{ii}\right)^2\right]\right.\\
&\qquad\left.+\left(\lambda\sigma_{ii}^p+\Delta\sigma_{ii}\right)-\left(\lambda R_{ij}^p+\Delta R_{ij}\right)\left(\lambda\sigma_{ji}^p+\Delta\sigma_{ji}\right)\right\}dV\\
&-\int_{V_0}\left[\frac{1}{4G}\left(\lambda^2\sigma_{ij}^p\sigma_{ij}^p-\frac{\nu}{1+\nu}\lambda^2\sigma_{ii}^{p2}\right)+\lambda\sigma_{ii}^p-\lambda^2R_{ij}^p\sigma_{ij}^p\right]dV
\end{aligned} \qquad \text{VI.B(5)}$$

From Eq. VI.B(5) by expanding the first, second and fourth terms and simplifying, one obtains

$$\begin{aligned}
&\pi^*(\lambda R_{ij}^p+\Delta R_{ij},\lambda\sigma_{ij}^p+\Delta\sigma_{ij})-\pi^*(\lambda R_{ij}^p,\lambda\sigma_{ij}^p)\\
&=\int_{V_0}\left\{\frac{1}{4G}\left[\left(2\lambda\sigma_{ij}^p\Delta\sigma_{ij}+\Delta\sigma_{ij}\Delta\sigma_{ij}\right)-\frac{\nu}{1+\nu}\left(2\lambda\sigma_{jj}^p\Delta\sigma_{ii}+\Delta\sigma_{ii}\Delta\sigma_{jj}\right)\right]+\Delta\sigma_{ii}\right.\\
&\qquad\left.-\left(\lambda R_{ij}^p\Delta\sigma_{ji}+\lambda\Delta R_{ij}\sigma_{ji}^p+\Delta R_{ij}\Delta\sigma_{ji}\right)\right\}dV
\end{aligned} \qquad \text{VI.B(6)}$$

By substituting Eq. VI.B(4) into Eq. VI.B(6), one obtains

$$\pi^*(\lambda R_{ij}^p + \Delta R_{ij}, \lambda\sigma_{ij}^p + \Delta\sigma_{ij}) - \pi^*(\lambda R_{ij}^p, \lambda\sigma_{ij}^p)$$
$$= \int_{V_0} \left\{ \frac{1}{2G}\left[\left(\lambda\sigma_{ij}^p \Delta\sigma_{ij}\right) - \frac{\nu}{1+\nu}\left(\lambda\sigma_{jj}^p\Delta\sigma_{ii}\right)\right] + \frac{1}{4G}\left[\left(\Delta\sigma_{ij}\Delta\sigma_{ij}\right) - \frac{\nu}{1+\nu}\left(\Delta\sigma_{ii}\right)^2\right] \right.$$
$$- \left(\varepsilon_{imj}\Delta\phi_m\lambda\sigma_{ji}^p + \frac{1}{2}\Delta\phi_i\Delta\phi_j\lambda\sigma_{ji}^p - \delta_{ij}\frac{1}{2}\Delta\phi_m\Delta\phi_m\lambda\sigma_{ji}^p \right) \qquad \text{VI.B(7)}$$
$$\left. - \left(\varepsilon_{imj}\Delta\phi_m\Delta\sigma_{ji} + \frac{1}{2}\Delta\phi_i\Delta\phi_j\Delta\sigma_{ji} - \delta_{kj}\frac{1}{2}\Delta\phi_m\Delta\phi_m\Delta\sigma_{ji}\right)\right\} dV$$

By nothing that $\delta_{ij}\sigma_{ji}^p = \sigma_{jj}^p$ and rearranging Eq. VI.B(7), one obtains

$$\pi^*(\lambda R_{ij}^p + \Delta R_{ij}, \lambda\sigma_{ij}^p + \Delta\sigma_{ij}) - \pi^*(\lambda R_{ij}^p, \lambda\sigma_{ij}^p)$$
$$= \int_{V_0} \left\{ \left(\frac{1}{2}\Delta\sigma_{ii}\Delta\phi_m\Delta\phi_m - \frac{1}{2}\Delta\sigma_{ji}\Delta\phi_i\Delta\phi_j \right) + \frac{1}{2G}\left[\left(\lambda\sigma_{ij}^p\Delta\sigma_{ij}\right) - \frac{\nu}{1+\nu}\left(\lambda\sigma_{jj}^p\Delta\sigma_{ii}\right)\right] \right.$$
$$- \varepsilon_{imj}\Delta\phi_m\lambda\sigma_{ji}^p - \varepsilon_{imj}\Delta\phi_m\Delta\sigma_{ji} \qquad \text{VI.B(8)}$$
$$\left. + \left(\frac{1}{2}\lambda\sigma_{ii}^p\Delta\phi_m\Delta\phi_m - \frac{1}{2}\lambda\sigma_{ji}^p\Delta\phi_i\Delta\phi_j \right) + \frac{1}{4G}\left[\left(\Delta\sigma_{ij}\Delta\sigma_{ij}\right) - \frac{\nu}{1+\nu}\left(\Delta\sigma_{ii}\right)^2\right]\right\} dV$$

The first variation of the complementary energy at the onset of buckling vanishes since the compatibility is satisfied i.e.,

$$\delta\pi^*(\lambda R_{ij}^p, \lambda\sigma_{ij}^p) = \int_{V_0} \left[\frac{1}{4G}\left(2\lambda\sigma_{ij}^p\Delta\sigma_{ij} - \frac{\nu}{1+\nu}2\lambda\sigma_{ii}^p\Delta\sigma_{jj}\right) + \delta\left(\lambda\sigma_{ii}^p - \lambda^2 R_{ij}^p\sigma_{ji}^p\right)\right] dV = 0 \qquad \text{VI.B(9)}$$

Since $\lambda R_{ij}^p = \delta_{ij}$ at the onset of buckling one obtains $\lambda\sigma_{ii}^p - \lambda^2 R_{ij}\sigma_{ji}^p = 0$ and the first variation of the complementary energy at the onset of buckling becomes

$$\delta\pi^*(\lambda R_{ij}^p, \lambda\sigma_{ij}^p) = \int_{V_0} \left[\frac{1}{2G}\left(\lambda\sigma_{ij}^p\Delta\sigma_{ij} - \frac{\nu}{1+\nu}\lambda\sigma_{ii}^p\Delta\sigma_{jj}\right)\right] dV = 0 \qquad \text{VI.B(10)}$$

By using the symmetry of the Jaumann stress tensor i.e., $\varepsilon_{imj}\Delta\phi_m\lambda\sigma_{ji}^p = 0$ and $\varepsilon_{imj}\Delta\phi_m\lambda\Delta\sigma_{ji} = 0$, neglecting third order small terms i.e., $\Delta\sigma_{ii}\Delta\phi_m\Delta\phi_m = 0$ and

$\Delta\sigma_{ji}\Delta\phi_i\Delta\phi_j = 0$ and by substituting Eq. VI.B(10) into Eq. VI.B(8) to yield the second variation of the complementary energy as

$$\frac{1}{2}\delta^2\pi^* = \int_{V_0}\frac{1}{2}\left(\lambda\sigma_{ii}^P\Delta\phi_m\Delta\phi_m - \lambda\sigma_{ij}^P\Delta\phi_j\Delta\phi_i\right) + \frac{1}{4G}\left[\Delta\sigma_{ij}\Delta\sigma_{ij} - \frac{\nu}{(1+\nu)}\left(\Delta\sigma_{ii}\right)^2\right]dV \qquad \text{VI.B(11)}$$

Equation VI.B(11) is the one in Eq. (VI.47).

Appendix VI.C -Deriving the Compatibility Equations and Boundary Conditions

This appendix is starting with the second variation of complementary energy in Eq. (VI.157) to formulate the compatibility Equations and Boundary conditions by evoking the stationarity condition.

The internal stress resultant fields ΔM_y, ΔB, ΔT_{sv}, $\Delta V_{x\alpha}$, ΔT_α and angle of twist (due to buckling) $\Delta\phi_z$ appearing in Eq. (VI.157) are the independent fields of the second variation of the complementary energy functional $\delta^2\pi^*$. By taking the variation of Eq. (VI.157) one obtains

$$\delta\left(\frac{1}{2}\delta^2\pi^*\right)$$
$$=\frac{1}{\lambda}\int_L\left\langle\left(-\Delta M_y{}'-\Delta V_{x\alpha}+\lambda V_y^p\Delta\phi_Z\right)\quad\left(\Delta B'+\Delta T_{sv}-\Delta T_\alpha\right)\right\rangle\mathbf{C}_{2\times2}^{-1}\begin{Bmatrix}\delta\left(-\Delta M_y{}'-\Delta V_{x\alpha}+\lambda V_y^p\Delta\phi_Z\right)\\ \delta\left(\Delta B'+\Delta T_{sv}-\Delta T_\alpha\right)\end{Bmatrix}dz$$
$$+\int_L\left\{\frac{1}{E}\left\langle\Delta M_y\quad\Delta B\right\rangle\mathbf{D}_{r2\times2}^{-1}\begin{Bmatrix}\delta\Delta M_y\\ \delta\Delta B\end{Bmatrix}+\frac{1}{G}\left\langle-\Delta M_y{}'\quad\Delta B'\right\rangle\boldsymbol{\chi}_{2\times2}^{-1}\begin{Bmatrix}-\delta\Delta M_y{}'\\ \delta\Delta B'\end{Bmatrix}+\delta\Delta T_{sv}\frac{\Delta T_{sv}}{GJ_d}\right\}dz \qquad \text{VI.C(1)}$$

From Eq. (VI.56) by substituting into Eq. VI.C(1) one obtains

$$\delta\left(\frac{1}{2}\delta^2\pi^*\right)=\int_L\left\langle\Delta u'\quad\Delta\phi_Z{}'\right\rangle\begin{Bmatrix}\delta\left(-\Delta M_y{}'-\Delta V_{x\alpha}+\lambda V_y^p\Delta\phi_Z\right)\\ \delta\left(\Delta B'+\Delta T_{sv}-\Delta T_\alpha\right)\end{Bmatrix}dz$$
$$+\int_L\left\{\frac{1}{E}\left\langle\Delta M_y\quad\Delta B\right\rangle\mathbf{D}_{r2\times2}^{-1}\begin{Bmatrix}\delta\Delta M_y\\ \delta\Delta B\end{Bmatrix}+\frac{1}{G}\left\langle-\Delta M_y{}'\quad\Delta B'\right\rangle\boldsymbol{\chi}_{2\times2}^{-1}\begin{Bmatrix}-\delta\Delta M_y{}'\\ \delta\Delta B'\end{Bmatrix}+\delta\Delta T_{sv}\frac{\Delta T_{sv}}{GJ_d}\right\}dz \qquad \text{VI.C(2)}$$

Equation VI.C(2) can be re-written as

$$\delta\left(\frac{1}{2}\delta^2\pi *\right)\left(\Delta u',\Delta\phi_Z,\Delta\phi_Z',\Delta M_y,\Delta M_y',\Delta B,\Delta B',\Delta T_{sv},\Delta T_\alpha,\Delta V_{x\alpha}\right)=$$

$$\int_L\left\langle \Delta u' \quad \Delta\phi_z'\right\rangle\begin{Bmatrix}\delta\left(-\Delta M_y'\right)\\ \delta\left(\Delta B'\right)\end{Bmatrix}dz-\int_L\left\langle \Delta u' \quad \Delta\phi_Z'\right\rangle\begin{Bmatrix}\delta\left(\Delta V_{x\alpha}\right)\\ \delta\left(\Delta T_\alpha\right)\end{Bmatrix}dz$$

$$+\int_L\left\langle \Delta u' \quad \Delta\phi_z'\right\rangle\begin{Bmatrix}\delta\left(\lambda V_y^p\Delta\phi_Z\right)\\ \delta\left(\Delta T_{sv}\right)\end{Bmatrix}dz \tag{VI.C(3)}$$

$$+\int_L\frac{1}{E}\left\langle \Delta M_y \quad \Delta B\right\rangle\mathbf{D}_{r2\times2}^{-1}\begin{Bmatrix}\delta\Delta M_y\\ \delta\Delta B\end{Bmatrix}dz$$

$$+\int_L\frac{1}{G}\left\langle -\Delta M_y' \quad \Delta B'\right\rangle\boldsymbol{\chi}_{2\times2}^{-1}\begin{Bmatrix}-\delta\Delta M_y'\\ \delta\Delta B'\end{Bmatrix}dz$$

$$+\int_L\delta\Delta T_{sv}\frac{\Delta T_{sv}}{GJ_d}dz$$

By performing integration by parts, for the first, second and fifth terms in Eq. VI.C(3) and noting that $\Delta V_{x\alpha}'=0$ and $\Delta T_\alpha'=0$ .one obtains

$$\delta\left(\frac{1}{2}\delta^2\pi *\right)=\left[\left\langle \Delta u' \quad \Delta\phi_Z'\right\rangle\begin{Bmatrix}\delta\left(-\Delta M_y\right)\\ \delta\left(\Delta B\right)\end{Bmatrix}\right]_0^L-\int_L\left\langle \Delta u'' \quad \Delta\phi_Z''\right\rangle\begin{Bmatrix}\delta\left(-\Delta M_y\right)\\ \delta\left(\Delta B\right)\end{Bmatrix}dz$$

$$-\left[\left\langle \Delta u \quad \Delta\phi_Z\right\rangle\begin{Bmatrix}\delta\left(\Delta V_{x\alpha}\right)\\ \delta\left(\Delta T_\alpha\right)\end{Bmatrix}\right]_0^L$$

$$+\int_L\left[\left\langle \Delta u' \quad \Delta\phi_Z'\right\rangle\begin{Bmatrix}\delta\left(\lambda V_y^p\Delta\phi_Z\right)\\ \delta\left(\Delta T_{sv}\right)\end{Bmatrix}\right]dz \tag{VI.C(4)}$$

$$+\int_L\frac{1}{E}\left\langle \Delta M_y \quad \Delta B\right\rangle\mathbf{D}_{r2\times2}^{-1}\begin{Bmatrix}\delta\Delta M_y\\ \delta\Delta B\end{Bmatrix}dz$$

$$+\frac{1}{G}\left\langle -\Delta M_y' \quad \Delta B'\right\rangle\boldsymbol{\chi}_{2\times2}^{-1}\begin{Bmatrix}-\delta\Delta M_y\\ \delta\Delta B\end{Bmatrix}_0^L-\int_L\frac{1}{G}\left\langle -\Delta M_y'' \quad \Delta B''\right\rangle\boldsymbol{\chi}_{2\times2}^{-1}\begin{Bmatrix}-\delta\Delta M_y\\ \delta\Delta B\end{Bmatrix}dz$$

$$+\int_L\delta\Delta T_{sv}\frac{\Delta T_{sv}}{GJ_d}dz$$

Eq. VI.C(4) can be expanded to yield

$$\delta\left(\frac{1}{2}\delta^2\pi^*\right)=\left[\delta\left(-\Delta M_y\right)\Delta u'\right]_0^L+\left[\delta\left(\Delta B\right)\Delta\phi_Z'\right]_0^L-\int_L \Delta u''\delta\left(-\Delta M_y\right)dz-\int_L \Delta\phi_Z''\delta\left(\Delta B\right)dz$$
$$-\left[\delta\left(\Delta V_{x\alpha}\right)\Delta u\right]_0^L-\left[\delta\left(\Delta T_\alpha\right)\Delta\phi_Z\right]_0^L+\int_L \Delta u'\delta\left(\lambda V_y^p\Delta\phi_z\right)dz+\int_L \Delta\phi_Z'\delta\left(\Delta T_{sv}\right)dz$$
$$+\int_L\frac{1}{E}\left\langle \Delta M_y \quad \Delta B\right\rangle \mathbf{D}_{r2\times2}^{-1}\begin{Bmatrix}1\\0\end{Bmatrix}\delta\Delta M_y dz+\int_L\frac{1}{E}\left\langle \Delta M_y \quad \Delta B\right\rangle \mathbf{D}_{r2\times2}^{-1}\begin{Bmatrix}0\\1\end{Bmatrix}\delta\Delta B dz$$
$$+\frac{1}{G}\left[\left\langle -\Delta M_y' \quad \Delta B'\right\rangle \boldsymbol{\chi}_{2\times2}^{-1}\begin{Bmatrix}-1\\0\end{Bmatrix}\delta\Delta M_y\right]_0^L+\frac{1}{G}\left[\left\langle -\Delta M_y' \quad \Delta B'\right\rangle \boldsymbol{\chi}_{2\times2}^{-1}\begin{Bmatrix}0\\1\end{Bmatrix}\delta\Delta B\right]_0^L \qquad \text{VI.C(5)}$$
$$-\int_L\frac{1}{G}\left\langle -\Delta M_y'' \quad \Delta B''\right\rangle \boldsymbol{\chi}_{2\times2}^{-1}\begin{Bmatrix}-1\\0\end{Bmatrix}\delta\Delta M_y dz-\int_L\frac{1}{G}\left\langle -\Delta M_y'' \quad \Delta B''\right\rangle \boldsymbol{\chi}_{2\times2}^{-1}\begin{Bmatrix}0\\1\end{Bmatrix}\delta\Delta B dz$$
$$+\int_L \delta\Delta T_{sv}\frac{\Delta T_{sv}}{GJ_d}dz$$

By grouping the factors of $\delta\Delta M_y, \delta\Delta B, \delta\Delta T_{sv}, \delta\Delta V_{x\alpha}$ and $\delta\Delta T_{x\alpha}$ one obtains

$$\delta\left(\frac{1}{2}\delta^2\pi^*\right)=$$
$$\int_L \delta\Delta M_y\left[\Delta u''+\frac{1}{E}\left\langle \Delta M_y \quad \Delta B\right\rangle \mathbf{D}_{r2\times2}^{-1}\begin{Bmatrix}1\\0\end{Bmatrix}-\frac{1}{G}\left\langle -\Delta M_y'' \quad \Delta B''\right\rangle \boldsymbol{\chi}_{2\times2}^{-1}\begin{Bmatrix}-1\\0\end{Bmatrix}\right]dz$$
$$+\int_L \delta\Delta B\left[-\Delta\phi_Z''+\frac{1}{E}\left\langle \Delta M_y \quad \Delta B\right\rangle \mathbf{D}_{r2\times2}^{-1}\begin{Bmatrix}0\\1\end{Bmatrix}-\frac{1}{G}\left\langle -\Delta M_y'' \quad \Delta B''\right\rangle \boldsymbol{\chi}_{2\times2}^{-1}\begin{Bmatrix}0\\1\end{Bmatrix}\right]dz$$
$$+\int_L \delta\Delta T_{sv}\left[\Delta\phi_Z'+\frac{\Delta T_{sv}}{GJ_d}\right]dz$$
$$+\int_L\left[\delta\left(\Delta\phi_Z\right)\lambda V_y^p\Delta u'\right]dz$$
$$+\delta\Delta M_y\left[\frac{1}{G}\left\langle -\Delta M_y' \quad \Delta B'\right\rangle \boldsymbol{\chi}_{2\times2}^{-1}\begin{Bmatrix}-1\\0\end{Bmatrix}-\Delta u'\right]_0^L$$
$$+\delta\Delta B\left[\frac{1}{G}\left\langle -\Delta M_y' \quad \Delta B'\right\rangle \boldsymbol{\chi}_{2\times2}^{-1}\begin{Bmatrix}0\\1\end{Bmatrix}+\Delta\phi_Z'\right]_0^L \qquad \text{VI.C(6)}$$
$$-\left[\delta\Delta V_{x\alpha}\Delta u\right]_0^L-\left[\delta\Delta T_{x\alpha}\Delta\phi_Z\right]_0^L$$

By substituting the relations $\Delta\phi_X(z,x)=\left(a_x-x\right)\Delta\phi_Z'$ and $\Delta\phi_Y(z,y)=\Delta u'(z)-\left(y-a_y\right)\Delta\phi_Z'$

into Eqs. (VI.23 a-d), one obtains

$$-\lambda\sigma_{zx}^{p}\left(x-a_x\right)\Delta\phi_Z'=0 \qquad \text{VI.C(7)}$$

and

$$\lambda\sigma_{yz}^{p}\left[\Delta u'(z)-\left(y-a_y\right)\Delta\phi_Z'\right]=0 \qquad \text{VI.C(8)}$$

By substituting the relations $x-a_x=h\sin\alpha$, $y-a_y=-h\cos\alpha$ into Eqs. VI.C(7) and VI.C(8) respectively, summing and integrating over the cross-sectional area, one obtains

$$\lambda\int_A \sigma_{zx}^{p}\left[-h\sin\alpha\Delta\phi_z'\right]+\sigma_{yz}^{p}\left[\Delta u'(z)+h\cos\alpha\Delta\phi_z'\right]dA=0 \qquad \text{VI.C(9)}$$

By substituting the relations $\sigma_{zx}\sin\alpha-\sigma_{zy}\cos\alpha=0$ and $\int_A \sigma_{yz}^{p}dA=V_y^p$ into Eq. VI.C(9) one obtains

$$\lambda V_y^p\Delta u'(z)=0 \qquad \text{VI.C(10)}$$

Equation VI.C(10) suggests that $\int_L \lambda V_y^p\Delta u'(z)dz$ vanishes in the last integral terms of Eq. VI.C(6). This outcome is consistent with the assumptions made. From Eq. VI.C(6), one obtains the field equations as

$$\Delta u''+\frac{1}{E}\left\langle \Delta M_y \quad \Delta B\right\rangle \mathbf{D}_{r2\times2}^{-1}\begin{Bmatrix}1\\0\end{Bmatrix}+\frac{1}{G}\left\langle -\Delta M_y'' \quad \Delta B''\right\rangle \boldsymbol{\chi}_{2\times2}^{-1}\begin{Bmatrix}1\\0\end{Bmatrix}=0$$

$$-\Delta\phi_Z''+\frac{1}{E}\left\langle \Delta M_y \quad \Delta B\right\rangle \mathbf{D}_{r2\times2}^{-1}\begin{Bmatrix}0\\1\end{Bmatrix}-\frac{1}{G}\left\langle -\Delta M_y'' \quad \Delta B''\right\rangle \boldsymbol{\chi}_{2\times2}^{-1}\begin{Bmatrix}0\\1\end{Bmatrix}=0 \qquad \text{VI.C(11)a-c}$$

$$\Delta\phi_Z'+\frac{\Delta T_{sv}}{GJ_d}=0$$

and the boundary conditions can be obtained as

Either ΔM_y is specified or $-\Delta u'+\frac{1}{G}\left\langle -\Delta M_y' \quad \Delta B'\right\rangle \boldsymbol{\chi}_{2\times2}^{-1}\begin{Bmatrix}-1\\0\end{Bmatrix}=0$

Either ΔB is specified or $\Delta\phi_Z{}'+\frac{1}{G}\left\langle -\Delta M_y{}' \quad \Delta B'\right\rangle \chi_{2\times 2}^{-1}\begin{Bmatrix}0\\1\end{Bmatrix}=0$ VI.C(12)a-d

Either $\Delta V_{x\alpha}$ is specified or $\Delta u = 0$

Either ΔT_α is specified or $\Delta\phi_Z = 0$

Simplification under Orthogonal Coordinates

From Equation VI.C(6), by adopting principal orthogonal coordinates i.e., $S_x = S_y = J_{xy} = J_{\omega x} = J_{\omega y} = 0$, one obtains

$$\delta\left(\frac{1}{2}\delta^2\pi^*\right)=$$

$$\int_L\left[\delta\Delta M_y\left(\Delta u''+\frac{\Delta M_y}{EJ_{yy}}-\frac{\Delta M_y{}''}{G\chi_{11}}\right)+\delta\Delta B\left(-\Delta\phi_Z{}''+\frac{\Delta B}{EJ_{ww}}-\frac{\Delta B''}{G\chi_{22}}\right)+\delta\Delta T_{sv}\left(\Delta\phi_Z{}'+\frac{\Delta T_{sv}}{GJ_d}\right)\right]dz \quad \text{VI.C(13)}$$

$$+\delta\Delta M_y\left[-\Delta u'+\frac{\Delta M_y{}'}{G\chi_{11}}\right]_0^L+\delta\Delta B\left[\Delta\phi_Z{}'+\frac{\Delta B'}{G\chi_{22}}\right]_0^L-\delta\Delta V_{x\alpha}\left[\Delta u\right]_0^L-\delta\Delta T_\alpha\left[\Delta\phi_Z\right]_0^L$$

From Eq. VI.C(13) the field equations are

$$\Delta\Delta u''+\frac{\Delta M_y}{EJ_{yy}}-\frac{\Delta M_y{}''}{G\chi_{11}}=0$$

$$-\Delta\phi_Z{}''+\frac{\Delta B}{EJ_{ww}}-\frac{\Delta B''}{G\chi_{22}}=0 \quad \text{VI.C(14)a-c}$$

$$\Delta\phi_Z{}'+\frac{\Delta T_{sv}}{GJ_d}=0$$

and the boundary conditions are

Either ΔM_y is specified or $-\Delta u'+\frac{\Delta M_y{}'}{G\chi_{11}}=0$

Either ΔB is specified or $\Delta\phi_Z{}'+\frac{\Delta B'}{G\chi_{22}}=0$ VI.C(15)a-d

Either $\Delta V_{x\alpha}$ is specified or $\Delta u = 0$

Either ΔT_{α} is specified or $\Delta \phi_{Z} = 0$

Equations VI.C(14)a-c are compatibility relations while Eq. VI.C(15)a-c are the boundary conditions.

Appendix VI.D-Element Matrices

In this appendix, the sub-matrices of the element geometric stiffness matrix $\mathbf{K}^{(i)}_{\mathbf{g}\ 8\times8}$ and matrix $\mathbf{B}^{(i)}_{13\times13}$ are explicitly given for an element (i) of length $L^{(i)}$.

Geometric Stiffness Matrix $\mathbf{K}^{(i)}_{\mathbf{g}\ 8\times8}$

In Eq. (VI.94), sub-matrices $\mathbf{K}^{(i)}_{\mathbf{g1}\ 4\times4}$ and $\mathbf{K}^{(i)}_{\mathbf{g2}\ 4\times4}$ were introduced to express the geometric stiffness matrix $\mathbf{K}^{(i)}_{\mathbf{g}\ 8\times8}$. The entries of $\mathbf{K}^{(i)}_{\mathbf{g1}\ 4\times4}$ and $\mathbf{K}^{(i)}_{\mathbf{g2}\ 4\times4}$ are

$$\mathbf{K}^{(i)}_{\mathbf{g1}\ 4\times4} = \begin{bmatrix} \frac{6}{5L^{(i)}} & \frac{1}{10} & -\frac{6}{5L^{(i)}} & \frac{1}{10} \\ \frac{1}{10} & \frac{2L^{(i)}}{15} & -\frac{1}{10} & -\frac{L^{(i)}}{30} \\ -\frac{6}{5L^{(i)}} & -\frac{1}{10} & \frac{6}{5L^{(i)}} & -\frac{1}{10} \\ \frac{1}{10} & -\frac{L^{(i)}}{30} & -\frac{1}{10} & \frac{2L^{(i)}}{15} \end{bmatrix} \qquad \text{VI.D(1)}$$

$$\mathbf{K}^{(i)}_{\mathbf{g2}\ 4\times4} = \begin{bmatrix} \frac{3}{5} & \frac{L^{(i)}}{10} & \frac{-3}{5} & 0 \\ \frac{L^{(i)}}{10} & \frac{\left(L^{(i)}\right)^2}{30} & -\frac{L^{(i)}}{10} & -\frac{\left(L^{(i)}\right)^2}{60} \\ -\frac{3}{5} & -\frac{L^{(i)}}{10} & \frac{3}{5} & 0 \\ 0 & -\frac{\left(L^{(i)}\right)^2}{60} & 0 & \frac{\left(L^{(i)}\right)^2}{10} \end{bmatrix} \qquad \text{VI.D(2)}$$

Matrix $\mathbf{B}^{(i)}_{13\times13}$

In Eq. (VI.97), matrix $\mathbf{B}^{(i)}_{13\times13}$ was partitioned into submatrices $\mathbf{B}^{(i)}_{\mathbf{t}\ 1\times1}$, $\mathbf{B}^{(i)}_{\mathbf{tf}\ 1\times4}$, $\mathbf{B}^{(i)}_{\mathbf{td}\ 1\times8}$, $\mathbf{B}^{(i)}_{\mathbf{f}\ 4\times4}$, $\mathbf{B}^{(i)}_{\mathbf{fd}\ 4\times8}$ and $\mathbf{B}^{(i)}_{\mathbf{d}\ 8\times8}$. The entries for these submatrices are formulated in the following. From Eqs. (VI.86) through (VI.91) by expressing in terms of the vectors using the vectors $\mathbf{\Delta t}^{(i)}_{1\times1}$, $\mathbf{\Delta f}^{(i)T}_{\mathbf{N}\ 1\times4}$ and $\mathbf{\Delta d}^{(i)T}_{\mathbf{N}\ 1\times8}$ defined in Eqs. (VI.96) through (VI.98), one can express the internal stress resultant fields for element i as

$$\begin{Bmatrix} \Delta M_y^{(i)} \\ \Delta B^{(i)} \end{Bmatrix} = \lambda\left(\mathbf{m}^{(i)}{}_{2\times4}\mathbf{\Delta f}^{(i)}_{\mathbf{N}\ 4\times1} + \mathbf{m}^{(i)}_{\mathbf{d}\ 2\times8}\mathbf{\Delta d}^{(i)}_{\mathbf{N}\ 8\times1} + \mathbf{m}^{(i)}_{\mathbf{dv}2\times8}\mathbf{\Delta d}^{(i)}_{\mathbf{N}\ 8\times1}\right) \qquad \text{VI.D(3)}$$

$$\begin{Bmatrix} \Delta V_x^{(i)} \\ \Delta T_w^{(i)} \end{Bmatrix} = \lambda\left(\mathbf{v}^{(i)}{}_{2\times4}\mathbf{\Delta f}^{(i)}_{\mathbf{N}\ 4\times1} + \mathbf{v}^{(i)}_{\mathbf{d}\ 2\times8}\mathbf{\Delta d}^{(i)}_{\mathbf{N}\ 8\times1} + \mathbf{v}^{(i)}_{\mathbf{dv}2\times8}\mathbf{\Delta d}^{(i)}_{\mathbf{N}\ 8\times1}\right) \qquad \text{VI.D(4)}$$

$$\Delta T_{sv}^{(i)} = \lambda\left(\mathbf{\Delta t}^{(i)}_{1\times1} - \mathbf{t}^{(i)}{}_{1\times4}\mathbf{\Delta f}^{(i)}_{\mathbf{N}\ 4\times1} + \mathbf{t}^{(i)}_{\mathbf{d}\ 1\times8}\mathbf{\Delta d}^{(i)}_{\mathbf{N}\ 8\times1}\right) \qquad \text{VI.D(5)}$$

In Eqs. VI.D(3) through VI.D (5), matrices $\mathbf{m}^{(i)}{}_{2\times4}$, $\mathbf{m}^{(i)}_{\mathbf{d}\ 2\times8}$, $\mathbf{m}^{(i)}_{\mathbf{dv}2\times8}$, $\mathbf{v}^{(i)}{}_{2\times4}$, $\mathbf{v}^{(i)}_{\mathbf{d}\ 2\times8}$, $\mathbf{v}^{(i)}_{\mathbf{dv}2\times8}$, $\mathbf{t}^{(i)}{}_{1\times4}$ and $\mathbf{t}^{(i)}_{\mathbf{d}\ 1\times8}$ contain the interpolation functions and are defined as

$$\mathbf{m}^{(i)}{}_{2\times4} = \left[\begin{array}{cc|cc} \left(1-z/L^{(i)}\right) & z/L^{(i)} & 0 & 0 \\ \hline 0 & 0 & \left(1-z/L^{(i)}\right) & z/L^{(i)} \end{array}\right] \qquad \text{VI.D(6)}$$

$$\mathbf{m}^{(i)}_{\mathbf{d}\ 2\times8} = \left[\begin{array}{c|c} -N^{p(i)}\mathbf{H}(z)^T_{1\times4} & \left(M_{x0}^{p(i)} - a_y N^{p(i)}\right)\mathbf{H}(z)^T_{1\times4} \\ \hline -\left(M_{x0}^{p(i)} - a_y N^{p(i)}\right)\mathbf{H}(z)^T_{1\times4} & \left[N^{p(i)}\left(r_{N0}{}^2 + a_y{}^2 + a_x{}^2\right) + \beta_{Nx} M_{x0}^{p(i)}\right]\mathbf{H}(z)^T_{1\times4} \end{array}\right] \qquad \text{VI.D(7)}$$

$$\mathbf{m}^{(i)}_{\mathbf{dv}2\times8} = \left[\begin{array}{c|c} 0_{1\times4} & V_y^{pi}\left(\mathbf{Q}(z)^T_{1\times4} + \mathbf{G}(z)^T_{1\times4}\right) \\ \hline -V_y^{p(i)}\left(\mathbf{Q}(z)^T_{1\times4} + \mathbf{G}(L^{(i)})^T_{1\times4} z/L^{(i)}\right) & V_y^{p(i)}\beta_{Nx}\left(\mathbf{Q}(z)^T_{1\times4} + \mathbf{G}(L^{(i)})^T_{1\times4} z/L^{(i)}\right) \end{array}\right] \qquad \text{VI.D(8)}$$

in which $\mathbf{Q}(z)^T_{1\times4} = \int z\mathbf{H'}(z)^T_{1\times4}\,dz$

$$\mathbf{v}^{(i)}{}_{2\times4} = \left[\begin{array}{cc|cc} 1/L^{(i)} & -1/L^{(i)} & 0 & 0 \\ \hline 0 & 0 & -1/L^{(i)} & 1/L^{(i)} \end{array}\right] \qquad \text{VI.D(9)}$$

$$\mathbf{v}^{(i)}_{\mathbf{d}\ 2\times8} = \left[\begin{array}{c|c} N^{p(i)}\mathbf{H'}(z)^T_{1\times4} & -\left(M_{x0}^{p(i)} - a_y N^{p(i)}\right)\mathbf{H'}(z)^T_{1\times4} \\ \hline -\left(M_{x0}^{p(i)} - a_y N^{p(i)}\right)\mathbf{H'}(z)^T_{1\times4} & \left[N^{p(i)}\left(r_{N0}{}^2 + a_y{}^2 + a_x{}^2\right) + \beta_{Nx} M_{x0}^{p(i)}\right]\mathbf{H'}(z)^T_{1\times4} \end{array}\right]$$

VI.D(10)

$$\mathbf{v}^{(i)}_{\mathbf{dv}\,2\times8}=\left[\begin{array}{c|c} 0_{1\times4} & -V_y^{p(i)}\left(z\mathbf{H'}(z)^T_{1\times4}+\mathbf{H}(z)^T_{1\times4}\right) \\ \hline -V_y^{p(i)}\left(z\mathbf{H'}(z)^T_{1\times4}+\mathbf{G}(L^{(i)})^T_{1\times4}/L^{(i)}\right) & V_y^{p(i)}\beta_{Nx}\left(z\mathbf{H'}(z)^T_{1\times4}+\mathbf{G}(L^{(i)})^T_{1\times4}/L^{(i)}\right) \end{array}\right] \quad \text{VI.D(11)}$$

$$\mathbf{t}^{(i)}{}_{1\times4}=\left\langle 0 \quad 0 \mid -1/L^{(i)} \quad 1/L^{(i)}\right\rangle \quad \text{VI.D(12)}$$

$$\mathbf{t}^{(i)}_{\mathbf{d}\;1\times8}=\left\langle \frac{V_y^{p(i)}}{2} \quad \frac{V_y^{p(i)}L^{(i)}}{12} \quad \frac{V_y^{p(i)}}{2} \quad -\frac{V_y^{p(i)}L^{(i)}}{12} \;\middle|\; \frac{-V_y^{pi}\beta_{Nx}}{2} \quad \frac{-V_y^{pi}\beta_{Nx}L^{(i)}}{12} \quad \frac{-V_y^{p(i)}\beta_{Nx}}{2} \quad \frac{V_y^{p(i)}\beta_{Nx}L^{(i)}}{12}\right\rangle$$

VI.D(13)

From Eqs. VI.D(3) through VI.D(5), by substituting into Eq. (VI.94), one obtains the second variation of complementary energy for element i as

$$\begin{aligned}
\delta^2\pi^{*(i)}=\lambda\Big\{ & N\Delta\mathbf{u}^{(i)T}_{\mathbf{N}\,1\times4}\mathbf{K}^{(i)}_{\mathbf{g1}\,4\times4}\Delta\mathbf{u}^{(i)}_{\mathbf{N}\,4\times1}-2\Delta\mathbf{u}^{(i)T}_{\mathbf{N}\,1\times4}\left[\left(M^{p\,i}_{x0}-a_yN\right)\mathbf{K}^{(i)}_{\mathbf{g1}\,4\times4}+V_y^{pi}\mathbf{K}^{(i)}_{\mathbf{g2}\,4\times4}\right]_{4\times4}\Delta\boldsymbol{\varphi}^{(i)}_{\mathbf{N}\,4\times1} \\
&+\Delta\boldsymbol{\varphi}^{(i)T}_{\mathbf{N}\,1\times4}\left\{\left[N^{p(i)}\left(r_{N0}{}^2+a_y{}^2+a_x{}^2\right)+\beta_{Nx}M^{p(i)}_{x0}\right]\mathbf{K}^{(i)}_{\mathbf{g1}\,4\times4}\right\}_{4\times4}\Delta\boldsymbol{\varphi}^{(i)}_{\mathbf{N}\,4\times1} \\
&+\beta_{Nx}V_y^{p(i)}\Delta\boldsymbol{\varphi}^{(i)T}_{\mathbf{N}\,1\times4}\mathbf{K}^{(i)}_{\mathbf{g2}\,4\times4}\Delta\boldsymbol{\varphi}^{(i)}_{\mathbf{N}\,4\times1}\Big\} \\
&+\lambda^2\int_{L^i}\Big\{\frac{1}{E}\Delta\mathbf{f}^{(i)T}_{\mathbf{N}\,1\times4}\mathbf{m}^{(i)T}{}_{4\times2}\mathbf{D}^{-1}_{\mathbf{r}\,2\times2}\left[\mathbf{m}^{(i)}{}_{2\times4}\Delta\mathbf{f}^{(i)}_{\mathbf{N}\,4\times1}+\left(\mathbf{m}^{(i)}_{\mathbf{d}\;2\times8}+\mathbf{m}^{(i)}_{\mathbf{dv}\,2\times8}\right)\Delta\mathbf{d}^{(i)}_{\mathbf{N}\,8\times1}\right] \\
&\quad+\frac{1}{E}\Delta\mathbf{d}^{(i)T}_{\mathbf{N}\,1\times8}\mathbf{m}^{(i)T}_{\mathbf{d}\;8\times2}\mathbf{D}^{-1}_{\mathbf{r}\,2\times2}\left[\mathbf{m}^{(i)}{}_{2\times4}\Delta\mathbf{f}^{(i)}_{\mathbf{N}\,4\times1}+\left(\mathbf{m}^{(i)}_{\mathbf{d}\;2\times8}+\mathbf{m}^{(i)}_{\mathbf{dv}\,2\times8}\right)\Delta\mathbf{d}^{(i)}_{\mathbf{N}\,8\times1}\right] \\
&\quad+\frac{1}{E}\Delta\mathbf{d}^{(i)T}_{\mathbf{N}\,1\times8}\mathbf{m}^{(i)T}_{\mathbf{dv}\,8\times2}\mathbf{D}^{-1}_{\mathbf{r}\,2\times2}\left[\mathbf{m}^{(i)}{}_{2\times4}\Delta\mathbf{f}^{(i)}_{\mathbf{N}\,4\times1}+\left(\mathbf{m}^{(i)}_{\mathbf{d}\;2\times8}+\mathbf{m}^{(i)}_{\mathbf{dv}\,2\times8}\right)\Delta\mathbf{d}^{(i)}_{\mathbf{N}\,8\times1}\right] \\
&\quad+\frac{1}{G}\Delta\mathbf{f}^{(i)T}_{\mathbf{N}\,1\times4}\mathbf{v}^{(i)T}{}_{4\times2}\boldsymbol{\chi}^{-1}_{2\times2}\left[\mathbf{v}^{(i)}{}_{2\times4}\Delta\mathbf{f}^{(i)}_{\mathbf{N}\,4\times1}+\left(\mathbf{v}^{(i)}_{\mathbf{d}\;2\times8}+\mathbf{v}^{(i)}_{\mathbf{dv}\,2\times8}\right)\Delta\mathbf{d}^{(i)}_{\mathbf{N}\,8\times1}\right] \\
&\quad+\frac{1}{G}\Delta\mathbf{d}^{(i)T}_{\mathbf{N}\,1\times8}\mathbf{v}^{(i)T}_{\mathbf{d}\;8\times2}\boldsymbol{\chi}^{-1}_{2\times2}\left[\mathbf{v}^{(i)}{}_{2\times4}\Delta\mathbf{f}^{(i)}_{\mathbf{N}\,4\times1}+\left(\mathbf{v}^{(i)}_{\mathbf{d}\;2\times8}+\mathbf{v}^{(i)}_{\mathbf{dv}\,2\times8}\right)\Delta\mathbf{d}^{(i)}_{\mathbf{N}\,8\times1}\right] \\
&\quad+\frac{1}{G}\Delta\mathbf{d}^{(i)T}_{\mathbf{N}\,1\times8}\mathbf{v}^{(i)T}_{\mathbf{dv}\,8\times2}\boldsymbol{\chi}^{-1}_{2\times2}\left[\mathbf{v}^{(i)}{}_{2\times4}\Delta\mathbf{f}^{(i)}_{\mathbf{N}\,4\times1}+\left(\mathbf{v}^{(i)}_{\mathbf{d}\;2\times8}+\mathbf{v}^{(i)}_{\mathbf{dv}\,2\times8}\right)\Delta\mathbf{d}^{(i)}_{\mathbf{N}\,8\times1}\right] \\
&\quad+\frac{1}{GJ_d}\left(\Delta\mathbf{t}^{(i)}_{1\times1}-\mathbf{t}^{(i)}{}_{1\times4}\Delta\mathbf{f}^{(i)}_{\mathbf{N}\,4\times1}\right)^2+\frac{1}{GJ_d}\left(\mathbf{t}^{(i)}_{\mathbf{d}\;1\times8}\Delta\mathbf{d}^{(i)}_{\mathbf{N}\,8\times1}\right)^2 \\
&\quad+\frac{1}{GJ_d}2\mathbf{t}^{(i)}_{\mathbf{d}\;1\times8}\Delta\mathbf{d}^{(i)}_{\mathbf{N}\,8\times1}\left(\Delta\mathbf{t}^{(i)}_{1\times1}-\mathbf{t}^{(i)}{}_{1\times4}\Delta\mathbf{f}^{(i)}_{\mathbf{N}\,4\times1}\right)\Big\}dz
\end{aligned}$$

VI.D(14)

By substituting Eqs. VI.D(6) through VI.D(12) into Eq. VI.D(14), one obtains

$$
\begin{aligned}
\delta^2\pi^{*(i)} = \lambda\Big\{ & N\Delta\mathbf{u}^{(i)T}_{\mathbf{N}\ 1\times4}\mathbf{K}^{(i)}_{\mathbf{g1}\ 4\times4}\Delta\mathbf{u}^{(i)}_{\mathbf{N}\ 4\times1} \\
& -2\Delta\mathbf{u}^{(i)T}_{\mathbf{N}\ 1\times4}\Big[\Big(M^{p\,i}_{x0}-a_yN\Big)\mathbf{K}^{(i)}_{\mathbf{g1}\ 4\times4}+V^{pi}_y\mathbf{K}^{(i)}_{\mathbf{g2}\ 4\times4}\Big]_{4\times4}\Delta\boldsymbol{\varphi}^{(i)}_{\mathbf{N}\ 4\times1} \\
& +\Delta\boldsymbol{\varphi}^{(i)T}_{\mathbf{N}\ 1\times4}\Big\{\Big[N^{p(i)}\Big(r_{N0}{}^2+a_y{}^2+a_x{}^2\Big)+\beta_{Nx}M^{p(i)}_{x0}\Big]\mathbf{K}^{(i)}_{\mathbf{g1}\ 4\times4}\Big\}_{4\times4}\Delta\boldsymbol{\varphi}^{(i)}_{\mathbf{N}\ 4\times1} \\
& +\beta_{Nx}V^{p(i)}_y\Delta\boldsymbol{\varphi}^{(i)T}_{\mathbf{N}\ 1\times4}\mathbf{K}^{(i)}_{\mathbf{g2}\ 4\times4}\Delta\boldsymbol{\varphi}^{(i)}_{\mathbf{N}\ 4\times1}\Big\} \\
+\lambda^2\Big\langle \Delta\mathbf{t}^{(i)}_{1\times1} \ \Big|\ & \Delta\mathbf{f}^{(i)T}_{\mathbf{N}\ 1\times4}\ \Big|\ \Delta\mathbf{d}^{(i)T}_{\mathbf{N}\ 1\times8}\Big\rangle
\left[\begin{array}{c|c|c}
\mathbf{B}^{(i)}_{\mathbf{t}\ 1\times1} & \mathbf{B}^{(i)}_{\mathbf{tf}\ 1\times4} & \mathbf{B}^{(i)}_{\mathbf{td}\ 1\times8} \\ \hline
\mathbf{B}^{(i)T}_{\mathbf{tf}\ 4\times1} & \mathbf{B}^{(i)}_{\mathbf{f}\ 4\times4} & \mathbf{B}^{(i)}_{\mathbf{fd}\ 4\times8} \\ \hline
\mathbf{B}^{(i)T}_{\mathbf{td}\ 8\times1} & \mathbf{B}^{(i)T}_{\mathbf{fd}\ 8\times4} & \mathbf{B}^{(i)}_{\mathbf{d}\ 8\times8}
\end{array}\right]
\left\{\begin{array}{c}
\Delta\mathbf{t}^{(i)}_{1\times1} \\ \hline
\Delta\mathbf{f}^{(i)}_{\mathbf{N}\ 4\times1} \\ \hline
\Delta\mathbf{d}^{(i)}_{\mathbf{N}\ 8\times1}
\end{array}\right\}
\end{aligned}
\qquad \text{VI.D(15)}
$$

In Eq. VI.D(15), sub-matrices $\mathbf{B}^{(i)}_{\mathbf{t}\ 1\times1}$, $\mathbf{B}^{(i)}_{\mathbf{tf}\ 1\times4}$, $\mathbf{B}^{(i)}_{\mathbf{td}\ 1\times8}$, $\mathbf{B}^{(i)}_{\mathbf{f}\ 4\times4}$, $\mathbf{B}^{(i)}_{\mathbf{fd}\ 4\times8}$ and $\mathbf{B}^{(i)}_{\mathbf{d}\ 8\times8}$ are defined as

$$\mathbf{B}^{(i)}_{\mathbf{t}\ 1\times1} = \frac{L^{(i)}}{GJ_d} \qquad \text{VI.D(16)}$$

$$\mathbf{B}^{(i)}_{\mathbf{tf}\ 1\times4} = -\frac{1}{GJ_d}\int_{L^{(i)}}\mathbf{t}^{(i)}{}_{1\times4}dz \qquad \text{VI.D(17)}$$

$$\mathbf{B}^{(i)}_{\mathbf{td}\ 1\times8} = \frac{1}{GJ_dL^{(i)}}\int_{L^{(i)}}\mathbf{t}^{(i)}_{\mathbf{d}\ 1\times8}dz \qquad \text{VI.D(18)}$$

$$\mathbf{B}^{(i)}_{\mathbf{f}\ 4\times4}=\frac{1}{E}\int_{L^{(i)}}\mathbf{m}^{(i)T}{}_{4\times2}\mathbf{D}^{-1}_{\mathbf{r}2\times2}\mathbf{m}^{(i)}{}_{2\times4}dz+\frac{1}{G}\int_{L^{(i)}}\mathbf{v}^{(i)T}{}_{4\times2}\boldsymbol{\chi}^{-1}_{2\times2}\mathbf{v}^{(i)}{}_{2\times4}dz+\frac{1}{GJ_d}\int_{L^{(i)}}\mathbf{t}^{(i)T}{}_{4\times1}\mathbf{t}^{(i)}{}_{1\times4}dz \qquad \text{VI.D(19)}$$

$$
\begin{aligned}
\mathbf{B}^{(i)}_{\mathbf{fd}\ 4\times8}= & \frac{1}{E}\int_{L^{(i)}}\mathbf{m}^{(i)T}{}_{4\times2}\mathbf{D}^{-1}_{\mathbf{r}2\times2}\mathbf{m}^{(i)}_{\mathbf{d}\ 2\times8}dz+\frac{1}{E}\int_{L^{(i)}}\mathbf{m}^{(i)T}{}_{4\times2}\mathbf{D}^{-1}_{\mathbf{r}2\times2}\mathbf{m}^{(i)}_{\mathbf{dv}2\times8}dz-\frac{1}{GJ_dL^{(i)}}\int_{L^{(i)}}\mathbf{t}^{(i)T}{}_{4\times1}\mathbf{t}^{(i)}_{\mathbf{d}\ 1\times8}dz \\
& +\frac{1}{G}\int_{L^{(i)}}\mathbf{v}^{(i)T}{}_{4\times2}\boldsymbol{\chi}^{-1}_{2\times2}\mathbf{v}^{(i)}_{\mathbf{d}\ 2\times8}dz+\frac{1}{G}\int_{L^{(i)}}\mathbf{v}^{(i)T}{}_{4\times2}\boldsymbol{\chi}^{-1}_{2\times2}\mathbf{v}^{(i)}_{\mathbf{dv}2\times8}dz
\end{aligned}
\qquad \text{VI.D(20)}
$$

and

$$
\begin{aligned}
\mathbf{B}^{(i)}_{\mathbf{d}\ 8\times8}= & \frac{1}{E}\int_{L^{(i)}}\mathbf{m}^{(i)T}_{\mathbf{d}\ 8\times2}\mathbf{D}^{-1}_{\mathbf{r}2\times2}\mathbf{m}^{(i)}_{\mathbf{d}\ 2\times8}dz+\frac{1}{E}\int_{L^{(i)}}\mathbf{m}^{(i)T}_{\mathbf{dv}8\times2}\mathbf{D}^{-1}_{\mathbf{r}2\times2}\mathbf{m}^{(i)}_{\mathbf{dv}2\times8}dz+\frac{1}{E}\int_{L^{(i)}}\mathbf{m}^{(i)T}_{\mathbf{d}\ 8\times2}\mathbf{D}^{-1}_{\mathbf{r}2\times2}\mathbf{m}^{(i)}_{\mathbf{dv}2\times8}dz \\
& +\frac{1}{E}\int_{L^{(i)}}\mathbf{m}^{(i)T}_{\mathbf{dv}8\times2}\mathbf{D}^{-1}_{\mathbf{r}2\times2}\mathbf{m}^{(i)}_{\mathbf{d}\ 2\times8}dz+\frac{1}{G}\int_{L^{(i)}}\mathbf{v}^{(i)T}_{\mathbf{d}\ 8\times2}\boldsymbol{\chi}^{-1}_{2\times2}\mathbf{v}^{(i)}_{\mathbf{d}\ 2\times8}dz+\frac{1}{G}\int_{L^{(i)}}\mathbf{v}^{(i)T}_{\mathbf{dv}8\times2}\boldsymbol{\chi}^{-1}_{2\times2}\mathbf{v}^{(i)}_{\mathbf{dv}2\times8}dz \\
& +\frac{1}{G}\int_{L^{(i)}}\mathbf{v}^{(i)T}_{\mathbf{d}\ 8\times2}\boldsymbol{\chi}^{-1}_{2\times2}\mathbf{v}^{(i)}_{\mathbf{dv}2\times8}dz+\frac{1}{G}\int_{L^{(i)}}\mathbf{v}^{(i)T}_{\mathbf{dv}8\times2}\boldsymbol{\chi}^{-1}_{2\times2}\mathbf{v}^{(i)}_{\mathbf{d}\ 2\times8}dz+\frac{1}{GJ_d\left(L^{(i)}\right)^2}\int_{L^{(i)}}\mathbf{t}^{(i)T}_{\mathbf{d}\ 8\times1}\mathbf{t}^{(i)}_{\mathbf{d}\ 1\times8}dz
\end{aligned}
\qquad \text{VI.D(21)}
$$

Appendix VI.E- Details of ABAQUS models

In this appendix, mesh, boundary condition and loading details for ABAQUS FEA models used in Examples VI.1 through VI.9 are provided.

Example VI.1

Mesh

In Example VI.1, each half flange is subdivided into 5 equal elements and web into 10 equal elements. The beam span is subdivided into 200 equal elements as shown in Fig. VI.E.1. Thus, a total of 6,000 S4R shell elements are used.

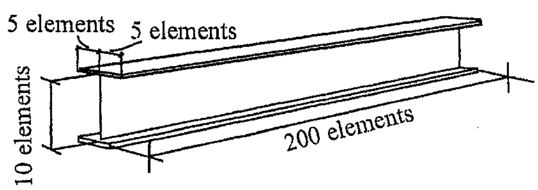

Fig. VI.E.1 ABAQUS mesh for Examples 1, 2 and 3

MPC type SLIDER constraint

The multiple point constraints MPC type SLIDER keeps; a) every node on the bottom flange (e.g., nodes r_1 and r_2 in Fig. VI.E.2) along the straight line defined by the nodes at the tip (node A) and the center (node B) of the bottom flange (Fig. VI.E.2), b) every node on the web (e.g., nodes s_1 and s_2) along the straight line defined by the nodes at the end (node B) and center (node C) of the web, and c) every node on the top flange (e.g., nodes t_1 and t_2) along the straight line defined by the nodes at the tip (node D) and the center (node E) of the top flange. These artificial multipoint constraints approximately simulate the Vlasov first assumption

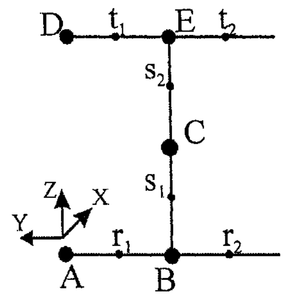

Fig. VI.E.2 Nodes defining straight lines for MPC type SLIDER constraint

Boundary Conditions

Simply supported boundary conditions are applied by restraining; a) the nodes at the centroid of the section (nodes C_0 and C_L located at both ends of the beam) in lateral (Y), and vertical (Z) directions at both ends in order to prevent horizontal and vertical translations as shown in Fig. VI.E.3 a and b, b) the node at the centroid of the section (node C_0) in axial (X) direction at only one end in order to prevent rigid body longitudinal translation (Fig. VI.E.3 a), and c) the nodes at the centroid of the top flange (nodes E_0 and E_L located at both ends of the beam) along the lateral (Y) direction at both ends in order to prevent angle of twist at both ends.

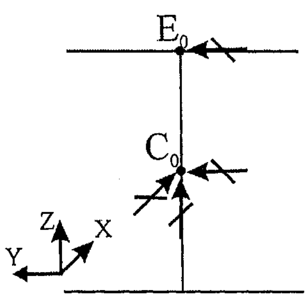

a) at left end

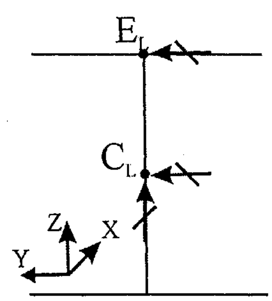

b) at right end

Fig. VI.E.3 Simply supported boundary conditions

Loading

In ABAQUS model, a compression force is applied by twenty 0.05 kN loads (i.e., totally $0.05 \times 20 = 1kN$) acting at the nodes of the bottom and top flanges a) in X direction at left end, b) in opposite to X direction at right end as shown Fig. VI.E.4 and b.

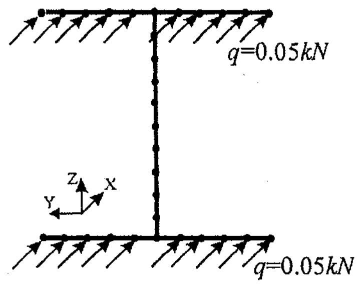

a) at left end

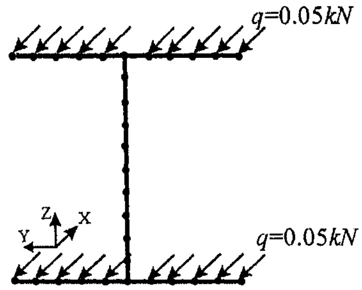

b) at right end

Fig. VI.E.4 Application of axial force

Example VI.2

Mesh

In both cases of Example VI.2, the mesh of the beams is identical to the one given in Example VI.1.

MPC type SLIDER constraint

The MPC type SLIDER constraint is applied as explained in Example VI.1.

Boundary Conditions

Fixed end boundary condition at the left end of the beams are applied by restraining all master nodes (nodes A_0, B_0, D_0 and E_0 in Fig.VI.E.5) in all three directions. Thus, the section translations in longitudinal, horizontal and vertical directions are prevented as well as the warping of the cross-section and rotations about the X, Y and Z axes.

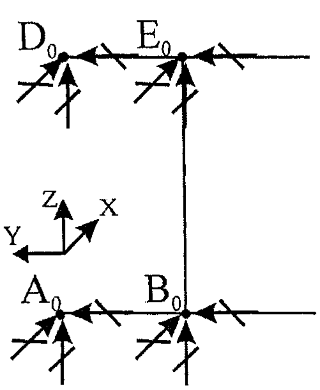

Fig. VI.E.5 Imposing fixity conditions

Simply supported boundary conditions at the right end of the beam in Case 1 is applied in a manner identical to one shown in Fig. VI.E.3b.

Loading

The compressive load is applied identical to the one shown in Fig. VI.E.4b. Thus, by applying twenty 0.05 kN loads acting at the nodes of bottom and top flanges.

Example VI.3

Mesh

In all cases of Example VI.3 the mesh of the beams is identical to the one given in Example VI.1.

MPC type SLIDER constraint

The MPC type SLIDER constraint is applied as explained in Example VI.1.

Boundary Conditions

Simply supported boundary conditions at both ends of the beams are applied in a manner identical to that shown in Fig. VI.E.3.

Loading

The bending moment is applied at left end through ten 0.5 kN loads applied to nodes of the top flange along the X direction, and ten 0.5 kN loads applied to nodes of the bottom flange in the negative X direction ($0.2 \times 0.5 \times 10 = 1kNm$) as shown in Fig. VI.E.6. A similar loading scheme is adopted at the right end.

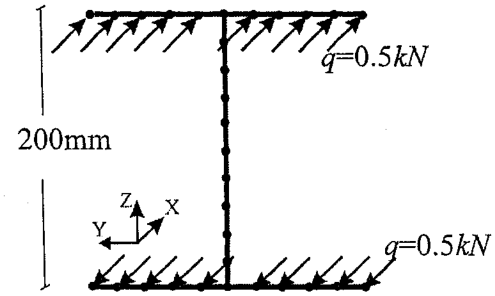

Fig. VI.E.6 Loading scheme for bending moment (1 *kNm*) at left end

Example VI.5

Mesh

The mesh of the beam is identical to that given in Example VI.1.

MPC type SLIDER constraint

The MPC type SLIDER constraint is applied as explained in Example VI.1.

Boundary Conditions

Fixed end boundary condition at left end of the beam are enforced in a manner identical to one shown in Fig. VI.E.5.

Loading

The bending moment is applied at the right end through ten 0.5 *kN* loads acting at the nodes of the top flange in the negative X direction, and ten 0.5 *kN* loads acting at the nodes of the bottom flange along the X direction as shown in Fig. VI.E.7.

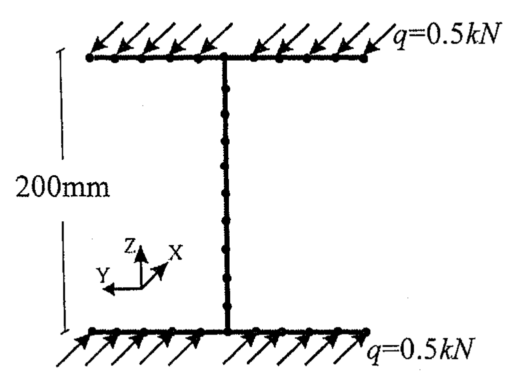

Fig. VI.E.7 Bending moment (1 *kNm*) at right end

Example VI.6

Mesh

In Example VI.6, each flange is subdivided into 5 equal elements and web into 10 equal elements. The beam span is divided into 200 equal elements as shown in Fig. VI.E.8. Thus, a total of 4,000 S4R shell elements are used.

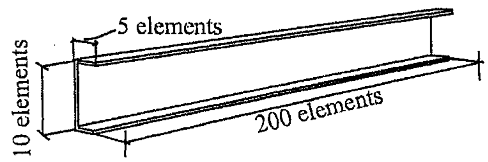

Fig. VI.E.8 ABAQUS mesh for Example 6

MPC type SLIDER constraint

The multiple point constraints MPC type SLIDER keeps; a) every node on the bottom flange (e.g., node r_1 in Fig. VI.E.9) along the straight line defined by the nodes at the end (node A) and the center (node B) of the bottom flange (Fig. VI.E.9), b) every node on the web (e.g., nodes s_1 and s_2) along the straight line defined by the nodes at the end (node A) and center (node C) of the web, and c) every node on the top flange (e.g., nodes t_1 and t_2) along the straight line defined by the nodes at the end (node D) and the center (node) of the top flange.

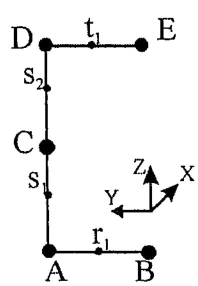

Fig. VI.E.9 Nodes defining straight lines for MPC type SLIDER constraint

Boundary Conditions

Fixed end boundary condition at the left end of the beams are applied by restraining all master nodes (nodes A_0, B_0, D_0 and E_0 in Fig.VI.E.10) in all three directions, which corresponds to restraining translations along the longitudinal, horizontal and vertical directions as well as warping of the cross-section and the rotations about X, Y and Z axes ($w = u = v = \phi = u' = v' = \phi' = 0$).

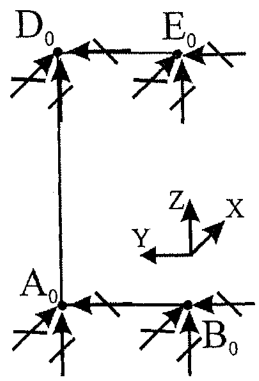

Fig. VI.E.10 Fixed end boundary condition in ABAQUS model for C shape cross-section

Loading

The vertical load P is applied through steel bars of circular cross-section with a diameter of 500mm connected to a) the top flange in Fig. VI.E.11a, b) the center node of the web in Fig. VI.E.11b, and c) the bottom flange in Fig. VI.E.11c.

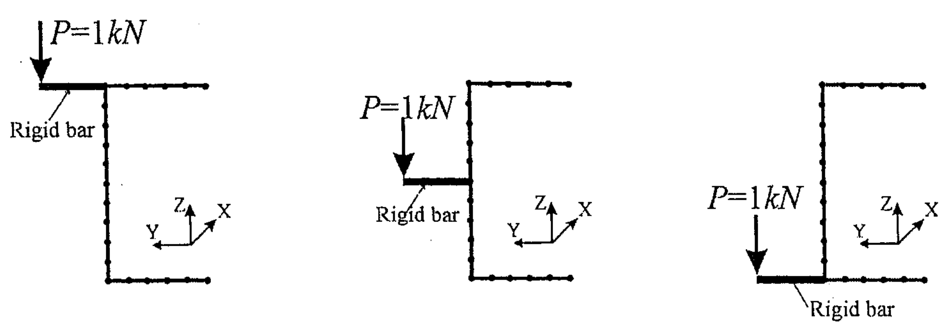

a) at top flange b) at shear center c) at bottom flange

Fig. VI.E.11Vertical Loads in Example VI.6

Example VI.7

Mesh

In Example VI.7, each half of the top flange is subdivided into 5 equal elements, each half of the bottom flange is subdivided into 2 equal elements and web into 10 equal elements. The beam span is subdivided into 100 equal elements as shown in Fig. VI.E.12. Thus, a total of 1,400 S4R shell elements are used.

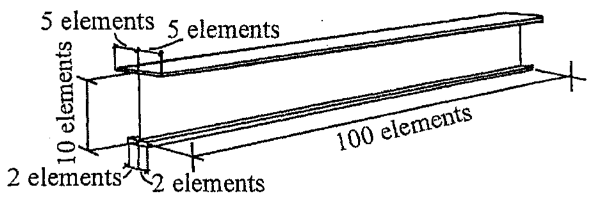

Fig. VI.E.12 ABAQUS mesh for Example 7

MPC type SLIDER constraint

The multiple point constraints MPC type SLIDER keeps; a) every node on the bottom flange (e.g., nodes r_1 and r_2 in Fig. VI.E.13) along the straight line defined by the nodes at the end (node A) and the center (node B) of the bottom flange (Fig. VI.E.13), b) every node on the web (e.g., nodes s_1 and s_2) along the straight line defined by the nodes at the end (node B) and center (node C) of the web, and c) every node on the top flange (e.g., nodes t_1 and t_2) along the straight line defined by the nodes at the end (node D) and the center (node E) of the top flange.

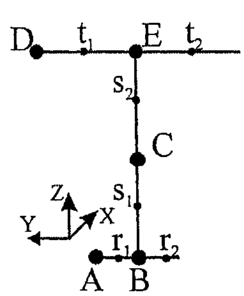

Fig. VI.E.13 Nodes defining straight lines for MPC type SLIDER constraint

Boundary Conditions

Simply supported boundary conditions are applied to the beam by restraining; a) the nodes at the centroid of the section (nodes C_0 and C_L) in horizontal (Y direction), and vertical (in Z direction) directions at both ends in order to prevent horizontal and vertical translations as shown in Fig. VI.E.14 a and b, b) the node at the centroid of the section (node C_0) in axial direction at only one end in order to prevent longitudinal translation (Fig. VI.E.14 a), and c) the nodes at the centroid of the top flange (nodes E_0 and E_L) in horizontal (Y direction) direction at both ends in order to prevent angle of twist.

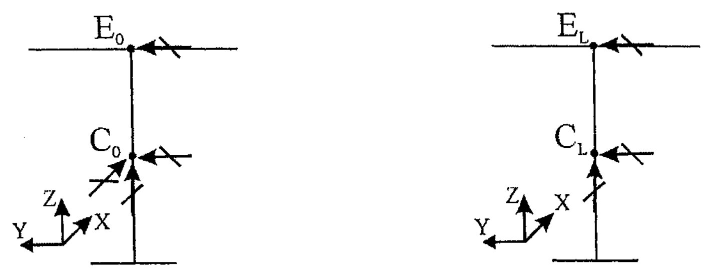

a) at right end b) at left end

Fig. VI.E.14 Simply supported boundary conditions

Loading

The bending moment is applied at left end by ten 0.5 *kN* loads spread to nodes of the top flange in X direction, and four 1.25 *kN* loads spread to nodes of the bottom flange in opposite to X direction as shown in Fig. VI.E.6. The bending moment is applied at right end by applying ten 0.5 *kN* loads spread to nodes of the top flange in opposite to X direction, and four 1.25 *kN* loads spread to nodes of the bottom flange in X direction as shown in Fig. VI.E.7.

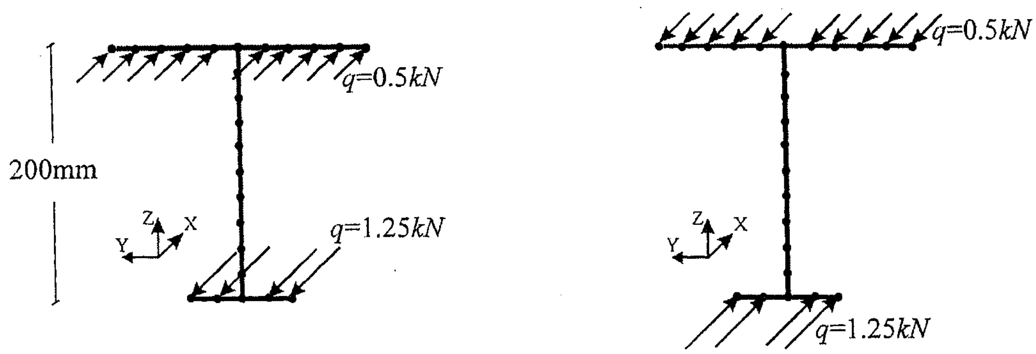

a) at right end b) at left end

Fig. VI.E.15 Bending moments applied to a Mono-symmetric section

Example VI.8

Mesh

The mesh of the beams is identical to that given in Example VI.7.

MPC type SLIDER constraint

The MPC type SLIDER constraint is applied as explained in Example VI.7.

Boundary Conditions

Simply supported boundary conditions at both ends of the beams are applied identical to one shown in Fig. VI.E.14.

Loading

The vertical load (1 kN) at the mid-span is applied at the center of the top flange in Z direction as shown in Fig. VI.E.16.

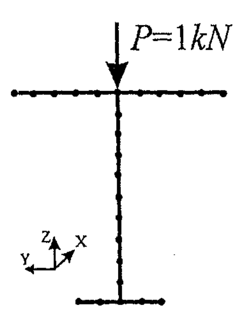

Fig. VI.E.16. Vertical load ($1kN$) applied at the top flange

Example VI.9

Mesh

In modeling the beam, the web is divided into 10 equal elements, the top flange is divided into 10 elements, the bottom flange is divided into 4 elements, and the beam span is divided into 40 equal elements as shown in Fig. VI.E.17.

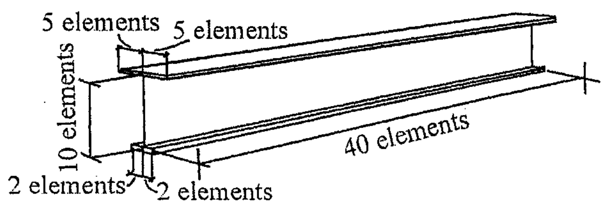

Fig. VI.E.17 ABAQUS mesh for Example 9

MPC type SLIDER constraint

The MPC type SLIDER constraint is applied as explained in Example VI.7.

Boundary Conditions

Fixed end boundary condition at the left end of the beams are applied by restraining all master nodes (nodes A_0, B_0, D_0 and E_0 in Fig.VI.E.18) in all three directions, thus the translations in longitudinal, horizontal and vertical directions are prevented as well as warping of the cross-section and the rotations about X, Y and Z axes.

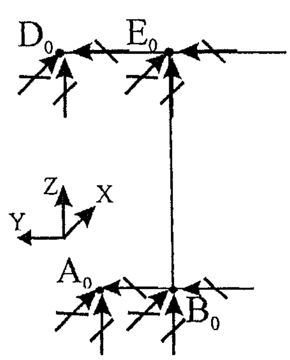

Fig. VI.E.18 Fixed end boundary condition in ABAQUS model for Mono-symmetric section

Simply supported boundary conditions at z=1000*mm* is applied identical to one shown in Fig. VI.E.14b.

Loading

Vertical load (1 *kN*) at the tip of the beam (z=1600*mm*) is applied at the center of the top flange in Z direction as shown in Fig. VI.E.16.

Appendix VI.F-Eigenvalues Corresponding to Higher Modes

The eigenvalue corresponding to first mode is the one needed to obtain the buckling load factor for practical purposes. In this appendix, however, the eigenvalues corresponding to the higher modes on BECE, BECES, ABAQUS solutions and results available in literature are presented. The comparison of higher buckling modes provides a stricter test to show the validity of the new solution. It can also be observed that for higher modes, the effect of shear deformation becomes more significant. The first five eigenvalue predictions are provided for the examples. For Example 6.6, no closed form solution exists for buckling mode shapes and in ABAQUS model the analysis has been pursued until the 30th mode and all of the higher modes contain local buckling effect, thus a comparison could not be made.

Example VI.1 Flexural and Torsional Buckling of Simply-Supported column

Table VI.F.1 Third mode for Example VI.1

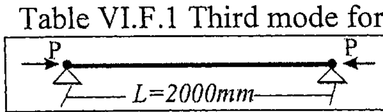	ABAQUS (kN)	Closed form (kN)	BECE (kN)	BECES (kN)
Mode 3- strong axis bending * 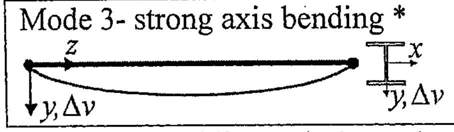	35,500	43,425	43,426	34,584

*Flexural buckling solutions about strong axis with BECE and BECES are obtained by rotating the cross-section 90 degrees about its longitudinal axis.

Until the 30th mode the rest of the modes involve local buckling in ABAQUS model. 3 Deformed shape in a local buckling mode is shown in Fig. VI.F.1. Comparison of the higher modes is made with closed form solutions in which the shear deformation effect is not included.

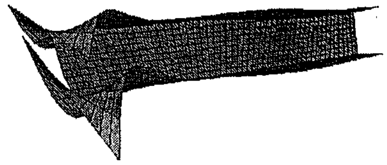

Fig. VI.F.1 3 D deformed shape in a local buckling mode based on ABAQUS analysis

Table VI.F.2 Fourth and fifth modes for Example VI.1

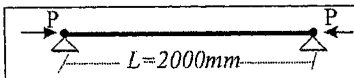	Closed form (kN)	BECE (kN)	BECES (kN)
Mode 4- weak axis bending 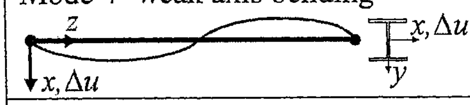	52,633	52,638	47,696
Mode 5- torsion 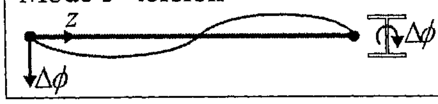	55,850	55,881	51,255

Example VI.2 Effect of Boundary Conditions on Column Flexural Buckling

Table VI.F.3 Higher modes for Example VI.2 Case1

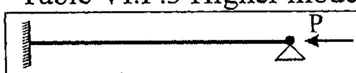	ABAQUS (kN)	BECE (kN)	BECES (kN)
Mode 2- weak axis bending 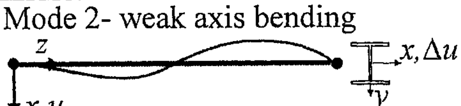	4,910	4,973	4,922
Mode 3- strong axis bending * 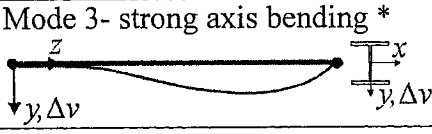	5,410	5,552	5,343
Mode 4- torsion 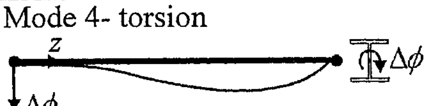	9,270	9,695	9,544
Mode 5- weak axis bending 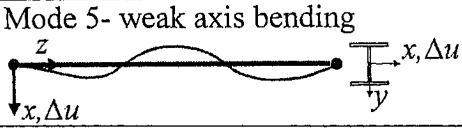	9,720	9,908	9,713

Table VI.F.4 Higher modes for Example VI.2 Case2

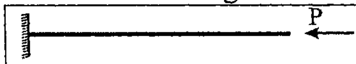	ABAQUS (kN)	BECE (kN)	BECES (kN)
Mode 2- strong axis bending * 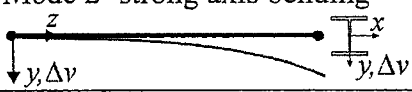	679	679	676
Mode 3- weak axis bending 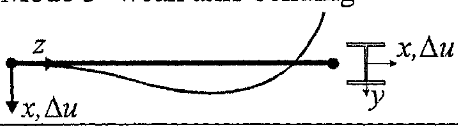	1,830	1,851	1,844
Mode 4- weak axis bending 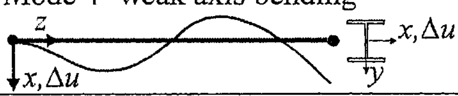	5,070	5,140	5,089
Mode 5- strong axis bending 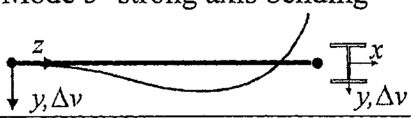	5,950	6,107	5,891

Example VI.3 Lateral Torsional Buckling of Beams with doubly symmetric cross-section

Table VI.F.5 Higher modes for Example VI.3 Case1

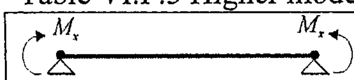	ABAQUS (kNm)	BECE (kNm)	BECES (kNm)
Mode 2 flexure and torsion 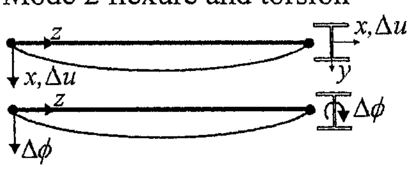	-274	-285	-283
Mode 3 flexure and torsion 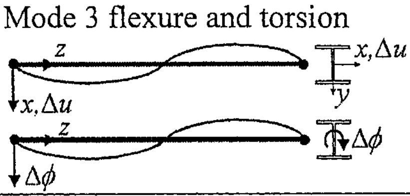	612	635	628
Mode 4 flexure and torsion 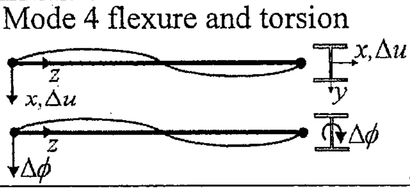	-617	-635	-628
Mode 5 flexure and torsion 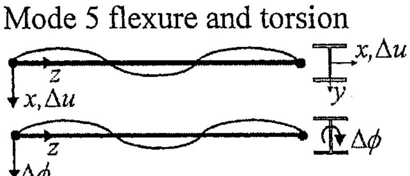	1,070	1,096	1,079

Table VI.F.6 Higher modes for Example VI.3 Case2

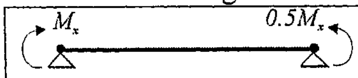	ABAQUS (kNm)	BECE (kNm)	BECES (kNm)
Mode 2 flexure and torsion 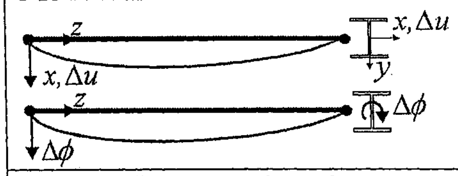	-361	-375	-371
Mode 3 flexure and torsion 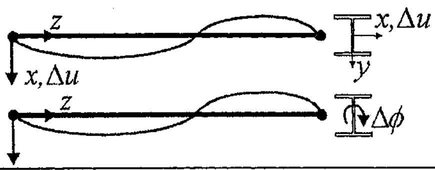	820	849	840
Mode 4 flexure and torsion 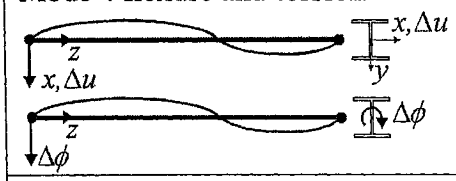	-825	-849	-840
Mode 5 flexure and torsion 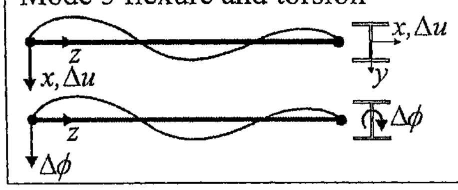	1,440	1,473	1,449

Table VI.F.7 Higher modes for Example VI.3 Case3

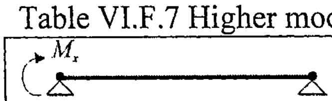	ABAQUS (kNm)	BECE (kNm)	BECES (kNm)
Mode 2 flexure and torsion 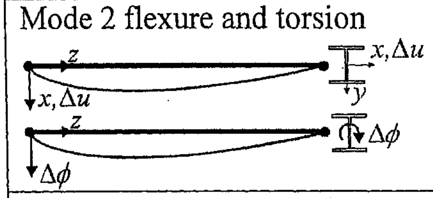	-492	-512	-505
Mode 3 flexure and torsion 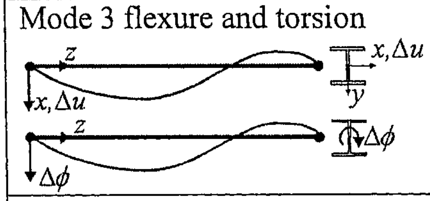	1,220	1,263	1,242
Mode 4 flexure and torsion 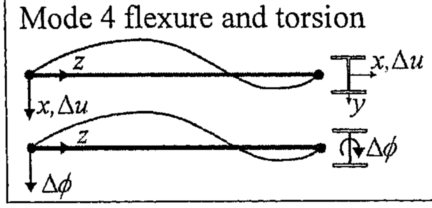	-1,230	-1,263	-1,242

Mode 5 flexure and torsion 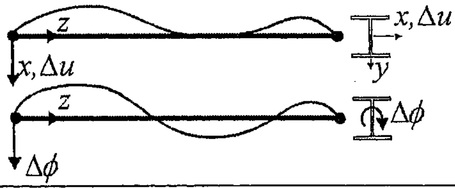	2,230	2,290	2,236

Table VI.F.8 Higher modes for Example VI.3 Case4

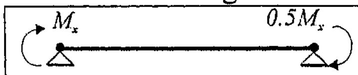	ABAQUS (kNm)	BECE (kNm)	BECES (kNm)
Mode 2 flexure and torsion 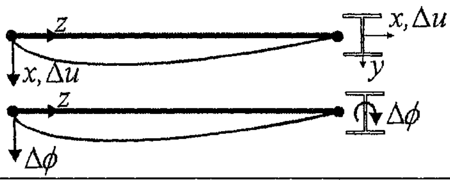	-659	-689	-682
Mode 3 flexure and torsion 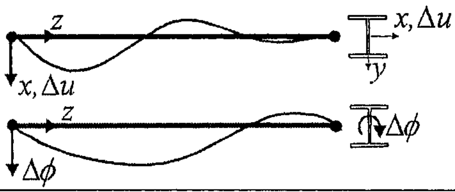	1,810	1,881	1,846
Mode 4 flexure and torsion 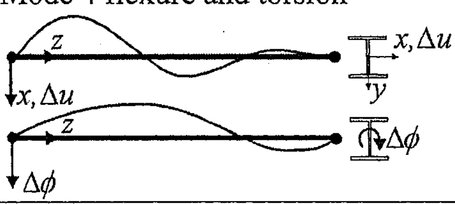	-1,820	-1,881	-1,846
Mode 5 flexure and torsion 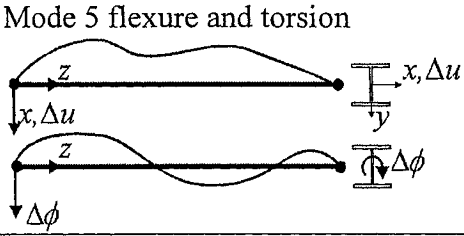	2,860	3,047	2,944

Table VI.F.9 Higher modes for Example VI.3 Case5

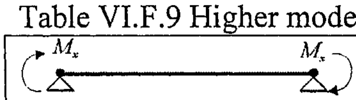	ABAQUS (kNm)	BECE (kNm)	BECES (kNm)
Mode 2 flexure and torsion 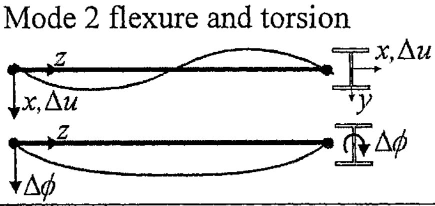	-717	-752	-744

Mode 3 flexure and torsion 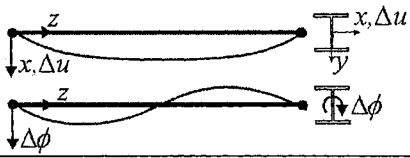	1,090	1,158	1,135
Mode 4 flexure and torsion 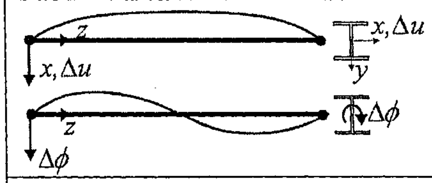	-1,090	-1,158	-1,135
Mode 5 flexure and torsion 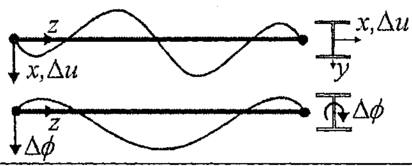	2,580	2,678	2,608

Example VI. 4 Lateral Torsional Buckling of a fixed-pinned beam under uniform moment(L=4000mm)

Table VI.F.10 Higher modes for Example VI.4

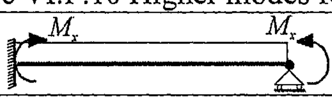	Trahair (kNm)	BECE (kNm)	BECES (kNm)
Mode 2 flexure and torsion 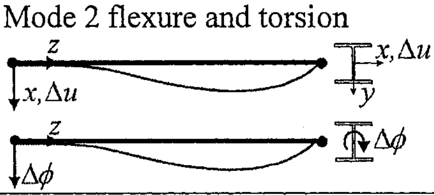	-1,032	-1,029	-1,013
Mode 3 flexure and torsion 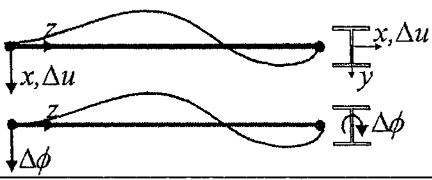	2,402	2,391	2,303
Mode 4 flexure and torsion 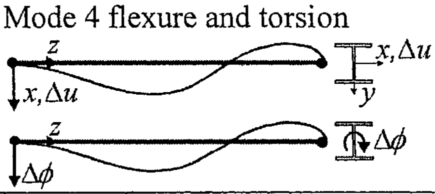	-2,402	-2,391	-2,303
Mode 5 flexure and torsion 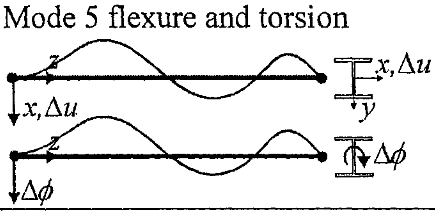	4,396	4,377	4,069

Example VI.5 Lateral Torsional Buckling of a cantilever under uniform moment (L=4000mm)

Table VI.F.11 Higher modes for Example VI.5

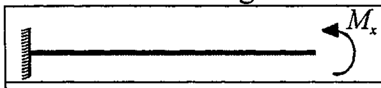	ABAQUS (kNm)	BECE (kNm)	BECES (kNm)
Mode 2 flexure and torsion 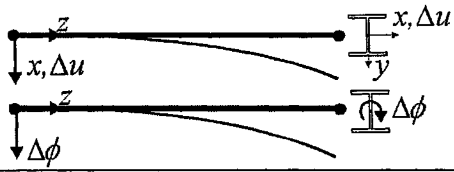	-271	-285	-283
Mode 3 flexure and torsion 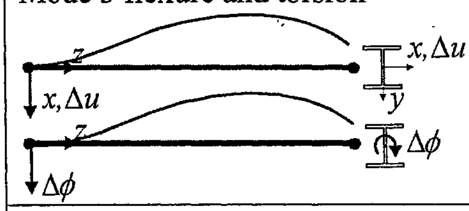	1,057	1,102	1,085
Mode 4 flexure and torsion 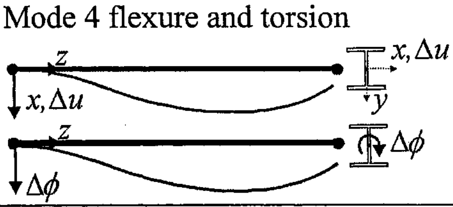	-1,060	-1,102	-1,085
Mode 5 flexure and torsion 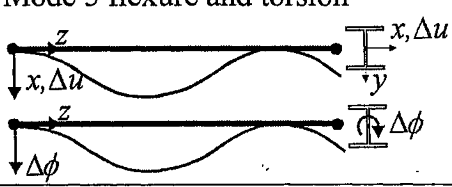	2,350	2,459	2,371

Example VI.6 Load Position Effect for a Cantilever under transverse load (L=4000mm)

Table VI.F.12 Higher modes for Example VI.6 Case1

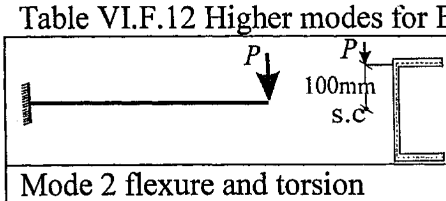	ABAQUS (kN)	BECE (kN)	BECES (kN)
Mode 2 flexure and torsion 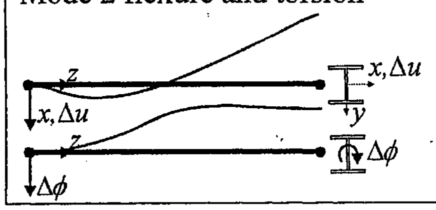	-92.8	-95.5	-93.8

Mode 3 flexure and torsion 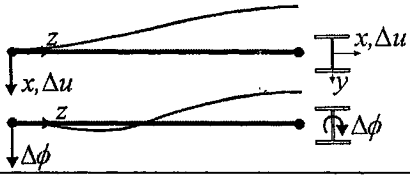	190	201	196
Mode 4 flexure and torsion 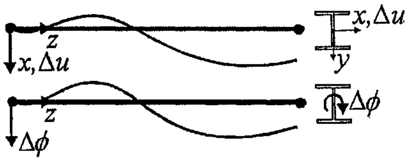	-257	-265	-257
Mode 5 flexure and torsion 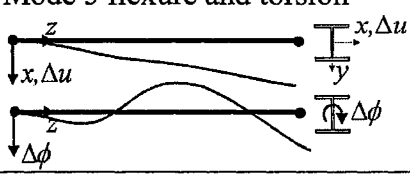	357	380	366

Table VI.F.13 Higher modes for Example VI.6 Case2

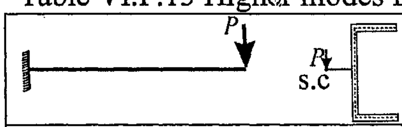	ABAQUS (kN)	BECE (kN)	BECES (kN)
Mode 2 flexure and torsion 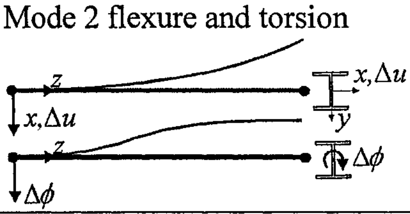	82	85	83
Mode 3 flexure and torsion 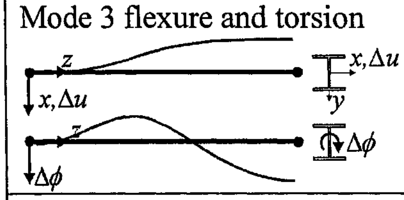	-234	-243	-237
Mode 4 flexure and torsion 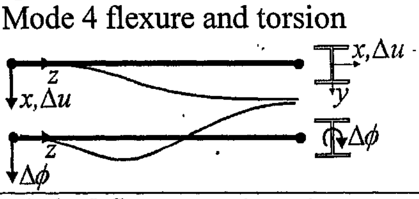	235	243	237
Mode 5 flexure and torsion 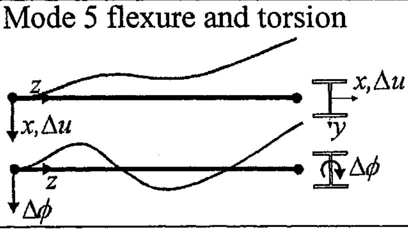	-435	-461	-439

Note that the higher modes for bottom flange loadings can be obtained by changing the signs of the top flange loading case

Example VI.7 Lateral torsional buckling of mono-symmetric beams under uniform moment (L=4000mm)

Table VI.F.14 Higher modes for Example VI.7

	ABAQUS (kNm)	BECE (kNm)	BECES (kNm)
Mode2 flexure and torsion 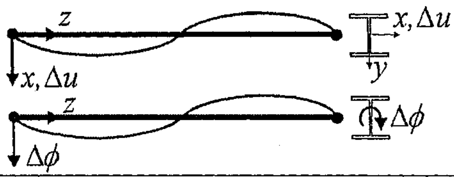	359	390	382
Mode3 flexure and torsion 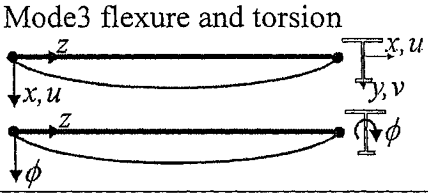	-491	-508	-502
Mode4 flexure and torsion 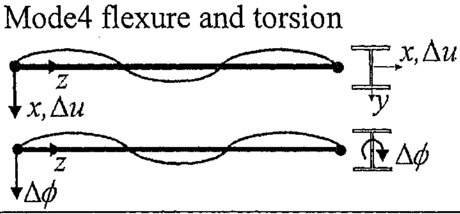	492	534	524
Mode5 flexure and torsion 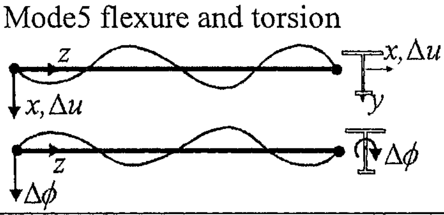	651	708	692

Example VI.8 Lateral torsional buckling of mono-symmetric beams under mid-span load (L=4000mm)

Table VI.F.15 Higher modes for Example VI.8

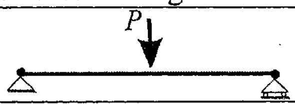	ABAQUS (kN)	BECE (kN)	BECES (kN)
Mode 2 flexure and torsion 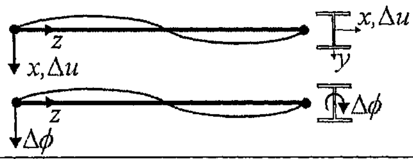	3,074	3,486	3,411
Mode 3 flexure and torsion 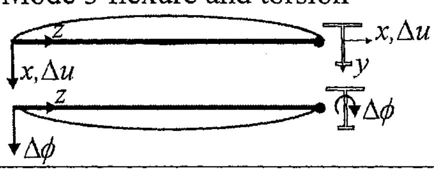	3,470	3,650	2,781
Mode 4 flexure and torsion 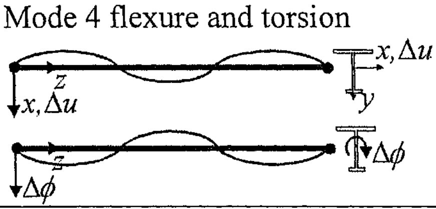	6,917	8,135	6,054
Mode 4 flexure and torsion 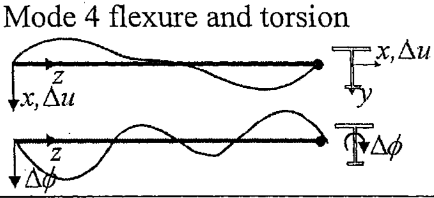	11,444	13,819	12,577

Appendix VI.G - Lower Bound Condition for Eigenvalue Predictions in Torsional Buckling of Columns

The flexural buckling load based on the element BECE is equivalent to Timoshenko's quotient (Westergaard 1941). Thus, the approximate buckling load obtained by interpolating only the displacement field into the complementary functional is always an upper bound to true buckling load since the interpolated displacement field can be conceived as a constraint displacement applied to the true field (Timoshenko 1961). This directly results from the min-max principle (Courant and Hilbert 1953) which states that when a constraint condition is applied to a buckling problem, the eigenvalue of the problem after imposition of the constraint will increase (or at least will not decrease) compared to the unconstrained system. A formal proof of the upper bound property of the eigenvalue and the superior convergence of Timoshenko's quotient in comparison to solutions based on total potential energy were reported in Lang (1947).

On the other hand, when the buckling mode involves torsional behavior (e.g., torsional buckling of columns, torsional flexural buckling of columns, or lateral torsional buckling of beams) element BECE can provide a lower bound prediction of the buckling load. The objective of this Appendix is to show that, in contrast to the assured upper bound solutions in flexural buckling modes, it is possible to obtain a lower bound solution for torsional buckling modes as a result of the independent interpolation of the St. Venant twisting moment due to buckling ΔT_{sv}. The proof is provided for the simple case a simply supported column with a doubly symmetric cross-section undergoing torsional buckling under concentric axial loading. In order to further simplify the argument, the contribution of shear is omitted from the proof.

The second variation of the complementary energy functional consists of the external load potential W^* and the internal strain energy U^* due to buckling i.e.,

$$\delta^2\pi^* = -\lambda W^* + \lambda^2 U^* \qquad \text{VI.G(1)}$$

In Eq. VI.G(1), symbol λ represents the buckling load factor. At the buckling load, the variation of the second variation of the potential energy vanishes i.e., $\delta\left(\delta^2\pi^*\right) = -\lambda\delta W^* + \lambda^2\delta U^* = 0$, or $\delta W^* - \lambda\delta U^* = 0$. By defining a quotient as $\lambda_T = W^*/U^*$, one can show that when λ_T is stationary, the quotient λ_T is equal to the buckling load factor λ.

$$\delta\lambda_T = 0 = \delta\frac{W^*}{U^*} = \frac{\left(U^*\,\delta W^* - W^*\,\delta U^*\right)}{U^{*2}} = \frac{\left(\delta W^* - \lambda_T\delta U^*\right)}{U^*} \qquad \text{VI.G(2)}$$

Thus, when $\lambda_T = \lambda$, Eq. VI.G(2) is satisfied. Hence, λ_T can be conceived as a scalar that coinciding with the buckling load factor λ, only when it has a stationary value. By replacing tensile force with a compressive force in Eq. (VI.54) i.e., $P = -N$ and selecting an orthogonal system of coordinates in which the sectorial origin and the shear center coincide with the centroid i.e., $a_x = a_y = 0$ and $r_{N0} = r_0$, the second variation of the complementary energy functional corresponding to a pure torsional buckling mode (i.e., $u = M_x = V_y = 0$) for a member with a doubly symmetric cross-section can be expressed as

$$\delta^2\pi^* = -\lambda\int_L\left(Pr_0^{\,2}\Delta\phi_Z{}'^2\right)dz + \lambda^2\int_L\left(\frac{\Delta B^2}{\lambda^2 EJ_{ww}} + \frac{\Delta T_{sv}^{\,2}}{\lambda^2 GJ_d}\right)dz \qquad \text{VI.G(3)}$$

From Eqs. VI.G(1) and VI.G(3), quotient λ_T can be expressed as

$$\lambda_T = \frac{Pr_0^2 \int_L (\Delta\phi_Z')^2\, dz}{\int_L \left(\frac{\Delta B^2}{\lambda^2 EJ_{ww}} + \frac{\Delta T_{sv}^{\ 2}}{\lambda^2 GJ_d} \right) dz} \qquad \text{VI.G(4)}$$

The compatibility equations in Eq. (VI.61) are exactly satisfied when the functions ϕ_{Zm}, ΔB_m and ΔT_{svm} associated with the m^{th} buckling mode meet the conditions

$$\Delta\phi_{Zm}'' - \frac{\Delta B_m}{EJ_{\omega\omega}} = 0 \qquad \text{VI.G(5)}$$

and

$$\Delta\phi_{Zm}' + \frac{\Delta T_{svm}}{GJ_d} = 0 \qquad \text{VI.G(6)}$$

By using the equilibrium condition in Eq. (VI.45) for mode m, one obtains

$$\Delta B_m = \Delta B_{m\alpha} + \Delta T_{m\alpha} z - \lambda_m Pr_0^2 \Delta\phi_{Zm} - \int \Delta T_{svm} dz \qquad \text{VI.G(7)}$$

By substituting Eq. VI.G(7) into Eq. VI.G(5) one obtains

$$\Delta\phi_{Zm}'' = \frac{\Delta B_{\alpha m} + \Delta T_{\alpha m} z - \lambda_m Pr_0^2 \Delta\phi_{Zm} - \int \Delta T_{svm} dz}{EJ_{\omega\omega}} \qquad \text{VI.G(8)}$$

From the identity $\int_L \Delta\phi_{Zm}' \Delta\phi_{Zn}' dz = \Delta\phi_{Zm} \Delta\phi_{Zn}'\big|_0^L - \int_L \Delta\phi_{Zm} \Delta\phi_{Zn}'' dz$, along with Eqs. VI.G(6) and VI.G(8) and the boundary conditions $\Delta\phi_{Zm}(0) = \Delta\phi_{Zm}(L) = 0$ for a simply supported column, one obtains

$$\int_L \Delta\phi_{Zm}' \Delta\phi_{Zn}' dz = \lambda_n \frac{Pr_0^2}{EJ_{\omega\omega}} \delta_{mn} - \frac{GJ_d}{EJ_{\omega\omega}} \delta_{mn} - \int_L \Delta\phi_{Zm} \left(\frac{\Delta B_{\alpha n} + \Delta T_{\alpha n} z}{EJ_{\omega\omega}} \right) dz \qquad \text{VI.G(9)}$$

In Eq. VI.G(9), symbol δ_{mn} represents the Kronecker delta function. In obtaining Eq. VI.G(9), it has been assumed that the eigenvectors have been scaled so that

$$\int_L \Delta\phi_{Zm}\Delta\phi_{Zn}dz = \delta_{mn} \qquad \text{VI.G(10)}$$

An assumed interpolation rotation field $\Delta\phi_z$ and St.Venant torsion field ΔT_{sv} can be expressed as a superposition of the buckling modes. The existence of such a representation is assured when the Fourier transformability conditions are satisfied i.e., a) functions $\Delta\phi_Z$ and ΔT_{sv} are piecewise continuous on every finite interval, and b) functions $\Delta\phi_Z$ and ΔT_{sv} are integrable with respect to z. Under these conditions, one can write

$$\Delta\phi_Z = \sum_{m=1}^{\infty} a_m \Delta\phi_{Zm} \qquad \text{VI.G(11)}$$

$$\Delta T_{sv} = -GJ_d \sum_{m=1}^{\infty} b_m \Delta\phi_{Zm}{}' \qquad \text{VI.G(12)}$$

In Eqs. VI.G(11) and VI.G(12), a_m and b_m are Fourier constants which represent the weighting of the associated mode $\Delta\phi_{Zm}$ or $\Delta\phi_{Zm}{}'$ in interpolation functions $\Delta\phi_Z$ and ΔT_{sv}. By enforcing the boundary conditions $\Delta\phi_{Zm}(0) = \Delta B_m(0) = \Delta\phi_{Zm}(L) = \Delta B_m(L) = 0$ into Eq. VI.G(7) one obtains

$$\Delta B_{\alpha m} = \int \Delta T_{svm} dz \Big|_0 \qquad \text{VI.G(13)}$$

and

$$\Delta T_{\alpha m} = \frac{1}{L}\int_0^L \Delta T_{svm} dz \qquad \text{VI.G(14)}$$

From Eq. VI.G(6), by substituting into Eqs. VI.G(13) and VI.G(14) one obtains

$$\Delta B_{\alpha m} = GJ_d \Delta\phi_{Zm}(0) = 0 \qquad \text{VI.G(15)}$$

and

$$\Delta T_{\alpha m} = \frac{GJ_d}{L}\left[\Delta\phi_{Zm}(0) - \Delta\phi_{Zm}(L)\right] = 0 \qquad \text{VI.G(16)}$$

By substituting Eqs. VI.G(16) and VI.G(15) into Eq. VI.G(9), one obtains

$$\int_L \Delta\phi_{Zm}{}'\,\Delta\phi_{Zn}{}'dz = \lambda_n \frac{Pr_0^2}{EJ_{\omega\omega}}\delta_{mn} - \frac{GJ_d}{EJ_{\omega\omega}}\delta_{mn} \qquad \text{VI.G(17)}$$

From Eqs. VI.G(7), VI.G(11) and VI.G(12) into Eq. VI.G(4) one obtains

$$\lambda_T = \frac{Pr_0^2 \int\limits_L \sum\limits_{m=1}^{\infty}\sum\limits_{n=1}^{\infty} a_m a_n \phi_{Zm}{}'\phi_{Zn}{}'dz}{\int\limits_L \left[\frac{1}{EJ_{\omega\omega}}\left(-Pr_0^2\sum\limits_{m=1}^{\infty} a_m\phi_{Zm} + GJ_d\sum\limits_{m=1}^{\infty}\frac{b_m}{\lambda_m}\phi_{Zm}\right)^2 + GJ_d\sum\limits_{m=1}^{\infty}\sum\limits_{n=1}^{\infty}\frac{b_m}{\lambda_m}\frac{b_n}{\lambda_n}\phi_{Zm}{}'\phi_{Zn}{}'\right]dz} \qquad \text{VI.G(18)}$$

From Eqs. VI.G(10) and VI.G(17), by substituting into Eq. VI.G(18) one obtains

$$\lambda_T = \frac{Pr_0^2\left(\frac{Pr_0^2}{EJ_{\omega\omega}}\sum\limits_{m=1}^{\infty}\lambda_m a_m^2 - \frac{GJ_d}{EJ_{\omega\omega}}\sum\limits_{m=1}^{\infty} a_m^2\right)}{\left[\frac{1}{EJ_{\omega\omega}}\sum\limits_{m=1}^{\infty}\left(Pr_0^2 a_m - GJ_d\frac{b_m}{\lambda_m}\right)^2 + \frac{GJ_d}{EJ_{\omega\omega}}\sum\limits_{m=1}^{\infty}\left(\lambda_m Pr_0^2 - GJ_d\right)\left(\frac{b_m}{\lambda_m}\right)^2\right]} \qquad \text{VI.G(19)}$$

In Eq. VI.G(19) the relations $\sum\limits_{m=1}^{\infty}\sum\limits_{n=1}^{\infty}\delta_{mn}(b_m/\lambda_m)(b_n/\lambda_n) = \sum\limits_{m=1}^{\infty}(b_m/\lambda_m)^2$, $\sum\limits_{m=1}^{\infty}\sum\limits_{n=1}^{\infty}\delta_{mn}a_m a_n = \sum\limits_{m=1}^{\infty}a_m^2$ and

$\sum\limits_{m=1}^{\infty}\sum\limits_{n=1}^{\infty}\left[Pr_0^2 a_m - GJ_d(b_m/\lambda_m)\right]\left[Pr_0^2 a_n - GJ_d(b_n/\lambda_n)\right]\delta_{mn} = \sum\limits_{m=1}^{\infty}\left[Pr_0^2 a_m - GJ_d(b_m/\lambda_m)\right]^2$ were used. By eliminating the multiplier $EJ_{\omega\omega}$ in Eq. VI.G(19), expanding the first term in the denominator and performing several simplifications, one obtains

$$\lambda_T = \frac{Pr_0^2 \sum_{m=1}^{\infty} \lambda_m a_m^2 - GJ_d \sum_{m=1}^{\infty} a_m^2}{Pr_0^2 \sum_{m=1}^{\infty} a_m^2 - 2GJ_d \sum_{m=1}^{\infty} a_m \frac{b_m}{\lambda_m} + GJ_d \sum_{m=1}^{\infty} \frac{b_m^2}{\lambda_m}} \qquad \text{VI.G(20)}$$

By dividing the numerator and the denominator of equation VI.G(20) by $a_1^2\left(Pr_0^2 - GJ_d/\lambda_1\right)$ in which λ_1 is the load factor corresponding to the first buckling mode i.e., $\lambda_1 = \left[GJ_d + \pi^2 EJ_{\omega\omega}/L^2\right]/\left(Pr_0^2\right)$, Eq. VI.G(20) can be expressed as

$$\lambda_T = \lambda_1 \left(\frac{1+\varepsilon_1}{1+\varepsilon_2}\right) \qquad \text{VI.G(21)}$$

in which

$$\varepsilon_1 = \frac{Pr_0^2 \sum_{m=2}^{\infty} \lambda_m a_m^2 - GJ_d \sum_{m=2}^{\infty} a_m^2}{a_1^2\left(\lambda_1 Pr_0^2 - GJ_d\right)} \qquad \text{VI.G(22)}$$

and

$$\varepsilon_2 = \frac{\lambda_1 Pr_0^2 \sum_{m=2}^{\infty} a_m^2 + GJ_d\left[\left(a_1 - b_1\right)^2 - 2\lambda_1 \sum_{m=2}^{\infty} a_m \frac{b_m}{\lambda_m} + \lambda_1 \sum_{m=2}^{\infty} \frac{b_m^2}{\lambda_m}\right]}{a_1^2\left(\lambda_1 Pr_0^2 - GJ_d\right)} \qquad \text{VI.G(23)}$$

One can show that the condition $\left(1+\varepsilon_2\right) > 0$ is always satisfied. Thus by substituting the relation $\lambda_1 Pr_0^2 = GJ_d + \pi^2 EJ_{\omega\omega}/L^2$ into Eq. VI.G(23) one obtains

$$\left(1+\varepsilon_2\right) = \frac{\frac{\pi^2 EJ_{\omega\omega}}{L^2} \sum_{m=1}^{\infty} a_m^2 + GJ_d \sum_{m=1}^{\infty}\left(a_m^2 - 2\lambda_1 a_m \frac{b_m}{\lambda_m} + \lambda_1 \frac{b_m^2}{\lambda_m}\right)}{a_1^2 \frac{\pi^2 EJ_{\omega\omega}}{L^2}} \qquad \text{VI.G(24)}$$

By using the relation $\lambda_m \geq \lambda_1$ in Eq. VI.G(24), one obtains

$$(1+\varepsilon_2) \geq \frac{\frac{\pi^2 EJ_{\omega\omega}}{L^2}\sum_{m=1}^{\infty} a_m{}^2 + GJ_d \sum_{m=1}^{\infty} \frac{\lambda_1}{\lambda_m}(a_m - b_m)^2}{a_1{}^2 \frac{\pi^2 EJ_{\omega\omega}}{L^2}} > 0 \qquad \text{VI.G.(25)}$$

From Eq. VI.G(21), since $(1+\varepsilon_2)$ is always positive, one can verify that when $\varepsilon_2 > \varepsilon_1$ one obtains $\lambda_T < \lambda_1$. Thus, for the approximate load factor λ_T to be smaller than the load factor corresponding to the first torsional buckling mode λ_1, one must have

$$\lambda_1 Pr_0{}^2 \sum_{m=2}^{\infty} a_m{}^2 + GJ_d \left[(a_1 - b_1)^2 - 2\lambda_1 \sum_{m=2}^{\infty} a_m \frac{b_m}{\lambda_m} + \lambda_1 \sum_{m=2}^{\infty} \frac{b_m{}^2}{\lambda_m} \right] > Pr_0{}^2 \sum_{m=2}^{\infty} \lambda_m a_m{}^2 - GJ_d \sum_{m=2}^{\infty} a_m{}^2 \qquad \text{VI.G(26)}$$

For example, the condition in Eq. VI.G(26) is met when the assumed rotation field $\Delta\phi_Z$ is chosen equal to the eigenvector of the first buckling mode i.e., $\Delta\phi_Z = a_1 \Delta\phi_{Z1}$, i.e., $a_2 = a_3 = \ldots a_\infty = 0$ and the assumed St. Venant torsion field ΔT_{sv} is chosen to have the more general expression $\Delta T_{sv} = -GJ_d \sum_{m=1}^{\infty} b_m \Delta\phi_{Zm}{}'$. In this case, by considering that $GJ_d > 0$, one can show that the inequality in Eq. VI.G(26) reduces to the condition

$$(a_1 - b_1)^2 + \lambda_1 \sum_{m=2}^{\infty} \frac{b_m{}^2}{\lambda_m} > 0 \qquad \text{VI.G(27)}$$

which is met for any combination of b_m constant s. For the special case where the assumed rotation field is $\Delta\phi_Z = a_1 \Delta\phi_{Z1}$ and the assumed St.Venant torsion field is $\Delta T_{sv} = -GJ_d a_1 \Delta\phi_{Z1}{}'$, Eq. VI.G(20) gives $\lambda_T = \lambda_1$, as expected and Eqs. VI.G(22) and VI.G(23) can be shown to lead to the conditions $\varepsilon_1 = 0$ and $\varepsilon_2 = 0$.

When the contribution of the St.Venant torsion is omitted i.e., $GJ_d = 0$, the buckling load factor corresponding to the first torsional buckling mode is obtained by using the formula $\lambda_1 = (\pi^2 EJ_{\omega\omega})/(Pr_0^2 L^2)$ (Bazant 1991). In this case, Eq. VI.G(26) is never satisfied for any assumed rotation field $\Delta\phi_Z = \sum_{m=1}^{\infty} a_m \Delta\phi_{Zm}$. Thus the eigenvalues predicted by setting $GJ_d = 0$ are always upper bounds to the load factor obtained by using the formula i.e., $\lambda_1 = (\pi^2 EJ_{\omega\omega})/(Pr_0^2 L^2)$ which is a lower value than the true buckling load obtained by using the formula i.e., $\lambda_1 = \left[GJ_d + \pi^2 EJ_{\omega\omega}/L^2\right]/(Pr_0^2)$. This is numerically illustrated and confirmed in Example VI.1 Table VI.3.

Appendix VI.H - Obtaining Buckling Mode Shapes

This appendix describes the procedures used to obtain the deformed shapes corresponding to buckling loads.

Step 1. The nodal values of the buckling mode shapes of elements BECE and BECES are obtained as from the eigenvector solution of Eq. (VI.126).

Step 2. The nodal displacement and rotation values extracted for the eigenvectors in Step1 are interpolated by using Hermitian polynomials.

The mode shape predictions obtained in this manner are in very good agreement with the conventional finite element solutions in Trahair (1993) and the ABAQUS shell model for the case of uniform moments i.e., $V_y^P = 0$ (For instance, this is the case in Fig. VI.18 of Example VI.3 Case 1 in Table VI.7).

However, when the loading condition causes moment gradient i.e., $V_y^P \neq 0$, although the buckling load predictions and the mode shape prediction for angle of twist are in very good agreement with those based on Trahair (1993) and ABAQUS results, the initial mode shape predictions for lateral displacements are rather poor (Fig. VI.H.1). This is possibly a result of the field identity $\lambda V_y^P \Delta u'(z) = 0$ (Eq. VI.C10) which naturally arose from the assumptions of the formulation. This field identity implies a constant lateral displacement field, which is in contradiction with the assumed cubic displacement field.

The mode shape predictions can be refined through the following additional steps

Step 3. The interpolated displacement field obtained in step 2 above is substituted into equilibrium equations i.e., (Eqs. (VI.41) and (VI.44)) which are then solved for the internal stress resultant fields. Note that the integration in Eqs. (VI.41) and (VI.44) constants can be also obtained from the displacement field by using the inter-element continuity and force boundary conditions.

Step 4. From the internal stress resultant fields obtained in Step 3, by substituting into the compatibility relations (Eq. (VI.57)) another set of displacement fields are obtained. Indeed, under the corrective scheme proposed in Steps 3 and 4, very good agreement with ABAQUS mode shapes is observed (e.g., Ex. VI.4, VI.6, VI.8 and VI.9).

The four step procedure of the corrective scheme is illustrated for Example 6 in which the load is applied at the top flange of the cantilever (Table VI.11 Case 1). In Step 1, the nodal displacements $\mathbf{\Delta d}_{\mathrm{NG}1\times4N}^{T} = \left\langle 0 \mid \mathbf{\Delta d}_{\mathrm{r}} \right\rangle_{1\times4N}^{T}$ are obtained from the eigenvector $\mathbf{\Delta d}_{\mathrm{r}}$ in Eq. (VI.126). By following Step 2, the lateral displacement and angle of twist for the first mode are obtained as given in Fig. VI.H.1 a and b respectively.

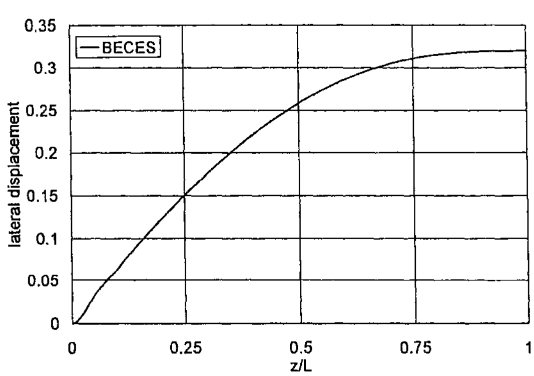

a-Lateral displacement

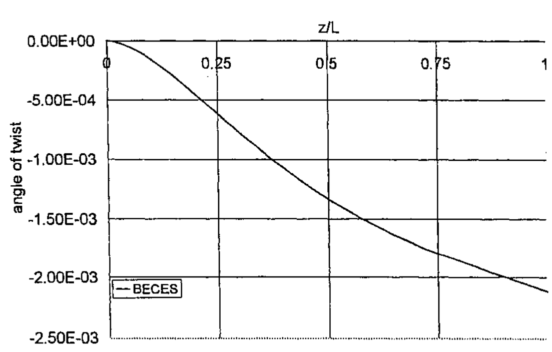

b-Angle of twist

Fig. VI.H.1 Buckling Mode for Case 1 in Table VI.11

In Step 3, the internal stress resultant filed is obtained by using the discretized form of the equilibrium conditions. Thus, the nodal displacement vector $\Delta\mathbf{d}_{\mathrm{NG}4N\times 1}$ is substituted into Eq. (VI.122) to solve for the vector of independent torsional constants $\Delta\mathbf{t}_{\mathrm{b}tb\times 1}$ and the moment and bimoment constants $\Delta\mathbf{f}_{\mathrm{Nt}sh\times 1}$.

$$\mathbf{B}^{\mathbf{G2}}_{\mathbf{t}\ tb\times tb}\Delta\mathbf{t}_{\mathrm{b}tb\times 1}+\mathbf{B}^{\mathbf{G2}}_{\mathbf{tf}\ tb\times sh}\Delta\mathbf{f}_{\mathrm{Nt}sh\times 1}=-\mathbf{B}^{\mathbf{G2}}_{\mathbf{td}\ tb\times 4N}\Delta\mathbf{d}_{\mathrm{NG}4N\times 1} \qquad \text{VI.H(1)}$$

$$\mathbf{B}^{\mathbf{G2}T}_{\mathbf{tf}\ sh\times tb}\Delta\mathbf{t}_{\mathrm{b}tb\times 1}+\mathbf{B}^{\mathbf{G2}}_{\mathbf{f}\ sh\times sh}\Delta\mathbf{f}_{\mathrm{Nt}sh\times 1}=-\mathbf{B}^{\mathbf{G}}_{\mathbf{fd}\ sh\times 4N}\Delta\mathbf{d}_{\mathrm{NG}4N\times 1} \qquad \text{VI.H(2)}$$

Because of the torsional continuity condition, all of the components are equal for this single span problem i.e., $\Delta T^{(r)}=\Delta T^{(i)}(i=1,16)$. Since the boundary condition for the last element is $\Delta T^{(16)}_{\alpha}=0$, all of the components of vector $\Delta\mathbf{t}_{\mathrm{b}tb\times 1}$ vanish. Thus, from Eqs. VI.H(1) and VI.H(2), one obtains

$$\mathbf{B}^{\mathbf{G2}}_{\mathbf{f}\ sh\times sh}\Delta\mathbf{f}_{\mathrm{Nt}sh\times 1}=-\mathbf{B}^{\mathbf{G2}}_{\mathbf{fd}\ sh\times 4N}\Delta\mathbf{d}_{\mathrm{NG}4N\times 1} \qquad \text{VI.H(3)}$$

From Eq. VI.H(3) one obtains the vector $\Delta\mathbf{f}_{\mathrm{Nt}sh\times 1}$, which can be written as $\Delta\mathbf{f}^{T}_{\mathrm{Nt}1\times 16}=\left\langle \Delta B^{(1)}_{\alpha} \quad \Delta B^{(2)}_{\alpha}...\Delta B^{(16)}_{\alpha}\right\rangle$ since the moment integration constants $\Delta M^{(2)}_{y\alpha}$ to $\Delta M^{(16)}_{y\alpha}$ are eliminated due to the shear continuity condition, constants $\Delta M^{(17)}_{y\alpha}$, $\Delta B^{(17)}_{\alpha}$ are eliminated due to free rotation and warping condition, and the constant $\Delta M^{(1)}_{y\alpha}$ is eliminated due to free translation condition. Note that, from the nodal displacement vector $\Delta\mathbf{d}_{\mathrm{NG}4N\times 1}$ one can easily obtains the element nodal displacement vectors $\Delta\mathbf{d}^{(i)}_{\mathrm{N}\ 8\times 1}$. From the free rotation and warping conditions, similar to Eqs. (VI.107) and (VI.108), constants $\Delta M^{(17)}_{y\alpha}$ and $\Delta B^{(17)}_{\alpha}$ can be recovered as

$$\Delta M^{(17)}_{y\alpha}=-\lambda\left[-N^{p(16)}\Delta u_{17}+\left(M^{p(16)}_{xl}-a_{y}N^{p(16)}\right)\Delta\phi_{Z17}\right] \qquad \text{VI.H(4)}$$

$$\Delta B_{\alpha}^{(17)} = -\lambda\left[\left(M_{xl}^{p(16)} - a_y N^{p(16)}\right)\Delta u_{17} + \left(N^{p(16)} r_{N0}^{\ 2} + M_{xl}^{p(16)} \beta_{Nx} + a_y^{\ 2} N^{p(16)}\right)\Delta\phi_{Z17}\right] \quad \text{VI.H(5)}$$

From the free translation condition, in a manner similar to Eq. (VI.110) constant $\Delta M_{y\alpha}^{1}$ can be recovered as

$$\Delta M_{y\alpha}^{(1)} = \Delta M_{y\alpha}^{(17)} = -\lambda\left[-N^{p(16)}\Delta u_{17} + \left(M_{xl}^{p(16)} - a_y N^{p(16)}\right)\Delta\phi_{Z17}\right] \quad \text{VI.H(6)}$$

From the shear continuity condition, constants $\Delta M_{y\alpha}^{2}$ to $\Delta M_{y\alpha}^{16}$ can be recovered.

$$\Delta M_{y\alpha}^{(j)} = \Delta M_{y\alpha}^{(1)}\left(\frac{L_r - \sum_{1}^{j} L^{(i)}}{L_r}\right) + \Delta M_{y\alpha}^{(17)}\left(\frac{\sum_{1}^{j} L^{(i)}}{L_r}\right) \quad \text{VI.H(7)}$$

From the element nodal displacement vectors $\mathbf{\Delta d}_{\mathrm{N}\ 8\times1}^{(i)}$, by substituting into relations $\Delta u^{(i)}(z) = \mathbf{H(z)}_{1\times4}^{T}\mathbf{\Delta u}_{\mathrm{N}\ 4\times1}^{(i)}$ and $\Delta\phi_{\mathrm{Z}}^{(i)}(z) = \mathbf{H(z)}_{1\times4}^{T}\mathbf{\Delta\varphi}_{\mathrm{N}\ 4\times1}^{(i)}$, one obtains the displacement field $\Delta u^{(i)}(z)$ and rotation field $\Delta\phi_{\mathrm{Z}}^{(i)}(z)$ for element i. By substituting these fields and the integration constants $\Delta T_{\alpha}^{(i)}$, $\Delta M_{y\alpha}^{(i)}$ and $\Delta B_{\alpha}^{(i)}$ obtained from Eqs. VI.H(1) through VI.H(7) into Eqs. (VI.90) and (VI.91), one obtains the internal moment ΔM_{y}^{i} and bimoment $\Delta B^{(i)}$ fields due to buckling for each element i ($i = 1,16$). From the fields $\Delta M_{y}^{(i)}$ and $\Delta B^{(i)}$ for each element one can plot the internal stress resultant fields ΔM_{y} and ΔB of the beam as shown in Fig. VI.H.2 a and b respectively.

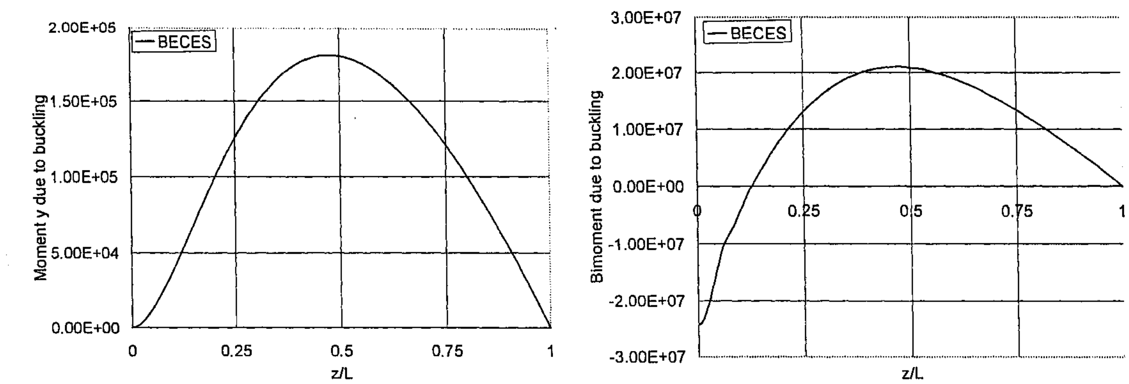

a- Moment due to buckling b-Bimoment due to buckling

Fig. VI.H.2 Buckling Mode for Case1 in Table VI.11

From Eq. (VI.58), by using the internal stress resultant fields ΔM_y and ΔB, one obtains the second derivative of the lateral displacement and angle of twist fields due to buckling as

$$\Delta u''+\frac{1}{E}\langle \Delta M_y \quad \Delta B\rangle \mathbf{D}_{r2\times2}^{-1}\begin{Bmatrix}1\\0\end{Bmatrix}+\frac{1}{G}\langle -\Delta M_y'' \quad \Delta B''\rangle \chi_{2\times2}^{-1}\begin{Bmatrix}1\\0\end{Bmatrix}=0 \qquad \text{VI.H(8)}$$

and

$$-\Delta\phi_Z''+\frac{1}{E}\langle \Delta M_y \quad \Delta B\rangle \mathbf{D}_{r2\times2}^{-1}\begin{Bmatrix}0\\1\end{Bmatrix}-\frac{1}{G}\langle -\Delta M_y'' \quad \Delta B''\rangle \chi_{2\times2}^{-1}\begin{Bmatrix}0\\1\end{Bmatrix}=0 \qquad \text{VI.H(9)}$$

By performing numerical integration twice on Eqs. VI.H(8) and VI.H(9) using thetrapezoidal rule of integration, one obtains the lateral displacement and angle of twist fields in terms of two integration constants for each equation. The integration constants are determined from the boundary conditions i.e., $u(0)=u'(0)=\phi(0)=\phi'(0)=0$. Thus, the lateral displacement and angle of twist predictions are obtained as shown in Fig. VI.28 a and b respectively. The deformed shapes presented in Figs. VI.16 through VI.35 are obtained by applying a similar procedure for each problem.

One should consider that in the proposed finite element method, by interpolating the displacement fields (i.e., u and ϕ) the internal stress resultant field is interpolated only indirectly. As a result of enforcing the variational principle one determines the internal stress resultant field. The displacement field can than be obtained from the internal stress resultant field through the compatibility equations. This procedure is just the opposite of that based on total potential energy, in which one determines the displacement field as a result of the variational principle and the internal stress resultant field through the equilibrium equations by using the displacement field.

Chapter VI References

[VI.1] Bathe, K.J. (1982), Finite Element Procedures in Engineering Analysis. Prentice-Hall Inc, Englewood Cliffs, New Jersey, USA.

[VI.2] Bazant, Z. P. and El Nimeri, M. (1973), "Large-Deflection Spatial Buckling of Thin-Walled Beams and Frames", *Jour. Eng. Mech. Div.* Vol. 99, No. EM6, pp.1259-1281.

[VI.3] Bazant, Z. P. (1991), *Stability of Structures*, Oxford University Press.

[VI.4] Boresi, A. P., Sidebottom, O. M. (1985), *Advanced Mechanics of Materials*, Fourth Edition, John Wiley & Sons, USA.

[VI.5] Bufler, H. (1983), "On the Work Theorems for Finite and Incremental Elastic Deformations with Discontinuous Fields: A Unified Treatment of Different Versions", *Comp. Meth. in Appl. Mech. and Eng.*, Vol.19, pp.235-255.

[VI.6] Chajes, A. and Winter, G. (1965), "Torsional-Flexural Buckling of Thin-Walled Members", *Journal of the Structural Division, ASCE,* Vol. 91, No. ST4, pp.103-125.

[VI.7] Chen, H. and Blandford, G. E. (1991), "Thin-Walled Space Frames. I: Large Deformation Analysis Theory", *Journal of the Structural Division, ASCE,* Vol. 117, No. 8, pp.2499-2520.

[VI.8] Courant, R. and Hilbert, D. (1962), *Methods of Mathematical Physics*, Vol.1, pp.233-273, Vol.2 pp.34-39, John Wiley and Sons.

[VI.9] Dabbas, A. (2002), *Lateral Stability of Partially Restraint Cantilever Supports*, M. Eng. Report, University of Ottawa, ON, Canada

[VI.10] De Veubeke, B. F. (1972), "A New Variational Principle for Finite Elastic Displacements", *Int. J. Engng. Sci.*, Vol.10, pp.745-763.

[VI.11] Dill, E. H. (1977), "The Complementary Energy Principle in Nonlinear Elasticity", *Letters in applied and Engineering Sciences*, Vol. 5, pp. 95-106.

[VI.12] Elias, M. Z. (1986), Theory and methods of Structural Analysis. John Wiley and Sons, NewYork, N.Y.

[VI.13] Erkmen, R. E. and Mohareb, M. "Non-orthogonal solution for thin-walled members-Generalized Expression for Stresses", accepted for presentation in The Eighth International Conference on Computational Structures Technology September 2006

[VI.14] Hancock, G. J., Trahair, N. S. and Bradford, M. A. (1980), "Web Distortion and Flexural-Torsional Buckling", *Journal of the Structural Division*, Vol. 106, No. 7, July 1980, pp. 1557-1571

[VI.15] John, F. (1960), "Plane Strain Problems for a perfectly Elastic Material of Harmonic Type", *Communications on Pure and Appl. Math.* Vol.13 pp.239-296.

[VI.16] Kim, M. Y. (1996), "Spatial Stability Analysis of Thin-Walled Space Frames", *Int. J. Num. Meth. Eng.*, Vol.39, pp.499-525

[VI.17] Kim, S. B and Kim, M. Y. (2000),"Improved formulation for spatial stability and free vibration of thin-walled tapered beams and space frames", *Eng. Struc*, Vol.22, pp.446-458.

[VI.18] Kim, M. Y., Kim, N. and Yun, H. T. (2003), " Exact dynamic and static stiffness matrices of shear deformable thin-walled beam-columns", *Journal of Sound and Vibration,* Vol.267, pp.29-55

[VI.19] Koiter, W. T. (1973), "On the principle of Stationary Complementary Energy in the nonlinear Theory of Elasticity", *SIAM J. Appl. Math.* Vol. 25, No.3, pp.424-434.

[VI.20] Koiter, W. T. (1975), "On the Complementary Energy theorem in nonlinear elasticity theory", WTHD Report 72, Delft University of Technology

[VI.21] Koiter, W. T. (1976), "Complementary Energy, neutral equilibrium and buckling", Proc. Kon. Ned. Akad., Wetensch., Series B, pp.183-200.

[VI.22] Krajcinovic, D. (1969), "A consistent discrete elements technique for thin wall assemblages", *Int. Jour. Solids and Structures*, Vol. 5, pp. 639-662.

[VI.23] Kutlukaya, O. (2003), *Lateral Stability of Planar Frames*, M. Eng. Report, University of Ottawa, ON, Canada

[VI.24] Lang, H. A. (1948), "Note on Rayleigh's Method and Non-uniform Strut", *Quart. Appl. Math.*, Vol.5, No.4, pp.510-511.

[VI.25] Levinson M. (1965), "The Complementary Energy Theorem in Finite Elasticity", Transactions of the ASME, Ser. E, *J. Appl. Mech.*, Vol.87, pp.826-828.

[VI.26] Lur'e, A. I. (1968), "Theory of Elasticity for semilinear Material", *PMM. J.Appl.Math and Mech*, Vol.32, no.6, pp.1053-1069

[VI.27] McGuire W., Gallagher R. H. and Ziemian R. D. (2000), *Matrix Structural Analysis*, John Wiley and sons, USA.

[VI.28] Masur, E. F. and Popelar, C. H. (1976), "On the Use of the Complementary Energy in the Solution of Buckling Problems", *Int. J. Solids and Structures* Vol. 12, pp.203-216

[VI.29] Mohareb, M. and Dabbas, A. (2003), "Lateral Stability of Partially Restrained Cantilever Supports", Annual Stability Conference Baltimore, Maryland, April , pp. 671-694.

[VI.30] Murakawa, H., Reed, K. W., Atluri, S. N. and Rubenstein, R. (1981), "Stability Analysis of Structures via Complementary Energy Method", *Comp. and Struc.*, Vol.13, pp.11-18.

[VI.31] Novozhilov, V.V. (1961), "*Theory of Elasticity*" Pergamon Press, Oxford

[VI.32] Ogden, R.W. (1977), "Inequalities Associated with the Inversion of Elastic Stress-Deformation Relations and Their Applications", *Math. Proc. Camb. Phil. Soc*,.Vol. 81, pp. 313-324.

[VI.33] Oran, C. (1967), "Complementary Energy Concept for Large Deformations", *Journal of the Structural Division*, Vol. 93, No. ST1, pp. 471-494.

[VI.34] Oran, C. (1967), "Complementary Energy Method for Buckling", *Journal of the Engineering Mechanics Division*, Vol. 93, No. EM1, pp. 57-75.

[VI.35] Oran, C. (1968), "Complementary Energy Method for Buckling of Plates", ASCE, J. Engng. Mech. Div., Vol. 94, pp. 621 -638.

[VI.36] Oran, C. (1971), "Upper bounds in Complementary Energy Method", *Journal of the Engineering Mechanics Division*, Vol. 97, No. EM4, pp. 1093-1102.

[VI.37] Pai, P. F. and Nayfeh, A. H. (1994), "A New Method for The Modeling of Geometric Nonlinearities in Structures", Computers & Structures Vol. 53, No. 4, pp. 877-895.

[VI.38] Pai, P.F. and Palazotto, A. N. (1995)," Polar Decomposition Theory in Nonlinear Analyses of Solids and Structures", *Journal of the Engineering Mechanics, ASCE*, Vol. 121, No. 4, pp. 568-581.

[VI.39] Pai, P.F., Palazotto, A. N. and Greer, J. M. (1998), "Polar Decomposition and Appropriate Strains and Stresses for Nonlinear Structural Analyses", *Computers & Structures* Vol. 66, No.6, pp.823-840.

[VI.40] C. Patterson, "Sufficient conditions for convergence in the Finite Element Method for any solution of Finite Energy", In J.R. Whiteman editor, The mathematics of Finite Elements and Applications: Proceedings of the Brunel university conference of the institute of Mathematics and its applications held in 1972, pages 213-224, NewYork 1973. Academic press.

[VI.41] Pi, Y.L and Trahair, N.S. (1992), "Energy Equation for Beam Lateral Buckling", *J. Struct. Eng.*, Vol. 118, No. 6, pp. 1462-1479.

[VI.42] Pi, Y.L and Trahair, N.S. (1992), "Prebuckling Deflections and Lateral Buckling. I:Theory", *J. Struct. Eng.*, Vol. 118, No. 11, pp. 2949-2967.

[VI.43] Pi, Y.L and Trahair,N.S. (1992), "Prebuckling Deflections and Lateral Buckling. II:Applications", *J. Struct. Eng.*, Vol. 118, No. 11, pp. 2967-2985.

[VI.44] Popelar, C. H. (1974), "Assured Upper Bounds via Complementary Energy", *Journal of Engineering Mechanics ASCE*, Vol. 100, No. 4, pp. 623-633.

[VI.45] Popelar, C. H. (1974), "Lower Bounds for the Buckling Loads and the Fundamental Frequencies of Elastic Bodies", *Journal of Appl. Mech.*, pp.151-154.

[VI.46] Roberts T. M. and Zaven G. Azizian (1983), "Instability of Thin-walled bars", *Journal of Engineering Mechanics ASCE*, Vol. 109, No. 3, pp. 781-794.

[VI.47] Schreyer, H. L. and Shih, P. (1973), "Lower Bounds to Column Buckling Loads", *Jour. Eng. Mech. Div.*, Vol. 99, No. EM5, pp. 1011-1022.

[VI.48] Souza, R.M. (2000), Force-based Finite Element for Large Displacement Inelastic Analysis of Frames, Ph.D Thesis, University of California, Berkeley.

[VI.49] Tabarrok, B. and Simpson, A. (1977), "An Equilibrium Finite Element Model for Buckling Analysis of Plates", *Int. J. Num. Meth. Eng.*, Vol.11, pp.1733-1751

[VI.50] Timoshenko (1913), "Sur la stabilite des systemes elastiques, Ann. Ponts et chausses". This paper also appears in "The collected papers of Stephen Timoshenko", pp. 92-224, McGraw-Hill Book Company, Inc., New York, 1954.

[VI.51] Timoshenko, S.P. (1945), "Theory of Bending, Torsion and Buckling of Thin-Walled Members of Open Cross Section", *J.Frankl.Inst.* Vol.239, No.3, pp.201-219.

[VI.52] Timoshenko, S.P. (1945), "Theory of Bending, Torsion and Buckling of Thin-Walled Members of Open Cross Section", *J.Frankl.Inst.* Vol.239, No.4, pp.249-268.

[VI.53] Timoshenko, S.P. (1945), "Theory of Bending, Torsion and Buckling of Thin-Walled Members of Open Cross Section", *J.Frankl.Inst.* Vol.239, No.5, pp.343-361.

[VI.54] Timoshenko, S.P. and Gere, J. M. (1961), *Theory of Elastic Stability*, second Edition, *McGraw-Hill Inc.*, NY

[VI.55] Timoshenko, S.P., Goodier, J. N. (1970), *Theory of Elasticity*, 3rd Edition, *McGraw-Hill Inc.*, NY

[VI.56] Trahair, N.S. and Bild, S. (1990), "Elastic Biaxial and Torsion of Thin-Walled Members", *Thin-Walled Structures.*, Vol.9, pp. 269-307.

[VI.57] Trahair, N.S. (1993), *Flexural-Torsional Buckling of Structures*, CRC Press, Boca Raton, FL, USA.

[VI.58] Trahair, N.S. and Pi, Y.L. (1997), "Torsion, Bending and Buckling of Steel Beams", *Eng. Struc.* Vol.19, No.5, pp.372-377.

[VI.59] Vlasov, V. Z. (1961), *Thin Walled Elastic Beams*, Second Edition, Israel Program for Scientific Translations, Jerusalem, Israel.

[VI.60] Wagner, H. (1936), *Torsion and Buckling of Open Sections*, Translated Technical Memorandum No. 807, NACA - National Advisory Committee for Aeronautics.

[VI.61] Washizu, K. (1982), *Variational Methods in elasticity and Plasticity*, Pergamon Press Third edition Oxford.

[VI.62] Westergaard, H. M. (1941), "On the Method of Complementary Energy and its applications to Structures Stressed beyond the Proportional Limit, to Buckling and Vibrations, and to Suspension Bridges", *Transactions ASCE*, Vol. 107, pp. 765-793.

[VI.63] Yoo, C.H. (1980), "Bimoment Contribution to stability of Thin-Walled Assamblages", *Comp. & Struc.* Vol.11 pp.465-471.

[VI.64] Zubov, L. M. (1970), “The stationary principle of complementary work in nonlinear theory of elasticity”, *PMM, J.Appl.Math and Mech,* Vol.34 No.2, pp.241-245.

Chapter VI List of symbols

A	=	cross-sectional area;
A_p	=	pole (Fig. VI.4);
a_x, a_y	=	coordinates of arbitrary pole A_p (Figs. VI.4b);
$\overline{A}, \overline{S}_x, \overline{S}_y, \overline{S}_\omega$	=	functions to relate stress resultant functions to constant component of Jaumann stress;
$\mathbf{B}^{(i)}{}_{13\times 13}$	=	element elastic matrix;
$\mathbf{B}^{\mathrm{G}}{}_{(7N-1)\times(7N-1)}$	=	globale elastic matrix after imposing moment and bimoment continuity conditions;
$\mathbf{B}^{\mathrm{G2}}{}_{(tb+sh+4N)\times(tb+sh+4N)}$	=	global elastic matrix after imposing moment and bimoment, shear force, torsion continuity and force boundary conditions;
$\mathbf{K}_{\mathrm{E}4N\times 4N}$	=	global elastic stiffness matrix after static condensation;
$\mathbf{K}_{\mathrm{G}4N\times 4N}$	=	global geometric stiffness matrix;
C	=	Centroid;
$\mathbf{C}_{2\times 2}$	=	matrix due to external loading;
$\mathbf{c}_{1(N-1)\times a}, \mathbf{c}_{2\,2N\times b}, \mathbf{c}_{3b\times s}$	=	matrix of constraint conditions to impose inter-element stress resultant continuity;
$\mathbf{c}_{4b\times 4N}, \mathbf{c}_{5s\times sh}, \mathbf{c}_{6s\times 4N}$	=	matrix of constraint conditions to impose inter-element stress resultant continuity;

$\mathbf{c}_{7a\times 4tb}$	=	matrix of constraint conditions to impose inter-element stress resultant continuity;
$\mathbf{D}_{4\times 4}$	=	matrix of cross-sectional properties;
$\mathbf{D}_{r2\times 2}$	=	reduced matrix of cross-sectional properties;
D_{ij}	=	first Piola-Kirchoff stress tensor;
dl_1	=	un-deformed length for an infinitesimal element along the principal direction;
dL_1	=	deformed length for an infinitesimal element along the principal direction;
$\vec{e}_0$	=	unit vectors along the principal strain directions of the *un-deformed* parallelepiped;
$\vec{e}$	=	unit vectors along the principal strain directions of the un-*deformed* parallelepiped;
f_j	=	forces acting on the surfaces of infinitesimal parallelepiped (Fig. VI.3);
E	=	modulus of elasticity;
F_{ij}	=	deformation gradient tensor;
G	=	shear modulus;
$\mathbf{H}(z)_{4\times 1}$	=	vector of Hermitian polynomials;
$h(s)$	=	normal distance between pole and the tangent to mid-surface;

$\vec{i}_{0j}$	=	unit vectors along X,Y and Z directions;
J_d	=	St. Venant's torsional constant;
$L^{(i)}$	=	length of finite element (i);
$J_{xx}, J_{yy}, J_{xy}, J_{\omega x}, J_{\omega y}$	=	section moments of inertia and products of inertia;
J_d	=	St. Venant's torsional constant;
$J_{\omega\omega}$	=	second moment of the sectorial coordinate;
$\mathbf{K}^{(i)}_{\mathbf{g}\ 8\times 8}$	=	geometric stiffness matrix;
$\mathbf{K}^{(i)}_{\mathbf{g1}\,4\times 4}$, $\mathbf{K}^{(i)}_{\mathbf{g2}\,4\times 4}$	=	components of geometric stiffness matrix;
N	=	Number of nodes;
$N^p, V_x^p, V_y^p, T^p, T_w^p, T_{sv}^p$	=	stress resultant functions in prebuckling analysis;
M_x, M_y	=	stress resultant functions in prebuckling analysis;
O	=	Origin;
R_{ij}	=	rigid body rotation tensor;
r	=	coordinate normal to the section mid surface (Fig. VI.5);
r_{N0}	=	radius of gyration in non-orthogonal coordinates;
s	=	curvilinear coordinate along mid surface (Fig. VI.4, Fig.VI.5);
S_0	=	sectorial origin (Figs. VI.4);
$S.C$	=	Shear Center;
S_x, S_y, S_w	=	first moments of area of coordinates x, y, and ω;
sh	=	Number associated with the bending and bimoment

		boundary conditions and number of elements;
$t(s)$	=	thickness of the thin-wall segment (Fig. VI.5);
T	=	total twisting moment;
T_{sv}	=	St.Venant torsion (Fig. VI.4);
T_w	=	warping torsion (Fig. VI.4);
tb	=	Number associated with the torsional boundary conditions and number of elements;
u_s, v_s, w_s	=	displacement fields along X, Y and Z directions;
U^*	=	complementary strain energy;
$u(z), v(z)$	=	displacements along x, y directions of arbitrary pole (Fig. VI.4a);
$u_s(s,z), v_s(s,z)$	=	horizontal and vertical displacements of arbitrary point B_p located on section mid-surface (Fig. VI.4a);
V	=	volume of element;
W	=	Wagner stress resultant;
W_i	=	Internal strain energy density;
x, y, z	=	material coordinates of a point (Figs. VI.1);
X,Y,Z	=	spatial coordinates of a point (Figs. VI.1);
α	=	angle between the tangent to the contour and the x axis;
β_{Nx}	=	mono-symmetry property in non-orthogonal coordinates;
δ_{ij}	=	right extensional strain;
$\Delta\mathbf{d}^{(i)}_{\mathrm{N}\ 8\times1}$	=	vector of nodal displacements of element i;

$\Delta\mathbf{f}_{\mathrm{N}\ 4\times 1}^{(i)}$ = vector of moment and bimoment integration constants of element i;

$\Delta\mathbf{f}_{\mathrm{NG}\,2N\times 1}$ = global vector of moment and bimoment integration constants after imposing moment and bimoment continuity conditions i;

$\Delta\mathbf{f}_{\mathrm{Nr}b\times 1}$ = vector of moment and bimoment integration constants after imposing shear force continuity conditions;

$\Delta\mathbf{f}_{\mathrm{Nm}s\times 1}$ = vector of moment and bimoment integration constants after imposing shear force continuity and moment and bimoment force boundary conditions;

$\Delta\mathbf{f}_{\mathrm{Nt}sh\times 1}$ = vector of moment and bimoment integration constants after imposing shear force continuity and all theforce boundary conditions;

$\Delta N, \Delta V_x, \Delta V_y$ = stress resultant increments due to buckling;

$\Delta T, \Delta T_w, \Delta T_{sv} M_x, M_y$ = stress resultant increments due to buckling;

$\Delta\mathbf{t}_{1\times 1}^{(i)}$ = vector of torsional constant of element i;

$\Delta\mathbf{t}_{\mathrm{NG}(N-1)\times 1}$ = vector of torsional constant after assamblage;

$\Delta\mathbf{t}_{\mathrm{r}a\times 1}$ = vector of torsional constant after imposing torsion continuity condition;

$\Delta\mathbf{t}_{\mathrm{b}tb\times 1}$ = vector of torsional constant after imposing torsion continuity and torsion boundary condition;

$\mathrm{D}u(z), \mathrm{D}v(z)$	=	displacements increments due to buckling along x, y directions of arbitrary pole;
ε_{ij}	=	right extensional strain tensor;
ε_{imj}	=	permutation symbol;
ϕ_X, ϕ_Y, ϕ_Z	=	rotation vector components about X, Y and Z directions;
γ_1, γ_2	=	angles due to shear deformation in Fig. VIA.1.b;
λ	=	buckling load factor;
$\chi_{2\times2}$	=	matrix associated with the distribution of shear stress on the cross-section;
ν	=	Poisson's ratio;
π^*	=	total complementary energy;
σ_{ij}	=	Jaumann stress tensor;
σ_c	=	constant component of Jaumann stress along the thickness;
σ_r	=	vanishing component of Jaumann stress (Fig. VI.5);
σ_{sv}	=	Jaumann stress due to St.Venant torsion (Fig. VI.5);
ω	=	sectorial area (Figs. VI.4b);

Chapter VI List of Tables

Table VI.F.1 Third mode for Example VI.1

Table VI.F.2 Fourth and fifth modes for Example VI.1

Table VI.F.3 Higher modes for Example VI.2 Case1

Table VI.F.4 Higher modes for Example VI.2 Case2

Table VI.F.5 Higher modes for Example VI.3 Case1

Table VI.F.6 Higher modes for Example VI.3 Case2

Table VI.F.7 Higher modes for Example VI.3 Case3

Table VI.F.8 Higher modes for Example VI.3 Case4

Table VI.F.9 Higher modes for Example VI.3 Case5

Table VI.F.10 Higher modes for Example VI.4

Table VI.F.11 Higher modes for Example VI.5

Table VI.F.12 Higher modes for Example VI.6 Case1

Table VI.F.13 Higher modes for Example VI.6 Case2

Table VI.F.14 Higher modes for Example VI.7

Table VI.F.15 Higher modes for Example VI.8

Chapter VI List of Figures

Figure VIH.1 Buckling Mode for the first problem in Table VI.11 Case a a) lateral displacement and b) angle of twist

Figure VIH.2 Increments in force fields due to buckling for the first problem in Table 11

Fig. VI.H.2 Buckling Mode for Case 1 in Table VI.11

CHAPTER VII

SUMMARY AND RECOMMENDATIONS FOR FUTURE WORK

In this chapter, the contributions made in this thesis are summarized. Recommendations for future work are also presented.

Summary

In Chapters II, III and IV, a general non-orthogonal solution scheme for the Vlasov thin-walled beam theory was developed.

In Chapter II, three finite elements were derived. Element NOVEE14 provides exact nodal values under the limitations of the Vlasov theory. Element NOVEC14 is suitable for modeling short elements while element NOVEL12 is suitable for modeling long elements.

In Chapter III, the advantages and modeling capabilities of the formulation were presented through four examples. It was shown that the new finite element solution is effective in seamlessly modeling members with stepwise cross-sectional changes, rectangular holes and longitudinal stiffeners, and eccentric supports.

In Chapter IV, expressions for normal and shear stresses in terms of stress resultants were developed for a general open thin-walled section based on non-orthogonal coordinate system. These expressions complement the finite element solutions derived in Chapter II.

In Chapter V, the shear deformation effect due to warping was included in torsional analysis of thin-walled beams and the field equation and boundary conditions were developed based on the principle of complementary energy. Two finite elements were developed, which capture shear deformation effects. Element THE4 yields nodal displacements in exact agreement with the closed form solution of the differential equations based on the developed theory. Element TLE4 provides lower bound solutions and converges to THE4 results when a refined mesh is adopted. For squat beams, shear deformation effects were shown to gain significance.

In Chapter VI, the buckling equilibrium equations for open section thin-walled members were obtained in terms of the stress resultants and displacement field based on the stress expressions of the Vlasov thin-walled beam theory. Field equations and boundary conditions based on a general non-orthogonal system of coordinates were derived by using the complementary energy principle. Two finite elements were developed for the buckling analysis of members with symmetric and mono-symmetric sections. In element BECE, the shear deformation effect is omitted whereas in element BECES, it is included. The validity of the new solution in predicting buckling loads of columns in flexural and torsional buckling modes and beams in lateral torsional buckling modes were demonstrated through comparisons to established solutions for a wide number of problems. The load position effect was successfully captured by adopting non-orthogonal coordinate systems. It was shown that omitting shear deformation effect significantly overestimates buckling load predictions in some cases.

Recommendations for Future Research

a) Several researchers (e.g., ref. V.2 and V.10) have modified the Vlasov theory to incorporate shear deformation effects. All solutions developed adopt displacement based variational solutions under orthogonal coordinates. To the author's knowledge there were no attempts to develop solutions for these advanced theories under non-orthogonal coordinates. The methodology developed in Chapter II could be extended to these advanced theories, with similar modeling advantages as those presented in Chapter III.

b) The complementary energy based solution adopted in Chapter V can be generalized to include the flexural behavior of the thin-walled members, by including the additional internal stresses induced by biaxial bending moments, biaxial shear and axial forces. Finite element formulation can be developed for the static analysis of thin-walled members either under orthogonal or non-orthogonal coordinates, which includes shear deformation effects.

c) Dynamic effects can be included in the virtual work expression in Chapter II or in the complementary energy expression in Chapter V to extend the finite element solutions to the vibration analysis of thin-walled members.

d) Distributed member load effects can be incorporated into the developments of Chapter VI.

e) The formulations in Chapters II, V and VI were applied for one dimensional structures. Extended applications of the new solutions to 2D structures can be achieved by developing suitable interfacing finite elements between non co-linear elements which model the elastic behaviour of connections.

f) A Hybrid element can be developed from the complementary energy functional for the buckling analysis of thin walled beams in which the force degrees of freedom are eliminated prior to assemblage, so that the assemblage process can be simplified which may be more suitable for assembling 3D structures.

g) It was noticed that the solutions of elements BECE and BECES can either underestimate or overestimate the buckling load (as predicted by closed form solutions or other established solutions). This is in contrast to displacement based formulations which always tend to overestimate buckling loads. A mathematical proof has been developed demonstrating that the eigenvalue predictions for torsional column buckling under BECE formulation can be a lower bound. It is of interest to possibly generalize the developments to describe the set of conditions under which this will be the case for beams or beam columns subject to lateral torsional buckling.